

“The truth may be puzzling. It may take some work to grapple with. It may be counterintuitive. It may contradict deeply held prejudices. It may not be consonant with what we desperately want to be true. But our preferences do not determine what's true.”

—

Carl Sagan (1934 – 1996)

University of Alberta

**Synthesis and Characterization of Novel Radiolabelled Substrates for
Imaging of GLUT5 Expression in Human Breast Cancer Using
Positron Emission Tomography**

by

Brendan Joseph Trayner

A thesis submitted to the Faculty of Graduate Studies and Research
in partial fulfillment of the requirements for the degree of

Doctor of Philosophy

Department of Physiology

©Brendan Joseph Trayner
Fall 2012
Edmonton, Alberta

Permission is hereby granted to the University of Alberta Libraries to reproduce single copies of this thesis and to lend or sell such copies for private, scholarly or scientific research purposes only. Where the thesis is converted to, or otherwise made available in digital form, the University of Alberta will advise potential users of the thesis of these terms.

The author reserves all other publication and other rights in association with the copyright in the thesis and, except as herein before provided, neither the thesis nor any substantial portion thereof may be printed or otherwise reproduced in any material form whatsoever without the author's prior written permission.

To my parents

—

For giving me the tools that I needed

Abstract

Overactive glucose transport and metabolism has been widely recognized as one of the fundamental hallmarks of cancer and its progression. The facilitative glucose transporter GLUT1 is widely overexpressed in many tumor types compared to their untransformed counterparts. Due to this, the glucose analogue, 2-deoxy-2-[¹⁸F]fluoro-D-glucose (FDG) has been used widely for the imaging of malignant neoplastic tissue through a non-invasive technique, positron emission tomography (PET). PET scans have been very successful in the imaging of many breast cancers expressing high levels of GLUT1, but unfortunately, many breast tumors do not express GLUT1 at high levels, if at all. Clinically, this lack of GLUT1 expression in tumors has led to false-negatives in patients' PET scans. Interestingly, in 1996 it was first identified that the fructose transporting facilitative hexose transporter GLUT5 is highly expressed in transformed breast tissue compared to the untransformed surrounding tissue. This finding has led to the suggestion that radiolabeled substrates for GLUT5 may be effective in imaging GLUT1 negative, GLUT5 positive tumors. We have rationally designed and synthesized several compounds based around previously performed structural studies and analyzed their behaviour both *in vitro* and *in vivo*. The C-6 labelled fructose analogue 6-deoxy-6-[¹⁸F]fluoro-D-fructose (6-FDF) has shown favourable *in vitro* and *in vivo* characteristics for the imaging of GLUT5 expressing breast tumors. Additionally, its dosimetry and excretory profile suggest the viability of the compound for a clinical trial. Other substrates based

on the C₂ symmetric fructose mimic 2,5-anhydro-D-mannitol (2,5-AM) have also been examined for their behaviour *in vitro* and *in vivo*. Further work will be spent on further characterizing additional fructose and 2,5-AM analogues that will shed more light on the structural requirements of GLUT5 and perhaps lead to other tracers that will show utility in the imaging of GLUT5 expressing breast cancer with PET.

Acknowledgements:

Science is a finicky thing.

Sometimes you feel like you have a grip on all of it and then suddenly, in an instant, it all goes tumbling through your fingers only for you to attempt pick it up all over again. It requires dedication, support, friendship, luck, and more importantly a well-honed sense of humour. I have many people to thank for their support throughout my last five years that has led to the creation of this document.

First and foremost I would like to thank my supervisor Dr. Chris Cheeseman for taking me on as a PhD student in his lab. The project that I have been entrusted with was more than I think many students could ever hope for, and the freedom and unwavering support given to me throughout the years I believe has truly transformed me into a well-rounded young scientist.

Next, are our collaborators from the Department of Chemistry who have made this project possible - Dr. Tina Grant, Dr. Olivier Soueidan, Dr. Fred West, Tom Scully and Dr. Jeff Henderson. They have all been exceedingly courteous and helpful throughout the years and did not complain once when I asked for “just a little more 6-FDF”.

The members of my committee Dr. John Mercer and Dr. David Murray have shared their wisdom, insight and support throughout my program, and have provided me with a sense of true collegiality that I believe not many students have been privy to.

Many of these experiments would not have been possible if it was not for the help of Dr. Melinda Wuest and her excellent technical knowledge in the field of radiopharmaceutical development and animal PET imaging. Her invaluable support and rigorous questioning has strengthened our publication record

substantially, and has set this project on the right path for future growth while maintaining very high quality levels of science.

I also would like to thank both Dr. Sandy McEwan and Dr. Frank Wuest. Dr. McEwan provided me the financial means as well as a “kick in the butt” to get me to start graduate studies. Dr. Wuest has always contributed greatly to our unique collaborative effort and always did so with a smile on his face. Both have had a lasting impact on my education and were a very important part of my time spent at the Cross Cancer Institute.

Thank you to Monica Wang and Bonnie Andrais for their excellent technical services throughout the preparation of this work.

I have had the distinct pleasure of meeting a whole swath of incredible people during my time in the Department of Physiology, all of whom have had an important part in turning me into the person I am today:

- Deb O’Neill – for being my “lab mom” and giving me the support, friendship, help and motivation I needed to work through this process. I will miss our daily chats and hilarious banter more than you know.
- Dr. Kate Witkowska – for being the closest thing that I’ve ever had to a sister. It’s been an incredible journey for the both of us over the last 5 years and I am glad I could share it with you.
- Mike Carew – for being a great roommate and an amazing friend who is there whenever I need to talk to someone.
- Jen Zwicker – for sharing the load with our student government responsibilities and always being someone I can reflect on the future with.
- Barbara Roggenbeck – for dealing with my constant sarcasm and sharing many laughs with me.

- Richard Kanyo – For always being there when beer was needed to be consumed.

Next, are my friends who I've met from outside the confines of science. You are too countless to name, but you know who you are. From weekend dance parties, lazy afternoons, to serious conversations about life, the world, politics, friendship and love – I appreciate and love you all.

Lastly and perhaps most importantly are my mother, father, Josh and Sean. You have shaped me into who I am today more than anyone or anything. You are my best friends, and those who I can always count on. Thank you for everything – this wouldn't have been possible without you.

Additional thanks goes to Dr. Melinda Wuest, Tom Scully and Dr. Olivier Soueidan for assistance in the preparation of this thesis.

CHAPTER 1: GENERAL INTRODUCTION	1
1.1 INTRODUCTION OUTLINE	2
1.2 INTRODUCTION TO CARRIER-MEDIATED GLUCOSE TRANSPORT	2
1.2.1 <i>Transport across cellular membranes.....</i>	2
1.2.2 <i>Principles and history of carrier mediated glucose transport and the 'simple carrier model' 3</i>	
1.3 FAMILY OF FACILITATIVE HEXOSE TRANSPORTER PROTEINS (GLUTs)	8
1.3.1 <i>General overview of the SLC2A family of facilitative hexose transporters</i>	8
1.4 CLONING AND INITIAL CHARACTERIZATION OF GLUT1 (SLC2A1)	10
1.4.1 <i>Cloning and characterization of GLUT1</i>	10
1.4.2 <i>GLUT1 substrate binding studies</i>	12
1.5 CLONING AND INITIAL CHARACTERIZATION OF GLUT2 (SLC2A2)	13
1.5.1 <i>Cloning and characterization of GLUT2</i>	13
1.5.2 <i>GLUT2 in the small intestine and kidney.....</i>	14
1.5.3 <i>GLUT2 in the liver and pancreas.....</i>	15
1.5.4 <i>GLUT2 as a glucose sensor and regulation</i>	16
1.5.5 <i>GLUT2 substrate binding studies</i>	16
1.6 CLONING AND INITIAL CHARACTERIZATION OF GLUT5 (SLC2A5)	17
1.6.1 <i>Cloning and characterization of GLUT5</i>	17
1.6.2 <i>GLUT5 in the small intestine</i>	18
1.6.3 <i>GLUT5 in the kidney.....</i>	19
1.6.4 <i>GLUT5 in spermatozoa.....</i>	20
1.6.5 <i>GLUT5 in skeletal muscle and adipose tissue.....</i>	20
1.6.6 <i>GLUT5 in the brain</i>	21
1.6.7 <i>Regulation of GLUT5.....</i>	22

1.6.8	<i>GLUT5 substrate binding studies</i>	23
1.7	INITIAL CHARACTERIZATION OF THE PRIMARY PHOSPHORYLATING ENZYMES OF GLUCOSE AND FRUCTOSE	25
1.7.1	<i>Hexokinase family</i>	25
1.7.2	<i>Ketohexokinase (KHK)</i>	30
1.8	A BRIEF OVERVIEW OF THE CHARACTERISTICS OF HEXOSE METABOLISM IN CANCER ..	31
1.8.1	<i>Brief overview of hexose metabolism and energy production</i>	31
1.8.2	<i>Glucose transport, Glycolysis and the TCA in cancerous tissue: An overview</i>	33
1.8.3	<i>GLUT1/GLUT3 expression in cancer</i>	35
1.8.4	<i>Hexokinase II in tumors</i>	37
1.8.5	<i>Additional factors accelerating glycolysis</i>	38
1.9	BREAST CANCER	40
1.9.1	<i>Overview of diagnosis and treatment</i>	40
1.9.2	<i>Changes in breast cancer glycolysis</i>	42
1.10	POSITRON EMISSION TOMOGRAPHY AND MOLECULAR IMAGING OF BREAST CANCER USING 2-DEOXY-2-[¹⁸F]FLUORO-D-GLUCOSE ([¹⁸F]FDG)	45
1.10.1	<i>Brief overview and history of positron emission tomography and its importance for imaging of cancer</i>	45
1.10.2	<i>History and characterisation of [¹⁸F]FDG as a radiotracer for PET</i>	47
1.10.3	<i>Molecular imaging of breast cancer with [¹⁸F]FDG PET</i>	51
1.10.4	<i>Brief explanation of standardized uptake value (SUV)</i>	56
1.11	RATIONAL DESIGN OF ALTERNATIVE HEXOSE BASED PROBES FOR IMAGING OF BREAST TUMORS USING POSITRON EMISSION TOMOGRAPHY	57
1.11.1	<i>GLUT5 and GLUT2 expression in breast cancer tissue</i>	57
1.11.2	<i>GLUT5 analogues for the imaging of breast cancer</i>	60

1.11.3	Thesis objectives.....	<i>Error! Bookmark not defined.</i>
1.12	BIBLIOGRAPHY	72
CHAPTER 2 - SYNTHESIS AND CHARACTERIZATION OF 6-DEOXY-6- FLUORO-D-FRUCTOSE AS A POTENTIAL COMPOUND FOR IMAGING BREAST CANCER WITH PET		
97		
2.1	INTRODUCTION	98
2.2	RESULTS AND DISCUSSION	102
2.2.1	Synthesis of 6-FDF.....	102
2.2.2	Hexose transport in MCF-7 and MDA-MB-231	103
2.2.3	Inhibition studies	106
2.2.4	Uptake of [¹⁴ C]6-FDF.....	107
2.3	EXPERIMENTAL / MATERIAL AND METHODS.....	108
2.3.1	Synthesis of 6-deoxy-6-fluoro-D-fructose.	108
2.3.2	Methyl 6- <i>O</i> -(<i>tert</i> -butyldimethylsilyl)-D-fructofuranoside, 3.....	109
2.3.3	Methyl 1,3,4-tri- <i>O</i> -acetyl-6- <i>O</i> -(<i>tert</i> -butyldimethylsilyl)-D-fructofuranoside, 4.....	110
2.3.4	Methyl 1,3,4-tri- <i>O</i> -acetyl-D-fructofuranoside, 5.	112
2.3.5	Methyl 1,3,4-tri- <i>O</i> -acetyl-6-deoxy-6-fluoro-D-fructofuranoside, 6.....	113
2.3.6	6-Deoxy-6-fluoro-D-fructose, 7.	115
2.3.7	Western Blots	116
2.3.8	Cell Culture and Fluxes.....	117
2.3.9	Immunocytochemistry	118
2.3.10	Analysis.....	119
2.4	BIBLIOGRAPHY	129

CHAPTER 3 - RADIOPHARMACOLOGICAL EVALUATION OF 6-DEOXY- 6-[¹⁸F]FLUORO-D-FRUCTOSE AS A RADIOTRACER FOR PET IMAGING OF GLUT5 IN BREAST CANCER	133
3.1 INTRODUCTION	134
3.2 MATERIALS AND METHODS	138
3.2.1 <i>Radiotracer synthesis.....</i>	138
3.2.2 <i>Western Blots of MCF-7, MDA-MB-231 and EMT-6</i>	139
3.2.3 <i>In vitro cell uptake and efflux studies</i>	140
3.2.4 <i>Animals</i>	141
3.2.5 <i>Biodistribution experiments.....</i>	142
3.2.6 <i>Small animal PET in normal and tumor-bearing mice</i>	143
3.2.7 <i>Phosphorylation with KHK</i>	144
3.2.8 <i>Determination of radioactive metabolites in mouse blood and urine</i>	145
3.2.9 <i>Data analysis</i>	145
3.3 RESULTS.....	146
3.3.1 <i>Radiotracer synthesis.....</i>	146
3.3.2 <i>Western Blots of MCF-7, MDA-MB-231 and EMT-6</i>	147
3.3.3 <i>Cell uptake studies.....</i>	147
3.3.4 <i>Biodistribution in normal mice.....</i>	149
3.3.5 <i>In vivo studies in tumor-bearing mice.....</i>	150
3.3.6 <i>Phosphorylation with KHK</i>	152
3.3.7 <i>Metabolite analysis</i>	152
3.4 DISCUSSION	153
3.4.1 <i>Summary.....</i>	153

3.4.2	<i>In vitro studies</i>	154
3.4.3	<i>In vivo studies</i>	157
3.5	CONCLUSION	162
3.6	BIBLIOGRAPHY	176

CHAPTER 4 - DOSIMETRY OF 6-DEOXY-6-[¹⁸F]FLUORO-D-FRUCTOSE

(6-[¹⁸F]FDF) FOR PET IMAGING OF GLUT5 DERIVED FROM A STUDY

IN RATS 181

4.1	INTRODUCTION	182
4.2	METHODS	182
4.2.1	<i>Synthesis of 6-[¹⁸F]FDF</i>	182
4.2.2	<i>Animals</i>	184
4.2.3	<i>Positron Emission Tomography</i>	184
4.2.4	<i>Biodistribution experiments</i>	185
4.2.5	<i>Radiation Dosimetry Analysis</i>	185
4.2.6	<i>Statistics</i>	187
4.3	RESULTS	187
4.4	DISCUSSION	188
4.5	BIBLIOGRAPHY	195

CHAPTER 5 - IN VITRO AND IN VIVO EVALUATION OF 1-DEOXY-1-

FLUORO-2,5-ANHYDRO-D-MANNITOL AS A POTENTIAL

RADIOTRACER FOR PET IMAGING OF GLUT5 IN BREAST CANCER. 197

5.1	INTRODUCTION	198
------------	---------------------------	------------

5.2	MATERIALS AND METHODS.....	203
5.2.1	<i>Synthesis of 1-deoxy-1-fluoro-2,5-anhydro-D-mannitol</i>	203
5.2.2	<i>Cell culture and transport experiments</i>	209
5.2.1	<i>Animals</i>	210
5.2.2	<i>Small animal PET in EMT-6 tumor-bearing mice</i>	211
5.2.3	<i>Data analysis</i>	213
5.3	RESULTS.....	213
5.3.1	<i>Inhibition of [¹⁴C]D-fructose transport with 2,5-AM</i>	213
5.3.2	<i>Inhibition of [¹⁴C]D-fructose transport by 1-FDAM</i>	214
5.3.3	<i>Uptake of [¹⁴C]1-FDAM</i>	214
5.3.4	<i>Inhibition of [¹⁴C]1-FDAM uptake by cytochalasin B.....</i>	215
5.3.5	<i>Inhibition of [¹⁴C]1-FDAM transport with D-fructose.....</i>	215
5.3.6	<i>Inhibition of 6-[¹⁸F]FDF uptake with 1-FDAM</i>	216
5.3.7	<i>Uptake of 1-[¹⁸F]FDAM into EMT-6 cells.....</i>	216
5.3.8	<i>Uptake of 1-[¹⁸F]FDAM, 1-[¹⁸F]FDF, 6-[¹⁸F]FDF and [¹⁸F]FDG into BALB/c mice with xenografted EMT-6 tumors.....</i>	217
5.4	DISCUSSION	218
5.5	CONCLUSION	223
5.6	BIBLIOGRAPHY	235

CHAPTER 6 - GENERAL DISCUSSION, CONCLUSIONS AND FUTURE

DIRECTIONS..... 240

6.1	THESIS GOALS REVISITED	ERROR! BOOKMARK NOT DEFINED.
6.2	FRUCTOSE DERIVATIVES FOR MOLECULAR IMAGING	241
6.2.1	<i>Molecular imaging of GLUT5</i>	241

6.2.2	<i>History and critique of previous work in the field</i>	242
6.2.3	<i>Initial in vitro characterization of 6-FDF, and model systems</i>	245
6.2.4	<i>6-FDF in vivo studies and preclinical work</i>	250
6.2.5	<i>1-FDAM in vitro characterization</i>	256
6.2.6	<i>Insight into binding to GLUT5 from 6-^[18F]FDF and 1-^[18F]FDAM</i>	257
6.3	SPECIAL COMMENT ON GOWRISHANKAR ET AL. 2011 – GLUT 5 IS NOT OVER-EXPRESSED IN BREAST CANCER CELLS AND PATIENT BREAST CANCER TISSUES.	260
6.4	FUTURE DIRECTIONS	263
6.4.1	<i>6-^[18F]FDF, GLUT expression in breast cancer and beyond</i>	263
6.4.2	<i>1-FDAM</i>	266
6.4.3	<i>Other 2,5-AM analogues</i>	267
6.4.4	<i>3-FDF</i>	267
6.5	BIBLIOGRAPHY	271
	APPENDIX A – MATERIALS.....	276
	A.1 MATERIALS	277
	APPENDIX B - CHARACTERIZATION OF 1-DEOXY-1-FLUORO-D-FRUCTOSE (1-FDF), 3-DEOXY-3-FLUORO-D-FRUCTOSE (3-FDF), AND 2-FLUORO-N-(1-DEOXY-2,5-ANHYDRO-D-MANNITOL)ACETAMIDE (AC-AM) FOR BREAST CANCER IMAGING VIA PET	284
	B.1 2-FLUORO-N-(1-DEOXY-2,5-ANHYDRO-D-MANNITOL)ACETAMIDE (AC-AM)	285
	<i>B.1.1 Experimental Design</i>	285
	<i>B.1.2 Results and Discussion</i>	285

B.2 1-DEOXY-1-FLUORO-D-FRUCTOSE (1-FDF)	286
<i>B.2.1 Experimental Design</i>	286
<i>B.2.2 Results and Discussion</i>	286
B.3 3-DEOXY-3-FLUORO-D-FRUCTOSE (3-FDF)	287
<i>B.3.1 Experimental Design</i>	287
<i>B.3.2 Results and Discussion</i>	288

Table List

Chapter 1

Table 1.1: Overview of the GLUTs - **Page 64**

Chapter 3

Table 3.1: Biodistribution table and graphical representation of 6- ^{18}F FDF in EMT-6 tumor bearing BALB/c mice - **Page 168**

Chapter 4

Table 4.1: Biodistribution table and graphical representation of 6- ^{18}F FDF in rats - **Page 192**

Table 4.2: Table and graphical representation of the calculated human absorbed doses and effective dose for 6- ^{18}F FDF - **Page 193**

Appendix A

Table A.1: Cell culture, transport assay and western blot materials - **Page 278-279**

Table A.2: Antibodies and recombinant enzymes - **Page 280**

Table A.3: Software and Equipment - **Page 281**

Table A.4 Composition of Phosphate buffered saline (PBS) - **Page 282**

Table A.5 Composition of Krebs-Ringer solution - **Page 282**

Table A.6 Western Blot Buffers - **Page 283**

Figure List

Chapter 1

Figure 1.1: Simple carrier model - **Page 62**

Figure 1.2: Topology model of the GLUT family - **Page 63**

Figure 1.3: Unrooted dendrogram tree of the human facilitative hexose transporter family - **Page 65**

Figure 1.4: Glucose binding and being translocated by GLUT1 - **Page 66**

Figure 1.5: Intestinal transport of dietary sugars - **Page 67**

Figure 1.6: Regulation of GLUT5 by fructose - **Page 68**

Figure 1.7: Previously published substrates for GLUT5 - **Page 69**

Figure 1.8: Differences in glycolysis between normal tissue and breast cancer - **Page 70**

Figure 1.9: The basics of PET imaging - **Page 71**

Chapter 2

Scheme 2.1: Synthesis of 6-FDF - **Page 120**

Figure 2.1: Hexose uptake in MCF-7 and MDA-MB-231 - **Page 121**

Figure 2.2: Western Blots of MCF-7 and MDA-MB-231 - **Page 122**

Figure 2.3: Confocal images - **Page 123**

Figure 2.4: Inhibition of [¹⁴C]D-fructose uptake with cytochalasin B - **Page 124**

Figure 2.5: 6-FDF inhibition studies of [¹⁴C]-D-glucose transport - **Page 125**

Figure 2.6: 6-FDF inhibition studies of [¹⁴C]-D-fructose transport - **Page 126**

Figure 2.7: [¹⁴C]6-FDF uptake time course - **Page 127**

Figure 2.8: Inhibition of [¹⁴C]6-FDF by cytochalasin B - **Page 128**

Chapter 3

Figure 3.1: Western blots of MCF-7, MDA-MB-231, EMT-6 and human liver homogenate - **Page 163**

Figure 3.2: Radiosynthesis of 6-[¹⁸F]FDF - **Page 164**

Figure 3.3: *In vitro* uptake studies - **Page 165**

Figure 3.4: Concentration-response curves - **Page 166**

Figure 3.5: 6-[¹⁸F]FDF in a normal BALB/c mouse 1 - **Page 167**

Figure 3.6: 6-[¹⁸F]FDF in normal BALB/c mice - **Page 169**

Figure 3.7: PET images of an EMT-6 tumor-bearing BALB/c mouse - **Page 170**

Figure 3.8: PET images of a MCF-7 tumor-bearing NIH-III mouse - **Page 171**

Figure 3.9: Time-activity curves (TAC) - **Page 172**

Figure 3.10A-B: Phosphorylation by ketohexokinase *in vitro* and distribution of radioactivity in blood compartments - **Page 173**

Figure 3.10C-E: Radio TLC of 6-[¹⁸F]FDF in saline and mouse plasma and blood compartments - **Page 174**

Figure 3.10F-G: Metabolism profile in mouse plasma and urine samples - **Page 175**

Chapter 4

Figure 4.1: Whole body distribution of 6-^[18F]FDF at 2 h post injection in a rat
- Page 192

Figure 4.2: Time-activity curves - Page 194

Chapter 5

Figure 5.1: Synthesis of 1-FDAM - Page 224

Figure 5.2: 2,5-AM inhibition of [¹⁴C]D-fructose transport - Page 225

Figure 5.3: 1-FDAM inhibition of [¹⁴C]D-fructose transport - Page 226

Figure 5.4: [¹⁴C]1-FDAM 60 minute time course - Page 227

Figure 5.5: Inhibition of [¹⁴C]1-FDAM by 50 μM cytochalasin B - Page 228

Figure 5.6: Fructose inhibition studies of [¹⁴C]1-FDAM transport - Page 229

Figure 5.7: Concentration-response curves for 6-FDF, fructose, 1-FDAM and 1-FDF - Page 230

Figure 5.8: In vitro 1-^[18F]FDAM uptake studies - Page 231

Figure 5.9: 1-^[18F]FDAM uptake into an EMT-6 tumor-bearing BALB/c mouse -
Page 232

Figure 5.10: 1-^[18F]FDAM and 6-^[18F]FDF in EMT-6 bearing BALB/c mice - Page
233

Figure 5.11: Time-activity curves (TAC) - Page 234

Chapter 6

Figure 6.1: Proposed metabolic pathway of 6-^[18F]FDF - Page 269

Figure 6.2: Binding of 6-FDF and 1-FDAM to GLUT5 - Page 270

Appendix B

Figure B.1: Structures of AC-AM, 3-FDF and 1-FDF - **Page 289**

Figure B.2: AC-AM inhibition of [^{14}C]D-fructose transport - **Page 290**

Figure B.3: 1- ^{18}F FDF injected EMT-6 tumor-bearing BALB/c mouse PET image - **Page 291**

Figure B.4: 3-FDF inhibition of [^{14}C]D-fructose transport - **Page 292**

Figure B.5: [^{14}C]3-FDF 60 minute time course - **Page 293**

Figure B.6: Inhibition of [^{14}C]3-FDF uptake by 50 μM cytochalasin B (+CB) and 500mM D-fructose - **Page 294**

Figure B.7: Concentration-response curves for 6-FDF, fructose, 1-FDAM 3-FDF and 1-FDF - **Page 295**

Symbols list

μg – microgram

μL – microliter

μM – micromolar

1,3BPG – 1,3-bisphosphoglycerate

1-FDAM – 1-deoxy-1-fluoro-2,5-anhydro-D-mannitol

1-FDF – 1-deoxy-1-fluoro-D-fructose

2,5-AM – 2,5-anhydro-D-mannitol

2-NBDG – 2-(N-(7-Nitrobenz-2-oxa-1,3-diazol-4-yl)Amino)-2-deoxyglucose

2-PG – 2-phosphoglycerate

2DG – 2-deoxy-D-glucose

3-FDF – 3-deoxy-3-fluoro-D-fructose

6-FDF – 6-deoxy-6-fluoro-D-fructose

^{18}F FDG – 2-deoxy-2- ^{18}F fluoro-D-glucose

AC-AM – 2-fluoro-N-(1-deoxy-2,5-anhydro-D-mannitol)acetamide

ADP – adenosine diphosphate

ALD – aldolase B

AMP – adenosine monophosphate

ATP – adenosine triphosphate

Bax – Bcl-2-associated X protein

Ca²⁺ – calcium cation

cAMP – cyclic AMP

CB – cytochalasin B

cDNA – complementary deoxyribonucleic acid

Cl⁻ – chloride anion

CT – X-ray computed tomograph

DHA – dehydroascorbic acid

DHAP – dihydroxyacetone phosphate

ENO – enolase

FADH₂ – flavin adenine dinucleotide

G3P – glyceraldehyde-3-phosphate

GAPDH – glyceraldehyde 3-phosphate dehydrogenase

HER2 – Human Epidermal Growth Factor Receptor 2

HIF-1 – hypoxia-inducible factor

HK – hexokinase family

IC₅₀ – half maximal inhibitory concentration

K⁺ – Potassium cation

KDa – kilodalton

KHK – ketohexokinase

K_m – Michaelis-Menten kinetic constant representing half-maximal saturation of a carrier by a substrate, also known as the apparent affinity of substrate for a given carrier

LDH – lactate dehydrogenase

mM – millimolar

MRI – magnetic resonance imaging

mRNA – messenger ribonucleic acid

Na⁺ – sodium cation

NAD⁺ – nicotinamide adenine dinucleotide – oxidizing agent

NADH – nicotinamide adenine dinucleotide – reducing agent

NHE1 – Na⁺/H⁺ exchanger 1

O₂ – oxygen

OXP – oxidative phosphorylation

p53 – tumor protein 54

PEP – phosphoenolpyruvate

PET – positron emission tomograph

PFK-1 – phosphofructokinase-1

PGI/AMF – phosphoglucose isomerase and its secreted form autocrine motility factor

MCT4 – monocarboxylate transporter 4

SDS-PAGE – sodium dodecyl sulfate polyacrylamide gel electrophoresis

SEM – standard error of mean

siRNA – small interfering ribonucleic acid

SLC2A – gene name for GLUT

Src – proto-oncogene tyrosine-protein kinase

SUV – standardized uptake value

TAC – time activity curves

TCA – tricarboxylic acid cycle (or citric acid cycle)

TLC – thin layer chromatography

TM – transmembrane

TPI – triosephosphate isomerase

VDAC – voltage dependent ion channel

V_{\max} – Michaelis-Menten kinetic constant representing the maximal rate of carrier-mediated transport, also referred to as a carrier's capacity to transport a substrate

Chapter 1: General Introduction

1.1 Introduction outline

The following chapter will deal with the expression, structure and function of the facilitative hexose transporter family known as the GLUTs. Specific care will be taken to elaborate on the cloning and the characterization of the glucose transporter GLUT1, fructose/glucose transporter GLUT2, and the fructose transporter GLUT5 and their roles in healthy tissue and the initial stages of hexose metabolism. Due to the perturbed hexose metabolism phenotype present in many tumors, the identity of altered expression and characteristics of these proteins in cancer will be identified and described, highlighting the work done in human breast cancer. Imaging of these tumors, with specific focus on Positron Emission Tomography (PET) will then centre on the glucose analogue [¹⁸F]FDG, and its use in the clinic. The identified variability of GLUT5 expression found within these tissues will lead into the proposed rational design, synthesis and characterisation of novel GLUT5 substrates for the imaging of breast tumors in vivo using PET.

1.2 Introduction to carrier-mediated glucose transport

1.2.1 Transport across cellular membranes

The facilitative transport of hexoses across the plasma membrane of cells is a necessary and ubiquitous action in the majority of eukaryotic cells. Initial work identifying how sugars enter cells elucidated that diffusion was unable to explain the movement observed, and instead it was identified to be due to the presence

of specialized, substrate specific integral membrane proteins. These proteins belong to either the Major Facilitative Superfamily (1) or the Sodium/Solute Symporter family (2), and rely on the concentration gradient present from the interior to the exterior of the cell. The concentration gradient is used to derive energy to move substrates across the membrane until reaching a state of trans-membrane equilibrium, or movement is coupled to that of another substrate moving down its concentration gradient.

Being classified in the SLC2A gene family, the group of facilitative hexose transporters known as GLUTs represent the most significant component of total hexose flux within the majority of mammalian cells. More uniquely perhaps, is that the GLUTs were the focal point of some of the first initial characterization of trans-membrane facilitative carrier proteins.

1.2.2 Principles and history of carrier mediated glucose transport and the 'simple carrier model'

In 1952, Widdas (3) thoroughly described sugar transport across the placental barrier and postulated that something other than diffusion was responsible for the movement of glucose. Widdas suggested that a "carrier mechanism" was responsible for the discrepancy, and that diffusion could not account for the translocation across the membrane since large concentration gradients only led to minimal observable amounts of transport. It was not until a year later however, that the phenomenon was more thoroughly examined using Michaelis-

Menten Kinetics in rat intestine (4). In combination with this quantitative determination of the K_m and V_{max} , and with later work in erythrocytes, the paradigm of membrane transport was subsequently shifted to that of the idea of a 'simple carrier' model of membrane transport (**Figure 1.1**). This simple carrier theory involves four distinctly separate but intrinsically related processes that occur during trans-cellular transport of substrates. The first two initial steps are initiated by substrate binding to the vestibule wherein it is recognized by amino acid side chains of the transporter protein – a process very similar to that observed with enzymes, but with no chemical modification of the substrate. After binding has occurred, the protein undergoes a stage of conformational change, reorienting the previously formed substrate-carrier complex into the opposite facing direction wherein the substrate is then released from the binding pocket. After the release of the substrate, the empty protein reorients the binding pocket to the side that was initially faced, allowing for the process to repeat. In the case of the facilitative transport, substrate movement can be bi-directional, so concentration gradients must be taken into account, and thus net movement must be considered (5).

To initiate the formation of this simple carrier model, Widdas made three astute assumptions. Firstly, that the carriers observed could adsorb glucose and not fructose suggesting substrate specificity of the transport process. Secondly, that the carriers in each side of the membrane interface are equally distributed which would allow for bidirectional transport. Lastly that the carriers present within the

membrane pass through the interface by thermal agitation regardless if they are saturated with glucose or not. He then went on to make a conclusion that the net movement of substrate was proportional to the differential saturation of the carriers on each side of the membrane, which would be directly related to the concentration of the substrate present on each side (3). An important note to mention is that Widdas did not relate the movement of glucose across the membrane to metabolism (6). He goes on to mention Ussing's (7) use of the word "Ferryboats" which provides an easily imagined qualitative description of the movement of the transporter-substrate that after "picking up" its cargo, the substrate-carrier complex then "unloads" its cargo on the other side. During his calculations, it was also assumed that the rate-determining step was the relatively slow movement non-saturated reorientation across the membrane which was later supported by trans-acceleration experiments (8). Widdas also suggested that the facilitated transfer of glucose might not just be a property of the tissues examined in his work, but may be a phenomenon present in other tissues beyond what had been studied.

It was not until Danielli that the idea of conformational changes within the structure of the protein was responsible for the shuttling of substrates across the membrane (9). He postulated that there was a single adsorption site on the protein present on one side of the membrane that underwent a conformational change, and ended up on the other side of the lipid bilayer. This was a significant shift in the carrier hypothesis, as it moved away from the idea of a mobile carrier

to a more stationary protein that just altered its shape in order to translocate the substrate. Later work by Wilbrandt and Rosenberg (10) attempted to more fully define kinetics of the glucose transporter. They suggested that the formation of a substrate-carrier complex and then movement across the membrane and subsequent release of the substrate was the mechanism responsible for cross-membrane sugar transport.

Most of the early work in defining the kinetics of glucose transport was done using red blood cells. They were easy to obtain, had a high expression of transport proteins, and were quite straightforward to work with. In 1961 LeFevre (11) noted that characteristics of carrier mediated transport were evident not only in human erythrocytes, but also muscle, adipose tissue, the blood-brain barrier, placenta, crystalline lens and also in several ascites tumor cells corresponding with Widdas' earlier hypothesis that this phenomena occurred in a wider range of tissues. He also noted that in adipose, ocular and muscle tissue the presence of insulin was required for full activation of sugar uptake (11,12). It was not until 1977 (13) however, that the erythrocyte D-glucose transporter was purified using reconstituted phospholipids vesicles, radio-labelled D-glucose to identify sugar penetration and L-glucose to gauge the amount crossing the membrane due to diffusion. After using SDS-PAGE, a protein with a glycosylated mass of approximately 55kDa and 46 kDa when deglycosylated was observed and set the stage for the molecular identification and classification for the remaining, currently unidentified SLC2A family members.

The purification of the human erythrocyte glucose transporter in reconstituted liposomes paved the way for the accurate determination of uptake kinetics, and determination of the asymmetrical structure of the protein (14). The formation of hydrogen bonds between specific hydroxyl groups present on hexoses and hydrophilic amino acid side chains in the transporter vestibule was postulated to be essential for transport (5). It was also elucidated that either side of the transporter, whether that be the internal or external facing vestibule, may be markedly different, suggesting that there is also asymmetry on the kinetic characteristics of each side (5,15). Wheeler's use of the cytoplasmic glucose transport inhibitor trypsin on the internal and external side of the liposomes, determined that transport was only inhibited by 40% of its original value. When trypsin was applied to both sides however, 80% inhibition occurred. These results pointed to the transporter protein being asymmetrical with respect to its binding site structure, since when reconstituted in liposomes, it is oriented in both directions (14). This characteristic of the protein allowed Wheeler to establish an accurate determination of the influx and efflux K_m of the transporter protein by applying the inhibitor to different sides of the membrane consistent with the hypothesis of an asymmetrical carrier protein. How hexoses interact with the binding vestibule of the family of GLUTs has been examined utilizing hexose analogues and examining uptake into cells transfected with specific GLUT family isoforms or into erythrocytes (16). This set the stage for further identification of required hydroxyl groups for the binding and transport of

hexose analogues via members of the GLUT family which will be discussed further on in this chapter. All this work culminated to the simple carrier model that we know today, and despite decades of research, it still represents the best representation of the phenomena of trans-cellular membrane hexose transport.

1.3 Family of facilitative hexose transporter proteins (GLUTs)

1.3.1 General overview of the SLC2A family of facilitative hexose transporters

The human erythrocyte glucose transporter was cloned in 1985, and was found to be a 492 amino acid protein expressed almost ubiquitously in all tissue types (17). Once differing kinetic parameters in disparate tissues were observed, it was assumed that there may be other transporters involved in the total hexose flux into tissues. Further expression cloning done in subsequent years quickly brought 4 more family members into the GLUT family, where it was also discovered that two of these new members also facilitated fructose transport, satisfying most tissue metabolic requirements. Within the last several decades however, molecular biology techniques have progressed to the point where the family of hexose transporters has been expanded from the original human erythrocyte transporter (GLUT1) and the initial first five GLUT members to a whole family encompassing 14 members subdivided into 3 classes with distinct and disparate tissue distribution and behaviour (**Figure 1.2**). Since mapping of the human genome, the 14 different GLUTs with similar sequences have been

identified, classified and characterised with varying expression patterns, and substrate specificity (**Table 1.1**) (5,18,19). The available kinetic information obtained indicates that they operate in an alternating conformation mechanism (5). These transporters have been split into 3 classes (I, II, and III) with respect to their sequence and structural similarity. The first initially characterized five glucose transporting GLUTs belong almost exclusively to class I, excluding the fructose transporting isoform GLUT5 that has been placed within class II with the high affinity glucose and fructose transporting GLUT7 and GLUT11 as well as with the recently identified urate/glucose/fructose transporting GLUT9 (20). Characteristically, the Class II GLUTs also show little to no galactose, 2-deoxy-D-glucose (2DG), or 2-deoxy-2-¹⁸F-fluoro-D-glucose (¹⁸F-FDG) transport, compared to the Class I GLUTs. This is despite the fact GLUT5 was initially identified using 2DG as a substrate until it was discovered that its true substrate was fructose (21–24). The typical structure of the SLC2A family of transporters is a protein with 12 trans membrane spanning helices, wherein both the N and C terminus are both present within the cytosol (**Figure 1.3**). X-ray crystallography indicates that 6 transmembrane (TM) helices form a barrel shaped structure wherein the binding site is present in the middle of the pore with a N-glycosylation site between TMs 1 and 2, and a long extracellular loop between TMs 6-7 in the Class I and II GLUTs (5). The Class III GLUTs however, vary slightly on their structural arrangement. While preserving the twelve helices of the class I and II GLUTs, the N-glycosylation site location is not between TMs 1 and 2, but instead appears to

be located on the extracellular loop between TMs 9 and 10. Additionally, the class IIIs possess retention motifs on their N- or C- terminal ends, insinuating that perhaps they play a role in subcellular compartments in normal conditions (25) .

The Class III GLUTs have presented a challenge to study as it's becoming clear that perhaps their physiological substrate is not primarily hexoses, but something markedly different. While this has been observed with GLUT2 transporting glucosamine (26), GLUTs 1, 3 and 4 transporting dehydroascorbic acid (DHA) (27) and recently GLUT9 being identified as a urate transporter(20), it is less clear what the primary substrate of these transporters may be. Despite their vital importance in maintaining homeostasis, the process of how these operate on a molecular level is still not well understood (28).What is clear is that tight maintenance of hexose concentrations in tissues is a multi factorial process involving many different players from the GLUT family. The upcoming section will describe the history and function of three important GLUT isoforms that have key roles in normal maintenance of health and perturbed expression in disease states. The known information on the parameters of binding and transport of substrates will also be described.

1.4 Cloning and initial characterization of GLUT1 (SLC2A1)

1.4.1 Cloning and characterization of GLUT1

In 1985, the human erythrocyte facilitated glucose transporter protein (GLUT1) was cloned from human HepG2 hepatoma cells using a cDNA clone library.

GLUT1 has been found to make up approximately 3-5% of total membrane protein in erythrocytes, and thus red blood cells were a valuable model system for early characterisation of this isoform (17,25). This clone sequence was first examined using fast atom bombardment and Edman degradation and was found to be extremely homologous to the human erythrocyte glucose transporter. Through SDS-PAGE it was determined to have a glycosylated mass of approximately 55kDa, and to be composed of 492 amino acids with an N-linked glycosylation site. Hydropathy plots indicated the presence of 12 TM domains present within the protein with a large intracellular loop between TMs 6 and 7 (17). Screenings were performed on various human tissues indicating that GLUT1 is a ubiquitous protein, and may be responsible for basal glucose uptake in most tissues. When expressed in *Xenopus laevis* oocytes, its substrates consist of D-glucose ($k_m = 5$ mM), galactose ($k_m = 5$ mM), 2DG ($k_m = 5$ mM), mannose and 3-O-methyl-glucose ($k_m = 20$ mM) (5,25,26,29). Transport with GLUT1 was also found to be inhibited by the cell permeable mycotoxin cytochalasin B (CB), phloretin, and phlorizin, and when examined in *S.cerevisiae* the IC_{50} for inhibition of D-glucose uptake was 0.44 μ M, 49 μ M, and 355 μ M respectively (30). GLUT1 is ubiquitously expressed in tissues, and is found in early mammalian embryo development from the oocyte to the blastocyst. Its expression also is prominent in epithelial like barriers in the brain, eye, peripheral nerve, placenta, and plays a large role in the maintenance of a hyper metabolic state in many tumor tissues (31,32). Overexpression of GLUT1 in cancer plays an important diagnostic role via

the facilitation of uptake of the fluorinated glucose analogue [¹⁸F]FDG which allows non-invasive imaging of tumors using Positron Emission Tomography (PET). On the other side of the coin, lack of GLUT1 expression through the autosomal-dominant human GLUT1 Deficiency Syndrome (also known as De Vivo disease) is characterized by infantile seizures, slow development, acquired microcephaly, and cases of ataxia. These disease states have been identified to be caused by lack of glucose transport between the circulation and that of the cerebrospinal fluid, limiting the amount of glucose available for neurologic metabolic processes and development (33,34). Regulation of GLUT1 expression and activity is controlled by several factors that will be discussed in a following section discussing its role in cancer (35).

1.4.2 GLUT1 substrate binding studies

The first experiments ascertaining the parameters of binding to GLUT1 were done in isolated human erythrocyte membranes which have high endogenous expression of the protein (36). Transport experiments undertaken using D-glucose analogues substituted at all the available hydroxyls found that transport required binding of the C-1, C-3 and C-4 hydroxyls as well as the pyranose ring oxygen (36). Later work by Barnett, Holman and Munday used more glucose variants and reconstituted erythrocytes in liposomes that allowed them to propose that the C-1 of D-glucose enters the extracellular vestibule first, while the C-6 end would first enter when binding to exit from the interior of the cell (**Figure 1.4**) (16). They also postulated that the sugar had to first bind to the

extracellular facing side of the protein to initiate a conformational change, and then the sugar would be exposed to the interior of the binding pocket – something that would be inhibited if bulky groups were present on any of the required hydroxyl groups. Derivatives of glucose including 2DG, [¹⁸F]FDG and even the bulky 2-NBDG have shown uptake into GLUT1 expressing tissues, suggesting that labelling at the C-2 position, even with large bulky groups is handled by the transporter (37,38).

1.5 Cloning and initial characterization of GLUT2 (SLC2A2)

1.5.1 Cloning and characterization of GLUT2

The lack of understanding how glucose uptake was occurring in hepatic and renal tissue prompted Thorens et al. to utilize cDNA of GLUT1 to probe hepatocyte cDNA libraries at a low stringency and perhaps identify another protein responsible for hexose uptake in these tissues (39). After doing so, they isolated a 2.5kb cDNA sequence with a 1.56 kb open reading frame coding for a 57 kDa, 522 amino acid protein. With 55% identical sequence to that of the human erythrocyte transporter (GLUT1), and possessing a virtually identical hydropathy plot, the later to be named GLUT2 was found to be a low affinity, high capacity transporter (39). GLUT2 facilitates the transport of glucose ($k_m = 11$ mM), galactose ($k_m = 86-92$ mM) , 2DG ($k_m = 11$ mM), D-fructose ($k_m = 11-76$ mM) and glucosamine with high affinity ($k_m = 0.8$ mM) and is also non competitively inhibited by cytochalasin B (5,26,40–44). GLUT2 glucose and fructose transport

activity was also shown to be inhibited by D-fructose mimics, including 2,5-anhydro-D-mannitol (2,5-AM), with 50mM causing >50% inhibition of total glucose and fructose transport (43). The discovery of this GLUT isoform identified how uptake was occurring in tissues where GLUT1 was not present such as liver, brain pancreatic β -cells, renal and intestinal tissue. GLUT2 serves several key roles within the mammalian system to maintain metabolic homeostasis. This includes intestinal, kidney sugar absorption, hexose transport in liver and pancreas tissue, and it also acts as a glucose sensor (45). More specifically, Thorens made an important observation that GLUT2 appeared to be functioning as the gateway for glucose in the basolateral membrane in intestinal epithelial cells, thus securing a vital role in supplying the body with dietary sugars (39).

1.5.2 GLUT2 in the small intestine and kidney

The Na^+ /glucose cotransporter SGLT1, using the sodium electrochemical gradient generated by the Na^+/K^+ ATPase present in the basolateral membrane, transports dietary glucose from the lumen of the small intestine across the apical membrane up its concentration gradient. Then the basolaterally expressed GLUT2 moves glucose from the interior of the cell into the extracellular intestinal tissue milieu and into the circulating plasma (**Figure 1.5**) (46,47). Rapid, transient GLUT2 insertion in the apical membrane from GLUT2 containing vesicles has also been observed once dietary sugars are present within the intestinal lumen increasing the uptake of glucose approximately three-fold (48). As circulating concentrations of glucose increase, and the lumen is cleared of sugars, insulin is

released causing the internalization of GLUT2 and return to basal levels (49,50). This is also the case within renal tissue, as upregulation and insertion of GLUT2 has been reported within apical tissue within proximal tubules acting to reabsorb lost hexoses within the urine (51,52).

1.5.3 GLUT2 in the liver and pancreas

Within the liver, GLUT2 acts as a bidirectional passageway for glucose. Glucose is produced in the liver during a fasting phase via the breakdown of glycogen by glycogen phosphorylase and phosphoglucomutase to produce glucose-6-phosphate that is dephosphorylated by glucose-6-phosphatase and then effluxed out of the cell via GLUT2. During the feeding phase, the metabolic machinery works in the opposite direction, since GLUT2 can take up dietary glucose from the circulation via hepatic portal vein to be stored as glycogen and lipids during phases of feeding. Regulation of expression of GLUT2 in liver has been shown to be upregulated by thyroid hormone, suggesting its role in the facilitation of increased hepatic glucose output (53).

Detection of variations in blood glucose concentrations by pancreatic β -cells and a subsequent appropriate secretion of insulin are key events in the control of glucose homeostasis. In the pancreas, GLUT2 transport of hexoses acts causing feeding induced insulin secretion. Glucose uptake within the β -cells and subsequent metabolism via glycolysis and mitochondrial metabolism, ATP/ADP ratios trigger the closure of ATP dependent potassium channels inducing

membrane depolarization, and release of intracellular Ca^{2+} stores. This release subsequently induces the exocytosis of insulin carrying secretory vesicles (45,54).

1.5.4 GLUT2 as a glucose sensor and regulator

GLUT2 also acts as a metabolic glucose sensor, affecting insulin release in B-cells (55). The levels of GLUT2 and glucose sensitive gene expression have also been shown to be closely correlated in hepatoma cells, suggesting that one of the cytoplasmic domains of the protein is activated by its interaction with sugar (56,57). This mechanism acts in a dose dependent manner, as increases in glucose concentration within the cell increase the stimulation of glucose-sensitive gene transcription. Glucose sensing via the hepatoportal glucose sensor relies on GLUT2 expression, although the exact mechanism by which this occurs is still unknown (58). To properly fulfil the role GLUT2 plays in glucose homeostasis, evidence has pointed to its expression in the liver, intestine and the pancreas being tightly regulated to circulating concentrations of glucose and fructose (59,60). This becomes vital in the case of the feeding/fasting cycle wherein hepatic stores of glycogen become important in the maintenance of circulating glucose levels.

1.5.5 GLUT2 substrate binding studies

Gwyn Gould's group in 1993 released a seminal paper examining the structural requirements for binding to the GLUT2 transporter expressed in the *X. laevis* heterologous expression system (61). Using a range of deoxy-glucose analogues

as well as other hexose analogues they identified required hydrogen bonding at the C-1, C-3, and the C-4 hydroxyls, and hydrophobic interactions at the C-6 position for proper glucose transport. The fructose mimic 2,5-AM locked in the furanose ring form was able to inhibit 2DG transport at an order of magnitude higher than that of the fructose analogue L-sorbose or D-fructose, suggesting a preference for fructose in the furanose form. The primary difference between glucose and fructose was suggested to be the absence of hydrogen bonds between GLUT2 and the substrate at the C-1 position, suggesting that hydrogen bonds from that position are not necessary for transport of fructose.

1.6 Cloning and initial characterization of GLUT5 (SLC2A5)

1.6.1 Cloning and characterization of GLUT5

GLUT5 was cloned from human small intestine and fetal skeletal muscle cDNA libraries using low stringency cross-hybridization with a fragment from GLUT1. During analysis, it was discovered to be a 501 amino acid protein with approximately 40% sequence identity with the other described GLUT1, GLUT2, GLUT3 and GLUT4 isoforms (22). Expression of GLUT5 mRNA was found to be highest within the small intestine, kidney, skeletal muscle, cartilage, spermatozoa, brain and adipose tissue (24,62,63). GLUT5 was characterised by using 2DG in the *X. Laevis* oocyte expression system, where it was shown to transport the substrate at very low levels, and be CB sensitive (22). Later work identified it to be a pH, CB and phloretin insensitive D-fructose transporter with a

K_m of approximately 5-14 mM (5,24,44,64). Out of the seven members of the GLUT family that do transport fructose, GLUT5 is the only member that does not transport glucose and galactose and acts as the primary fructose transporter in the human body (62). GLUT5's main role is the transporting of fructose in the small intestine, erythrocytes, brain, kidney and the testes and sperm. Fructose is naturally found in honey, fruits, berries and many root vegetables alone or linked with glucose in sucrose. Fructose has become a large part of the "western diet", as many Americans are consuming up to 22 teaspoons of sugar a day, and predominantly that is in the form of fructose (65). High levels of dietary fructose has been implicated in obesity, insulin resistance, hypertension, gout, hyperinsulinism and atherogenic dyslipidemia – all under the umbrella of metabolic syndrome (65).

1.6.2 GLUT5 in the small intestine

Apical fructose transport within the small intestine has been shown to be primarily facilitated by GLUT5 and transiently expressed GLUT2 (48). Once inside the cell, fructose follows the concentration gradient through GLUT5 and GLUT2 on the basolateral side into the intestinal milieu and into the bloodstream (**Figure 1.5**) (62,66). The small intestine has been found to express the largest amount of GLUT5 RNA of anywhere in humans as well as several other species such as rat, rabbit, chicken, horse and mouse (62). The fate of intestinal fructose and whether or not it is phosphorylated within the epithelium into fructose-1-phosphate via action of the enzyme ketohexokinase (KHK) and/or

phosphorylation at the 6 position with hexokinase forming fructose-6-phosphate (67). It is still unclear which of these pathways would occur preferentially, or if diet would also play a role in the regulation of this balance. cAMP levels have been shown to upregulate GLUT5 without increasing mRNA abundance in vivo, suggesting modulation of expression not on a transcriptional level, but perhaps in a post translational or regulatory manner (68). This was contrary to previously found mRNA increases in in-vitro settings using Caco-2 cells, something that may be attributed to the tissue macrostructure and variety of cell types present in the small intestine (67). Micro array studies done by Ron Ferraris' group indicate that other than GLUT5, fructose also has an impact on gluconeogenic regulatory enzymes, intracellular phosphate metabolism and even alterations in the ATP/ADP ratio may be involved in the "big picture" of small intestinal fructose transport and regulation (62,69).

1.6.3 GLUT5 in the kidney

The kidney expresses the second highest amount of GLUT5 which is targeted to the apical side of the S3 proximal tubule cells epithelium (70). Found to have a K_m of approximately 12.6mM in rats (71), it acts to recover dietary fructose that is lost through filtration in the glomerulus. Fructose flux from the lumen into the bloodstream is promoted by a downstream concentration gradient present between the lumen and the blood stream, as normal non-diabetic concentrations for fructose within the urine are around 0.035 mM, and within the blood it ranges between 0.008 and 0.03 mM (62). mRNA, protein and activity

levels of GLUT5 have also been shown to increase with an increase of fructose in the diet (62).

1.6.4 GLUT5 in spermatozoa

GLUT5 has been detected within the spermatozoa in multiple species (human, mouse, rat, bull, pig and dog) and it has been suggested that presence within this tissue allow sperm to utilize fructose, or may even play an important role in activating fertilization (72,73). The metabolic effect of fructose supplementation was found to be greater than that of glucose, showing increases in glycolytic intermediates and ATP levels compared to glucose supplemented cells. This finding provides further credence to the idea that fructose may be an important energy source (73).

1.6.5 GLUT5 in skeletal muscle and adipose tissue.

Skeletal muscle and adipose tissue express GLUT5 in humans, mice and rats (62,74). GLUT5 in human skeletal muscle represents a large proportion of the total hexose transporter protein in sarcolemma, wherein its role is to absorb dietary fructose present in the circulation (74). GLUT5 activity in skeletal muscle has also been shown to be insulin dependent. Extended exposure to high insulin levels has been shown to increase the expression functional activity of GLUT5 in skeletal muscle via the activation of the GLUT5 promoter, increasing de novo carrier synthesis (75). Not unlike skeletal muscle, adipose tissue shows plasma membrane expression of GLUT5, and hypoxia has the ability to increase the

expression of GLUT5 approximately 9-fold, and may play a role in nutrient uptake in those in later stages of obesity, when hypoxia in adipose tissue is a factor (76). Other studies have showed that GLUT5 expressing cells were able to grow at higher confluence levels than those not possessing GLUT5, conferring an ability to grow even in exceedingly close proximity and density with other cells suggesting that expression of GLUT5 may be able to confer resistance to hypoxic/high density environments (77).

1.6.6 GLUT5 in the brain

GLUT5's true physiological role within the brain is still unknown. Being present within human microglia, cerebellar Purkinje cells in human fetus, mouse cerebellum, the human blood-brain barrier, and rat hippocampus, one would assume that the brain would utilize free, circulating fructose as a substrate for its metabolic machinery (62,78,79). Not unlike GLUT1 which facilitates glucose transport across the blood-brain barrier and GLUT3 expression in neurons for the metabolically hungry brain tissue (43,80,81), it is logical to believe that GLUT5 which is also expressed in the cerebellum and glial cells would be doing the same (79,81,82). Studies have shown otherwise however, as rats injected with radiolabelled fructose had minimal accumulation within the brain (83). This is despite the fact that with high fructose diets rats displayed modest transcriptional upregulation of GLUT5 mRNA levels within the brain, signifying that fructose has entered the tissue as it is a potent and specific stimulator of GLUT5 transcription (84). Contrary to that finding, and muddying the waters

even further to GLUT5's physiological role within the brain, a study using a high fat, high fructose diet in a mouse model found the opposite of the rat study, as GLUT5 was not upregulated (85). Currently the true role that fructose has in the brain is unknown, and further work should be undertaken to fully understand its metabolic role in the brain.

1.6.7 Regulation of GLUT5

From what is known about GLUT5's regulatory mechanisms, they largely stem from the exposure of fructose to intracellular control mechanisms, although the response has been shown to vary between tissues (**Figure 1.6**). High fructose diets and artificial methods used to expose the lumen of the small intestine to high concentrations of fructose (ie. gavage, perfusion) have been consistently effective in increasing the luminal expression of GLUT5. Natural expression patterns appear to be developmentally sensitive, as fructose uptake has been shown to be reduced in infants and toddlers (86). GLUT5 expression does not arise until after weaning, and is expressed when the child would start to encounter fructose in their diet. The rat parallels this, as GLUT5 expression is low during suckling (0-14 days of age) and weaning (14-28 days) but increases dramatically after 28 days have passed (87). GLUT5 activity in rats has been also shown to increase during suckling and weaning stages when fructose is supplemented into their diet (88). Similarly in humans, fetal small intestine samples indicated lower levels of GLUT5 than that of adults – something that was markedly different than either GLUT2 or SGLT1 expression, suggesting a

unique substrate dependent regulatory role of fructose in the expression of GLUT5 (89). Interestingly, the metabolically inactive analogue 3-O-methylfructose had markedly decreased levels of GLUT5 upregulation on intestinal lumen in rats when compared to fructose. This suggests that not just fructose, but also its metabolites play a notable role in regulating GLUT5 expression (90).

1.6.8 GLUT5 substrate binding studies

Holman and associates' first paper on the evaluation of fructose analogues to competitively inhibit fructose via GLUT5 was published in 2000, and began to shed light on the structural requirements for binding and transport (91). Using a group of fructofuranosides and fructopyranosides inhibition was observed, indicating that GLUT5 accepts both ring forms (**see Figure 1.7A for structures**). Epimers of fructose were all found to be poorly tolerated, indicating the requirement of the hydroxyls to be in the fructo-configuration. All allyl substituted derivatives except for 6-O-allyl-D-fructo-furanose showed limited ability to inhibit normal D-fructose entry into their GLUT5 expressing Chinese Hamster Ovary model (91) indicating that perhaps bulky groups would still be tolerated by the transporter when placed at the 6 position.

The following work by Holman furthered these ideas by first replacing the hydroxyl present on C-1 of fructose with an allylamine group which was found to be moderately tolerated by GLUT5 (**see Figure 1.7B for structures**) (92). This surprising finding perhaps suggests that the amine group may facilitate the

formation of hydrogen bonds with the transporter, something that was missing with the allyl group examined in the earlier paper. Next, the symmetrical molecule 2,5-AM, a substrate for GLUT5 whose C-1 and C-6 positions are equivalent was labelled at the 1 position with an allylamino group. This was found to have an order of magnitude higher affinity than 1-allylamino-D-fructose indicating that bulky groups at the 1 position may influence binding to the transporter, and that the 2,5-AM derivative can enter the binding pocket by just “flipping around”. Holman’s group also synthesized a group of large, amide linked biotinylated photolabeling moieties at the primary position that surprisingly had no decreased affinity to that of 2,5-AM (**Figure 1.7B**). Dinitrophenyl groups substituted at the amine group on the 1 position showed very high affinity for the transporter suggesting that the 6 position of the D-fructofuranose configuration actually occupies an exposed position in the binding site of GLUT5 (**Figure 1.7B**). Derivatives with a longer spacer between these bulky groups and the fructofuranose ring actually increased affinity suggesting perhaps that the further the large groups would protrude into the cytosol, the less they would interfere with binding to the transporter. They concluded that the primary labelled allylamine derivatives of 2,5-AM were tolerated very well by GLUT5, secondary amine linked groups substituted at this position actually increased the affinity of the compound for the transporter, and large photolabel moieties are still able to inhibit transport (92). What is not clear however is whether or not these compounds are blocking the binding of D-

fructose to GLUT5 or actually are being transported into the cell. While it may be viable for these substrates to occupy the binding site present in the extracellular vestibule, bulky groups such as the dinitrophenyl and photolabel moieties may not be able to be transported by GLUT5. Further work needs to be done using radiolabeled molecules to determine their ability to enter the cell and until then this work will truly only be able to act as a guide for the initial steps of binding before translocation into the cell.

1.7 Initial characterization of the primary phosphorylating enzymes of glucose and fructose

1.7.1 Hexokinase family

Hexoses are a critical metabolic component for most prokaryotic and eukaryotic life on earth. The metabolism and subsequent conversion of hexoses to usable energy is a complex process involving dozens of distinct, regulated processes, all of which funnel the metabolized hexose into a variety of paths to be used for biosynthesis of needed cellular materials. Glucose is also able to be stored within the polymeric form glycogen and is important for maintaining homeostasis in a variety of organisms. How sugars are utilized ultimately depends on the tissue, its metabolic demands, and activity of the enzymatic pathways within the cell of interest.

After the transport of glucose across the membrane, the first step for metabolism in both eukaryotic and many prokaryotic cells is phosphorylation

catalysed by one of the members of the hexokinase family to form glucose-6-phosphate. The metabolism and conversion of the entirety of glucose that enters the cell into cellular materials is undoubtedly crucial for whole organism homeostasis and maintenance of health, so in accordance with that the first step of glucose metabolism must be tightly controlled.

History of hexokinase: Initial work on the first steps of glucose metabolism was done in 1964 by Gonzalez et al. where four distinct isozymes (I, II, III, and IV) of hexokinase in rat liver were separated by ion exchange (93) wherein the fourth isoform has been mainly known as glucokinase (94). The hexokinase family of enzymes are approximately 100 kDa in size and are thought to have arisen from gene duplication and fusion of a 50 kDa ancestral hexokinase. Sequence homology between both C and N 'halves' of the protein as well as with the 50 kDa hexokinase enzymes found in other organisms has lent credence to this notion (95,96). The hexokinases have a high affinity for glucose permitting initiation of glycolysis even when blood glucose levels are relatively low. Glucokinase, found in the liver and pancreatic β cells, requires a much higher glucose concentration for maximal activity ($k_m = 8-12$ mM) (97). It is thus most active when glucose concentrations are very high in the portal vein, immediately after consumption of a carbohydrate-rich meal. It has a high V_{max} , allowing the liver to effectively remove excess glucose, and minimize hyperglycemia after eating.

The first step in the metabolic regulation of hexokinase is the potent inhibitory effect of glucose-6-phosphate, a finding consistent with not only the Type I-III isoforms in mammals, but also extending to the 50 kDa forms found in lower organisms. This is a very important regulatory step, since it prevents the consumption of too much cellular ATP to form glucose-6-phosphate when glucose concentrations are high. This finding has suggested that this product feedback mechanism evolved early, and before the duplication and formation of the 100 kDa mammalian isoforms. Despite the apparent duplication, mutation has altered the C and N terminal halves of the Type I and Type III hexokinase isoforms so that unlike Type II, its catalytic activity now solely resides in the C-terminal half (98,99).

Hexokinase appears to have a simple job. Why then are there multiple isoforms that appear to have the same task? Wilson postulated that the main 3 reasons for the existence of these isoforms are that firstly, they may differ in their catalytic, kinetic or regulatory properties that may suit them for a specific role. Secondly, they all may possess varying transcriptional and translational mechanisms that may lead to selective behaviour, and expression in tissues. Lastly, multiple isoforms allows for distinct subcellular localization, allowing for the compartmentalization of glucose metabolism for the funnelling of glucose-6-phosphate into specific pathways (100,101).

Hexokinase I: Hexokinase I (HKI) was identified in brain homogenates in 1953 by Crane and Sols, and later work elucidated that it was associated with the outer mitochondrial membrane. Further work also identified mitochondrially bound HKI in many other tissues as well as some tumor lines (94). This binding is dependent on the hydrophobic N-terminal sequence, inserting into the hydrophobic centre of the mitochondrial membrane. HKI also associates with the voltage dependent anion channel (VDAC), a passageway for which metabolites are able to cross the outer mitochondrial membrane. The idea that HKI as the primary 'glycolytic' enzyme was associated with the site of oxidative phosphorylation had not been a new one (102). Access to the entry and exit point of ATP and ADP via binding to the exterior of the mitochondria was thought to allow for privileged access to ATP, and efficient phosphorylation of incoming glucose. Activity of mitochondrially bound HKI has been shown to be intrinsically linked to oxidative phosphorylation. In cells not undergoing oxidative phosphorylation, ATP is taken from the cytoplasm and when oxidative phosphorylation is underway, HKI is coupled to the intramitochondrial pool of ATP (94). Under normal conditions, the rate of glucose metabolism is tightly associated with the terminal stages of glucose metabolism and oxidative phosphorylation occurring in the mitochondria – a step that will ensure that introducing more glucose into glycolytic metabolism is on par with the terminal stages, and that excess toxic lactate is not produced (103). Having a k_m of

approximately 0.03 mM, HKI has the second highest affinity for glucose out of any of the members of the hexokinase family.

Hexokinase II: Hexokinase II (HKII) also possesses a hydrophobic N-terminal tail, allowing it to target to the mitochondria not unlike HKI. While a large proportion of HKII has been shown to be associated with mitochondrial fractions from cell lysate, large quantities are also found in the 'soluble' fraction, and in the cytoplasm using immunolocalization studies, suggesting a broader cellular distribution than HKI (94). Kinetic studies place the k_m of HKII at approximately 0.3 mM, a value that suggests a more relevant physiological concentration compared to either hexokinase I or III.

Hexokinase III: Hexokinase III (HKIII) lacks the N-terminal hydrophobic sequence that is necessary for mitochondrial binding, and instead appears to be targeted to the cytoplasm and nuclear periphery (104). The purpose of this targeting and HKIII's role is yet unknown, as its k_m for glucose is an order of magnitude higher than HKII (approximately 0.003 mM) despite having the lowest affinity for the binding of ATP of all the hexokinases. Furthermore, activity of HKII is the least product sensitive of the HK family (104). These characteristics lend towards the notion of an unclear physiological role. Perhaps like HKI and HKII, which are both associated with the mitochondria, HKIII fulfils a similar metabolic role being associated with the nucleus.

The HK family is known to be a primary phosphorylation enzyme of glucose, but it also has the ability to phosphorylate fructose at the 6 position, albeit with a much higher k_m of 1-10 mM (and 107 mM with glucokinase) (105,106). 2,5-AM has also been shown to be phosphorylated by HK with an approximate k_m of 6.3 mM (107). Additionally, binding studies have found that substitution at the C-1 on fructose is non-critical for enzyme activity (108). It has also been suggested that this phosphorylation of fructose may be outcompeted by physiological concentrations of glucose and thus HK's role is not well understood in fructose metabolism (109).

1.7.2 ***Ketohexokinase (KHK)***

KHK with a molecular weight of ~33 kDa acts on dietary fructose by catalysing the reaction with ATP to form fructose-1-phosphate, and has recently become more of interest due to high fructose western diets being correlated in epidemiological studies with the onset of diabetes, hypertension and gout (62,105). After being phosphorylated, fructose-1-phosphate is then cleaved into dihydroxyacetone phosphate and glyceraldehyde by fructose-1-phosphate aldolase (Aldolase B), an enzyme expressed highly within the liver, renal cortex and mucosa of the small intestine feeding into glycolysis and bypassing some of the first initial regulatory steps normally encountered by glucose (110). Other than the liver, KHK has been identified mainly in the kidney, intestine, and in lower levels, brain, pancreas, lung, parotid gland, muscle and the optic nerve. The exact distribution of these KHK expressing cells within these tissues and

functional information on its behaviour are not well known (105). In 1998, two distinct splice variants (KHK-A and KHK-C) were identified (111,112). Kinetically, KHK-A possesses a 10x higher K_m for fructose than KHK-C (8 mM vs 0.8 mM), suggesting a poor ability to phosphorylate fructose at physiological conditions (112). Due to this, the majority of studies have focused on high KHK-C expressing tissues such as the liver which acts on dietary fructose via the hepatic portal vein, kidney and the duodenum, without inclusion of the KHK-A isoform into their kinetic analysis, as the splice variants were not identified until later. An example of a disease state related to lack of hepatic KHK is the autosomal recessive disorder essential fructosuria where affected individuals display abnormally large shifts in blood fructose concentrations after ingestion of fructose (112). KHK expression and behaviour is still not well understood, and due to its critical role in the rapid handling of dietary fructose loads, more work needs to be done in order to ascertain its role in each tissue. Additionally, KHK isolated from beef liver has shown to phosphorylate 2,5-AM with a K_m of approximately 1.7 mM (113).

1.8 A brief overview of the characteristics of hexose metabolism in cancer

1.8.1 Brief overview of hexose metabolism and energy production

Rapid growth and proliferation have been identified as two of the hallmarks of cancer (114). It is becoming more clear however, that overactive sugar transport

and metabolism plays a vital part in oncogenesis, and is emerging as one of the most important hallmarks of cancer and of its progression (114). Since the identification of the “Warburg Effect” by the Nobel laureate Otto Warburg in 1929 (115,116), the metabolic pathways responsible for hexose metabolism in many cancers have been found to be significantly altered to adopt high levels of the less efficient anaerobic glycolysis instead of oxidative phosphorylation. The exact mechanisms behind this metabolic “reprogramming” of nutrient metabolism are unknown, but in many cancer cells there is a significant preference for glycolytic reactions instead of oxidative phosphorylation in the mitochondria.

Glycolysis is a ten step sequence that provides the cell with ATP and NADH, chemical energy biomolecules created by the multistep enzymatic processes and breakdown of glucose (**Figure 1.8**). In anaerobic organisms as well as tissues which have limited supply of O₂, glycolysis is the primary source of ATP. Glucose is metabolized into two molecules of pyruvate and has a net gain of 2 ATP per molecule of glucose. The pyruvate generated is subsequently metabolized by lactate dehydrogenase (LDH) to generate NAD⁺ for use as a component of further breakdown of glucose via glycolysis, and lactate can also be reconverted back to pyruvate.

In aerobic tissues, glycolysis occurs within the cytosol to produce two molecules of pyruvate which end up in the mitochondria to be converted into acetyl-CoA

and CO₂. From this, the multi-step tricarboxylic acid cycle (TCA) cycle generates high-energy electrons carried by the molecules NADH and FADH₂. These energetic electrons are subsequently passed through the electron transport chain present within the inner mitochondrial membrane, forming an electrochemical proton gradient, and through this process combining with O₂ to form H₂O. This is known as oxidative phosphorylation (OXPHOS) and drives the conversion of ADP into ATP via the enzyme ATP synthase present in the mitochondrial membrane. OXPHOS presents the most efficient method of energy production within aerobic tissue, yielding 36 molecules of ATP for every molecule of glucose. With the addition of steps within the mitochondria, it relies on more genes than anaerobic glycolysis as they are encoded by both nuclear and mitochondrial DNA, and thus have more steps of regulation than strict glycolysis. With the basics of normal glucose metabolism in place, one must then examine the perturbed phenotype of glucose metabolism present in many tumor types.

1.8.2 Glucose transport, Glycolysis and the TCA in cancerous tissue: An overview

Cancer cells depend largely on glycolysis for their energy supply (115), and changes have occurred in order to facilitate the production of the large quantity of energy required for these processes. Since glucose uptake is the first step in sugar metabolism, the overexpression of the major facilitative glucose transporter GLUT1 has been thought to be the limiting step in tumor glycolytic

flux (117). In step with this, GLUT1 has been identified to be overexpressed in breast, pancreatic, esophageal, brain, renal, lung, cutaneous, colorectal, ovarian, and cervical carcinomas compared to their normal, healthy tissue counterparts (118–127).

Cells with high levels of glycolysis can rapidly produce ATP due to the rapidity of glycolysis vs. the TCA and oxidative pathway and can quickly synthesize glycolytic intermediates such as fructose-6-phosphate and glyceraldehyde-3-phosphate for de novo nucleotide synthesis (116,128,129). HK enters glucose into the glycolytic pathway via the phosphorylation on C-6, and has been seen to be overexpressed in many tumor types (130). The next step in glucose metabolism after phosphorylation, glucose-6-phosphate isomerase has been identified to be overexpressed in tumor cells, and is correlated with cell growth in vitro, cell migration, invasion, and tumor survival (116).

Concurrently, a low pH in the extracellular environment is established through the excretion of the end products of anaerobic glycolysis such as H^+ and lactic acid using the overexpressed sodium proton exchanger NHE1 and the monocarboxylate transporter MCT4 (131–133). This can directly influence the invasiveness of tumors through the elimination of those cells within the tumor expressing functional p53 via apoptosis, and select for a more invasive phenotype (134,135). Additionally, some cells have found methods of overexpressing membrane bound carbonic anhydrases to generate HCO_3^- and

prevent cellular acidification in those cells using higher levels of anaerobic glycolysis (136,137). These in turn may select for a more aggressive phenotype and it has been suggested that this is critical for subsequent malignant growth of both primary and metastatic tumors (138). In correlation with increased levels of glycolysis, the gene expression of many components and regulatory mechanisms of the glycolytic pathway have been altered by transformation. Particularly, and the focus of this upcoming section, will be the primary steps of glycolysis.

1.8.3 GLUT1/GLUT3 expression in cancer

GLUT1, in concert with the HKs has been recognized to play a crucial role in contributing the main steps of control of tumor glycolysis. GLUT1 in particular has been recognized primarily as the rate limiting step in the initiation of glycolysis (117). Evidence points towards the activation of the oncogenes ras, c-myc, and src causing upregulation of the expression of GLUT1 in many tumors compared to normal tissue (139–142). It appears that both ras and src directly influence the enhancer region of the GLUT1 promoter (143), and c-myc through an Sp1 dependent mechanism (139,144,145). The comparative functional ability in tumor cells to take up glucose has been shown to be upwards of 10-12 times that of normal untransformed tissue (37) which provides these cells with enough metabolic fuel to make up for the preferential use of inefficient anaerobic glycolysis and conversion into lactate instead of oxidative phosphorylation (115,146,147). The glycolytic rate in tumor cells has been observed to be 30 times that of normal untransformed cells, which is sustained by the continual

regeneration of the essential glycolytic coenzyme NAD⁺ through the upregulation of the pyruvate to lactate converting enzyme LDH-A by HIF-1, a factor which will be discussed below (131,148,149). While the increase of GLUT1 expression has been primarily determined via mRNA or protein quantification, functional data is harder to come by, mostly due to the difficulty of the assays. However, several good kinetic dissections of glucose fluxes have been performed recently to examine *in vitro* glucose transport phenomena in tumor cells (4, 38). Despite the lack of a large amount of kinetic dissections of glucose transport in tumors, GLUT1 expression still has strong negative correlations with patient survival and aggressiveness (150), suggesting that GLUT1 expression is intrinsically linked with more invasive and fundamentally dangerous tumor development and progression (122,151–162). GLUT1 expression has been shown to directly correlate with several tumor phenotypes including higher proliferative ability, and tumor grade, as well as decreased differentiation. Inhibition of GLUT1 by antibodies has been shown to induce growth arrest, and to potentiate chemotherapeutic drugs in breast and lung cancer cell lines (163). The inhibition of GLUT1 and subsequent effects shows its vital importance in the metabolic health in GLUT1 expressing tissues. An important regulatory mechanism of GLUT1 involves the hypoxia-inducible factor 1 (HIF-1), which has been suggested to play a very important role in not only altering glucose metabolism, but also is tightly linked to the development of an invasive, aggressive, and often lethal tumor phenotype in hypoxic tumors (164,165). The

GLUT1 promoter possess a hypoxia-response element which binds HIF-1 in coordination with the co activator proteins P300 and the CREDB(CBP) binding protein. This in turn facilitates the transcription of the transporter (164). HIF-1 is a transcription factor made up of both the constitutively expressed HIF-1 β and the O₂ regulated HIF-1 α subunits (165,166). It has been documented that human tumors have significantly reduced O₂ concentrations compared to surrounding healthy tissue which leads to the upregulation of a large quantity of hypoxia related cellular mechanisms, particularly those involved with cell death, metabolism, and angiogenesis (165,167–169).

The high affinity glucose transporter GLUT3 ($K_m = 1$ mM) (5) has also been shown to be upregulated in several forms of cancer, including breast, endometrial, oral squamous cell carcinoma, brain, non-small cell lung carcinoma, testicular and cases of lymphoma (124,126,142,162,170,171). It has been suggested that this expression contributes to the overall glucose flux into the cells, contributes to poor patient survival and may play a role in the transport of the glucose analogue [¹⁸F]FDG for PET imaging of these tissues.

1.8.4 Hexokinase II in tumors

The family of HK isozymes play a large role in the initiation of glycolysis in normal and in cancerous cells. It has been suggested specifically that the mitochondrial associated HKII plays the most important regulatory, growth promoting and survival associated role in many transformed tissues(172–175) although HKI has

been found to be the main isoform overexpressed within brain tumors (94). HKII transcription has been shown to be increased by hypoxia (via HIF-1), glucose, insulin, glucagon, cAMP, and p53 (172,176). Placement in the mitochondrial membrane via its hydrophobic N-terminus and association with VDAC can help protect HKII from proteases, as well as increasing the access of the enzyme to ATP from the ATP synthase (177). Additionally, HKII in the mitochondrial membrane may also block the binding of the pro-apoptotic protein Bax, giving tumor cells protection from self-destruction by preventing Bax from releasing pro-apoptotic factors out of the mitochondria (178).

1.8.5 Additional factors accelerating glycolysis

After phosphorylation by HK, and transformation of glucose-6-phosphate to fructose-6-phosphate by glucose-6-phosphate isomerase, phosphofructokinase type 1 (PFK-1) represents an additional important step within cancers' glycolytic pathway, as it catalyzes the irreversible reaction committing the intermediate fructose-6-phosphate into the catabolic cycle (**Figure 1.8**). In many tumors the activity of the heterotetrameric PFK-1 is higher (approximately 56 times) than in normal cells due to the selective upregulation of expression of the L and M subunits that are less sensitive to phosphoenolpyruvate (PEP), a product of glycolysis and an allosteric inhibitor of PFK-1 (37,179). Also, the heterotetramer is much less sensitive to inhibition by ATP and citrate which allows glycolysis to push forward. Furthermore, the powerful allosteric activator of PFK-1, fructose-2,6-bisphosphate (F2,6BP), is increased by overexpression of the HIF-1 α

inducible enzyme PFK-2/PFB3 in several tumor types (180). High concentrations of F2,6BP overcome product inhibition by ATP and citrate from the TCA cycle, also allowing for further glycolytic stimulation (148).

Enhancement of HIF-1 expression has been correlated with increased expression of HKII, PFK-1, PFK-2, GAPDH, and LDH increasing glycolysis under anaerobic conditions (37). While HIF-1 α can be naturally upregulated due via O₂ sensitive degradation pathways, its expression can also be modulated via O₂ independent synthesis regulatory mechanisms (181). Some of these affected regulatory mechanisms include loss of function mutations in the von Hippel-Lindau protein responsible for binding to hydroxylated HIF-1 α , ubiquitylating it to be degraded rapidly by the proteasome (181).

It has become apparent from recent literature that all tumors may not rely strictly on anaerobic glycolysis and may still also utilize oxidative phosphorylation for their energy requirements (37). Many tumors still utilize aerobic respiration (182) although it is observed that in several cell lines that their total glycolytic ATP ranges from 50% to 70% of the total produced within the cell (37). Conversely, work blocking mitochondrial function has shown that ATP production was not significantly reduced in tumor cells (183). However, it is important to recognize that glycolysis is still the common pathway for nutrient to energy conversion, regardless of whether or not these cells are using strictly glycolysis or oxidative phosphorylation to derive their energy. As such, glycolysis

is still the rate limiting step, so while further metabolism may vary between tumor types, the initial steps of glycolysis are present and required for all tissues. The next section will investigate breast cancer – how it is diagnosed as well as its characteristics and glycolytic phenotype.

1.9 Breast cancer

1.9.1 Overview of diagnosis and treatment

Breast cancer represents the second leading cause of cancer related deaths in women. In 2005, estimates by the World Health Organization put the number of yearly diagnoses to 1.5 million people (184). These numbers truly show the prolific damage that breast cancer has for women from all backgrounds, races, nationalities, geographic location and socioeconomic status(185). A quarter of breast cancers occur before age 50, but in Western nations the mortality rate has decreased over recent years due to improved treatments and better methods of detection (186).

Many risk factors increase the chance that a woman will be afflicted with breast cancer during her lifetime. Examples of this include age, family history, high breast density, use of oral contraceptives, childhood radiation exposure, and mutations present within the patient such as the tumor suppressor BRCA1 and BRCA2 genes. A litany of other factors are able to reduce the risk of acquiring breast cancer including having an early age for a first term pregnancy, breast feeding, and other factors such as physical activity and proper exercise(185).

Diagnosis of breast cancer is based on clinical, radiological and pathological examination:

- Clinical examination includes physical examination of the breasts and locoregional lymph nodes.
- Radiological examination includes bilateral mammography, ultrasound, MRI, and/or CT.
- Pathological diagnosis stems from the identification of a core needle biopsy or aspiration identifying a cancerous histological subtype (186).

The identification and ensuing classification of the breast cancer occurs with the pathologist's report detailing grade, invasiveness histological subtype and expression of biomarkers such as HER2, estrogen and progesterone receptor status with immunocytochemistry. Furthermore, if preoperative treatment is planned, a chest x-ray, abdominal ultrasound, bone scintigraphy and/or a CT scan are performed to look for metastatic disease especially in those with family history, large tumors or histological indications of an invasive tumor type (186).

Treatment is a multi-disciplinary, multi-factorial process involving a variety of cancer treatment practitioners. Surgery is often the first choice, and based from information ascertained during the diagnosis, varies from patient to patient.

These include(186):

1. Breast conservation surgery
2. Mastectomy

3. Axillary staging
4. Risk reducing mastectomy

Radiation therapy is often used in concert with surgery, decreasing the chance of local recurrence by approximately two thirds. This includes patients with invasive carcinomas who have either undergone mastectomies and possess several positive axillary lymph nodes. Non-invasive patients have shown no increase in survival when treated with whole breast irradiation (186).

Systemic therapy is recommended if “a relevant reduction of the estimated risk of recurrence and death can be expected with an acceptable level of treatment-related adverse effects” (186). To determine what regimen the patient will undergo, estrogen and progesterone receptor status are the strongest predictors of subsequent treatment. Tumors expressing either of these receptors are deemed hormone receptor positive. From this, patients will undergo either a combination of chemotherapy and endocrine therapy, decisions of which hinge on the expression of the aforementioned receptors.

1.9.2 Changes in breast cancer glycolysis

Like many other cancers, breast cancer has been shown to have alterations in the expression of GLUT1, HKII, and PFK-1 that act as the main controlling steps of glycolysis in order to improve glycolytic efficiency (187–189). GLUT1's overexpression and increased uptake of the sugar analogue [¹⁸F]FDG has been correlated with immunohistochemistry of patient tumor samples (125,126,164).

In accordance with the facilitation of higher glucose uptake by increased GLUT1 expression, modulation of the of GLUT1 in an *in vitro* and *in vivo* tumor model has subsequently found that growth can be directly correlated to GLUT1 expression (190). Conversely, and still a matter of debate, other studies have investigated GLUT1 expression within breast cancers, determining that 28 to 47% of the selected sample were GLUT1 negative (191–193). Some other studies however have found little to no detectable GLUT1, in tumors that still possess a proliferative phenotype (159). The high affinity Class I transporter GLUT3 has been shown to have upregulated expression in poorly differentiated breast cancer and its expression has been identified to be stimulated by cAMP in an *in vitro* model of breast cancer (126,170).

Like other cancers, many components of glycolysis after transport and initial phosphorylation are upregulated in order to facilitate the phenotype allowing for large quantities of anaerobic glycolysis (**Figure 1.8**). Phosphoglucose isomerase and its secreted form autocrine motility factor (PGI/AMF), the protein that catalyses the reversible conversion of glucose-6-phosphate to fructose-6-phosphate has been correlated with breast cancer progression, poor prognosis, and initiation of metastases (194). As mentioned earlier, PFK-1 is also expressed in a way that promotes glycolytic efficiency in breast tumors, preferentially expressing the PFK-L over the M and P isoforms, increasing the conversion of fructose-6-phosphate to fructose-1,6-bisphosphate (189). Aldolase B(ALD), the enzyme that catalyses the reversible cleavage of fructose-1,6-bisphosphate into

dihydroxyacetone-phosphate (DHAP) and glyceraldehyde-3-phosphate (G3P) has been detected in higher levels in breast cancer, and has shown to be even more increased in metastases (195). The next enzyme, triosephosphate isomerase (TPI) that catalyzes the conversion of DHAP into G3P, has been identified to be upregulated in metastatic breast cancers, suggesting a role in advancement of a proliferative, invasive phenotype (196). Glyceraldehyde phosphate dehydrogenase (GAPDH), normally a standard used for normalizing protein expression and an important enzyme responsible for the catalysis of G3P to 1,3-bisphosphoglycerate (1,3BPG) has been found to have upregulated expression in breast cancer, and that expression is correlated with higher proliferation and aggressiveness of tissues (197). Enolase (ENO), the enzyme responsible for the penultimate step of glycolysis catalyses the conversion of 2-phosphoglycerate (2-PG) to phosphoenolpyruvate (PEP). In breast cancer especially that of estrogen receptor positive tumors, high enolase expression was correlated with poorer prognosis, larger tumor size, and relapse. Pyruvate kinase catalyses the conversion of PEP into pyruvate, and exists in several forms (R-PK, L-PK, M1-PK and M2-PK) that are all homotetrameric and have specific tissue distribution. The M2-PK is unique however as it is able to show a dimeric form, which displays low affinity for the conversion of PEP, and instead promotes the formation of glycolytic precursors for the formation of nucleic acids via glutaminolysis instead of the conversion of PEP to pyruvate (198). Advanced breast cancer has been associated with higher expression of the M2-PK isoform, suggesting that perhaps

it has an important metabolic role in providing glycolytic precursors for de novo nucleotide synthesis – this has yet to be fully elucidated however (198). Overexpression of LDH-A, a critical enzyme in glycolysis transforms pyruvate into lactate and generates NAD^+ for further glycolysis has been observed in breast cancer. LDH-A has been shown to be associated with tumor invasiveness, size and tumor progression (199). After silencing LDH-A, reduced proliferation, and increased apoptosis due to higher intracellular oxidative stress was observed.

It is clear that breast cancer shows many of the same alterations to its glycolytic phenotype as other cancers and so the question remains: How can this information be used to improve patient outcomes and care?

1.10 Positron Emission Tomography and molecular imaging of breast cancer using 2-deoxy-2- ^{18}F fluoro-D-glucose (^{18}F FDG)

1.10.1 Brief overview and history of positron emission tomography and its importance for imaging of cancer

Molecular imaging is defined as the “visualization, characterization and measurement of biological processes at the molecular and cellular level in humans and other living systems” by the Society of Nuclear Medicine (200). Positron emission tomography (PET) is one type of non-invasive molecular imaging that utilizes the high energy photons released from positron-electron annihilations to determine the localization of decaying radionuclides *in vivo*. A multitude of these radionuclides can be used for this purpose, including ^{11}C , ^{15}O ,

^{13}N , and ^{18}F all of which are often integrated into the structure of organic molecules such as glucose, ammonia, CO_2 , methionine, and water. These all have relatively short half-lives, and are often integrated into compounds that are often analogous to naturally occurring substances in the body. These bioactive compounds are used to “visualize characterize, and measure biological processes in living systems” (200). Synthesis and use of these tracers however may be limited only to certain centres, as a cyclotron and synthesis facilities required to produce these radionuclides are very expensive, albeit getting more widespread.

Unlike traditional computed tomography (CT) or magnetic resonance imaging (MRI), PET focuses on the imaging of biochemical processes occurring within the body, instead of relying on strictly anatomical information that would be provided by MRI and CT scans. Once the radionuclide labelled tracer is administered intravenously into the patient, it will undergo positron emission decay, releasing a positron, an antiparticle of the electron with an opposite charge (**Figure 1.9**). This particle travels for a very short distance ($\sim 1\text{mm}$) until it interacts with an electron and annihilates. Annihilation produces two 511 keV gamma photons travelling away at 180° from each other that then interact with scintillation detectors surrounding the patient. With this information, the PET machine is able to determine whether or not the two detection events on opposing sides are from the same annihilation. These are called “coincidence events”, and from this an image can be reconstructed using computer software.

In a nuclear medicine setting, this image is then used by physicians or radiologists for diagnosis, staging, etc.

The work that pioneered the use of PET for clinical oncology practice was that of Ido and colleagues in 1979 when they successfully synthesized a 2 labeled glucose analogue, [^{18}F]FDG (201). It was not until the late 1980s that it became apparent that the accumulation of [^{18}F]FDG by tumors would be able to assist and monitor with the care of patients with cancer. The ability to do whole body scans of individuals to determine the class and stage of the disease not only was revolutionary, but it changed the playing field for diagnosis and treatment of cancer in a fundamental way. With further advances in scanning technology as well as the creation of new radiolabeled probes for detection and identification of different disease states, we have only scratched the surface of the potential utility of PET for the management of malignant disease.

1.10.2 History and characterisation of [^{18}F]FDG as a radiotracer for PET

FDG's initial synthesis was performed by Elmon Coe in the Biochemistry Department at Northwestern University Medical School in Chicago, Illinois in 1971 (202). His rationale for synthesizing this molecule was that earlier work has indicated that the hydroxyl groups present on the C-1, C-3, C-6 and perhaps the C-4 of glucose were involved in the binding and enzyme activity of HK. He thought, if an analogue would be able to be synthesized, and subsequently phosphorylated by HK, then it would inhibit the first steps of normal glucose

metabolism(202). Using an in vitro ascites tumor model, FDG was applied and its effects on glycolysis were examined. He found that FDG, or its metabolites specifically inhibited glycolysis.

Rational design: The design of [^{18}F]FDG was based on 2DG, an analogue of glucose that possessed similar behavioural traits for transport. On the C-2 of 2-DG, the hydroxyl group is replaced by a single hydrogen atom, and while it does share similar characteristics, this modest change has implications for its biological activity. Metabolism, past the point of entry via GLUT1 and phosphorylation by one of the members of the HK family (203), does not proceed as the C-2 hydroxyl group is crucial for the next step in glycolysis – reaction with glucose-6-phosphate isomerase (204,205). This was first witnessed in 1954 by Sols and Crane (206) which suggested that 2-DG had advantages over glucose for experimental studies due to phosphorylated 2-DG not being inhibitory nor a substrate for any other metabolic step, thus “isolating the hexokinase reaction”. The first synthesis of a radiolabeled 2DG was with a [^{11}C] substitution, although ^{18}F was subsequently chosen as the C-F bond is strong, and the short 20 minute half-life of [^{11}C] was not amendable for transporting the compound the distances to where the first human studies were performed. ^{18}F possesses a much lengthier half-life of approximately 110 minutes. As discussed above, it was also logical that any modification of glucose would be at the 2 position in order to not interfere with binding and transport via GLUT1 and phosphorylation by HK whilst also not being a substrate for glucose-6-phosphate

isomerase. This would allow for metabolic trapping due to the fact that membrane permeability of hexose phosphates is low (205) and subsequent external imaging of glucose transport and phosphorylation via PET (**Figure 1.9**).

Pre-clinical work: [^{18}F]FDG was first synthesized by Ido et al at the Brookhaven National Laboratory in Upton New York in 1976 for the purpose of PET imaging. Initially examined in two normal patients, it was used for the purpose of mapping glucose utilization by the brain for utility in neuroscience research (207). These studies occurred despite of the findings that 2DG in high doses (>100mg/kg) produced toxic effects in humans and animals via its inhibitory effects on normal glucose metabolism (208,209). As such, further studies were needed to examine toxicity of [^{18}F]FDG. Subsequently, Som et al. in 1980 found no evidence of acute or chronic toxicity in animal models (210) and also that [^{18}F]FDG was identified to have utility for the imaging of malignant tumors in mice, rats, hamsters, rabbits and dog (211). They found that tumor to normal tissue and tumor to blood ratios were quite high and that levels of uptake were dependent on the type of tumor being scanned. This initial toxicological study set the stage for its eventual FDA approval, a process that while slow, started with approval for brain imaging, proceeded to cardiovascular disease imaging, and just after the year 2000 expanded to a wide range of tumor types including breast cancer (212). Now, most large cancer centres possess PET scanners and have access to synthesis facilities for the production of [^{18}F]FDG for the imaging of tumors in patients.

Biodistribution and clearance: [^{18}F]FDG readily enters tissues with high levels of glucose utilization, such as the brain and the myocardium, with less uptake observed in muscle, liver, kidneys and the intestine (213,214). [^{18}F]FDG PET can demonstrate abnormal metabolic activity in tissues and organs that may not be identified morphologically, and tumor imaging studies indicate that [^{18}F]FDG has very high signal to noise ratios due to upregulated hexose transport and glycolysis (115,116,159,204,210). Unlike glucose, [^{18}F]FDG is excreted into the urine because the missing hydroxyl on C-2 prevented reabsorption in the nephron via active transport mechanisms (213,215). This unexpected and beneficial result contributes to the relatively high signal to noise ratio that is frequently observed when performing [^{18}F]FDG based PET due to reduced blood and normal tissue levels of [^{18}F]FDG (204).

The combination of low background and high uptake into many cancerous tissues has put [^{18}F]FDG at the forefront for imaging of the vast majority of tumors in patients. Further work throughout the last 30 years has painted a very clear picture linking [^{18}F]FDG uptake with many different characteristics of cancer progression. The following section will look at the characteristics of [^{18}F]FDG, specifically related to its use for the diagnosis, monitoring and treatment of breast cancer.

1.10.3 Molecular imaging of breast cancer with [¹⁸F]FDG PET

The most widely used and studied tracer for the imaging of breast cancer is [¹⁸F]FDG, and the imaging data has been shown to be effective in the management of the disease (212,214,216–222). As mentioned earlier, [¹⁸F]FDG visualizes uptake via the hexose transporter GLUT1, and phosphorylation at the 6 position via HK to metabolically trap [¹⁸F]FDG. This trapping and cellular accumulation occurs since subsequent enzymatic reactions require the hydroxyl group on C-2. Normally, [¹⁸F]FDG is administered to the patient 45-90 minutes before visualization under the PET camera for effective detection of upregulated glucose transport and phosphorylation (214). [¹⁸F]FDG PET has been assessed for the detection and diagnosis of primary disease, evaluation of the efficacy of therapy, staging of local and distant metastases and estimation of the patient's long term prognosis. High levels of [¹⁸F]FDG uptake in breast tumors have been correlated with the Ki-67 proliferation index (a measurement of cellular proliferation), tumor grade (223,224), GLUT1 expression (125,159,164), angiogenic factors (225), high density tumor tissue, HK expression, and density of microvessels (226). A downside to the use of [¹⁸F]FDG is that uptake has also been linked with inflammatory vectors such as macrophages and neutrophils in the periphery of tumors and in independent inflammatory events, often leading to the overestimation of tumor size, and sometimes leading to false positives (227,228). Another confounding variable in distinguishing normal from malignant breast tissues is in the case of breast hypermetabolism that occurs during breast

feeding or breast infection when rapid white blood cell uptake may contribute to false positives (229,230). Lastly, low uptake may be observed because recent studies have shown that 28 to 47% of a selected sample were GLUT1 negative in breast cancer (191–193). In this section a breakdown of the clinical uses of [¹⁸F]FDG PET will be described and its respective utility in each role.

Early detection: Ideally, the spatial resolution of [¹⁸F]FDG-PET for breast cancer would be high enough to diagnose lesions that are unable to be discovered with conventional screening techniques such as mammography and self-examination. Widespread full body scans for early detection are unfeasible considering the cost of full body PET machines and related personnel as well as the lack of resolution to accurately detect <1.0cm in diameter malignancies in older machines. New generation PET machines do boast up to 4mm resolution for [¹⁸F], so this problem may be alleviated as older machines are retired. To overcome the issues with resolution and costs, positron emission mammography (PEM) for early stage diagnosis and detection is becoming more widely adopted, boasting higher resolution and being able to detect breast cancer as small as 3mm (214). A recent study has identified PEM to have a sensitivity of 90% and specificity of 86% for primary lesion detection, and in concert with conventional mammography, sensitivity increased to 91% and specificity to 93% (231). PEM and MRI have also been compared for their clinical utility, and PEM was found to be a good alternative to MRI as a presurgical breast imaging option that was not influenced by the patients hormonal status or breast density unlike what was

observed with mammography. MRI however, was better capable of detecting the need for mastectomy (250,251). These findings are indicative that [¹⁸F]FDG PEM has the possibility of being a useful technology for the diagnoses of primary tumors in patients.

Primary disease and lymph node diagnosis: Currently, [¹⁸F]FDG-PET is not recommended for primary disease diagnosis or detection of regional lymph node infiltration except in the case of patients with large primary tumors (>2cm) or aggressive malignancies. This is due to the high possibility of missing small, early stage lesions, and the risk of false negatives in patients(212). Well differentiated breast tumors such as ductal carcinoma in situ and slow growing tumors such as tubular carcinoma are difficult to diagnose with [¹⁸F]FDG, and invasive lobular carcinoma often shows low density cellular growth, correlated with limited [¹⁸F]FDG uptake (232,233). Additionally, with varied GLUT1 expression in tissues, sensitivity may be limited and false negative diagnoses may occur (191–193). A recent review assessing the clinical value of [¹⁸F]FDG-PET indicated 76 to 89% sensitivity and 73 to 80% specificity for the diagnosis of primary breast cancer (234). Varied and consistently poorer sensitivity and specificity than standard histological staging for axillary lymph nodes have warned policy makers and clinicians against using [¹⁸F]FDG PET for the assessment of axillary involvement (212,219). Low and very variable sensitivity (20 to 50%) was observed for the detection of axillary lymph node metastases (234). Axillary dissection and

assessment remains the gold standard with monitoring axillary lymph node status, as false positives have been observed when using [¹⁸F]FDG (235).

Metastatic disease: A recent review examined [¹⁸F]FDG PET for full body detection of metastases, and the reported specificity varied significantly (20-70%), although sensitivity remained quite high across the cases examined (78%-100%) (219). [¹⁸F]FDG PET has also shown higher sensitivity than traditional imaging with CT (236), mammography, MRI (237) and bone scintigraphy (specifically detection of osteolytic metastases) (238) when detecting local recurrence of disease or distant metastatic cancer in asymptomatic patients (214,218). Generally, [¹⁸F]FDG-PET has been recommended to be used in cases of advanced local or metastatic disease. While routine screening with [¹⁸F]FDG PET has also been recommended against, it should instead be used where high risk patients are likely to have undetected metastatic lesions or are feared to have recurrence (212).

Post-treatment monitoring: [¹⁸F]FDG PET's prognostic ability in the monitoring of chemotherapeutic efficacy has been thought to be another valuable clinical role. Several groups of investigators have found observable decreases in [¹⁸F]FDG uptake into treated tumors after the first cycle of treatment, reliably indicating responsive and non-responsive tumors (218). Despite this, the panel chaired by the American Society of Clinical Oncology has recommended against its

widespread use, as it still needs further work identifying its true benefit and to avoid possible treatment decisions that may endanger patients (212).

[¹⁸F]FDG PET/CT: Overall, [¹⁸F]FDG PET of breast cancer has shown significant clinical utility in the monitoring and identification of metastatic disease in many patients. Further work streamlining the imaging technology as well as clarifying [¹⁸F]FDG's behaviour in tumors undergoing treatment and understanding the fundamental mechanisms behind this modification in [¹⁸F]FDG uptake will only further clinicians ability to use this information to properly diagnose and treat these tumors. While [¹⁸F]FDG PET is able to identify abnormal metabolic activity in tissues, it is sometimes difficult to recognize and localize the position of this without the appearance of known anatomical landmarks. To overcome this, PET/CT scanners introduced in the late 90s combined functional metabolic information via the uptake of [¹⁸F]FDG, but also co-localize that with anatomical structures from the CT scan (232). This has given clinicians much higher accuracy in interpreting imaging results that would have previously been unclear with conventional PET imaging, improving the sensitivity and specificity of PET/CT compared to more traditional PET (239,240). PET/CT is especially useful in the examination of drug treated patients. This has shown superior accuracy than standard techniques such as mammography, detecting recurrences and metastatic lesions as anatomical landmarks and [¹⁸F]FDG uptake can prevent false positives and readily detect metastases (ie osteoblastic metastases) that may be invisible to conventional imaging (232). Ideally it appears that if available,

clinicians should prefer to give patients PET/CT scans as it adds added value and accuracy when staging breast cancers, examining metastases, evaluating of therapy and monitoring recurrence.

While more and more information is being gleaned through intensive study of [¹⁸F]FDG based PET and PET/CT, it is still clear that there are some fundamental hurdles to overcome such as the lack of efficacy in detecting small, well differentiated primary disease, the confounding influence of cancer associated and independent inflammatory tissue, as well as difficulty associating uptake with the efficacy of treatment. Perhaps while imaging technology improves, other novel radiolabeled tracers that are able to surmount these challenges may be an ideal choice to synthesize and evaluate for the *in vitro* imaging of breast tumors using PET. The next section will discuss a promising new avenue for the development of hexose based tracers based on both *in vitro* and *in vivo* findings with breast cancer and variability in its hexose transporter expression profile.

1.10.4 Brief explanation of standardized uptake value (SUV)

The standardized uptake value (SUV) is a simplified tool that was created in order to aid in interpretation of PET images. The formula used to calculate this is (241):

$$SUV = \frac{Q_{tissue}}{Q_{wholebody}} = \frac{Q_{tissue}}{ID}$$

- Q_{tissue} is the average activity per unit volume
- $Q_{wholebody}$ is the activity present in the body including excretions

- ID is the injected dose per unit body volume, weight or area.

SUVs have been helpful in determining the difference between benign and malignant lesions, although these protocols vary between institutions. In one meta-analysis, [¹⁸F]FDG breast cancer SUVs varied between 3.5 and 12.8 (242) giving credence to the conclusion that perhaps more standardized approaches need to be used in order to compare inter-institutional values. Overall SUVs can be a useful diagnostic tool and the development of more robust software and more universal protocols will improve inter-institution reliability.

1.11 Rational design of alternative hexose based probes for imaging of breast tumors using Positron Emission Tomography

1.11.1 GLUT5 and GLUT2 expression in breast cancer tissue

As mentioned previously, certain breast cancers have been found to express low, or no detectable GLUT1, but still manage to possess a proliferative phenotype (159). Despite the complexity involved with regards to the metabolic status present within breast cancer, it is clear that there are vastly increased levels of glucose flux, and glycolysis (37,114). Since these rapidly multiplying cells require a high level of energy and lack GLUT1 expression, they must be obtaining their energy from a different resource pool present within the blood. Mechanisms of sugar metabolism in breast cancer have large variability between tumor types, and conceivably the identified GLUT5 expression in transformed breast tissue is

of great importance with regards to the transporter's ability to provide alternative energy sources to the cell(44).

After GLUT5 expression levels were initially described in two breast adenocarcinoma cell lines using immunohistochemical techniques, western blots and functional analyses, it was proposed this could lead to novel strategies for earlier diagnoses and treatment regimens (44,125). A very comprehensive study performed by Godoy *et al.* (125) detected GLUT5 in 85% of immunostained breast tumors from patient samples as well as GLUT2 being overexpressed in 91% of invasive ductal carcinoma samples with moderate staining. Work done by Chan *et al.* identified that knockdown of GLUT5 with antisense oligonucleotides decreased the proliferative capacity of early and late stage models of breast cancer cells *in vitro*, indicating that GLUT5 might be a powerful contributor to tumor growth (243). Fructose exposure has been shown to increase the rate of transcription and GLUT5 mRNA stabilization in Caco-2 cells, indicating that a positive feedback mechanism may be in place (244). Furthermore, GLUT5 transfected CHO cells were also identified to grow at the same rate provided with either a glucose or fructose supplemented media and in a fructose only media, grow at a higher density. Given the increase in fructose consumption in western diet, this observation might in part explain the incidence of GLUT5 positive breast cancers in patients (62,77).

Breast cancer fructose metabolism begins with fructose entrance to the cell via a fructose transporting GLUT isoform (ie. GLUT2, GLUT5) (**Figure 1.8**) followed by phosphorylation by either KHK at the 1-position or at the 6-position by HK (245). Fructose-1-phosphate can enter glycolysis after it is broken down into glyceraldehyde (GA) and DHAP by aldolase B. Through enzymatic conversion by triokinase, GA can then be converted to glyceraldehyde-3-phosphate (246). In several widely accepted *in vitro* models of breast cancer, KHK is not expressed (245) suggesting a limited expression in breast tumors, but further work using clinical samples needs to be done to clarify this. Assuming that the level of KHK is low in breast tumors, phosphorylation of intracellular fructose by upregulated HK seems to be the main shuttling point of the sugar into the glycolytic pathway(246). The resulting fructose-6-phosphate is a common intermediate for glucose and fructose catabolism. Additionally, it has the potential to be enzymatically converted back into glucose-6-phosphate via glucose-6-phosphate isomerase, to be funnelled into *de novo* nucleotide synthesis via the pentose phosphate pathway (247). In the case of tumors expressing low or no GLUT1, it is reasonable to think that increased levels of fructose-6-phosphate, and the subsequent driving force of Le Chatelier's principle due to the lack of glucose uptake, will not only provide the cell with metabolic components for the remaining steps of glycolysis, but also the resources for proliferation, such as *de novo* synthesis of nucleotide precursors. The exact mechanisms that result in increased levels of GLUT5 and GLUT2 expression and fructose metabolism in

breast tumors are unknown, but GLUT5 upregulation in breast tissues has been able to be observed and presents a very valid target for the creation of radiolabeled probes to image these cell types via PET.

1.11.2 GLUT5 analogues for the imaging of breast cancer

The first work done to examine the ability of fluorinated fructose compounds for labelling of cancer tissue was done by Haradahira and co-workers wherein they described the labelling of fructose with [^{18}F] at the 1-position to yield 1-deoxy-1- [^{18}F]fluoro-D-fructose (1- [^{18}F]FDF). This was then evaluated in a xenograft fibrosarcoma mouse model where no trapping of 1- [^{18}F]FDF in the tumor was observed (248). More recently, Levi *et al.* labelled fructose with small fluorophores at the 1-position and showed uptake in GLUT5-expressing human breast cancer cells versus no uptake in cells lacking GLUT5 (240). This was the first work trying to take advantage of this GLUT5 expressing phenotype to label breast cancer, but despite the fact that uptake was observed into their model systems, their work met with very limited success (245). The investigators suggested that due to the size and electronic changes modified by the addition of such bulky fluorescent groups, uptake of their derivatives cannot be used as an analogue of fructose transport. Additionally, the lack of rigorous kinetic dissection of this transport also suggests that they were unable to show clear uptake via GLUT5.

Recently, our group recognized the potential of a fructose based PET-tracer to image GLUT5 expressing breast cancer and the potential of fluorinated compounds for the molecular imaging of GLUT5 expressing breast tumors. With the support of a multi-disciplinary team of physiologists, cell biologists, carbohydrate chemists and radiopharmacists all at the University of Alberta and The Cross Cancer Institute, we have successfully synthesized a panel of fructose based derivatives and examined their ability to label both selected cell and animal models of breast adenocarcinoma expressing GLUT5. This thesis will discuss the work done to ascertain the clinical relevance and possible utility for a new class of [^{18}F] labelled substrates for the imaging of GLUT5 and GLUT2 expressing tissues.

1.11.3 Hypothesis

The aim of this body of work is to develop and characterize a novel class of fluorinated fructose analogues for the *in vivo* imaging of GLUT5 expressing breast cancers using PET. From this additional data on the structural requirements of hexose based probes for proper binding and transport into several experimental models that express the fructose transporter GLUT5 can be determined. Furthermore, metabolism and subsequent safety of patients will be investigated in order to ascertain the viability of first in man trials using these novel substrates for GLUT5. Our goal is that through this work, patient outcomes may be improved by supplying a highly specific, safe, and effective range of molecules for improved diagnosis, staging and post-treatment follow up.

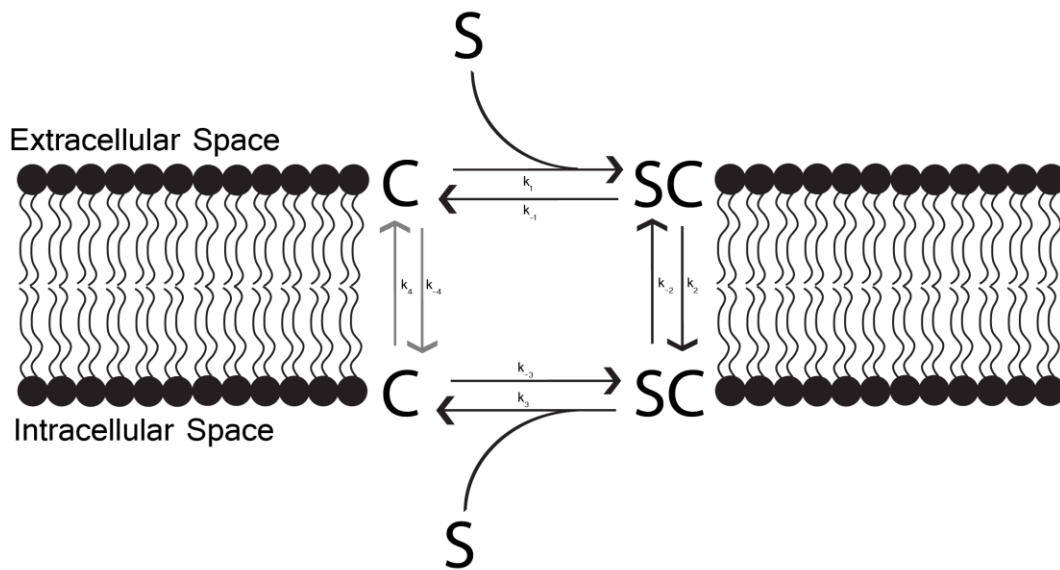


Figure 1.1: Simple carrier model – The model for carrier mediated transport of solutes is based upon Michaelis-Menten enzyme kinetics. The carrier (C) undergoes four separate and distinct steps in order to translocate the substrate(S) across the membrane, wherein each step is represented by separate and distinct kinetic constants (ie. k_1 and k_{-1}). Binding of the substrate is a unique and separate process from that of translocation. Additionally, the rate limiting step of the process has been shown through trans-stimulation experiments to be that of the reorientation of the empty carrier, shaded in lighter grey.

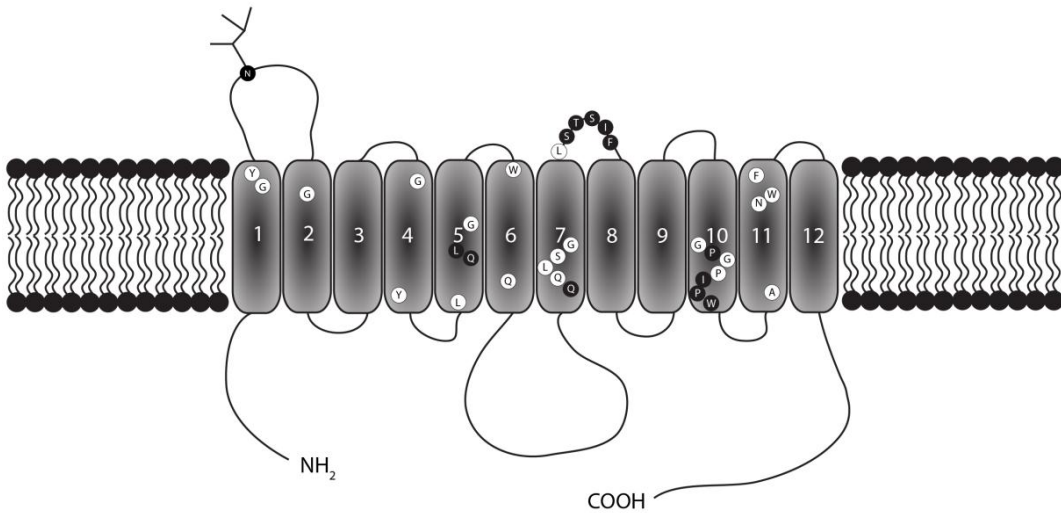
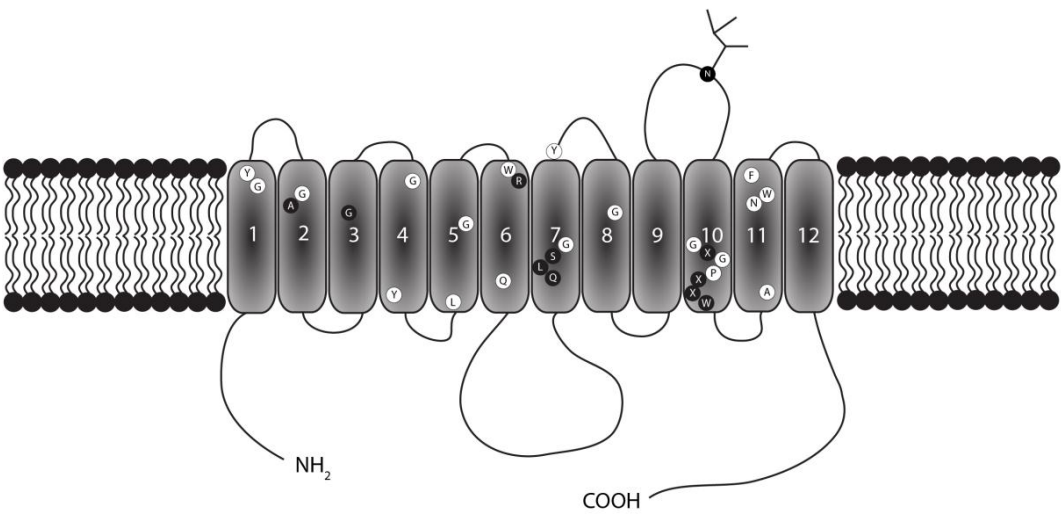
A**B**

Figure 1.2: Topology model of the GLUT family: Class I and II (A) share similar topology whilst Class III (B) differs, particularly in the location of the glycosylation site on the protein. Residues in white circles represent amino acids that are conserved between the GLUTs, and black distinguish Class I from that of Class III. Adapted from (29).

Table 1.1: Summary of the GLUTs – Adapted from (5).

GLUT isoform	K_m	Tissue	Substrate Specificity
<i>GLUT1</i>	5 mM	Ubiquitous, Red blood cells	glucose, galactose, DHA
<i>GLUT3 (GLUT14)</i>	1 mM	Neurons	glucose, galactose, DHA
<i>GLUT4</i>	5 mM	Fat, muscle	glucose, DHA
<i>GLUT2</i>	11 mM - glucose 11-76 mM – fructose 0.8 mM- glucosamine	Intestine, kidney, liver, beta-cells	glucose, galactose, fructose, glucosamine
<i>GLUT5</i>	5-14 mM	Intestine, muscle, sperm, kidney, brain	fructose, some 2DG
<i>GLUT7</i>	0.3 mM	Intestine	glucose, fructose
<i>GLUT9a and 9b</i>	0.3 mM	Kidney, Liver	urate, glucose, fructose
<i>GLUT11</i>	0.2 mM	Muscle, heart, fat, placenta, kidney, pancreas	glucose, fructose
<i>GLUT6</i>	High Km	Brain, spleen	glucose
<i>GLUT8</i>	2.4 mM – 2DG	Testes, brain fat, liver, spleen	glucose, some fructose
<i>GLUT10</i>	0.3 mM – 2DG	Heart, lung	glucose, galactose
<i>GLUT12</i>	4-5 mM	Insulin- sensitive tissues	glucose, galactose, fructose
<i>HMIT (GLUT13)</i>	0.1 mM	Brain	myo-inositol

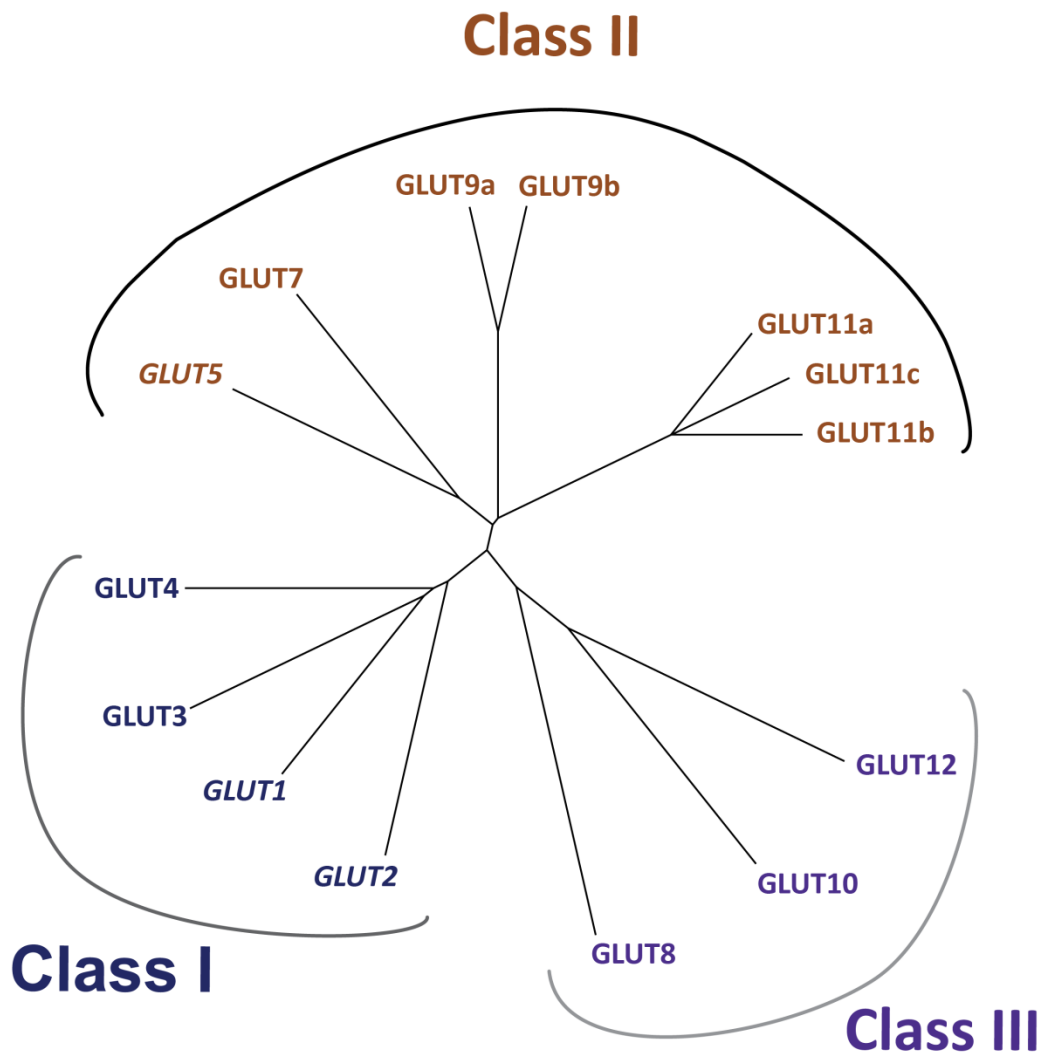


Figure 1.3: Unrooted dendrogram tree of the human facilitative hexose transporter family – Amino acid sequences of the SLC2A genes were aligned using ClustalW (<http://www.ebi.ac.uk/Tools/msa/clustalw2/>). Phylogenetic relationships were determined using Clustal W software (<http://align.genome.jp/>). The length of the branches represent relative evolutionary distance, and the Classes are separated by the curved lines.

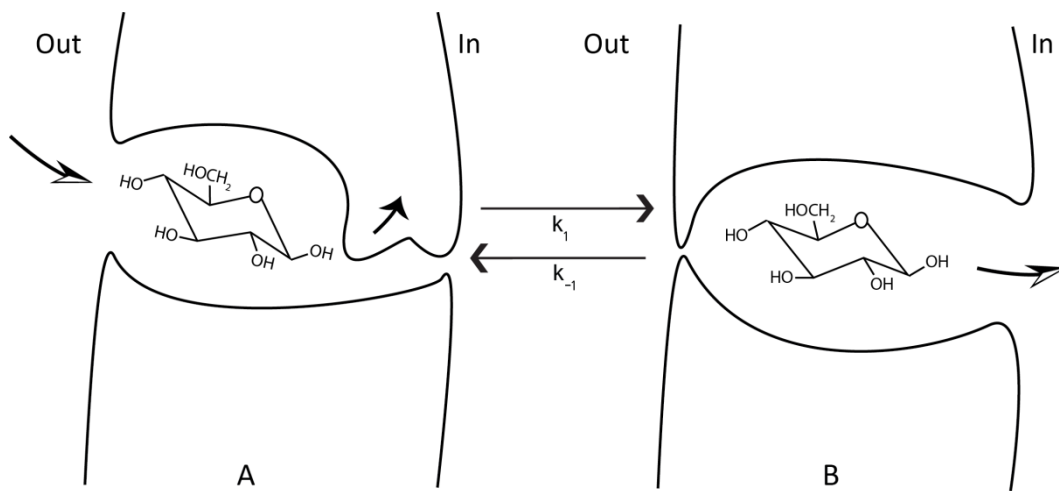


Figure 1.4: Glucose binding and being translocated by GLUT1 - C-1 of D-glucose enters the and binds to the extracellular vestibule to enter the cell. In situations of glucose efflux, C-6 binds to the intracellular binding pocket first, and then is translocated out of the cell. Adapted from (16).

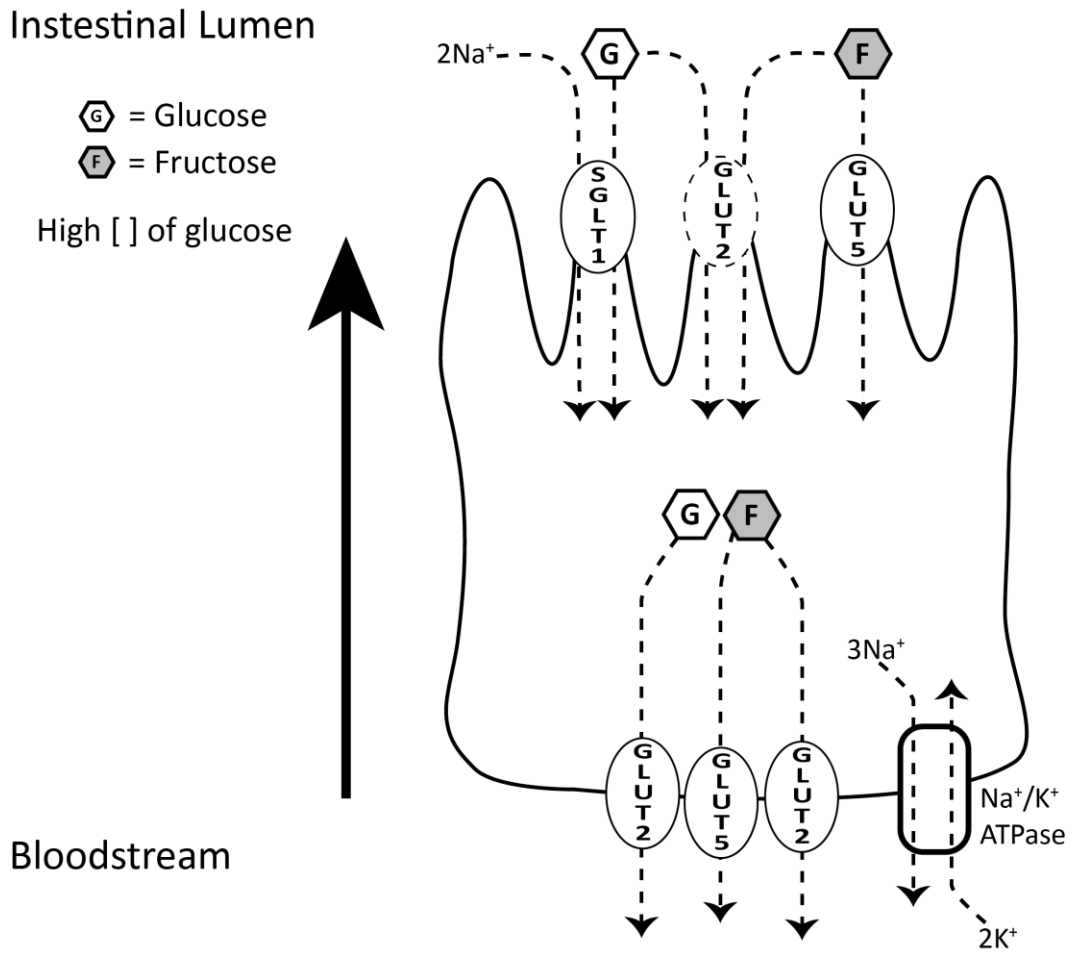


Figure 1.5: Intestinal transport of dietary sugars – expression of the facilitative transporters GLUT2 and GLUT5 is apparent on the basolateral membrane, as well as the Na⁺/K⁺ ATPase that maintains the sodium gradient required for active glucose transport via action of apically expressed SGLT1. GLUT2 is transiently expressed in the apical membrane in response to the presence of luminal hexoses.

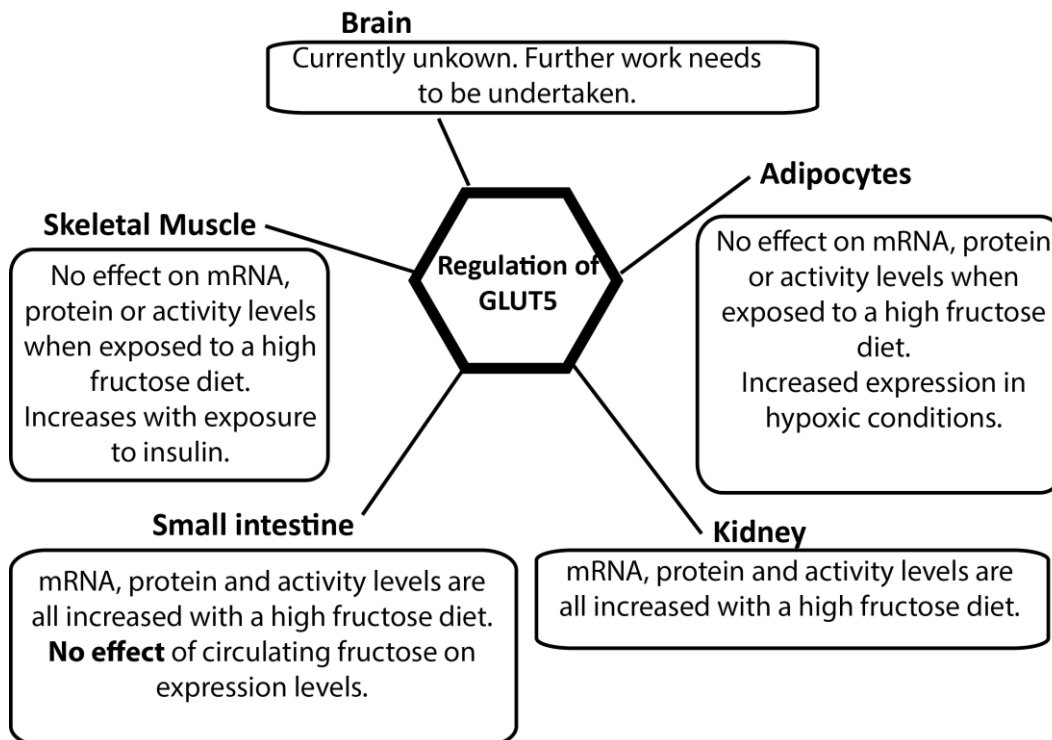


Figure 1.6: Regulation of GLUT5 by fructose – adapted from (62).

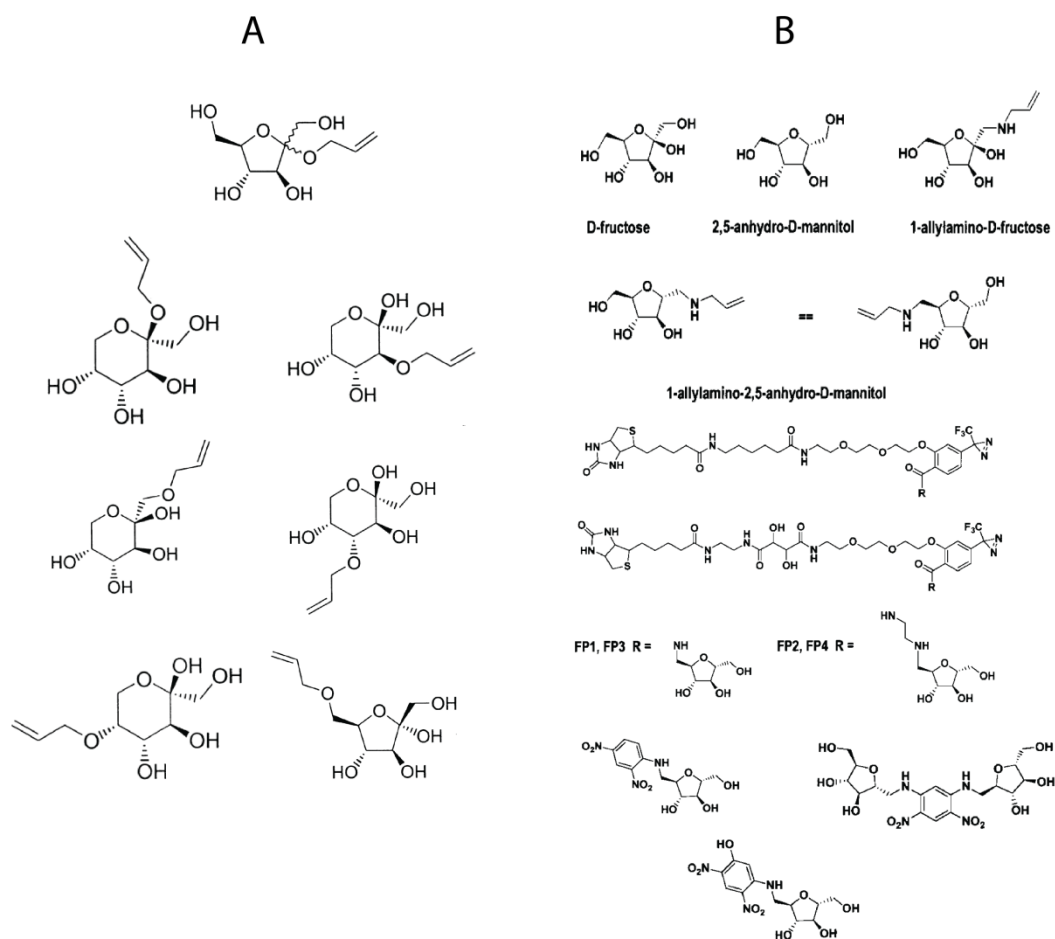


Figure 1.7: Previously published substrates for GLUT5 – (A) summarizes many of the allyl labelled fructofuranosides and fructopyranosides that were described previously to determine the structural requirements of GLUT5 (91). (B) summarizes the previously synthesized 2,5-AM derivatives used to inhibit fructose transport (92). Structures taken from (91,249).

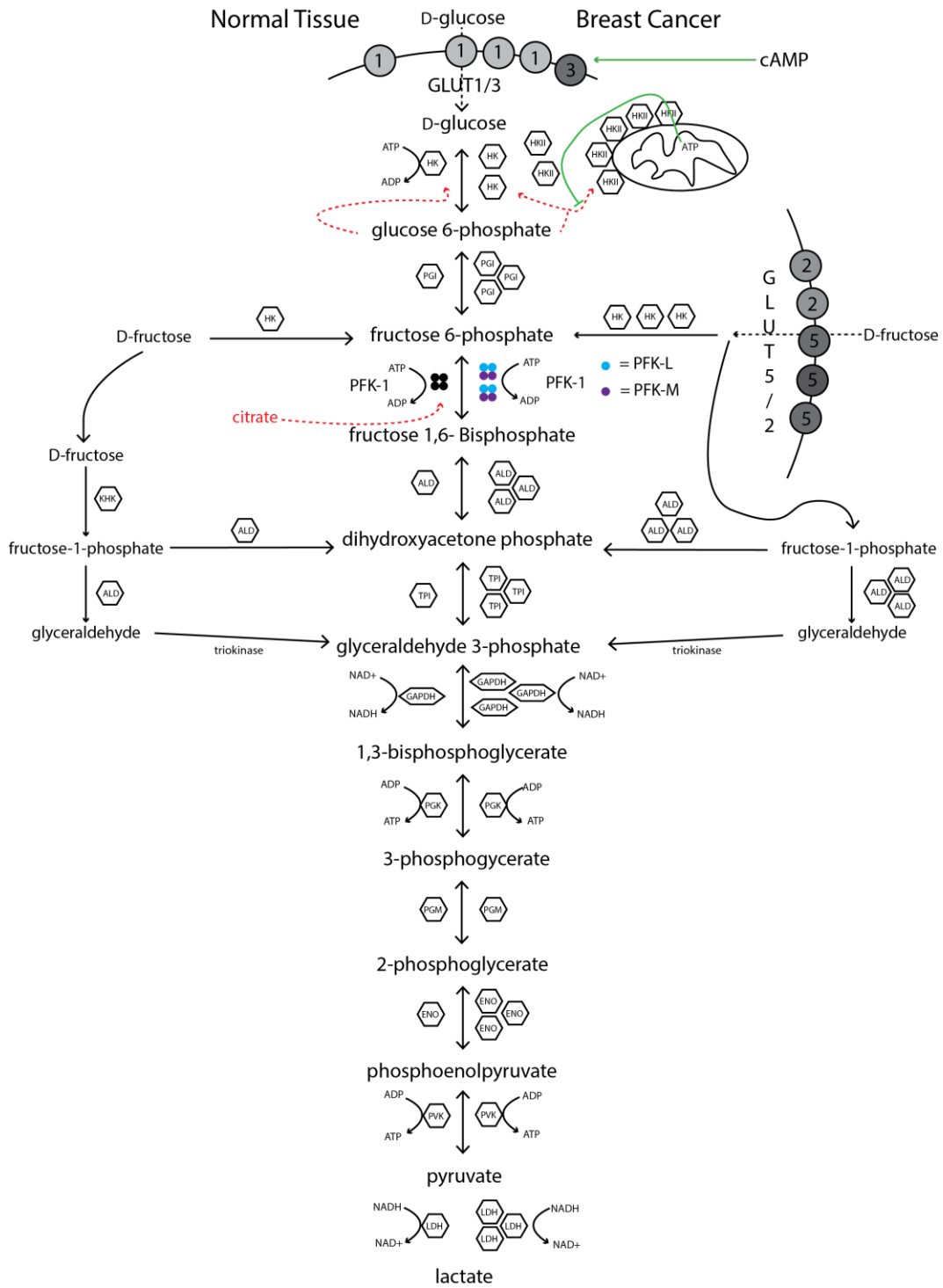


Figure 1.8: Differences in glycolysis between normal tissue and breast cancer – The glycolytic pathway in normal tissue (left) and breast tumor tissue (right). In breast tumor tissue there is an upregulation of many of the components of glycolysis compared to normal tissue. HKII overexpression and binding to the outer mitochondrial membrane improves access to newly synthesized ATP and can overcome product inhibition by glucose-6-phosphate. Adapted from (37).

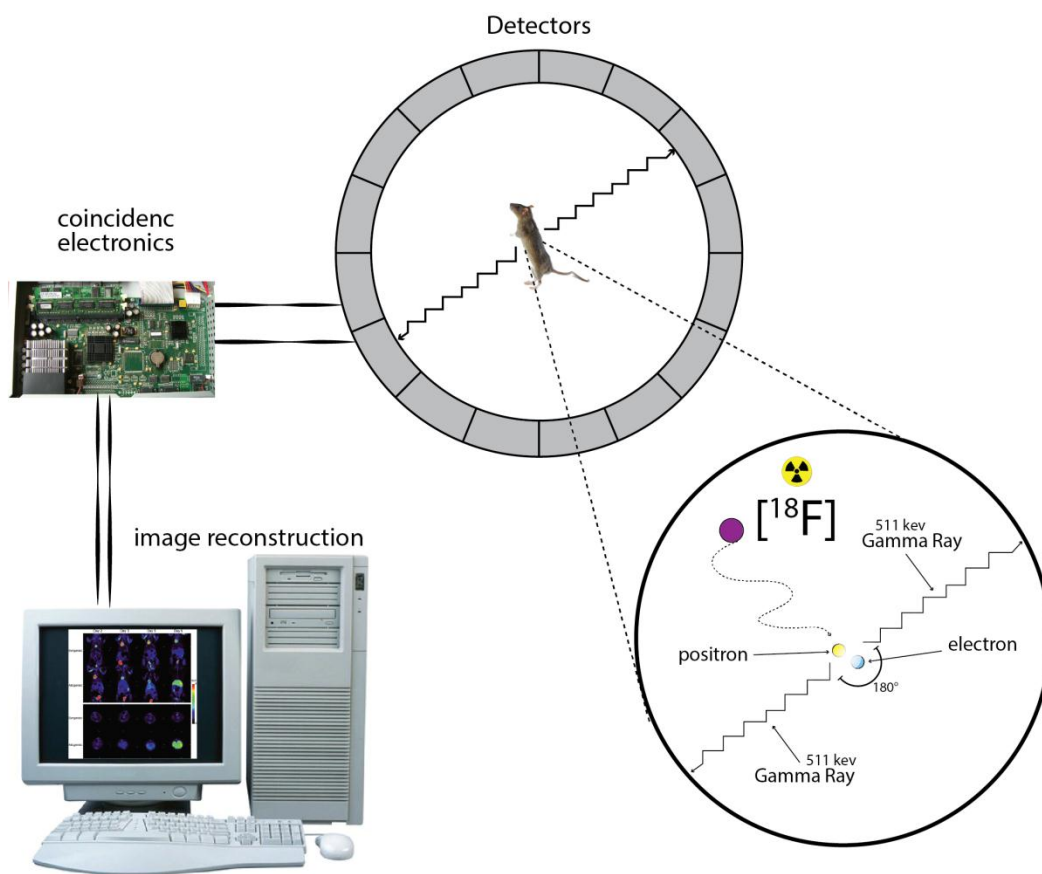


Figure 1.9: The basics of PET imaging - The radionuclide labelled tracer is administered intravenously into the patient or animal and it will undergo positron emission decay. This releases a positron, an antiparticle of the electron with an opposite charge (**Figure 1.9**). This particle travels for a very short distance ($\sim 1\text{mm}$) until it interacts with an electron and annihilates. Annihilation produces a duo of 511 keV gamma photons travelling away at 180° from each other that then interact with scintillation detectors surrounding the patient or animal. With this information, the PET machine is able to determine whether or not the two detection events on opposing sides are from the same annihilation. These are called “coincidence events”, and from this an image can be reconstructed using computer software.

1.12 Bibliography

1. Marger MD, Saier MH. A major superfamily of transmembrane facilitators that catalyse uniport, symport and antiport. *Trends in biochemical sciences*. 1993 Jan;18(1):13–20.
2. Reizer J, Reizer A, Saier MH. A functional superfamily of sodium/solute symporters. *Biochim Biophys Acta*. 1994;1197:133–66.
3. Widdas WF. Inability of diffusion to account for placental glucose transfer in the sheep and consideration of the kinetics of a possible carrier transfer. *The Journal of physiology*. 1952 Sep;118(1):23–39.
4. Fisher RB, Parsons DS. Glucose movements across the wall of the rat small intestine. *The Journal of physiology*. 1953 Feb 27;119(2-3):210–23.
5. Manolescu AR, Witkowska K, Kinnaird A, Cessford T, Cheeseman C. Facilitated hexose transporters: new perspectives on form and function. *Physiology (Bethesda, Md.)*. 2007 Aug;22:234–40.
6. Widdas WF. Facilitated transfer of hexoses across the human erythrocyte membrane. *The Journal of physiology*. 1954 Jul 28;125(1):163–80.
7. Ussing HH. Some aspects of the application of tracers in permeability studies. *Advances in enzymology and related subjects of biochemistry*. 1952 Jan;13:21–65.
8. Neame, K. D., and Richards TG. Elementary kinetics of membrane carrier transport. 1st ed. Blackwell Scientific Publications, Oxford, England; 1972.
9. Danielli JF. Phosphatases and other enzymes considered in relation to active transport and the functions of fibrous protein structures. *Proceedings of the Royal Society of London. Series B. Royal Society (Great Britain)*. 1954 Mar 25;142(907):146–54.
10. Wilbrandt W, Rosenberg T. The concept of carrier transport and its corollaries in pharmacology. *Pharmacological reviews*. 1961 Jun;13:109–83.
11. Lefevre PG. Sugar transport in the red blood cell: structure-activity relationships in substrates and antagonists. *Pharmacological reviews*. 1961 Mar;13:39–70.

12. Helmreich E, Cori CF. Studies of tissue permeability. II. The distribution of pentoses between plasma and muscle. *The Journal of biological chemistry*. 1957 Feb;224(2):663–79.
13. Kasahara M, Hinkle PC. Reconstitution and purification of the D-glucose transporter from human erythrocytes. *The Journal of biological chemistry*. 1977 Oct 25;252(20):7384–90.
14. Wheeler TJ, Hinkle PC. Kinetic properties of the reconstituted glucose transporter from human erythrocytes. *The Journal of biological chemistry*. 1981 Sep 10;256(17):8907–14.
15. Bourgeois F, Coady MJ, Lapointe J-Y. Determination of transport stoichiometry for two cation-coupled myo-inositol cotransporters: SMIT2 and HMIT. *The Journal of physiology*. 2005 Mar 1;563(Pt 2):333–43.
16. Barnett J, Holman G. An explanation of the asymmetric binding of sugars to the human erythrocyte sugar-transport systems (Short Communication). *Biochemical Journal*. 1973;:539–41.
17. Mueckler M, Caruso C, Baldwin SA, Panico M, Blench I, Morris HR, et al. Sequence and structure of a human glucose transporter. *Science (New York, N.Y.)*. 1985 Sep 6;229(4717):941–5.
18. Joost HG, Thorens B. The extended GLUT-family of sugar/polyol transport facilitators: nomenclature, sequence characteristics, and potential function of its novel members (review). *Molecular membrane biology*. 18(4):247–56.
19. Joost H-G, Bell GI, Best JD, Birnbaum MJ, Charron MJ, Chen YT, et al. Nomenclature of the GLUT/SLC2A family of sugar/polyol transport facilitators. *American journal of physiology. Endocrinology and metabolism*. 2002 Apr;282(4):E974–6.
20. Caulfield MJ, Munroe PB, O'Neill D, Witkowska K, Charchar FJ, Doblado M, et al. SLC2A9 is a high-capacity urate transporter in humans. *PLoS medicine*. 2008 Oct 7;5(10):e197.
21. Bell GI, Kayano T, Buse JB, Burant CF, Takeda J, Lin D, et al. Molecular biology of mammalian glucose transporters. *Diabetes care*. 1990 Mar;13(3):198–208.
22. Kayano T, Burant CF, Fukumoto H, Gould GW, Fan YS, Eddy RL, et al. Human facilitative glucose transporters. Isolation, functional

characterization, and gene localization of cDNAs encoding an isoform (GLUT5) expressed in small intestine, kidney, muscle, and adipose tissue and an unusual glucose transporter pseudogene-like. *The Journal of biological chemistry*. 1990 Aug 5;265(22):13276–82.

23. Davidson NO, Hausman AM, Ifkovits CA, Buse JB, Gould GW, Burant CF, et al. Human intestinal glucose transporter expression and localization of GLUT5. *The American journal of physiology*. 1992 Mar;262(3 Pt 1):C795–800.
24. Burant CF, Takeda J, Brot-Laroche E, Bell GI, Davidson NO. Fructose transporter in human spermatozoa and small intestine is GLUT5. *The Journal of biological chemistry*. 1992 Jul 25;267(21):14523–6.
25. Augustin R. The protein family of glucose transport facilitators: It's not only about glucose after all. *IUBMB life*. 2010 May;62(5):315–33.
26. Uldry M, Ibberson M, Hosokawa M, Thorens B. GLUT2 is a high affinity glucosamine transporter. *FEBS letters*. 2002 Jul 31;524(1-3):199–203.
27. Corti A, Casini AF, Pompella A. Cellular pathways for transport and efflux of ascorbate and dehydroascorbate. *Archives of biochemistry and biophysics*. 2010 Aug 15;500(2):107–15.
28. Mueckler M, Makepeace C. Model of the exofacial substrate-binding site and helical folding of the human Glut1 glucose transporter based on scanning mutagenesis. *Biochemistry*. 2009 Jun 30;48(25):5934–42.
29. Joost H-georg, Thorens B. The extended GLUT-family of sugar / polyol transport facilitators : nomenclature , sequence characteristics , and potential function of its novel members. *Mol Membr Biol*. 2001 Oct-Dec;18(4):247-56.
30. Kasahara T, Kasahara M. Expression of the rat GLUT1 glucose transporter in the yeast *Saccharomyces cerevisiae*. *The Biochemical journal*. 1996 Apr 1;315. Pt 1:177–82.
31. Illsley NP. Glucose transporters in the human placenta. *Placenta*. 2000 Jan;21(1):14–22.
32. Hanahan D, Weinberg RA. Hallmarks of cancer: the next generation. *Cell*. 2011 Mar 4;144(5):646–74.

33. Brockmann K. The expanding phenotype of GLUT1-deficiency syndrome. *Brain & development*. 2009 Aug;31(7):545–52.
34. Pascual JM, Wang D, Lecumberri B, Yang H, Mao X, Yang R, et al. GLUT1 deficiency and other glucose transporter diseases. *European journal of endocrinology / European Federation of Endocrine Societies*. 2004 May;150(5):627–33.
35. Behrooz A, Ismail-Beigi F. Dual control of glut1 glucose transporter gene expression by hypoxia and by inhibition of oxidative phosphorylation. *The Journal of biological chemistry*. 1997 Feb 28;272(9):5555–62.
36. Kahlenberg A, Dolansky D. Structural requirements of D-glucose for its binding to isolated human erythrocyte membranes. *Canadian journal of biochemistry*. 1972 Jun;50(6):638–43.
37. Moreno-Sánchez R, Rodríguez-Enríquez S, Marín-Hernández A, Saavedra E. Energy metabolism in tumor cells. *The FEBS journal*. 2007 Mar;274(6):1393–418.
38. O’Neil RG, Wu L, Mullani N. Uptake of a fluorescent deoxyglucose analog (2-NBDG) in tumor cells. *Molecular imaging and biology*. 2005. 7(6):388–92.
39. Thorens B, Sarkar HK, Kaback HR, Lodish HF. Cloning and functional expression in bacteria of a novel glucose transporter present in liver, intestine, kidney, and beta-pancreatic islet cells. *Cell*. 1988 Oct 21;55(2):281–90.
40. Gould GW, Holman GD. The glucose transporter family: structure, function and tissue-specific expression. *The biochemical journal*. 1993 Oct 15;295 (Pt 2):329–41.
41. Johnson JH, Newgard CB, Milburn JL, Lodish HF, Thorens B. The high Km glucose transporter of islets of Langerhans is functionally similar to the low affinity transporter of liver and has an identical primary sequence. *The Journal of biological chemistry*. 1990 Apr 25;265(12):6548–51.
42. Arbuckle MI, Kane S, Porter LM, Seatter MJ, Gould GW. Structure-function analysis of liver-type (GLUT2) and brain-type (GLUT3) glucose transporters: expression of chimeric transporters in *Xenopus* oocytes suggests an important role for putative transmembrane helix 7 in determining substrate selectivity. *Biochemistry*. 1996 Dec 24;35(51):16519–27.

43. Colville CA, Seatter MJ, Jess TJ, Gould GW, Thomas HM. Kinetic analysis of the liver-type (GLUT2) and brain-type (GLUT3) glucose transporters in *Xenopus* oocytes: substrate specificities and effects of transport inhibitors. *The biochemical journal*. 1993 Mar 15;290 (Pt 3):701–6.
44. Zamora-León SP, Golde DW, Concha II, Rivas CI, Delgado-López F, Baselga J, et al. Expression of the fructose transporter GLUT5 in human breast cancer. *Proceedings of the National Academy of Sciences of the United States of America*. 1996 Mar 5;93(5):1847–52.
45. Leturque A, Brot-Laroche E, Le Gall M, Stolarczyk E, Tobin V. The role of GLUT2 in dietary sugar handling. *Journal of physiology and biochemistry*. 2005 Dec;61(4):529–37.
46. Wright EM, Martín MG, Turk E. Intestinal absorption in health and disease—sugars. *Best practice & research. Clinical gastroenterology*. 2003 Dec;17(6):943–56.
47. Thorens B. Facilitated glucose transporters in epithelial cells. *Annual review of physiology*. 1993 Jan;55:591–608.
48. Leturque A, Brot-Laroche E, Le Gall M. GLUT2 mutations, translocation, and receptor function in diet sugar managing. *American journal of physiology. Endocrinology and metabolism*. 2009 May;296(5):E985–92.
49. Kellett GL. The facilitated component of intestinal glucose absorption. *The Journal of physiology*. 2001 Mar 15;531(Pt 3):585–95.
50. Gouyon F, Caillaud L, Carriere V, Klein C, Dalet V, Citadelle D, et al. Simple-sugar meals target GLUT2 at enterocyte apical membranes to improve sugar absorption: a study in GLUT2-null mice. *The Journal of physiology*. 2003 Nov 1;552(Pt 3):823–32.
51. Thorens B. Glucose transporters in the regulation of intestinal, renal, and liver glucose fluxes. *The American journal of physiology*. 1996 Apr;270(4 Pt 1):G541–53.
52. Marks J, Carvou NJC, Debnam ES, Srani SK, Unwin RJ. Diabetes increases facilitative glucose uptake and GLUT2 expression at the rat proximal tubule brush border membrane. *The Journal of physiology*. 2003 Nov 15;553(Pt 1):137–45.
53. Weinstein SP, O’Boyle E, Fisher M, Haber RS. Regulation of GLUT2 glucose transporter expression in liver by thyroid hormone: evidence for hormonal

- regulation of the hepatic glucose transport system. *Endocrinology*. 1994 Aug;135(2):649–54.
54. Henquin JC. Triggering and amplifying pathways of regulation of insulin secretion by glucose. *Diabetes*. 2000 Nov;49(11):1751–60.
 55. Matschinsky FM, Glaser B, Magnuson MA. Pancreatic beta-cell glucokinase: closing the gap between theoretical concepts and experimental realities. *Diabetes*. 1998 Mar;47(3):307–15.
 56. Antoine B, Lefrançois-Martinez AM, Le Guillou G, Leturque A, Vandewalle A, Kahn A. Role of the GLUT 2 glucose transporter in the response of the L-type pyruvate kinase gene to glucose in liver-derived cells. *The Journal of biological chemistry*. 1997 Jul 18;272(29):17937–43.
 57. Rencurel F, Waeber G, Antoine B, Rocchiccioli F, Maulard P, Girard J, et al. Requirement of glucose metabolism for regulation of glucose transporter type 2 (GLUT2) gene expression in liver. *The biochemical journal*. 1996 Mar 15;314 (Pt 3):903–9.
 58. Burcelin R, Dolci W, Thorens B. Glucose sensing by the hepatoportal sensor is GLUT2-dependent: in vivo analysis in GLUT2-null mice. *Diabetes*. 2000 Oct;49(10):1643–8.
 59. Asano T, Katagiri H, Tsukuda K, Lin JL, Ishihara H, Yazaki Y, et al. Upregulation of GLUT2 mRNA by glucose, mannose, and fructose in isolated rat hepatocytes. *Diabetes*. 1992 Jan;41(1):22–5.
 60. Rencurel F, Waeber G, Antoine B, Rocchiccioli F, Maulard P, Girard J, et al. Requirement of glucose metabolism for regulation of glucose transporter type 2 (GLUT2) gene expression in liver. *The biochemical journal*. 1996 Mar 15;314 (Pt 3):903–9.
 61. Colville CA, Seatter MJ, Gould GW. Analysis of the structural requirements of sugar binding to the liver, brain and insulin-responsive glucose transporters expressed in oocytes. *The biochemical journal*. 1993 Sep 15;294 (Pt 3):753–60.
 62. Douard V, Ferraris RP. Regulation of the fructose transporter GLUT5 in health and disease. *American journal of physiology. Endocrinology and metabolism*. 2008 Aug;295(2):E227–37.
 63. Ohara H, Tamayama T, Maemura K, Kanbara K, Hayasaki H, Abe M, et al. Immunocytochemical demonstration of glucose transporters in epiphyseal

growth plate chondrocytes of young rats in correlation with autoradiographic distribution of 2-deoxyglucose in chondrocytes of mice. *Acta histochemica*. 2001 Oct;103(4):365–78.

64. Kane S, Seatter MJ, Gould GW. Functional studies of human GLUT5: effect of pH on substrate selection and an analysis of substrate interactions. *Biochemical and biophysical research communications*. 1997 Sep 18;238(2):503–5.
65. Soleimani M. Dietary fructose, salt absorption and hypertension in metabolic syndrome: towards a new paradigm. *Acta physiologica (Oxford, England)*. 2011 Jan;201(1):55–62.
66. Blakemore SJ, Aledo JC, James J, Campbell FC, Lucocq JM, Hundal HS. The GLUT5 hexose transporter is also localized to the basolateral membrane of the human jejunum. *The biochemical journal*. 1995 Jul 1;309 (Pt 1):7–12.
67. Ellwood KC, Chatzidakis C, Failla ML. Fructose utilization by the human intestinal epithelial cell line, Caco-2. *Proceedings of the Society for Experimental Biology and Medicine*. Society for Experimental Biology and Medicine (New York, N.Y.). 1993 Apr;202(4):440–6.
68. Cui X-L, Ananian C, Perez E, Strenger A, Beuve AV, Ferraris RP. Cyclic AMP stimulates fructose transport in neonatal rat small intestine. *The journal of nutrition*. 2004 Jul;134(7):1697–703.
69. Cui X-L, Soteropoulos P, Toliás P, Ferraris RP. Fructose-responsive genes in the small intestine of neonatal rats. *Physiological genomics*. 2004 Jul 8;18(2):206–17.
70. Sugawara-Yokoo M, Suzuki T, Matsuzaki T, Naruse T, Takata K. Presence of fructose transporter GLUT5 in the S3 proximal tubules in the rat kidney. *Kidney international*. 1999 Sep;56(3):1022–8.
71. Mate A, de la Hermosa MA, Barfull A, Planas JM, Vázquez CM. Characterization of D-fructose transport by rat kidney brush-border membrane vesicles: changes in hypertensive rats. *Cellular and molecular life sciences : CMLS*. 2001 Nov;58(12-13):1961–7.
72. Angulo C, Rauch MC, Droppelmann A, Reyes AM, Slebe JC, Delgado-López F, et al. Hexose transporter expression and function in mammalian spermatozoa: cellular localization and transport of hexoses and vitamin C. *Journal of cellular biochemistry*. 1998 Nov 1;71(2):189–203.

73. Rigau T, Rivera M, Palomo MJ, Fernández-Novell JM, Mogas T, Ballester J, et al. Differential effects of glucose and fructose on hexose metabolism in dog spermatozoa. *Reproduction* (Cambridge, England). 2002 Apr;123(4):579–91.
74. Shepherd PR, Gibbs EM, Wesslau C, Gould GW, Kahn BB. Human small intestine facilitative fructose/glucose transporter (GLUT5) is also present in insulin-responsive tissues and brain. Investigation of biochemical characteristics and translocation. *Diabetes*. 1992 Oct;41(10):1360–5.
75. Hajduch E, Litherland GJ, Turban S, Brot-Laroche E, Hundal HS. Insulin regulates the expression of the GLUT5 transporter in L6 skeletal muscle cells. *FEBS letters*. 2003 Aug 14;549(1-3):77–82.
76. Wood IS, Wang B, Lorente-Cebrián S, Trayhurn P. Hypoxia increases expression of selective facilitative glucose transporters (GLUT) and 2-deoxy-D-glucose uptake in human adipocytes. *Biochemical and biophysical research communications*. 2007 Sep 21;361(2):468–73.
77. Wlaschin KF, Hu W-S. Engineering cell metabolism for high-density cell culture via manipulation of sugar transport. *Journal of biotechnology*. 2007 Aug 31;131(2):168–76.
78. Funari V a, Herrera VLM, Freeman D, Tolan DR. Genes required for fructose metabolism are expressed in Purkinje cells in the cerebellum. *Brain research. Molecular brain research*. 2005 Dec 14;142(2):115–22.
79. Funari VA, Crandall JE, Tolan DR. Fructose metabolism in the cerebellum. *Cerebellum* (London, England). 2007 Jan;6(2):130–40.
80. Pardridge WM, Boado RJ, Farrell CR. Brain-type glucose transporter (GLUT-1) is selectively localized to the blood-brain barrier. Studies with quantitative western blotting and in situ hybridization. *The Journal of biological chemistry*. 1990 Oct 15;265(29):18035–40.
81. Vannucci SJ, Maher F, Simpson IA. Glucose transporter proteins in brain: delivery of glucose to neurons and glia. *Glia*. 1997 Sep;21(1):2–21.
82. Payne J, Maher F, Simpson I, Mattice L, Davies P. Glucose transporter Glut 5 expression in microglial cells. *Glia*. 1997 Nov;21(3):327–31.
83. Oldendorf WH. Brain uptake of radiolabeled amino acids, amines, and hexoses after arterial injection. *The American journal of physiology*. 1971 Dec;221(6):1629–39.

84. Shu H-J, Isenberg K, Cormier RJ, Benz A, Zorumski CF. Expression of fructose sensitive glucose transporter in the brains of fructose-fed rats. *Neuroscience*. 2006 Jul 7;140(3):889–95.
85. Messier C, Whately K, Liang J, Du L, Puissant D. The effects of a high-fat, high-fructose, and combination diet on learning, weight, and glucose regulation in C57BL/6 mice. *Behavioural brain research*. 2007 Mar 12;178(1):139–45.
86. Buddington RK, Diamond JM. Ontogenetic development of intestinal nutrient transporters. *Annual review of physiology*. 1989 Jan;51:601–19.
87. Shu R, David ES, Ferraris RP. Dietary fructose enhances intestinal fructose transport and GLUT5 expression in weaning rats. *The American journal of physiology*. 1997 Mar;272(3 Pt 1):G446–53.
88. Shu R, David ES, Ferraris RP. Luminal fructose modulates fructose transport and GLUT-5 expression in small intestine of weaning rats. *The American journal of physiology*. 1998 Feb;274(2 Pt 1):G232–9.
89. Jones HF, Butler RN, Brooks DA. Intestinal fructose transport and malabsorption in humans. *American journal of physiology. Gastrointestinal and liver physiology*. 2011 Feb;300(2):G202–6.
90. Jiang L, Ferraris RP. Developmental reprogramming of rat GLUT-5 requires de novo mRNA and protein synthesis. *American journal of physiology. Gastrointestinal and liver physiology*. 2001 Jan;280(1):G113–20.
91. Tatibouët a, Yang J, Morin C, Holman GD. Synthesis and evaluation of fructose analogues as inhibitors of the D-fructose transporter GLUT5. *Bioorganic & medicinal chemistry*. 2000 Jul;8(7):1825–33.
92. Yang J, Dowden J, Tatibouët A, Hatanaka Y, Holman GD. Development of high-affinity ligands and photoaffinity labels for the D-fructose transporter GLUT5. *The biochemical journal*. 2002 Oct 15;367(Pt 2):533–9.
93. González C, Ureta T, Sánchez R, Niemeyer H. Multiple molecular forms of ATP:hexose 6-phosphotransferase from rat liver. *Biochemical and biophysical research communications*. 1964 Jul 1;16(4):347–52.
94. Wilson JE. Isozymes of mammalian hexokinase: structure, subcellular localization and metabolic function. *The Journal of experimental biology*. 2003 Jun;206(Pt 12):2049–57.

95. Bork P, Sander C, Valencia A. Convergent evolution of similar enzymatic function on different protein folds: the hexokinase, ribokinase, and galactokinase families of sugar kinases. *Protein science*. 1993 Jan;2(1):31–40.
96. Cárdenas ML, Cornish-Bowden A, Ureta T. Evolution and regulatory role of the hexokinases. *Biochimica et biophysica acta*. 1998 Mar 5;1401(3):242–64.
97. Board M, Colquhoun A, Newsholme EA. High Km glucose-phosphorylating (glucokinase) activities in a range of tumor cell lines and inhibition of rates of tumor growth by the specific enzyme inhibitor mannoheptulose. *Cancer research*. 1995 Aug 1;55(15):3278–85.
98. Tsai HJ, Wilson JE. Functional organization of mammalian hexokinases: characterization of the rat type III isozyme and its chimeric forms, constructed with the N- and C-terminal halves of the type I and type II isozymes. *Archives of biochemistry and biophysics*. 1997 Feb 15;338(2):183–92.
99. Tsai HJ, Wilson JE. Functional organization of mammalian hexokinases: characterization of chimeric hexokinases constructed from the N- and C-terminal domains of the rat type I and type II isozymes. *Archives of biochemistry and biophysics*. 1995 Jan 10;316(1):206–14.
100. Wilson JE. An introduction to the isoenzymes of mammalian hexokinase types I-III. *Biochemical Society transactions*. 1997 Feb;25(1):103–7.
101. Ovádi J, Srere PA. Macromolecular compartmentation and channeling. *International review of cytology*. 2000 Jan;192:255–80.
102. Rose IA, Warms JV. Mitochondrial hexokinase. Release, rebinding, and location. *The journal of biological chemistry*. 1967 Apr 10;242(7):1635–45.
103. BeltrandelRio H, Wilson JE. Coordinated regulation of cerebral glycolytic and oxidative metabolism, mediated by mitochondrially bound hexokinase dependent on intramitochondrially generated ATP. *Archives of biochemistry and biophysics*. 1992 Aug 1;296(2):667–77.
104. Preller A, Wilson JE. Localization of the type III isozyme of hexokinase at the nuclear periphery. *Archives of biochemistry and biophysics*. 1992 May 1;294(2):482–92.

105. Diggle CP, Shires M, Leitch D, Brooke D, Carr IM, Markham AF, et al. Ketohexokinase: expression and localization of the principal fructose-metabolizing enzyme. *The journal of histochemistry and cytochemistry*. 2009 Aug;57(8):763–74.
106. Cárdenas ML, Rabajille E, Niemeyer H. Fructose is a good substrate for rat liver “glucokinase” (hexokinase D). *The biochemical journal*. 1984 Sep 1;222(2):363–70.
107. Raushel FM, Cleland WW. The substrate and anomeric specificity of fructokinase. *The Journal of biological chemistry*. 1973 Dec 10;248(23):8174–7.
108. Purich DL, Fromm HJ, Rudolph FB. The hexokinases: kinetic, physical, and regulatory properties. *Advances in enzymology and related areas of molecular biology*. 1973 Jan;39:249–326.
109. Froesch E, Ginsberg J. Fructose Metabolism of Adipose Tissue. *Acta Med Scand Suppl*. 1972;542:37-46.
110. Van den Berghe G. Fructose: metabolism and short-term effects on carbohydrate and purine metabolic pathways. *Progress in biochemical pharmacology*. 1986 Jan;21:1–32.
111. Hayward BE, Bonthron DT. Structure and alternative splicing of the ketohexokinase gene. *European journal of biochemistry / FEBS*. 1998 Oct 1;257(1):85–91.
112. Asipu A, Hayward BE, O’Reilly J, Bonthron DT. Properties of normal and mutant recombinant human ketohexokinases and implications for the pathogenesis of essential fructosuria. *Diabetes*. 2003 Sep;52(9):2426–32.
113. Raushel FM, Cleland WW. The substrate and anomeric specificity of fructokinase. *The journal of biological chemistry*. 1973 Dec 10;248(23):8174–7.
114. Hanahan D, Weinberg RA. Hallmarks of cancer: the next generation. *Cell*. 2011 Mar 4;144(5):646–74.
115. Warburg O. On the origin of cancer cells. *Science (New York, N.Y.)*. 1956 Feb 24;123(3191):309–14.

116. Furuta E, Okuda H, Kobayashi A, Watabe K. Metabolic genes in cancer: their roles in tumor progression and clinical implications. *Biochimica et biophysica acta*. 2010 Apr;1805(2):141–52.
117. Rodríguez-Enríquez S, Marín-Hernández A, Gallardo-Pérez JC, Moreno-Sánchez R. Kinetics of transport and phosphorylation of glucose in cancer cells. *Journal of cellular physiology*. 2009 Dec;221(3):552–9.
118. Cantuaria G, Fagotti A, Ferrandina G, Magalhaes A, Nadji M, Angioli R, et al. GLUT-1 expression in ovarian carcinoma: association with survival and response to chemotherapy. *Cancer*. 2001 Sep 1;92(5):1144–50.
119. Baer SC, Casaubon L, Younes M. Expression of the human erythrocyte glucose transporter Glut1 in cutaneous neoplasia. *Journal of the American Academy of Dermatology*. 1997 Oct;37(4):575–7.
120. Wang BY, Kalir T, Sabo E, Sherman DE, Cohen C, Burstein DE. Immunohistochemical staining of GLUT1 in benign, hyperplastic, and malignant endometrial epithelia. *Cancer*. 2000 Jun 15;88(12):2774–81.
121. Rudlowski C, Becker AJ, Schroder W, Rath W, Büttner R, Moser M. GLUT1 messenger RNA and protein induction relates to the malignant transformation of cervical cancer. *American journal of clinical pathology*. 2003 Nov;120(5):691–8.
122. Haber RS, Rathan A, Weiser KR, Pritsker A, Itzkowitz SH, Bodian C, et al. GLUT1 glucose transporter expression in colorectal carcinoma: a marker for poor prognosis. *Cancer*. 1998 Jul 1;83(1):34–40.
123. Ozcan A, Shen SS, Zhai QJ, Truong LD. Expression of GLUT1 in primary renal tumors: morphologic and biologic implications. *American journal of clinical pathology*. 2007 Aug;128(2):245–54.
124. Nishioka T, Oda Y, Seino Y, Yamamoto T, Inagaki N, Yano H, et al. Distribution of the glucose transporters in human brain tumors. *Cancer research*. 1992 Jul 15;52(14):3972–9.
125. Reinicke K, Godoy A, Ulloa V, Rodri F, Medina RA, Yan AJ, et al. Differential Subcellular Distribution of Glucose Transporters GLUT1 – 6 and GLUT9 in Human Cancer : Ultrastructural Localization of GLUT1 and GLUT5 in Breast Tumor Tissues. *J Cell Physiol*. 2006;627(April 2005):614–27.
126. Krzeslak A, Wojcik-Krowiranda K, Forma E, Jozwiak P, Romanowicz H, Bienkiewicz A, et al. Expression of GLUT1 and GLUT3 Glucose Transporters

in Endometrial and Breast Cancers. Pathology oncology research : POR. 2012 Jul;18(3):721–8.

127. Tohma T, Okazumi S, Makino H, Cho A, Mochizuki R, Shuto K, et al. Overexpression of glucose transporter 1 in esophageal squamous cell carcinomas: a marker for poor prognosis. Diseases of the esophagus : official journal of the International Society for Diseases of the Esophagus / I.S.D.E. 2005 Jan;18(3):185–9.
128. Boren J, Cascante M, Marin S, Comín-Anduix B, Centelles JJ, Lim S, et al. Gleevec (STI571) influences metabolic enzyme activities and glucose carbon flow toward nucleic acid and fatty acid synthesis in myeloid tumor cells. The Journal of biological chemistry. 2001 Oct 12;276(41):37747–53.
129. Boros LG, Torday JS, Lim S, Bassilian S, Cascante M, Lee WN. Transforming growth factor beta2 promotes glucose carbon incorporation into nucleic acid ribose through the nonoxidative pentose cycle in lung epithelial carcinoma cells. Cancer research. 2000 Mar 1;60(5):1183–5.
130. Mathupala SP, Ko YH, Pedersen PL. Hexokinase-2 bound to mitochondria: cancer's stygian link to the "Warburg Effect" and a pivotal target for effective therapy. Seminars in cancer biology. 2009 Feb;19(1):17–24.
131. Ganapathy V, Thangaraju M, Prasad PD. Nutrient transporters in cancer: relevance to Warburg hypothesis and beyond. Pharmacology & therapeutics. 2009 Jan;121(1):29–40.
132. Gallagher SM, Castorino JJ, Wang D, Philp NJ. Monocarboxylate transporter 4 regulates maturation and trafficking of CD147 to the plasma membrane in the metastatic breast cancer cell line MDA-MB-231. Cancer research. 2007 May 1;67(9):4182–9.
133. Pinheiro C, Longatto-Filho A, Scapulatempo C, Ferreira L, Martins S, Pellerin L, et al. Increased expression of monocarboxylate transporters 1, 2, and 4 in colorectal carcinomas. Virchows Archiv : an international journal of pathology. 2008 Feb;452(2):139–46.
134. Gatenby RA, Gillies RJ. Why do cancers have high aerobic glycolysis? Nature reviews. Cancer. 2004 Nov;4(11):891–9.
135. Yalcin A, Telang S, Clem B, Chesney J. Regulation of glucose metabolism by 6-phosphofructo-2-kinase/fructose-2,6-bisphosphatases in cancer. Experimental and molecular pathology. 2009 Jun;86(3):174–9.

136. Parks SK, Chiche J, Pouyssegur J. pH control mechanisms of tumor survival and growth. *Journal of cellular physiology*. 2011 Feb;226(2):299–308.
137. Pouyssegur J, Dayan F, Mazure NM. Hypoxia signalling in cancer and approaches to enforce tumor regression. *Nature*. 2006 May 25;441(7092):437–43.
138. Adamski JK, Estlin EJ, Makin GWJ. The cellular adaptations to hypoxia as novel therapeutic targets in childhood cancer. *Cancer treatment reviews*. 2008 May;34(3):231–46.
139. Osthus RC, Shim H, Kim S, Li Q, Reddy R, Mukherjee M, et al. Deregulation of glucose transporter 1 and glycolytic gene expression by c-Myc. *The journal of biological chemistry*. 2000 Jul 21;275(29):21797–800.
140. Birnbaum MJ, Haspel HC, Rosen OM. Transformation of rat fibroblasts by FSV rapidly increases glucose transporter gene transcription. *Science (New York, N.Y.)*. 1987 Mar 20;235(4795):1495–8.
141. Flier JS, Mueckler MM, Usher P, Lodish HF. Elevated levels of glucose transport and transporter messenger RNA are induced by ras or src oncogenes. *Science (New York, N.Y.)*. 1987 Mar 20;235(4795):1492–5.
142. Yamamoto T, Seino Y, Fukumoto H, Koh G, Yano H, Inagaki N, et al. Over-expression of facilitative glucose transporter genes in human cancer. *Biochemical and biophysical research communications*. 1990 Jul 16;170(1):223–30.
143. Murakami T, Nishiyama T, Shirotani T, Shinohara Y, Kan M, Ishii K, et al. Identification of two enhancer elements in the gene encoding the type 1 glucose transporter from the mouse which are responsive to serum, growth factor, and oncogenes. *The journal of biological chemistry*. 1992 May 5;267(13):9300–6.
144. Le HB, Vaisanen PA, Johnson JL, Raney AK, McLachlan A. Regulation of transcription from the human muscle phosphofructokinase P2 promoter by the Sp1 transcription factor. *DNA and cell biology*. 1994 May;13(5):473–85.
145. Hwang D-Y, Ismail-Beigi F. Control of Glut1 promoter activity under basal conditions and in response to hyperosmolarity: role of Sp1. *American journal of physiology. Cell physiology*. 2006 Feb;290(2):C337–44.

146. Shaw RJ. Glucose metabolism and cancer. *Current opinion in cell biology*. 2006 Dec;18(6):598–608.
147. Ristow M. Oxidative metabolism in cancer growth. *Current opinion in clinical nutrition and metabolic care*. 2006 Jul;9(4):339–45.
148. Marín-Hernández A, Rodríguez-Enríquez S, Vital-González PA, Flores-Rodríguez FL, Macías-Silva M, Sosa-Garrocho M, et al. Determining and understanding the control of glycolysis in fast-growth tumor cells. Flux control by an over-expressed but strongly product-inhibited hexokinase. *The FEBS journal*. 2006 May;273(9):1975–88.
149. Iyer NV, Kotch LE, Agani F, Leung SW, Laughner E, Wenger RH, et al. Cellular and developmental control of O₂ homeostasis by hypoxia-inducible factor 1 alpha. *Genes & development*. 1998 Jan 15;12(2):149–62.
150. Ito S, Fukusato T, Nemoto T, Sekihara H, Seyama Y, Kubota S. Coexpression of glucose transporter 1 and matrix metalloproteinase-2 in human cancers. *Journal of the National Cancer Institute*. 2002 Jul 17;94(14):1080–91.
151. Sung J-Y, Kim GY, Lim S-J, Park Y-K, Kim YW. Expression of the GLUT1 glucose transporter and p53 in carcinomas of the pancreatobiliary tract. *Pathology, research and practice*. 2010 Jan 15;206(1):24–9.
152. Fenske W, Völker H-U, Adam P, Hahner S, Johanssen S, Wortmann S, et al. Glucose transporter GLUT1 expression is an stage-independent predictor of clinical outcome in adrenocortical carcinoma. *Endocrine-related cancer*. 2009 Sep;16(3):919–28.
153. Mori Y, Tsukinoki K, Yasuda M, Miyazawa M, Kaneko A, Watanabe Y. Glucose transporter type 1 expression are associated with poor prognosis in patients with salivary gland tumors. *Oral oncology*. 2007 Jul;43(6):563–9.
154. Tohma T, Okazumi S, Makino H, Cho A, Mochizuki R, Shuto K, et al. Overexpression of glucose transporter 1 in esophageal squamous cell carcinomas: a marker for poor prognosis. *Diseases of the esophagus : official journal of the International Society for Diseases of the Esophagus / I.S.D.E*. 2005 Jan;18(3):185–9.
155. Cleven AHG, van Engeland M, Wouters BG, de Bruïne AP. Stromal expression of hypoxia regulated proteins is an adverse prognostic factor in

colorectal carcinomas. *Cellular oncology : the official journal of the International Society for Cellular Oncology*. 2007 Jan;29(3):229–40.

156. Hoskin PJ, Sibtain A, Daley FM, Wilson GD. GLUT1 and CAIX as intrinsic markers of hypoxia in bladder cancer: relationship with vascularity and proliferation as predictors of outcome of ARCON. *British journal of cancer*. 2003 Oct 6;89(7):1290–7.
157. Mineta H, Miura K, Takebayashi S, Misawa K, Araki K, Misawa Y, et al. Prognostic value of glucose transporter 1 expression in patients with hypopharyngeal carcinoma. *Anticancer research*. 2002;22(6B):3489–94.
158. Schönberger J, Rüschoff J, Grimm D, Marienhagen J, Rümmele P, Meyringer R, et al. Glucose transporter 1 gene expression is related to thyroid neoplasms with an unfavorable prognosis: an immunohistochemical study. *Thyroid : official journal of the American Thyroid Association*. 2002 Sep;12(9):747–54.
159. Kang SS, Chun YK, Hur MH, Lee HK, Kim YJ, Hong SR, et al. Clinical significance of glucose transporter 1 (GLUT1) expression in human breast carcinoma. *Japanese journal of cancer research : Gann*. 2002 Oct;93(10):1123–8.
160. Kim YW, Park Y-K, Yoon TY, Lee SM. Expression of the GLUT1 glucose transporter in gallbladder carcinomas. *Hepato-gastroenterology*. 2002;49(46):907–11.
161. Kawamura T, Kusakabe T, Sugino T, Watanabe K, Fukuda T, Nashimoto A, et al. Expression of glucose transporter-1 in human gastric carcinoma: association with tumor aggressiveness, metastasis, and patient survival. *Cancer*. 2001 Aug 1;92(3):634–41.
162. Younes M, Brown RW, Stephenson M, Gondo M, Cagle PT. Overexpression of Glut1 and Glut3 in stage I nonsmall cell lung carcinoma is associated with poor survival. *Cancer*. 1997 Sep 15;80(6):1046–51.
163. Rastogi S, Banerjee S, Chellappan S, Simon GR. Glut-1 antibodies induce growth arrest and apoptosis in human cancer cell lines. *Cancer letters*. 2007 Nov 18;257(2):244–51.
164. Chen C-L, Chu J-S, Su W-C, Huang S-C, Lee W-Y. Hypoxia and metabolic phenotypes during breast carcinogenesis: expression of HIF-1 α , GLUT1, and CAIX. *Virchows Archiv : an international journal of pathology*. 2010 Jul;457(1):53–61.

165. Semenza GL. HIF-1: upstream and downstream of cancer metabolism. *Current opinion in genetics & development*. 2010 Feb;20(1):51–6.
166. Wang GL, Jiang BH, Rue EA, Semenza GL. Hypoxia-inducible factor 1 is a basic-helix-loop-helix-PAS heterodimer regulated by cellular O₂ tension. *Proceedings of the National Academy of Sciences of the United States of America*. 1995 Jun 6;92(12):5510–4.
167. Matsumoto S, Yasui H, Mitchell JB, Krishna MC. Imaging cycling tumor hypoxia. *Cancer research*. 2010 Dec 15;70(24):10019–23.
168. Sakata K-ichi, Someya M, Nagakura H, Nakata K, Oouchi A, Hareyama M, et al. A clinical study of hypoxia using endogenous hypoxic markers and polarographic oxygen electrodes. *Strahlentherapie und Onkologie*. 2006 Sep;182(9):511–7.
169. Greer SN, Metcalf JL, Wang Y, Ohh M. The updated biology of hypoxia-inducible factor. *The EMBO journal*. 2012 May 4;
170. Meneses AM, Medina RA, Kato S, Pinto M, Jaque MP, Lizama I, et al. Regulation of GLUT3 and glucose uptake by the cAMP signalling pathway in the breast cancer cell line ZR-75. *Journal of cellular physiology*. 2008 Jan;214(1):110–6.
171. Khandani AH, Dunphy CH, Meteesatien P, Dufault DL, Ivanovic M, Shea TC. Glut1 and Glut3 expression in lymphoma and their association with tumor intensity on 18F-fluorodeoxyglucose positron emission tomography. *Nuclear medicine communications*. 2009 Aug;30(8):594–601.
172. Pedersen PL, Mathupala S, Rempel A, Geschwind JF, Ko YH. Mitochondrial bound type II hexokinase: a key player in the growth and survival of many cancers and an ideal prospect for therapeutic intervention. *Biochimica et biophysica acta*. 2002 Sep 10;1555(1-3):14–20.
173. Mathupala SP, Rempel A, Pedersen PL. Aberrant glycolytic metabolism of cancer cells: a remarkable coordination of genetic, transcriptional, post-translational, and mutational events that lead to a critical role for type II hexokinase. *Journal of bioenergetics and biomembranes*. 1997 Aug;29(4):339–43.
174. Brown RS, Goodman TM, Zasadny KR, Greenson JK, Wahl RL. Expression of hexokinase II and Glut-1 in untreated human breast cancer. *Nuclear medicine and biology*. 2002 May;29(4):443–53.

175. Bayley J-P, Devilee P. The Warburg effect in 2012. *Current opinion in oncology*. 2012 Jan;24(1):62–7.
176. Mathupala SP, Heese C, Pedersen PL. Glucose catabolism in cancer cells. The type II hexokinase promoter contains functionally active response elements for the tumor suppressor p53. *The Journal of biological chemistry*. 1997 Sep 5;272(36):22776–80.
177. Beutner G, Rück A, Riede B, Brdiczka D. Complexes between porin, hexokinase, mitochondrial creatine kinase and adenylate translocator display properties of the permeability transition pore. Implication for regulation of permeability transition by the kinases. *Biochimica et biophysica acta*. 1998 Jan 5;1368(1):7–18.
178. Pastorino JG, Shulga N, Hoek JB. Mitochondrial binding of hexokinase II inhibits Bax-induced cytochrome c release and apoptosis. *The Journal of biological chemistry*. 2002 Mar 1;277(9):7610–8.
179. Vora S, Halper JP, Knowles DM. Alterations in the activity and isozymic profile of human phosphofructokinase during malignant transformation in vivo and in vitro: transformation- and progression-linked discriminants of malignancy. *Cancer research*. 1985 Jul;45(7):2993–3001.
180. Atsumi T, Chesney J, Metz C, Leng L, Donnelly S, Makita Z, et al. High expression of inducible 6-phosphofructo-2-kinase/fructose-2,6-bisphosphatase (iPFK-2; PFKFB3) in human cancers. *Cancer research*. 2002 Oct 15;62(20):5881–7.
181. Semenza GL. Targeting HIF-1 for cancer therapy. *Nature reviews. Cancer*. 2003 Oct;3(10):721–32.
182. Zu XL, Guppy M. Cancer metabolism: facts, fantasy, and fiction. *Biochemical and biophysical research communications*. 2004 Jan 16;313(3):459–65.
183. Ramanathan A, Wang C, Schreiber SL. Perturbational profiling of a cell-line model of tumorigenesis by using metabolic measurements. *Proceedings of the National Academy of Sciences of the United States of America*. 2005 Apr 26;102(17):5992–7.
184. Jemal A, Murray T, Ward E, Samuels A, Tiwari RC, Ghafoor A, et al. *Cancer statistics, 2005*. CA: a cancer journal for clinicians. 2005. 55(1):10–30.

185. Dumitrescu RG, Cotarla I. Understanding breast cancer risk -- where do we stand in 2005? *Journal of cellular and molecular medicine*. 2005. 9(1):208–21.
186. Aebi S, Davidson T, Gruber G, Cardoso F. Primary breast cancer: ESMO Clinical Practice Guidelines for diagnosis, treatment and follow-up. *Annals of oncology : official journal of the European Society for Medical Oncology / ESMO*. 2011 Sep;22 Suppl 6:vi12–24.
187. Medina RA, Owen GI. Glucose transporters: expression, regulation and cancer. *Biological research*. 2002 Jan;35(1):9–26.
188. Hennipman A, Smits J, van Oirschot B, van Houwelingen JC, Rijksen G, Neyt JP, et al. Glycolytic enzymes in breast cancer, benign breast disease and normal breast tissue. *Tumor biology : the journal of the International Society for Oncodevelopmental Biology and Medicine*. 1987 Jan;8(5):251–63.
189. Zancan P, Sola-Penna M, Furtado CM, Da Silva D. Differential expression of phosphofructokinase-1 isoforms correlates with the glycolytic efficiency of breast cancer cells. *Molecular genetics and metabolism*. 2010 Aug;100(4):372–8.
190. Young CD, Lewis AS, Rudolph MC, Ruehle MD, Jackman MR, Yun UJ, et al. Modulation of glucose transporter 1 (GLUT1) expression levels alters mouse mammary tumor cell growth in vitro and in vivo. *PloS one*. 2011 Jan;6(8):e23205.
191. Younes M, Brown RW, Mody DR, Fernandez L, Laucirica R. GLUT1 expression in human breast carcinoma: correlation with known prognostic markers. *Anticancer research*. 15(6B):2895–8.
192. Ravazoula P, Batistatou A, Aletra C, Ladopoulos J, Kourounis G, Tzigounis B. Immunohistochemical expression of glucose transporter Glut1 and cyclin D1 in breast carcinomas with negative lymph nodes. *European journal of gynaecological oncology*. 2003 Jan;24(6):544–6.
193. Laudański P, Koda M, Kozłowski L, Swiatecka J, Wojtukiewicz M, Sulkowski S, et al. Expression of glucose transporter GLUT-1 and estrogen receptors ER-alpha and ER-beta in human breast cancer. *Neoplasma*. 2004 Jan;51(3):164–8.

194. Funasaka T, Hogan V, Raz A. Phosphoglucose isomerase/autocrine motility factor mediates epithelial and mesenchymal phenotype conversions in breast cancer. *Cancer research*. 2009 Jul 1;69(13):5349–56.
195. Hennipman A, van Oirschot BA, Smits J, Rijksen G, Staal GE. Glycolytic enzyme activities in breast cancer metastases. *Tumor biology : the journal of the International Society for Oncodevelopmental Biology and Medicine*. 1988 Jan;9(5):241–8.
196. Thongwatchara P, Promwikorn W, Srisomsap C, Chokchaichamnankit D, Boonyaphiphat P, Thongsuksai P. Differential protein expression in primary breast cancer and matched axillary node metastasis. *Oncology reports*. 2011 Jul;26(1):185–91.
197. Révillion F, Pawlowski V, Hornez L, Peyrat JP. Glyceraldehyde-3-phosphate dehydrogenase gene expression in human breast cancer. *European journal of cancer (Oxford, England : 1990)*. 2000 May;36(8):1038–42.
198. Hoopmann M, Warm M, Mallmann P, Thomas A, Göhring U-J, Schöndorf T. Tumor M2 pyruvate kinase--determination in breast cancer patients receiving trastuzumab therapy. *Cancer letters*. 2002 Dec 10;187(1-2):223–8.
199. Wang Z-Y, Loo TY, Shen J-G, Wang N, Wang D-M, Yang D-P, et al. LDH-A silencing suppresses breast cancer tumorigenicity through induction of oxidative stress mediated mitochondrial pathway apoptosis. *Breast cancer research and treatment*. 2012 Feb;131(3):791–800.
200. Mankoff DA. A definition of molecular imaging. *Journal of nuclear medicine : official publication, Society of Nuclear Medicine*. 2007 Jun;48(6):18N, 21N.
201. Ido T, Wan C-N, Casella V, Fowler JS, Wolf AP, Reivich M, et al. Labeled 2-deoxy-D-glucose analogs. 18F-labeled 2-deoxy-2-fluoro-D-glucose, 2-deoxy-2-fluoro-D-mannose and 14C-2-deoxy-2-fluoro-D-glucose. *Journal of labelled compounds and radiopharmaceuticals*. 1978;14:175–83.
202. Coe EL. Inhibition of glycolysis in ascites tumor cells preincubated with 2-deoxy-2-fluoro-D-glucose. *Biochimica et biophysica acta*. 1972 Apr 21;264(2):319–27.
203. Bessell EM, Foster AB, Westwood JH. The use of deoxyfluoro-D-glucopyranoses and related compounds in a study of yeast hexokinase specificity. *The biochemical journal*. 1972 Jun;128(2):199–204.

204. Fowler JS, Ido T. Initial and subsequent approach for the synthesis of ¹⁸F-DG. *Seminars in nuclear medicine*. 2002 Jan;32(1):6–12.
205. Thomas P, Bessel EM. The effect of substitution at C-2 of D-glucose 6-phosphate on the rate of dehydrogenation by yeast glucose 6-phosphate dehydrogenase. *The biochemical journal*. 1972 Nov;130(1):21P.
206. Sols A, Crane RK. Substrate specificity of brain hexokinase. *The Journal of biological chemistry*. 1954 Oct;210(2):581–95.
207. Reivich M, Kuhl D, Wolf A, Greenberg J, Phelps M, Ido T, et al. The [¹⁸F]fluorodeoxyglucose method for the measurement of local cerebral glucose utilization in man. *Circulation research*. 1979 Jan;44(1):127–37.
208. Bessell EM, Courtenay VD, Foster AB, Jones M, Westwood JH. Some in vivo and in vitro antitumor effects of the deoxyfluoro-D-glucopyranoses. *European journal of cancer*. 1973 Jul;9(7):463–70.
209. Laszlo J, Harlan WR, Klein RF, Kirshner N, Estes EH, Bogdonoff MD. The effect of 2-deoxy-D-glucose infusions on lipid and carbohydrate metabolism in man. *The journal of clinical investigation*. 1961 Jan;40:171–6.
210. Som P, Atkins HL, Bandoypadhyay D, Fowler JS, MacGregor RR, Matsui K, et al. A fluorinated glucose analog, 2-fluoro-2-deoxy-D-glucose (F-18): nontoxic tracer for rapid tumor detection. *Journal of nuclear medicine : official publication, Society of Nuclear Medicine*. 1980 Jul;21(7):670–5.
211. Som P, Atkins HL, Bandoypadhyay D, Fowler JS, MacGregor RR, Matsui K, et al. A fluorinated glucose analog, 2-fluoro-2-deoxy-D-glucose (F-18): nontoxic tracer for rapid tumor detection. *Journal of nuclear medicine : official publication, Society of Nuclear Medicine*. 1980 Jul;21(7):670–5.
212. Fletcher JW, Djulbegovic B, Soares HP, Siegel BA, Lowe VJ, Lyman GH, et al. Recommendations on the use of ¹⁸F-FDG PET in oncology. *Journal of nuclear medicine : official publication, Society of Nuclear Medicine*. 2008 Mar;49(3):480–508.
213. Gallagher BM, Fowler JS, Gutterson NI, MacGregor RR, Wan CN, Wolf AP. Metabolic trapping as a principle of radiopharmaceutical design: some factors responsible for the biodistribution of [¹⁸F] 2-deoxy-2-fluoro-D-glucose. *Journal of nuclear medicine : official publication, Society of Nuclear Medicine*. 1978 Oct;19(10):1154–61.

214. Oude Munnink TH, Nagengast WB, Brouwers AH, Schröder CP, Hospers GA, Lub-de Hooge MN, et al. Molecular imaging of breast cancer. *Breast (Edinburgh, Scotland)*. 2009 Oct;18 Suppl 3:S66–73.
215. Silverman M, Aganon MA, Chinard FP. Specificity of monosaccharide transport in dog kidney. *The American journal of physiology*. 1970 Mar;218(3):743–50.
216. Lavayssière R, Cabée A-E, Filmont J-E. Positron Emission Tomography (PET) and breast cancer in clinical practice. *European journal of radiology*. 2009 Jan;69(1):50–8.
217. Lind P, Igerc I, Beyer T, Reinprecht P, Hausegger K. Advantages and limitations of FDG PET in the follow-up of breast cancer. *European journal of nuclear medicine and molecular imaging*. 2004 Jun;31 Suppl 1(June):S125–34.
218. Quon A, Gambhir SS. FDG-PET and beyond: molecular breast cancer imaging. *Journal of clinical oncology : official journal of the American Society of Clinical Oncology*. 2005 Mar 10;23(8):1664–73.
219. Hodgson NC, Gulenchyn KY. Is there a role for positron emission tomography in breast cancer staging? *Journal of clinical oncology : official journal of the American Society of Clinical Oncology*. 2008 Feb 10;26(5):712–20.
220. Santiago JFY, Gonen M, Yeung H, Macapinlac H, Larson S. A retrospective analysis of the impact of 18F-FDG PET scans on clinical management of 133 breast cancer patients. *The quarterly journal of nuclear medicine and molecular imaging : official publication of the Italian Association of Nuclear Medicine (AIMN) [and] the International Association of Radiopharmacology (IAR), [and] Section of the Society of Radiopharmaceutica*. 2006 Mar;50(1):61–7.
221. Mavi A, Urhan M, Yu JQ, Zhuang H, Houseni M, Cermik TF, et al. Dual time point 18F-FDG PET imaging detects breast cancer with high sensitivity and correlates well with histologic subtypes. *Journal of nuclear medicine : official publication, Society of Nuclear Medicine*. 2006 Sep;47(9):1440–6.
222. Weir L, Worsley D, Bernstein V. The value of FDG positron emission tomography in the management of patients with breast cancer. *The breast journal*. 2005;11(3):204–9.

223. Buck A, Schirrmeister H, Kühn T, Shen C, Kalker T, Kotzerke J, et al. FDG uptake in breast cancer: correlation with biological and clinical prognostic parameters. *European journal of nuclear medicine and molecular imaging*. 2002 Oct;29(10):1317–23.
224. Kim BS, Sung SH. Usefulness of 18F-FDG uptake with clinicopathologic and immunohistochemical prognostic factors in breast cancer. *Annals of nuclear medicine*. 2012 Feb;26(2):175–83.
225. Groves AM, Shastry M, Rodriguez-Justo M, Malhotra A, Endozo R, Davidson T, et al. 18F-FDG PET and biomarkers for tumor angiogenesis in early breast cancer. *European journal of nuclear medicine and molecular imaging*. 2011 Jan;38(1):46–52.
226. Bos R, van Der Hoeven JJM, van Der Wall E, van Der Groep P, van Diest PJ, Comans EFI, et al. Biologic correlates of (18)fluorodeoxyglucose uptake in human breast cancer measured by positron emission tomography. *Journal of clinical oncology : official journal of the American Society of Clinical Oncology*. 2002 Jan 15;20(2):379–87.
227. Kubota R, Kubota K, Yamada S, Tada M, Ido T, Tamahashi N. Microautoradiographic study for the differentiation of intratumoral macrophages, granulation tissues and cancer cells by the dynamics of fluorine-18-fluorodeoxyglucose uptake. *Journal of nuclear medicine : official publication, Society of Nuclear Medicine*. 1994 Jan;35(1):104–12.
228. Alavi A, Zhuang H. Finding infection--help from PET. *Lancet*. 2001 Oct 27;358(9291):1386.
229. Shor M, Dave N, Reddy M, Ali A. Asymmetric FDG uptake in a lactating breast. *Clinical nuclear medicine*. 2002 Jul;27(7):536.
230. Ginat DT, Puri S. FDG PET/CT manifestations of hematopoietic malignancies of the breast. *Academic radiology*. 2010 Aug;17(8):1026–30.
231. Berg WA, Weinberg IN, Narayanan D, Lobrano ME, Ross E, Amodei L, et al. High-resolution fluorodeoxyglucose positron emission tomography with compression (“positron emission mammography”) is highly accurate in depicting primary breast cancer. *The breast journal*. 2006;12(4):309–23.
232. Lim HS, Yoon W, Chung TW, Kim JK, Park JG, Kang HK, et al. FDG PET/CT for the detection and evaluation of breast diseases: usefulness and limitations. *Radiographics : a review publication of the Radiological Society of North America, Inc*. 2007 Oct;27 Suppl 1:S197–213.

233. Kumar R, Alavi A. Fluorodeoxyglucose-PET in the management of breast cancer. *Radiol Clin North Am.* 2004;42:1113–22.
234. Facey K, Bradbury I, Laking G, Payne E. Overview of the clinical effectiveness of positron emission tomography imaging in selected cancers. *Health technology assessment (Winchester, England).* 2007 Oct;11(44):iii-iv, xi–267.
235. Buck AK, Schirrmeister H, Mattfeldt T, Reske SN. Biological characterisation of breast cancer by means of PET. *Eur J Nucl Med Mol Imaging.* 2004 Jun;31 Suppl 1:S80-7.
236. Mahner S, Schirmacher S, Brenner W, Jenicke L, Habermann CR, Avril N, et al. Comparison between positron emission tomography using 2-[fluorine-18]fluoro-2-deoxy-D-glucose, conventional imaging and computed tomography for staging of breast cancer. *Annals of oncology : official journal of the European Society for Medical Oncology / ESMO.* 2008 Jul;19(7):1249–54.
237. Yang WT, Le-Petross HT, Macapinlac H, Carkaci S, Gonzalez-Angulo AM, Dawood S, et al. Inflammatory breast cancer: PET/CT, MRI, mammography, and sonography findings. *Breast cancer research and treatment.* 2008 Jun;109(3):417–26.
238. Minn H, Soini I. [18F]fluorodeoxyglucose scintigraphy in diagnosis and follow up of treatment in advanced breast cancer. *European journal of nuclear medicine.* 1989 Jan;15(2):61–6.
239. Iagaru A, Masamed R, Keesara S, Conti PS. Breast MRI and 18F FDG PET/CT in the management of breast cancer. *Annals of nuclear medicine.* 2007 Jan;21(1):33–8.
240. Kluetz PG, Meltzer CC, Villemagne VL, Kinahan PE, Chander S, Martinelli MA, et al. Combined PET/CT Imaging in Oncology. Impact on Patient Management. *Clinical positron imaging : official journal of the Institute for Clinical P.E.T.* 2000 Nov;3(6):223–30.
241. Thie J. Understanding the standardized uptake value, its methods, and implications for usage. *Journal of nuclear medicine.* 2004:1431–4.
242. Thie JA, Hubner KF, Smith GT. The diagnostic utility of the lognormal behavior of PET standardized uptake values in tumors. *Journal of nuclear medicine : official publication, Society of Nuclear Medicine.* 2000 Oct;41(10):1664–72.

243. Chan KK, Chan JYW, Chung KKW, Fung K-P. Inhibition of cell proliferation in human breast tumor cells by antisense oligonucleotides against facilitative glucose transporter 5. *Journal of cellular biochemistry*. 2004 Dec 15;93(6):1134–42.
244. Gouyon F, Onesto C, Dalet V, Pages G, Leturque A, Brot-Laroche E. Fructose modulates GLUT5 mRNA stability in differentiated Caco-2 cells: role of cAMP-signalling pathway and PABP (polyadenylated-binding protein)-interacting protein (Paip) 2. *The biochemical journal*. 2003 Oct 1;375(Pt 1):167–74.
245. Levi J, Cheng Z, Gheysens O, Patel M, Chan CT, Wang Y, et al. Fluorescent fructose derivatives for imaging breast cancer cells. *Bioconjugate chemistry*. 2007;18(3):628–34.
246. Heman RH, Zakim D. Fructose metabolism. I. The fructose metabolic pathway. *The American journal of clinical nutrition*. 1968 Mar;21(3):245–9.
247. Lu X, Bennet B, Mu E, Rabinowitz J, Kang Y. Metabolomic changes accompanying transformation and acquisition of metastatic potential in a syngeneic mouse mammary tumor model. *The Journal of biological chemistry*. 2010 Mar 26;285(13):9317–21.
248. Haradahira T, Tanaka A, Maeda M, Kanazawa Y, Ichiya YI, Masuda K. Radiosynthesis, rodent biodistribution, and metabolism of 1-deoxy-1-[18F]fluoro-D-fructose. *Nuclear medicine and biology*. 1995 Aug;22(6):719–25.
249. Yang J, Dowden J, Tatiboue A, Hatanaka Y, Holman GD. Development of high-affinity ligands and photoaffinity labels for the D-fructose transporter GLUT5. *Biochemical journal*. 2002 Oct 15;367(Pt 2):533-9.
250. Schilling K, Narayanan D, Kalinyak JE, The J, Velasquez MV, Kahn S, Saady M, Mahal R, Chrystal L. Positron emission mammography in breast cancer presurgical planning: comparisons with magnetic resonance imaging. *Eur J Nucl Med Mol Imaging*. 2011 Jan;38(1):23-36.
251. Berg WA, Madsen KS, Schilling K, Tartar M, Pisano ED, Larsen LH, Narayanan D, Kalinyak JE. Comparative effectiveness of positron emission mammography and MRI in the contralateral breast of women with newly diagnosed breast cancer. *AJR Am J Roentgenol*. 2012 Jan;198(1):219-32.

Chapter 2 - Synthesis and characterization of 6-deoxy-6-fluoro-D-fructose as a potential compound for imaging breast cancer with PET

A version of this chapter has been published:

Trayner BJ, Grant TN, West FG, Cheeseman CI. Synthesis and characterization of 6-deoxy-6-fluoro-D-fructose as a potential compound for imaging breast cancer with PET. *Bioorganic & Medicinal Chemistry*. 2009. 17(15):5488–95.

This work presented in this chapter represents a collaboration between the authors on the paper. BJT performed all in vitro experiments and analysis herein. All chemistry was done by TNG.

2.1 Introduction

Positron emission tomography (PET) is widely used as an effective diagnostic tool in the detection of breast cancer. The traditional method of tumor imaging with PET uses 2-deoxy-2- ^{18}F fluoro-D-glucose (^{18}F FDG) as the imaging agent, which takes advantage of the characteristic overexpression of facilitated hexose transporter isoform GLUT1 (SLC2A1) in cancerous cells. FDG is subsequently trapped and accumulated within the cells as the result of phosphorylation at the 6-position by hexokinase II, an enzyme that is also overexpressed in many cancers(1–3). ^{18}F FDG-PET has been most successfully used in the evaluation of metastatic and recurring cancer, but has also shown to be effective in detection in certain cases of the primary disease (4–7). Unfortunately, while FDG has been used to the benefit of many patients, it cannot be transported by any of the Class II GLUTs (GLUTs 5, 7, 9 and 11), which may explain why FDG-PET sensitivity and specificity of primary disease are often less than desired (8). Particularly in the case of breast cancer, it has become recognized that the Class II hexose transporter GLUT5, which can readily move fructose across the cell membrane, is more highly expressed in transformed breast tissue compared to normal, untransformed tissue (9–12). Not only is GLUT5 overexpressed, but the Class I glucose/fructose-transporting isoform GLUT2 is also overexpressed in cancerous breast tissue (10) which likely contributes to increased fructose uptake in these tumor cells. The increased expression of both GLUT5 and GLUT2 may be indicative of the cells' broadening

their substrate preference to compensate for an increased demand for metabolic fuel. This theory is supported by the observed ability of anti-sense oligonucleotide induced knockdown of GLUT5 to decrease the proliferation of breast cancer cells *in vivo*(13). The knowledge that breast cancers exhibit overexpression of GLUT5 and GLUT2 has prompted many researchers to hypothesize that an ¹⁸F-labelled fructose analogue may have great potential for the imaging and diagnosis of these tumors since [¹⁸F]FDG cannot be transported by GLUT5 or any of the other class II GLUTs (9,10,14). Thus, radiolabelled fructose analogues that are targeted to the Class II fructose-transporting GLUT5 and the Class I glucose/fructose-transporting GLUT2 may reveal a new avenue for improved imaging of breast cancer and perhaps other cancers with similar GLUT expression profiles.

While [¹⁸F]FDG-PET imaging has been very useful in the clinical setting (2,4,5,15–20) it is unfortunately not very effective in the detection of small tumors, and more differentiated sub-types such as tubular carcinomas or lobular carcinomas (6,21,22). GLUT1, the primary entry point for glucose and FDG into cancer cells has also shown variability in its expression in breast cancer, that may lead to false-negatives using [¹⁸F]FDG -PET (23–25). Imaging with ¹⁸F-labelled fructose derivatives may provide an improvement in this and other areas, including the monitoring of cancer progression in response to treatment with chemotherapeutic agents. Another exciting prospect for the use of fructose-based PET tracers is the potential for improved image resolution with clear

distinction of tumor cells from surrounding inflammation. Macrophages and other immune cells involved in inflammatory processes throughout the body have been implicated in the generation of false positives when using FDG-PET due to increased uptake of large quantities of glucose and FDG by these cells(26). Macrophages are also strongly associated with tumor sites and contribute a large percentage of the total cell count, especially after treatment with chemotherapeutics when macrophage numbers actually increase due to the destruction of tumor cells. This phenomenon can be responsible for an increase in the observed [^{18}F]FDG uptake by PET, generating false-positives in images used to monitor treatment efficacy (27,28). In this respect, an ^{18}F -labelled fructose analogue might circumvent this issue since it would not be transported well into immune cells, which have characteristically low expression of both GLUT2 and GLUT5 compared to GLUT1 and GLUT3. Therefore, a fructose-based PET tracer has the potential to clearly illuminate tumor cells associated with fructose uptake and metabolism, improving image resolution by eliminating the contribution from immune cells. The development of new ^{18}F -labelled fructose derivatives for use with PET may very well lead to a powerful tool for clinicians, providing clear images, uptake into GLUT1 negative, GLUT5 expressing tumor tissues and perhaps may assist in determining a more accurate picture of the status and health of a tumor.

When designing an ^{18}F -labelled fructose compound for use with PET, it is important to consider the placement of the fluorine as it can have important

implications with regard to its transport and subsequent metabolism. This fact was exemplified by Maeda's work wherein substitution of ^{18}F at the 1-position of fructose afforded a compound that was taken up into cells, but not specifically localized or trapped in tissues with high fructose metabolism (14). It also demonstrated that metabolism of the fructose analogue was dramatically influenced by fluorination at C-1, although transport remained unaffected. Holman and co-workers' (29,30) investigation into high-affinity ligands for GLUT5 has shown that substitution at the 6-position is well tolerated by the transporter and, in some instances, can actually increase the molecule's affinity. An increase in substrate affinity would be a considerable advantage for a fructose analogue that is to be used with PET since, when working with patients, relatively small concentrations of tracer will be injected requiring high affinity transport *in vivo* to ensure its efficacy as a PET tracer. For these reasons, our initial investigations into the development of fructose-derived PET tracers have focused on the incorporation of fluorine at the C-6 position.

A significant factor that must also be considered when designing a novel PET tracer is the potential for that tracer to be retained within tumor cells once transported inside. As previously mentioned, FDG is transported into cells and phosphorylated once, which leads to the accumulation of ^{18}F in these locations for facile imaging with PET. Fructose analogues can enter cancerous cells and be trapped and accumulated via one of two possible routes involving phosphorylation by hexokinase at the C-6 position or ketohexokinase (KHK) at

position 1 (12). Each enzyme possesses a different affinity and reactivity towards fructose, so the placement of fluorine at either the C-6 or C-1 position would still leave the other position open for phosphorylation by the other enzyme. We postulate that 6-deoxy-6-fluoro-D-fructose (6-FDF) would be readily transported by GLUT5 and thereafter be subject to phosphorylation by KHK. We present herein the successful chemical synthesis of 6-FDF, a fluorinated fructose derivative that has now been thoroughly characterized as a substrate for transport by GLUT2 and GLUT5 in two breast cancer cell lines.

2.2 Results and discussion

2.2.1 *Synthesis of 6-FDF*

The synthesis of 6-FDF was accomplished in 7 steps from fructose (**Scheme 2.1**). Treatment of fructose with acidic methanol afforded a mixture of methyl α/β -D-fructofuranosides **2**, which could be separated using standard silica gel chromatography or, alternatively, carried on as a mixture. Selective protection of the primary C-6 hydroxyl with *tert*-butyldimethylchlorosilane (TBDMSCl) in pyridine, followed by global acetylation afforded intermediate **4** in moderate yield over the 2 steps. Subsequently, the silyl protecting group was removed by treatment with aqueous trifluoroacetic acid in dichloromethane to provide the known intermediate **5** in 91% (30). This compound was then fluorinated *via* triflation under standard conditions and immediate treatment with 3 equivalents of cesium fluoride in refluxing *tert*-amyl alcohol (31). The success of the quick

and clean fluoride displacement reaction is very encouraging since, in the future, this step will be imperative to the installation of ^{18}F for initial imaging experiments. Standard deprotection of the acetates using sodium methoxide followed by acidic hydrolysis of the methyl fructofuranoside provided 6-FDF (**7**) as a white solid in 62% (2 steps).

2.2.2 Hexose transport in MCF-7 and MDA-MB-231

Before we examined 6-FDF transport, we chose to characterize hexose uptake and the pattern of expression of specific GLUTs in two human breast cancer cell lines. A cell culture transport model was utilized with the two cell lines MCF-7 and MDA-MB-231 based on their use in recent investigations of fructose transport in breast tumors and their representation of early and late stage breast cancer, respectively (12,13). Initially, experiments were carried out in order to ascertain the ability of both MDA-MB-231 and MCF-7 to transport glucose and fructose. A 30 minute time course was performed with [^{14}C]-D-glucose and [^{14}C]-D-fructose and, after correcting the data for residual extracellular levels of hexose, we saw clear uptake of both substrates (**Figure 2.1**) with what appears to be the start of a plateau at around 30 minutes. MDA-MB-231 cells showed a much higher level of glucose uptake than MCF-7 cells, and fructose transport was comparable between the two cell lines. The large disparity in glucose transport between the two cell lines is most likely indicative of differential levels of GLUT1 in the membrane, which corresponds with previous literature and the consequence of which will be discussed below (23,32).

The breast adenocarcinoma cells used in this experiment are known to express several of the GLUT isoforms, which made it important to dissect the components of these fluxes in order to see which GLUTs contributed to glucose, and more importantly, fructose transport. We utilized several techniques in order to determine the influence of each GLUT in the system. Firstly, Western blots utilizing a wide range of anti-GLUT antibodies were performed (**Figure 2.2**), allowing us to visualize which isoforms may actually be contributing to total transport in these cell lines, and to confirm previous expression data from the literature (9,13,23). Secondly, immunocytochemistry provided information regarding the localization of the GLUT proteins detected in the Western blots and isoform contributions to uptake due to their presence in the membrane (**Figure 2.3**). Thirdly, and most importantly, was the use of the Class I GLUT inhibitor cytochalasin B (33,34) (**Figure 2.4 and 2.8**), which inhibits fructose transport mediated by GLUT2 and therefore, by subtraction, provides direct insight into the contribution of GLUT5 to the total fructose flux. While both the Western blots and immunocytochemistry clarified some characteristics of hexose transport in the cells, functional data presents a much more definitive picture.

Western blots utilizing 25µg of total protein obtained from both MCF-7 and MDA-MB-231 (**Figure 2.2**) indicate that both cell lines express GLUT5 and GLUT2. Functional data however, points towards MDA-MB-231 having much higher membrane expression of GLUT2 (**Figure 2.4**). Immunocytochemistry for both cell lines also show clear cytosolic and membrane expression of both fructose

transporting isoforms, which is in agreement with previous literature(9). The major glucose-transporting isoform GLUT1, was much more highly expressed within MDA-MB-231 cells compared to MCF-7 which is also in agreement with the literature(23). Low levels of GLUT9 are also present in both cell lines and appear to be localized in the perinuclear region (immunocytochemistry data not shown). The localization and recent recognition of GLUT9 as a mediator of urate transport(35) leads us to believe that it would have very minimal influence on the total hexose flux across the membrane.

Despite what has previously been reported(36), neither the Western blots nor immunocytochemistry indicated the presence of GLUT12 in MCF-7 while the lack of expression in MDA-MB-231 is consistent (immunocytochemistry data not shown). Finally, both functional and Western blot data suggest that the MDA-MB-231 cell line displays more GLUT1 in the membrane compared to MCF-7 cells and consequently higher glucose flux observed in MDA-MB-231 cells (**Figure 2.2**), which is consistent with previous observations.

Localization analysis with immunocytochemistry showed that both GLUT2 and GLUT5 are present in the membrane and in the cytoplasm of the two cell lines (**Figure 2.4**); however, functional data suggests that the quantities of each isoform in the membranes vary (**Figure 2.5**). Data obtained utilizing [¹⁴C]-D-fructose and treatment with 100 μM CB has shown that GLUT2 plays a minor part in the total fructose flux across the membrane of MCF-7 cells (~12%), while

in MDA-MB-231 cells approximately 30% of the total fructose flux is mediated by GLUT2. These results provide evidence that GLUT5 mediates the largest component of fructose transport in both cell lines. Recognition of the minor influence of GLUT2 on the total fructose flux, along with the large body of literature focusing on GLUT5 in human breast cancer (9,10,12), prompted our selection of MCF-7 cells as a good model system for further investigation into the transportability of 6-FDF.

2.2.3 *Inhibition studies*

Since we have clearly demonstrated the expression of GLUT2 and GLUT5 as well as the transport of fructose mediated by both isoforms in the two cell lines, the next step was to examine substrate competition and inhibition of fructose and glucose transport by 6-FDF. We performed hexose transport inhibition studies with both MCF-7 and MDA-MB-231 cells and saw clear dose dependent inhibition of [¹⁴C]-D-fructose and [¹⁴C]-D-glucose transport by increasing the concentrations of 6-FDF in the incubation media. The influence of GLUT2 on the total flux was evident as glucose transport can be inhibited by 6-FDF with a IC₅₀ of approximately 1.05 ± 0.30 mM in MCF-7 (**Figure 2.5A**) and a IC₅₀ of 6.21 ± 2.86 mM MDA-MB-231 (**Figure 2.5B**). Fructose transport was also clearly inhibited by increasing concentrations of 6-FDF, and the IC₅₀ obtained for MCF-7 was 0.18 ± 0.05 mM (**Figure 2.6A**) and MDA-MB-231 (**Figure 2.6B**) had an IC₅₀ of 0.33 ± 0.15 mM.

2.2.4 Uptake of [¹⁴C]6-FDF

Inhibition of fructose transport by 6-FDF indicates that the fluorinated fructose analogue can bind to both GLUT2 and GLUT5 with high affinity in both cell lines. Glucose transport inhibition by 6-FDF is also a strong indicator that 6-FDF binds to GLUT2. While the inhibition of both glucose and fructose transport is evidence for binding, confirmation of transport into the cells is needed to prove that 6-FDF is being moved across the membrane. In order to perform uptake experiments, ¹⁴C-labelled 6-FDF was synthesized using the previously described synthetic pathway (**Scheme 2.1**) and [¹⁴C]-D-fructose as starting material. The synthesis of [¹⁴C]6-FDF (SA ~ 1 μCi/mL) was accomplished after 7 steps with a 13% overall yield. Only 3 purification steps were performed during this synthesis so as to limit unnecessary exposure to the radiolabeled compound.

A 90 minute time course experiment was performed for each cell line, using the [¹⁴C]6-FDF and uptake was observed into both cell lines (**Figure 2.7**). Current literature reports that neither MCF-7 nor MDA-MB-231 cells express ketohexokinase (12), which would suggest that the potential for phosphorylation of a 6-fluorinated fructose compound would be limited; however, it is unknown based on this data whether there are other interactions within the cell that prevent the efflux of 6-FDF. [¹⁴C]6-FDF uptake in our GLUT5 model cell line (MCF-7) was also performed and the inhibitory effect of the class I inhibitor cytochalasin B was observed. After a 60 minute incubation, a student's t-test determined a non-significant impact on [¹⁴C]6-FDF transport into MCF-7 (**Figure**

2.8). This result confirms our previous observation that GLUT5 is the major contributor to fructose movement across the plasma membrane, while also strongly implicating GLUT5 in the successful transport of [¹⁴C]6-FDF into MCF-7 cells.

Our experimental results have demonstrated the ability of 6-FDF to inhibit fructose transport mediated by GLUT2 and GLUT5 with a low IC₅₀ and uptake of [¹⁴C]6-FDF in both MCF-7 and MDA-MB-231 cells, which supports the idea that a [¹⁸F]-labelled 6-FDF compound has a great deal of promise with regard to the *in vivo* imaging of breast cancer. We have developed an efficient procedure for the automated synthesis of [¹⁸F]6-FDF in order to proceed with *in vivo* imaging trials using mouse xenograft models, and this will be discussed in the upcoming chapter.

2.3 Experimental / Material and methods

Please see **Appendix A** for a detailed materials list.

2.3.1 Synthesis of 6-deoxy-6-fluoro-D-fructose.

Reactions were carried out in flame-dried glassware under a positive argon atmosphere unless otherwise stated. Transfer of anhydrous solvents and reagents was accomplished with oven-dried syringes or cannulae. Solvents were distilled before use: methylene chloride (CH₂Cl₂) from calcium hydride, and pyridine from KOH. Thin layer chromatography was performed on glass plates precoated with 0.25 mm Kieselgel 60 F₂₅₄ (Merck). Flash chromatography

columns were packed with 230-400 mesh silica gel (Silicycle). Optical rotations were measured at 22 ± 2 °C. Proton nuclear magnetic resonance spectra (^1H NMR) were recorded at 400 MHz or 500 MHz and coupling constants (J) are reported in Hertz (Hz). Standard notation was used to describe the multiplicity of signals observed in ^1H NMR spectra: broad (br), multiplet (m), singlet (s), doublet (d), triplet (t), etc. Carbon nuclear magnetic resonance spectra (^{13}C NMR) were recorded at 100 MHz or 125 MHz and are reported (ppm) relative to the centre line of the triplet from chloroform-*d* (77.00 ppm). Infrared (IR) spectra were measured with a Mattson Galaxy Series FT-IR 3000 spectrophotometer. Mass spectra were determined on a PerSeptive Biosystems Mariner high-resolution electrospray positive ion mode spectrometer.

2.3.2 ***Methyl 6-O-(tert-butyldimethylsilyl)-D-fructofuranoside, 3.***

The methyl α/β -D-fructofuranoside (1.1 g, 5.6 mmol) was dissolved in freshly distilled pyridine (0.5 M). The reaction mixture was cooled to $\sim 0^\circ\text{C}$ (ice/water bath) and tert-Butyldimethylsilyl chloride (7.3 mmol, 1.1 g) was added in a single portion. The reaction was left to stir overnight with gradual warming to room temperature. After overnight stirring, the reaction was quenched by the addition of water and dilution with CH_2Cl_2 . The organic/aqueous layers were separated and the aqueous layer extracted with CH_2Cl_2 (2 x 15 mL). The combined organic layers were washed with 10% H_2SO_4 solution and water. The organic layer was dried (MgSO_4) and filtered before removing the solvent *in vacuo*. The 1,6-di-*O*-silylated product (0.071 g, 0.17 mmol, 3%) was isolated as a

clear, colourless oil, while the desired 6-*O*-silylated product (1.0 g, 3.3 mmol, 58%) was obtained as a white solid after purification by flash column chromatography (silica gel, 5% MeOH in CH₂Cl₂). **3 α** : m.p. 68-70°C; *R_f* 0.34 (CH₂Cl₂/MeOH 49:1); [α]_D +62.2 (*c* 0.6, MeOH); IR (thin film) 3453, 3322, 2952, 2929, 2858, 1461, 1253, 1150, 1072, 1009 cm⁻¹; ¹H NMR (500 MHz, CDCl₃) δ 4.22 (d, *J* = 11.0 Hz, 1H), 4.15 (br s, 1H), 4.05 (br d, *J* = 11.5 Hz, 1H), 3.99 (d, *J* = 11.0 Hz, 1H), 3.84 (d, *J* = 6.5 Hz, 2H), 3.83 (m, 2H), 3.37 (s, 3H), 3.12 (d, *J* = 11.5 Hz, 1H), 2.03 (t, *J* = 7.0 Hz, 1H), 0.92 (s, 9H), 0.13 (s, 6H); ¹³C NMR (125 MHz, CDCl₃) δ 109.9, 86.6, 78.8, 78.2, 63.2, 58.2, 50.4, 48.6, 25.7, 18.3, -5.6 (2C); HRMS (ESI, [M+Na]⁺) for C₁₃H₂₈O₆SiNa calcd 331.1547, found: *m/z* 331.1545.

3 β : m.p. 107-108°C; *R_f* 0.18 (CH₂Cl₂/MeOH 49:1); [α]_D -21.8 (*c* 0.5, MeOH); IR (thin film) 3390, 2952, 2929, 2858, 1463, 1255, 1130, 1036, 837 cm⁻¹; ¹H NMR (500 MHz, CDCl₃) δ 4.18 (br s, 1H), 4.14 (t, *J* = 7.0 Hz, 1H), 3.85 (dt, *J* = 7.0, 5.0 Hz, 1H), 3.75 (d, *J* = 5.0 Hz, 2H), 3.69 (br s, 2H), 3.38 (br s, 1H), 3.35 (s, 3H), 3.29 (br s, 1H), 2.66 (br s, 1H), 0.91 (s, 9H), 0.09 (s, 6H); ¹³C NMR (125 MHz, CDCl₃) δ 103.2, 81.9, 79.0, 77.1, 64.1, 61.3, 49.2, 25.9, 18.4, -5.4 (2C); HRMS (ESI, [M+Na]⁺) for C₁₃H₂₈O₆SiNa calcd 331.1547, found: *m/z* 331.1546.

2.3.3 ***Methyl 1,3,4-tri-*O*-acetyl-6-*O*-(*tert*-butyldimethylsilyl)-*D*-fructofuranoside, 4.***

Methyl 6-*O*-(*tert*-butyldimethylsilyl)- α/β -*D*-fructofuranoside (0.94 g, 3.0 mmol) was dissolved in freshly distilled pyridine (0.25 M). The temperature of the

reaction mixture was dropped to 0°C (ice/water bath) and acetic anhydride (61.0 mmol, 5.8 mL) was added at low temperature *via* syringe. The reaction mixture was allowed to stir overnight with gradual warming to room temperature. The reaction was then quenched by the addition of water with subsequent stirring for 30 min. The reaction mixture was then diluted with CH₂Cl₂. The organic/aqueous layers were separated and the aqueous layer extracted with CH₂Cl₂ (2 x 10 mL). The combined organic layers were washed with 10% H₂SO₄ solution and water. The organic layer was then dried (MgSO₄) and filtered before removing the solvent *in vacuo*. Methyl 1,3,4-tri-*O*-acetyl-6-*O*-(*tert*-butyldimethylsilyl)- α/β -D-fructofuranoside (1.15 g, 2.6 mmol, 87%) was isolated as a pale yellow oil after purification by flash column chromatography (silica gel, 2% MeOH in CH₂Cl₂). **4 α** : R_f 0.82 (CH₂Cl₂/MeOH 49:1); [α]_D +75.6 (*c* 0.6, MeOH); IR (thin film) 2955, 2931, 2858, 1752, 1371, 1231, 1070, 838 cm⁻¹; ¹H NMR (500 MHz, CDCl₃) δ 5.28 (d, *J* = 2.0 Hz, 1H), 5.04 (dd, *J* = 5.5, 2.0 Hz, 1H), 4.42 (d, *J* = 12.0 Hz, 1H), 4.08 (d, *J* = 12.0 Hz, 1H), 3.99 (dt, *J* = 5.5, 4.5 Hz, 1H), 3.84 (d, *J* = 4.5 Hz, 2H), 3.30 (s, 3H), 2.08 (s, 3H), 2.06 (s, 3H), 2.04 (s, 3H), 0.90 (s, 9H), 0.07 (s, 3H), 0.07 (s, 3H); ¹³C NMR (125 MHz, CDCl₃) δ 170.2, 170.0, 168.9, 106.6, 82.8, 80.5, 78.1, 62.4, 58.3, 48.5, 25.8, 20.8, 20.7, 20.6, 18.3, -5.3, -5.4; HRMS (ESI, [M+Na]⁺) for C₁₉H₃₄O₉SiNa calcd 457.1864, found: m/z 457.1864.

4 β : R_f 0.82 (CH₂Cl₂/MeOH 49:1); [α]_D -8.0 (*c* 0.7, MeOH); IR (thin film) 2956, 2932, 2858, 1754, 1369, 1230, 1055, 839 cm⁻¹; ¹H NMR (500 MHz, CDCl₃) δ 5.51 (t, *J* = 7.0 Hz, 1H), 5.46 (d, *J* = 7.0 Hz, 1H), 4.24 (d, *J* = 12.0 Hz, 1H), 4.16 (d, *J* =

11.5 Hz, 1H), 4.02 (q, $J = 5.5$ Hz, 1H), 3.81 (dd, $J = 11.0, 5.0$ Hz, 1H), 3.74 (dd, $J = 11.0, 5.5$ Hz, 1H), 3.38 (s, 3H), 2.12 (s, 3H), 2.10 (s, 3H), 2.07 (s, 3H), 0.90 (s, 9H), 0.08 (s, 3H), 0.07 (s, 3H); ^{13}C NMR (125 MHz, CDCl_3) δ 170.2, 170.1, 170.0, 102.7, 80.3, 77.1, 75.7, 63.5, 62.8, 49.8, 25.8, 20.8, 20.8, 20.7, 18.3, -5.5, -5.5; HRMS (ESI, $[\text{M}+\text{Na}]^+$) for $\text{C}_{19}\text{H}_{34}\text{O}_9\text{SiNa}$ calcd 457.1864, found: m/z 457.1864.

2.3.4 Methyl 1,3,4-tri-*O*-acetyl-*D*-fructofuranoside, 5.

Methyl 1,3,4-tri-*O*-acetyl-6-*O*-(*tert*-butyldimethylsilyl)- α/β -*D*-fructofuranoside (0.98 g, 2.3 mmol) was dissolved in CH_2Cl_2 (25 mL). Water (1 mL) and trifluoroacetic acid (9 mL) were subsequently added *via* plastic syringe at room temperature. The reaction mixture was allowed to stir for 30 min. before being neutralized with the addition of 2N NaOH aq. solution. The organic/aqueous layers were separated and the aqueous layer extracted with CH_2Cl_2 (20 mL). The organic layer was then washed with saturated NaHCO_3 aq. and brine solution. The organic layer was dried (MgSO_4) and filtered before removing the solvent *in vacuo*. Methyl 1,3,4-tri-*O*-acetyl- α/β -*D*-fructofuranoside (0.48 g, 1.5 mmol, 65%) was obtained as a clear, colorless oil after purification by flash column chromatography (silica gel, 5% MeOH in CH_2Cl_2). **5 α** : R_f 0.43 ($\text{CH}_2\text{Cl}_2/\text{MeOH}$ 49:1); $[\alpha]_D^{+25}$ +95.8 (c 0.7, MeOH); IR (thin film) 3487, 2942, 1747, 1373, 1235, 1065, 892 cm^{-1} ; ^1H NMR (500 MHz, CDCl_3) δ 5.31 (d, $J = 2.0$ Hz, 1H), 4.98 (dd, $J = 5.5, 2.5$ Hz, 1H), 4.44 (d, $J = 12.5$ Hz, 1H), 4.10 (d, $J = 12.0$ Hz, 1H), 4.02 (q, $J = 4.0$ Hz, 1H), 3.87 (ddd, $J = 12.0, 4.0, 4.0$ Hz, 1H), 3.77 (ddd, $J = 12.5, 8.0, 4.5$ Hz, 1H), 3.31 (s, 3H), 2.26 (dd, $J = 8.0, 5.0$ Hz, 1H), 2.09 (s, 3H), 2.07 (s, 3H), 2.04 (s, 3H); ^{13}C NMR

(125 MHz, CDCl₃) δ 170.5, 170.1, 168.9, 106.5, 82.9, 79.8, 77.8, 61.9, 58.5, 48.6, 20.7, 20.7, 20.6; HRMS (ESI, [M+Na]⁺) for C₁₃H₂₀O₉Na calcd 343.0999, found: m/z 343.1000.

5 β : R_f 0.43 (CH₂Cl₂/MeOH 49:1); [α]_D -13.7 (c 0.9, MeOH); IR (thin film) 3496, 2953, 1747, 1371, 1238, 1055, 905 cm⁻¹; ¹H NMR (500 MHz, CDCl₃) δ 5.51 (d, *J* = 7.5 Hz, 1H), 5.35 (t, *J* = 6.0 Hz, 1H), 4.25 (d, *J* = 12.0 Hz, 1H), 4.16 (d, *J* = 12.0 Hz, 1H), 4.01 (q, *J* = 6.0 Hz, 1H), 3.82 (ddd, *J* = 11.5, 5.5, 5.5 Hz, 1H), 3.71 (ddd, *J* = 12.0, 6.0, 6.0 Hz, 1H), 3.37 (s, 3H), 2.45 (t, *J* = 6.5 Hz, 1H), 2.10 (s, 3H), 2.08 (s, 6H); ¹³C NMR (125 MHz, CDCl₃) δ 170.9, 170.1, 169.8, 102.4, 81.0, 77.2, 76.4, 76.1, 63.4, 62.3, 49.8, 20.8, 20.6, 20.6; HRMS (ESI, [M+Na]⁺) for C₁₃H₂₀O₉Na calcd 343.0999, found: m/z 343.1000. This data is in close correlation with the previously reported data.[21]

2.3.5 *Methyl 1,3,4-tri-O-acetyl-6-deoxy-6-fluoro-D-fructofuranoside, 6.*

Methyl 1,3,4-tri-*O*-acetyl- α/β -D-fructofuranoside (0.41 g, 1.3 mmol) was dissolved in freshly distilled CH₂Cl₂ (0.1 M, 13 mL). The temperature of the reaction was lowered to -10°C (ice/acetone bath). Pyridine (1.9 mmol, 0.15 mL) and triflic anhydride (1.4 mmol, 0.24 mL) were subsequently added *via* syringe. The reaction mixture was allowed to stir at low temperature for 45 min. before being quenched with the addition of water. The organic/aqueous layers were separated and the aqueous layer extracted with CH₂Cl₂ (2 x 10 mL). The combined organic layers were washed with 10% H₂SO₄ solution and water. The

organic layer was then dried (MgSO_4) and filtered before removing the solvent *in vacuo*. The 6-*O*-triflyl product was obtained as a pale yellow oil.

The crude oil was directly dissolved in *tert*-amyl alcohol (0.33 M, 3.9 mL) and cesium fluoride (3.9 mmol, 0.58 g) was added in a single portion. The reaction was equipped with a reflux condenser and set to reflux at $\sim 90^\circ\text{C}$ (oil bath). After 20 min. the reaction was cooled to room temperature, then water and CH_2Cl_2 were added. The organic/aqueous layers were separated and the aqueous layer extracted with CH_2Cl_2 (2 x 5 mL). The combined organic layers were washed with water (2 x 5 mL) and then dried (MgSO_4). After filtration, the solvent was removed *in vacuo* to provide an orange oil. Methyl 1,3,4-tri-*O*-acetyl-6-deoxy-6-fluoro- α/β -D-fructofuranoside (0.35 g, 1.1 mmol, 84%) was isolated as a clear, colourless oil after purification by flash column chromatography (silica gel, 5% MeOH in CH_2Cl_2). **6 α** : R_f 0.55 ($\text{CH}_2\text{Cl}_2/\text{MeOH}$ 49:1); $[\alpha]_D +74.7$ (c 0.9, MeOH); IR (thin film) 2958, 1748, 1372, 1230, 1071, 892 cm^{-1} ; ^1H NMR (500 MHz, CDCl_3) δ 5.29 (br s, 1H), 4.93 (dd, $J = 5.5, 2.0$ Hz, 1H), 4.65 (ddd, $^2J_{\text{H-F}} = 47.0$ Hz, $J_{\text{H-H}} = 10.5, 2.5$ Hz, 1H), 4.60 (ddd, $^2J_{\text{H-F}} = 47.0$ Hz, $J_{\text{H-H}} = 10.5, 5.0$ Hz, 1H), 4.44 (d, $J = 12.0$ Hz, 1H), 4.14 (d, $J = 12.0$ Hz, 1H), 4.10 (dddd, $^3J_{\text{H-F}} = 23.5$ Hz, $J_{\text{H-H}} = 4.5, 4.5, 2.5$ Hz, 1H), 3.31 (s, 3H), 2.10 (s, 3H), 2.07 (s, 3H), 2.03 (s, 3H); ^{13}C NMR (125 MHz, CDCl_3) δ 170.2, 170.0, 168.9, 106.9, 81.8 (d, $^1J_{\text{C-F}} = 105.1$ Hz), 81.1 (d, $^2J_{\text{C-F}} = 49.8$ Hz), 79.6 (d, $^4J_{\text{C-F}} = 1.0$ Hz), 77.2 (d, $^3J_{\text{C-F}} = 7.1$ Hz), 58.0, 48.6, 20.6, 20.6, 20.6; HRMS (ESI, $[\text{M}+\text{Na}]^+$) for $\text{C}_{13}\text{H}_{19}\text{O}_8\text{FNa}$ calcd 345.0956, found: m/z 345.0956.

6 β : R_f 0.55 (CH₂Cl₂/MeOH 49:1); $[\alpha]_D$ -28.1 (*c* 1.1, MeOH); IR (thin film) cm⁻¹; ¹H NMR (300 MHz, CDCl₃) δ 5.52 (d, *J* = 7.2 Hz, 1H), 5.40 (t, *J* = 6.9 Hz, 1H), 4.63 (ddd, ²*J*_{H-F} = 48.0 Hz, *J*_{H-H} = 10.2, 3.0 Hz, 1H), 4.49 (ddd, ²*J*_{H-F} = 47.4 Hz, *J*_{H-H} = 10.5, 6.0 Hz, 1H), 4.26 (d, *J* = 11.7 Hz, 1H), 4.17 (d, *J* = 11.7 Hz, 1H), 4.16 (dddd, ³*J*_{H-F} = 20.7 Hz, *J*_{H-H} = 6.0, 6.0, 3.3 Hz, 1H), 3.38 (s, 3H), 2.11 (s, 3H), 2.09 (s, 3H), 2.09 (s, 3H); ¹³C NMR (125 MHz, CDCl₃) δ 170.3, 170.1, 169.9, 102.8, 82.5 (d, ¹*J*_{C-F} = 174.9 Hz), 78.9 (d, ²*J*_{C-F} = 19.6 Hz), 76.3 (d, ⁴*J*_{C-F} = 1.8 Hz), 74.7 (d, ³*J*_{C-F} = 7.5 Hz), 62.1, 49.7, 20.7, 20.7, 20.7; HRMS (ESI, [M+Na]⁺) for C₁₃H₁₉O₈FNa calcd 345.0956, found: *m/z* 345.0955.

2.3.6 6-Deoxy-6-fluoro-D-fructose, 7.

Methyl 1,3,4-tri-*O*-acetyl-6-deoxy-6-fluoro- α/β -D-fructofuranoside (0.20 g, 0.62 mmol) was dissolved in anhydrous MeOH (6 mL). At room temperature, NaOMe in MeOH (1.5 M, 0.14 mL) was added to the reaction mixture *via* plastic syringe. The reaction was allowed to stir for 10 min. before the addition of 1N HCl to quench the reaction. Upon neutralization of the reaction mixture, the volatiles were removed *in vacuo* to provide a pale yellow residue.

The crude material from the previous reaction was directly dissolved in 1,4-dioxane (1.5 mL). 1N HCl aq. solution (1 mL) was then added and the reaction mixture allowed to stir at room temperature overnight. The reaction was then quenched by neutralization with the addition of 2N NaOH aq. solution. The solvent was removed *in vacuo* and the crude oil immediately purified by

flash column chromatography (silica gel, 5–10% MeOH in CH₂Cl₂). 6-Deoxy-6-fluoro-D-fructose (6-FDF) was obtained as a white solid (0.077 g, 0.42 mmol, 69%). 6-FDF exists as an inseparable 1:4 mixture of α : β -anomers in the furanose conformation, as observed by ¹H NMR in D₂O: m.p. 74-76°C; R_f 0.11 (CH₂Cl₂/MeOH 95:5); [α]_D -6.39 (*c* 1.8, MeOH); IR (thin film) 3339, 2954, 1649, 1454, 1048, 938 cm⁻¹; HRMS (ESI, [M+Na]⁺) for C₆H₁₁O₅FNa calcd 205.0483, found: m/z 205.0484; Anal. Calcd for C₆H₁₁FO₅: C, 39.56; H, 6.09. Found: C, 39.11; H, 6.07. **7 α** : Partial ¹H NMR (500 MHz, D₂O) δ 4.69 (ddd, ²J_{H-F} = 50.5 Hz, J_{H-H} = 10.5, 2.5 Hz, 1H), 4.59 (ddd, ²J_{H-F} = 47.5 Hz, J_{H-H} = 11.0, 5.5 Hz, 1H), 3.67 (d, J = 12.0 Hz, 1H), 3.64 (d, J = 12.0 Hz, 1H); ¹³C NMR (125 MHz, CDCl₃) δ 105.6, 83.4 (d, ¹J_{C-F} = 167.4 Hz), 82.7, 80.6 (d, ²J_{C-F} = 17.7 Hz), 76.1 (d, ³J_{C-F} = 7.2 Hz), 63.6.

7 β : ¹H NMR (500 MHz, D₂O) δ 4.64 (ddd, ²J_{H-F} = 47.5 Hz, J_{H-H} = 11.0, 2.5 Hz, 1H), 4.56 (ddd, ²J_{H-F} = 47.5 Hz, J_{H-H} = 10.5, 5.0 Hz, 1H), 4.19 (t, J = 8.5 Hz, 1H), 4.14 (d, J = 8.5 Hz, 1H), 3.97 (dddd, ³J_{H-F} = 24.0 Hz, J_{H-H} = 8.0, 5.5, 2.5 Hz, 1H), 3.60 (d, J = 12.0 Hz, 1H), 3.55 (d, J = 12.0 Hz, 1H); ¹³C NMR (125 MHz, CDCl₃) δ 102.6, 83.9 (d, ¹J_{C-F} = 168.4 Hz), 79.7 (d, ²J_{C-F} = 18.2 Hz), 75.9, 74.1 (d, ³J_{C-F} = 7.5 Hz), 63.4.

2.3.7 Western Blots

Isolated whole cell samples were lysed with Cellytic™ M (Sigma), combined with a protease inhibitor cocktail as per the manufacturers specifications (Sigma, Canada) and a Bradford protein quantification assay was used for total protein to determine the concentrations of the samples. The 25 μ g samples were then run

on a 10% separating gel, and then transferred to a nitrocellulose membrane where we then labelled the protein using the particular rabbit primary polyclonal antibodies of the GLUT isoform being examined with concentrations ranging from 1:250 to 1:1000 (GLUT1, 2, 4 - Chemicon, GLUT5 - Biogenesis, GLUT7 - Chemicon, GLUT9 – Gift from Dr. Kelle Molle, GLUT11- GLUT12 - Gift from Dr. Sue Rogers). After the primary antibody was applied overnight, it was then labelled with ECL™ Antirabbit IgG Horseradish peroxidase linked whole antibody and then was visualized using the ECL™ Western Blot detection reagents (Amersham Biosciences).

2.3.8 Cell Culture and Fluxes

Both MCF-7 and MDA-MB-231 cells (Gifts from Dr. David Murray, Cross Cancer Institute) were grown in a 37°C, 5% CO₂ incubator, in Gibco® DMEM-F12 supplemented with 15mM HEPES, L-Glutamine, 10% Fetal Bovine Serum and 1% Penicillin/Streptomycin with media renewal every 2 to 3 days. For cell flux studies, cells were grown to confluence in 12-well plates with media renewal every two days. Two hours before performing the flux experiment, the media was removed, and the cells washed 2x with Phosphate Buffered Saline solution (PBS). Next, glucose free Krebs-Ringer solution was added to the wells (120mM NaCl, 25mM NaHCO₃, 4mM KCl, 1.2mM KH₂PO₄, 2.5mM MgSO₄, 70uM CaCl₂, pH 7.4) in order to deprive the cells of nutrients and to set up a *zero-trans* experiment. After the two hours, cells were removed from the incubator, and the respective experiments were performed. Radioactive “Hot” flux solutions

were made up using the Krebs-Ringer solution previously mentioned and radiolabeled [¹⁴C]-D-glucose (Amersham), [¹⁴C]-D-fructose (Moravek Biochemicals), or [¹⁴C]6-FDF (proprietary) at a specific activity of approximately 1 μCi/mL. For determining background levels of radioactivity, a Sodium reduced Krebs solution was made (70mM NaCl, 25mM NaHCO₃, 4mM KCl, 1.2mM KH₂PO₄, 2.5mM MgSO₄, 70μM CaCl₂, pH 7.4) with the addition of either 100 mM D-glucose or 100 mM D-fructose to outcompete the binding sites of the specific GLUT transporters we are examining. After applying the test flux solution, incubations lasted for 25 minutes, where the cells were then rinsed 2x with ice-cold Krebs-Ringer to stop the transport, and then lysed using 500 μL 5% trichloroacetic acid and let sit on a shaker bed overnight. Next, three 150 μL samples from each well were placed into scintillation counter vials, and 4 mLs of ScintiSafe™ liquid scintillation fluid (Fisher) was added. The vials were then placed in a Beckman LS 6500 multi-purpose liquid scintillation counter to be quantified. All counts were then normalized to standards and corrected for background accumulation of isotope.

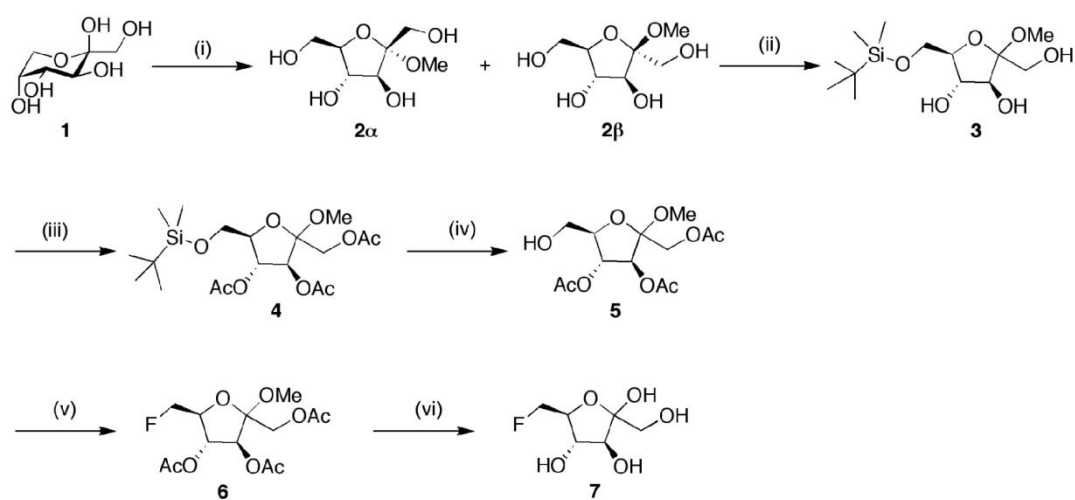
2.3.9 *Immunocytochemistry*

Cells were grown on 25 mm glass coverslips in 6-well plates until they were at the desired confluence. At this time, the cell culture media was removed, and the cells were rinsed 2x with PBS. Afterwards, a 50% methanol/PBS solution was added into the wells, and left on a shaker at a low speed for 5 minutes. After the 5 minutes had passed, the PBS/methanol solution was aspirated, and 100%

methanol was added to each well before putting the cells into the -20°C freezer to be stored until needed. After removing the cells from the freezer for immunofluorescence, the methanol was aspirated, and PBS was added and left to rinse the cells on the shaker for 5 minutes. The PBS is then aspirated, and a 5% skim milk solution was left on the cells to block for 1 hour. Primary antibody solutions were then prepared in the 5% skim milk solution at concentrations appropriate for each individual GLUT isoform (GLUT1, 2 - Chemicon, GLUT5 - Biogenesis, GLUT7 - Chemicon, GLUT9 - Gift from Dr. Kelle Molle, GLUT12 - Gift from Dr. Sue Rogers). The antibody solutions were then placed on the coverslips and let sit at room temperature for 1 hour. Afterwards, the coverslips were rinsed in a .01% PBS-Tween solution. The secondary antibody (anti-rabbit Alexafluor 488 - Invitrogen) was then allowed to bind to the primary antibody for another hour and then the coverslips with the cells were washed in PBS. Lastly, the coverslips were then mounted on slides using ProLong[®] Gold anti-fade reagent with DAPI (Invitrogen) before letting them sit to dry for 30 minutes and then being placed in the darkness in a 4°C refrigerator.

2.3.10 Analysis

All uptake values were corrected for their respective adhering extracellular substrate, and IC₅₀ values were determined using non-linear regression in Graphpad Prism 5. Student's t-tests were also performed in Graphpad Prism 5.



Scheme 2.1: Synthesis of 6-FDF - Reagents and conditions: (i) H_2SO_4 , MeOH, 91%; (ii) TBDMSCl, pyridine, 0°C , 57%; (iii) Ac_2O , pyridine, 88%; (iv) TFA: H_2O (9:1), CH_2Cl_2 , 91%; (v) Tf_2O , pyridine, CH_2Cl_2 , -10°C ; then CsF, t-Amyl alcohol, 80°C , 77%; (vi) NaOMe, MeOH; then 1N HCl, dioxane, 62%.

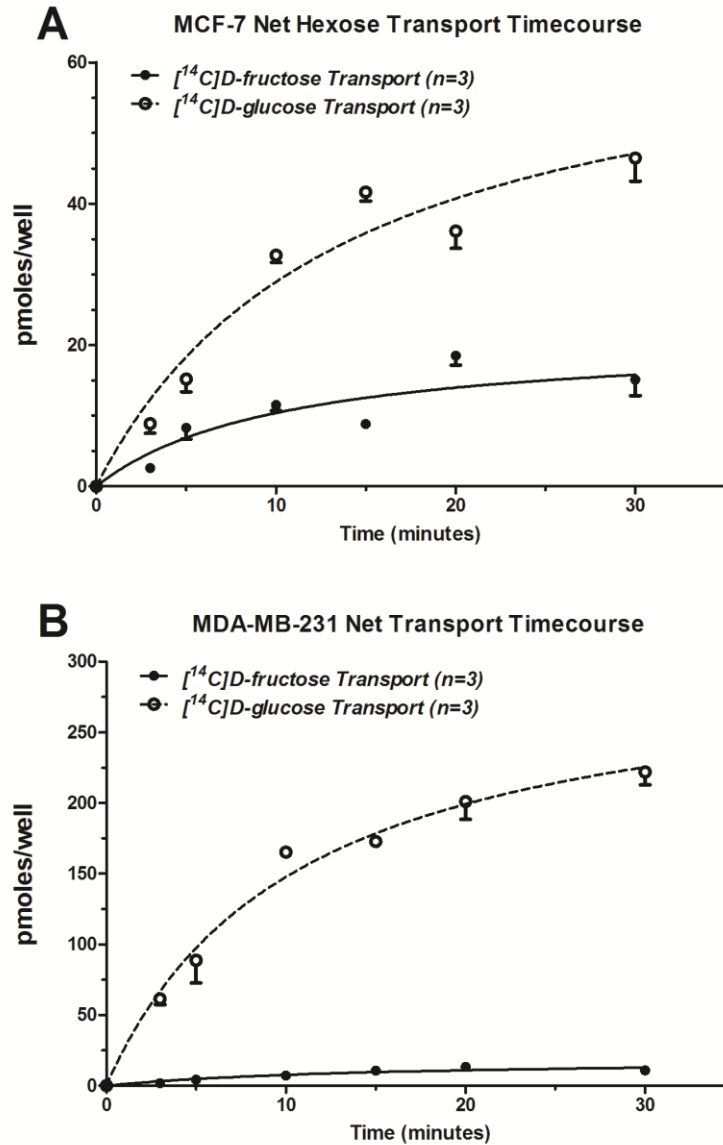


Figure 2.1: Hexose uptake in MCF-7 and MDA-MB-231- Hexose flux assays with both fructose (•) and glucose (°) in both MCF-7 (A) and MDA-MB-231 (B) show clear uptake after being corrected for non-carrier mediated uptake of hexose. MDA-MB-231 has significantly higher uptake of glucose compared to that of MCF-7, while fructose uptake in both lines is similar. Each data point represents n = 3 and the error bars the standard errors.

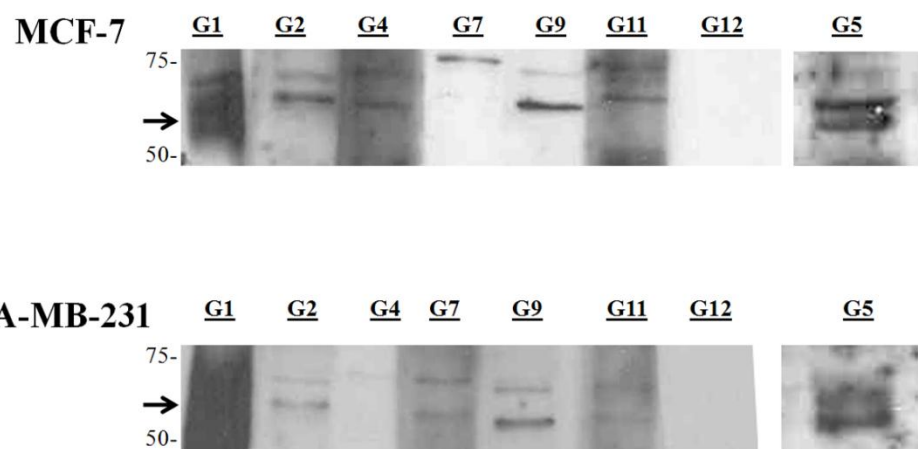


Figure 2.2: Western Blots of MCF-7 and MDA-MB-231 – Each lane was loaded with 25 μg of whole cell protein. Protein ladder indicates the location of 75 kDa and 50 kDa sized bands and the arrow refers to the approximate location of each of the GLUT isoforms to appear if detected. The doublet represents both glycosylated and unglycosylated forms.

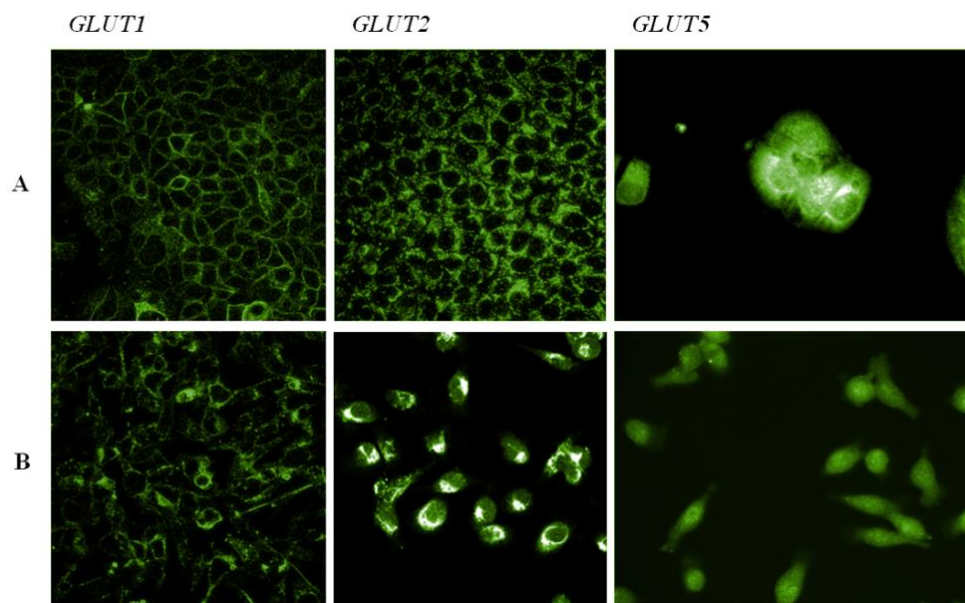


Figure 2.3: Confocal images - MCF-7 (A) and MDA-MB-231 (B) labelled using anti-GLUT1, GLUT2, and GLUT5 antibodies.

[¹⁴C]-D-fructose Uptake in MCF-7 and MDA-MB-231

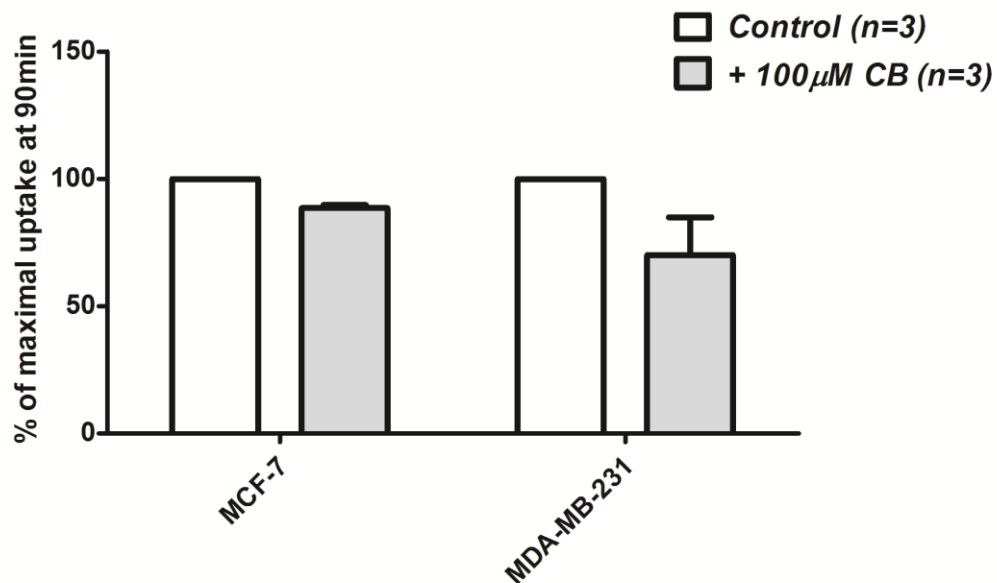


Figure 2.4: : Inhibition of [¹⁴C]D-fructose uptake with cytochalasin B - Ninety minute flux using [¹⁴C]D-fructose performed on both cell lines with and without treatment with 100 μM of the Class I GLUT inhibitor cytochalasin B (+CB represented by the shaded bars). Inhibition of the Class I GLUT isoform GLUT2 is apparent in both lines, although a much larger inhibition is shown in MDA-MB-231. All values are corrected for non-mediated uptake and extracellularly bound hexose. Each data point represents n = 3. Error bars represent SEM

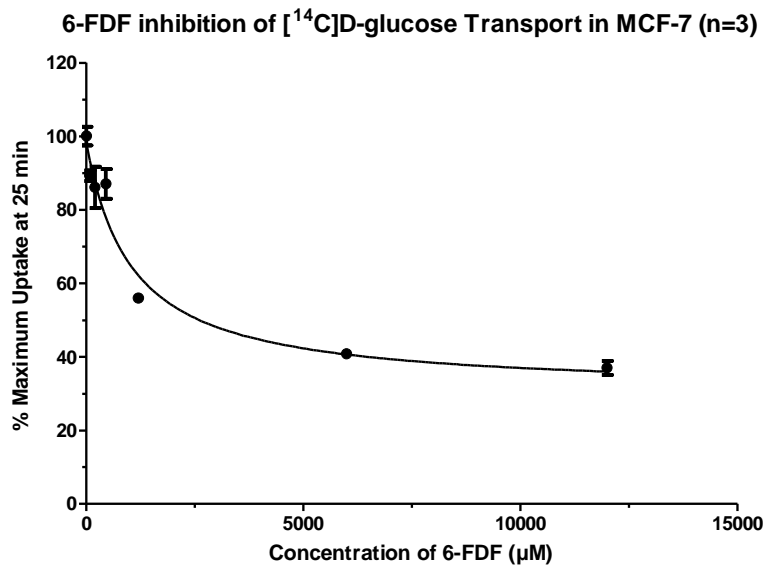
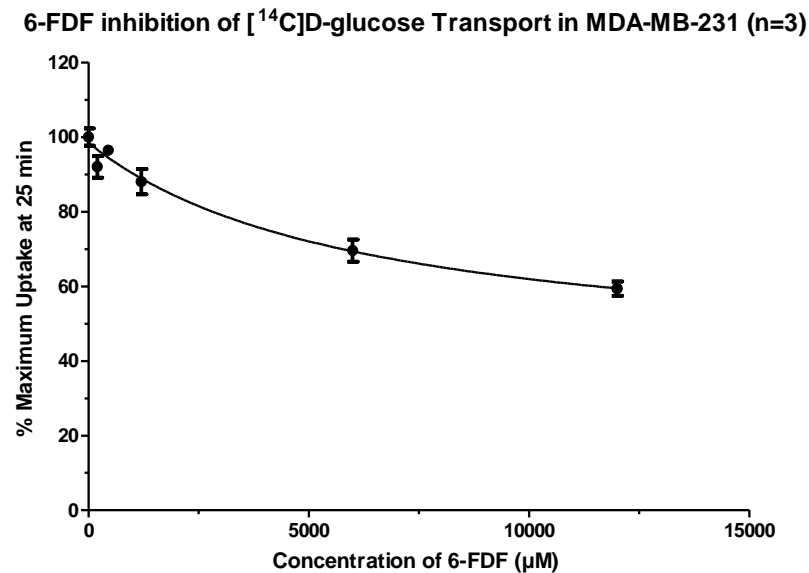
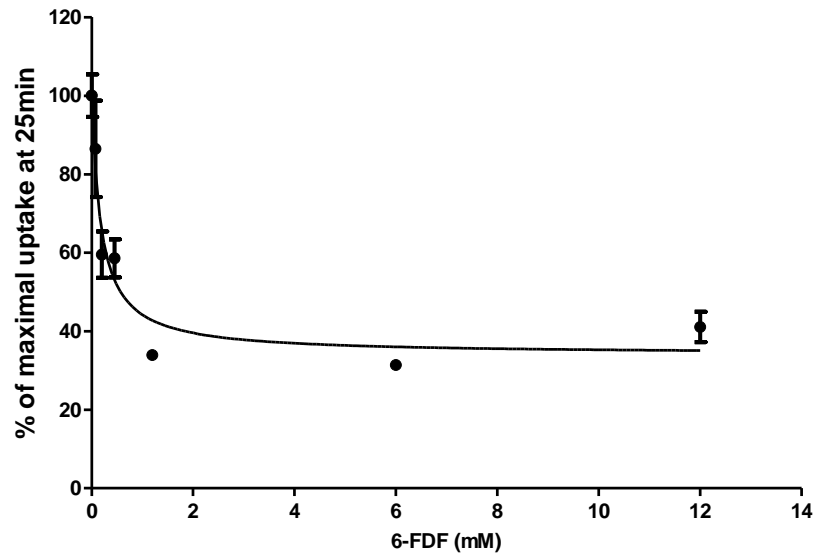
A**B**

Figure 2.5: : 6-FDF inhibition studies of [¹⁴C]-D-glucose transport - 6-FDF inhibition studies of [¹⁴C]-D-glucose transport after a 25 min incubation in both MCF-7 (A) and MDA-MB-231 (B) using increasing concentrations of 6-FDF. Glucose transport was inhibited by 6-FDF with a IC_{50} of approximately 1.05 ± 0.30 mM in MCF-7 (A) and a IC_{50} of 6.21 ± 2.86 mM in MDA-MB-231 (B). Each data point represents $n = 3$ and the error bars the SEM.

A 6-FDF inhibition of D-fructose transport in MCF-7 (n=3)



B

6-FDF inhibition of D-fructose transport in MDA-MB-231 (n=3)

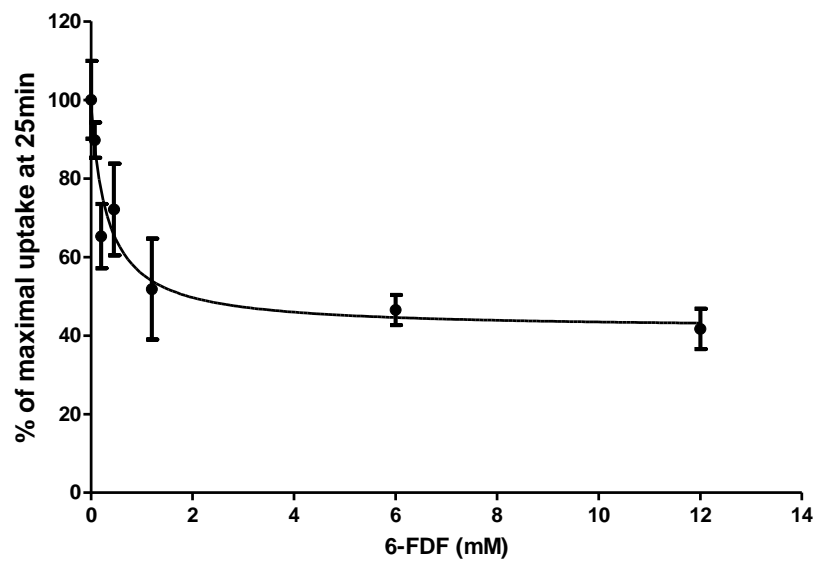


Figure 2.6: 6-FDF inhibition studies of [¹⁴C]-D-fructose transport - 6-FDF inhibition studies of [¹⁴C]-D-fructose transport after a 25 min incubation with both MCF-7 (A) and MDA-MB-231 (B) using increasing concentrations of 6-FDF. Fructose transport was inhibited by increasing concentrations of 6-FDF, and the IC₅₀ obtained for MCF-7 (A) was 0.18 ± 0.05 mM and MDA-MB-231 (B) had an IC₅₀ of 0.33 ± 0.15 mM. Each data point represents n = 3. Error bars represent SEM.

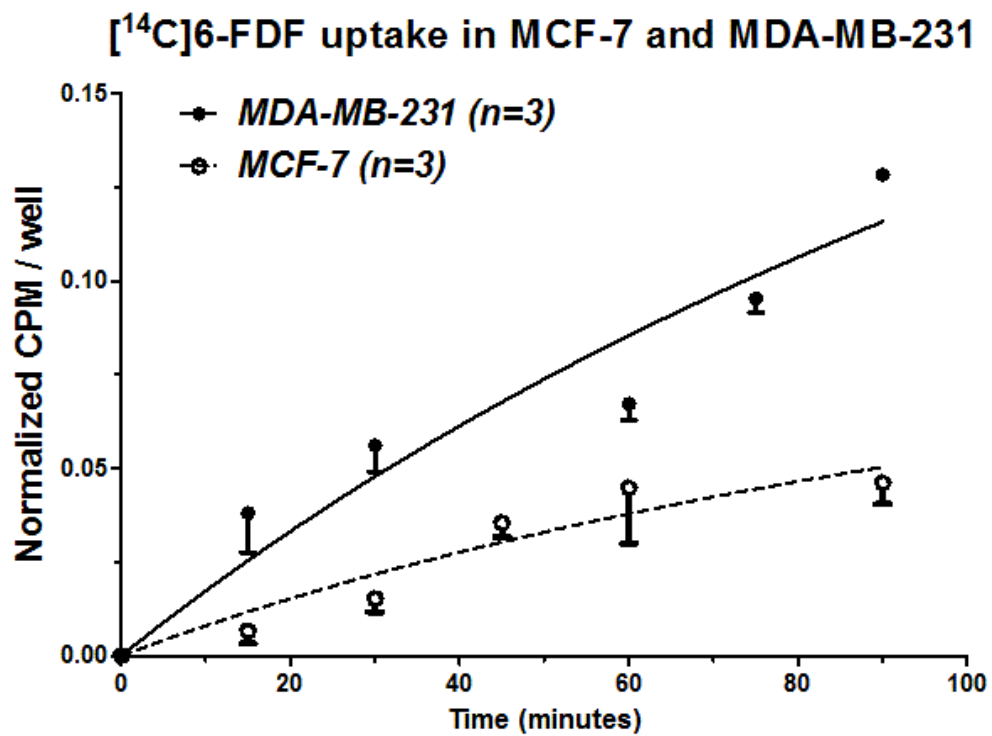


Figure 2.7: [¹⁴C]6-FDF uptake time course - [¹⁴C]6-FDF uptake 90 minute time course in both MCF-7 (○) and MDA-MB-231 (●) corrected for non-mediated hexose uptake. Uptake is observed in both cell types after a 90 min incubation and each data point represents n = 3. Error bars represent the SEM.

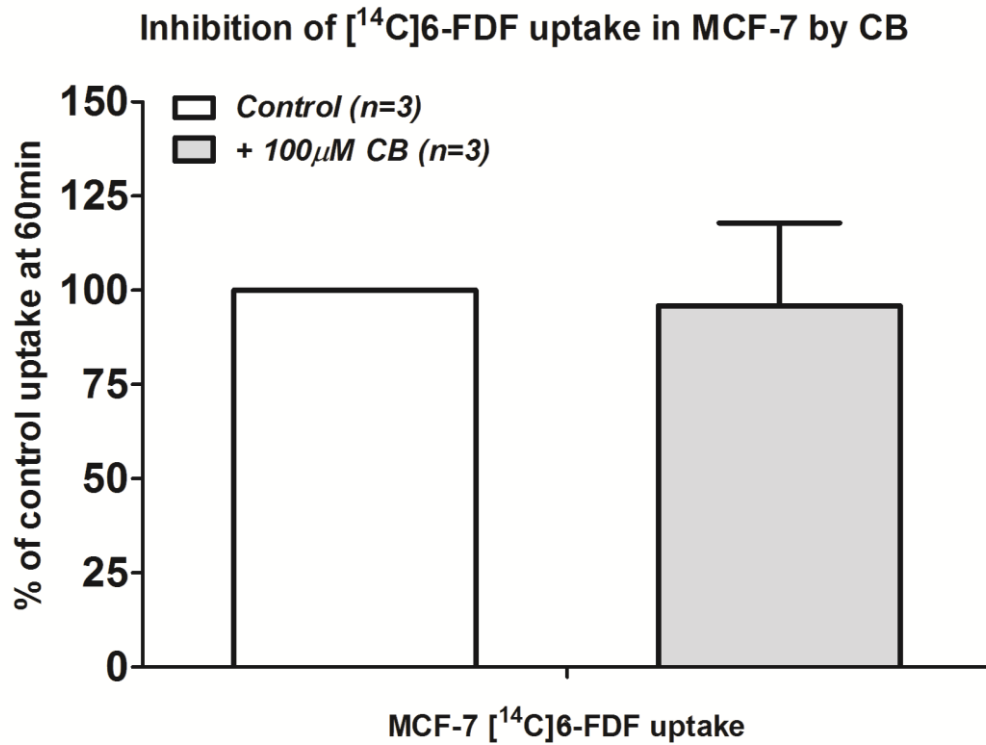


Figure 2.8: Inhibition of [¹⁴C]6-FDF by cytochalasin B - Inhibition by 100 μM cytochalasin B (+CB) is represented by the shaded bars) of [¹⁴C]6-FDF uptake into MCF-7 cells. Incubations lasted 60 min and uptakes were corrected for non-mediated fluxes. Error bars represent the SEM. No significant difference was observed between the control and treated groups.

2.4 Bibliography

1. Buerkle A, Weber W a. Imaging of tumor glucose utilization with positron emission tomography. *Cancer metastasis reviews*. 2008 Dec;27(4):545–54.
2. Santiago JFY, Gonen M, Yeung H, Macapinlac H, Larson S. A retrospective analysis of the impact of 18F-FDG PET scans on clinical management of 133 breast cancer patients. *The quarterly journal of nuclear medicine and molecular imaging*. 2006 Mar;50(1):61–7.
3. Bos R, van Der Hoeven JJM, van Der Wall E, van Der Groep P, van Diest PJ, Comans EFI, et al. Biologic correlates of (18)fluorodeoxyglucose uptake in human breast cancer measured by positron emission tomography. *Journal of clinical oncology : official journal of the American Society of Clinical Oncology*. 2002 Jan 15;20(2):379–87.
4. Eubank WB, Mankoff DA. Evolving Role of Positron Emission Tomography in Breast Cancer Imaging. *Semin Nucl Med*. 2005 Apr;35(2):84-99.
5. Weir L, Worsley D, Bernstein V. The value of FDG positron emission tomography in the management of patients with breast cancer. *The breast journal*. 2005;11(3):204–9.
6. Kumar R, Alavi A. Fluorodeoxyglucose-PET in the management of breast cancer. *Radiol Clin North Am*. 2004 Nov;42(6):1113-22, ix.
7. Fletcher JW, Djulbegovic B, Soares HP, Siegel BA, Lowe VJ, Lyman GH, et al. Recommendations on the use of 18F-FDG PET in oncology. *Journal of nuclear medicine : official publication, Society of Nuclear Medicine*. 2008 Mar;49(3):480–508.
8. Facey K, Bradbury I, Laking G, Payne E. Overview of the clinical effectiveness of positron emission tomography imaging in selected cancers. *Health technology assessment (Winchester, England)*. 2007 Oct;11(44):iii-iv, xi–267.
9. Zamora-León SP, Golde DW, Concha II, Rivas CI, Delgado-López F, Baselga J, et al. Expression of the fructose transporter GLUT5 in human breast cancer. *Proceedings of the national academy of sciences of the united states of america*. 1996 Mar 5;93(5):1847–52.

10. Reinicke K, Godoy A, Ulloa V, Rodri F, Medina RA, Yan AJ, et al. Differential Subcellular Distribution of Glucose Transporters GLUT1 – 6 and GLUT9 in Human Cancer : Ultrastructural Localization of GLUT1 and GLUT5 in Breast Tumor Tissues. *J Cell Physiol.* 2006 Jun;207(3):614-27.
11. Pontén F, Jirström K, Uhlen M. The Human Protein Atlas--a tool for pathology. *The Journal of pathology.* 2008 Dec;216(4):387–93.
12. Levi J, Cheng Z, Gheysens O, Patel M, Chan CT, Wang Y, et al. Fluorescent fructose derivatives for imaging breast cancer cells. *Bioconjugate chemistry.* 2007;18(3):628–34.
13. Chan KK, Chan JYW, Chung KKW, Fung K-P. Inhibition of cell proliferation in human breast tumor cells by antisense oligonucleotides against facilitative glucose transporter 5. *Journal of cellular biochemistry.* 2004 Dec 15;93(6):1134–42.
14. Haradahira T, Tanaka A, Maeda M, Kanazawa Y, Ichiya YI, Masuda K. Radiosynthesis, rodent biodistribution, and metabolism of 1-deoxy-1-[18F]fluoro-D-fructose. *Nuclear medicine and biology.* 1995 Aug;22(6):719–25.
15. Schirmer M, Calamia KT, Wenger M, Klauser a, Salvarani C, Moncayo R. 18F-fluorodeoxyglucose-positron emission tomography: a new explorative perspective. *Experimental gerontology.* 2003 Apr;38(4):463–70.
16. Lavayssière R, Cabée A-E, Filmont J-E. Positron Emission Tomography (PET) and breast cancer in clinical practice. *European journal of radiology.* 2009 Jan;69(1):50–8.
17. Lind P, Igerc I, Beyer T, Reinprecht P, Hausegger K. Advantages and limitations of FDG PET in the follow-up of breast cancer. *European journal of nuclear medicine and molecular imaging.* 2004 Jun;31 Suppl 1(June):S125–34.
18. Quon A, Gambhir SS. FDG-PET and beyond: molecular breast cancer imaging. *Journal of clinical oncology : official journal of the American Society of Clinical Oncology.* 2005 Mar 10;23(8):1664–73.
19. Hodgson NC, Gulenchyn KY. Is there a role for positron emission tomography in breast cancer staging? *Journal of clinical oncology : official*

journal of the American Society of Clinical Oncology. 2008 Feb 10;26(5):712–20.

20. Mavi A, Urhan M, Yu JQ, Zhuang H, Houseni M, Cermik TF, et al. Dual time point 18F-FDG PET imaging detects breast cancer with high sensitivity and correlates well with histologic subtypes. *Journal of nuclear medicine : official publication, Society of Nuclear Medicine*. 2006 Sep;47(9):1440–6.
21. Buck A, Schirrmeister H, Kühn T, Shen C, Kalker T, Kotzerke J, et al. FDG uptake in breast cancer: correlation with biological and clinical prognostic parameters. *European journal of nuclear medicine and molecular imaging*. 2002 Oct;29(10):1317–23.
22. Crippa F, Agresti R, Seregni E, Greco M, Pascali C, Bogni A, et al. Prospective evaluation of fluorine-18-FDG PET in presurgical staging of the axilla in breast cancer. *Journal of nuclear medicine : official publication, Society of Nuclear Medicine*. 1998 Jan;39(1):4–8.
23. Ludański P, Koda M, Kozłowski L, Swiatecka J, Wojtukiewicz M, Sulkowski S, et al. Expression of glucose transporter GLUT-1 and estrogen receptors ER-alpha and ER-beta in human breast cancer. *Neoplasma*. 2004 Jan;51(3):164–8.
24. Younes M, Brown RW, Mody DR, Fernandez L, Laucirica R. GLUT1 expression in human breast carcinoma: correlation with known prognostic markers. *Anticancer research*. 1995 Nov-Dec;15(6B):2895–8.
25. Ravazoula P, Batistatou A, Aletra C, Ladopoulos J, Kourounis G, Tzigounis B. Immunohistochemical expression of glucose transporter Glut1 and cyclin D1 in breast carcinomas with negative lymph nodes. *European journal of gynaecological oncology*. 2003 Jan;24(6):544–6.
26. Alavi A, Zhuang H. Finding infection--help from PET. *Lancet*. 2001 Oct 27;358(9291):1386.
27. Kubota R, Kubota K, Yamada S, Tada M, Ido T, Tamahashi N. Microautoradiographic study for the differentiation of intratumoral macrophages, granulation tissues and cancer cells by the dynamics of fluorine-18-fluorodeoxyglucose uptake. *Journal of nuclear medicine : official publication, Society of Nuclear Medicine*. 1994 Jan;35(1):104–12.

28. Lim HS, Yoon W, Chung TW, Kim JK, Park JG, Kang HK, et al. FDG PET/CT for the detection and evaluation of breast diseases: usefulness and limitations. *Radiographics : a review publication of the Radiological Society of North America, Inc.* 2007 Oct;27 Suppl 1:S197–213.
29. Yang J, Dowden J, Tatibouët A, Hatanaka Y, Holman GD. Development of high-affinity ligands and photoaffinity labels for the D-fructose transporter GLUT5. *The Biochemical journal.* 2002 Oct 15;367(Pt 2):533–9.
30. Tatibouët a, Yang J, Morin C, Holman GD. Synthesis and evaluation of fructose analogues as inhibitors of the D-fructose transporter GLUT5. *Bioorganic & medicinal chemistry.* 2000 Jul;8(7):1825–33.
31. Kim DW, Ahn D-S, Oh Y-H, Lee S, Kil HS, Oh SJ, et al. A new class of SN2 reactions catalyzed by protic solvents: Facile fluorination for isotopic labeling of diagnostic molecules. *Journal of the American Chemical Society.* 2006 Dec;128(50):16394–7.
32. Laudański P, Swiatecka J, Kovalchuk O, Wołczyński S. Expression of GLUT1 gene in breast cancer cell lines MCF-7 and MDA-MB-231. *Ginekologia polska.* 2003 Sep;74(9):782–5.
33. Uldry M, Thorens B. The SLC2 family of facilitated hexose and polyol transporters. *Pflügers Archiv : European journal of physiology.* 2004 Feb;447(5):480–9.
34. Manolescu AR, Witkowska K, Kinnaird A, Cessford T, Cheeseman C. Facilitated hexose transporters: new perspectives on form and function. *Physiology (Bethesda, Md.).* 2007 Aug;22:234–40.
35. Caulfield MJ, Munroe PB, O’Neill D, Witkowska K, Charchar FJ, Doblado M, et al. SLC2A9 is a high-capacity urate transporter in humans. *PLoS medicine.* 2008 Oct 7;5(10):e197.
36. Macheda ML, Rogers S, Best JD. Molecular and cellular regulation of glucose transporter (GLUT) proteins in cancer. *Journal of cellular physiology.* 2005 Mar;202(3):654–62.

Chapter 3 - Radiopharmacological evaluation of 6-deoxy-6-[¹⁸F]fluoro-D-fructose as a radiotracer for PET imaging of GLUT5 in breast cancer

A version of this chapter has been published as:

Wuest M, **Trayner BJ**, Grant TN, Jans H-S, Mercer JR, Murray D, West FG, McEwan AJB, Wuest F, Cheeseman CI. Radiopharmacological evaluation of 6-deoxy-6-[¹⁸F]fluoro-D-fructose as a radiotracer for PET imaging of GLUT5 in breast cancer. *Nuclear Medicine and Biology*. 2011 May;38(4):461–75.

This work presented in this chapter represents a collaboration between the authors on the paper. BJT performed all *in vitro* experiments and analysis. *In vivo* experiments and analysis were performed by MW with assistance by BJT. All chemical syntheses were performed by TNG.

3.1 Introduction

Breast cancer represents the second leading cause of cancer related deaths in women. Advances in early diagnosis and treatment have led to a decline of mortality, despite an increase in breast cancer incidence. Breast cancer remains a major health care problem in women, and early detection in order to improve prognosis remains the cornerstone of breast cancer research and clinical applications. Most primary cancers are detected by physical examination or mammography, although mammography is limited by only moderate sensitivity and specificity. Therefore, other imaging methodologies like ultrasound, CT and MRI have been investigated to complement and increase the diagnostic accuracy for breast cancer (1–4).

In the clinic, increased glucose uptake and metabolism in cancer cells is used to identify tumors in patients and to assess tumor metabolism in response to therapy by using ^{18}F -labeled 2-deoxy-2-fluoro-D-glucose ($[^{18}\text{F}]\text{FDG}$) with positron emission tomography (PET) (5–7). $[^{18}\text{F}]\text{FDG}$ is the most commonly used PET radiotracer for diagnosis and management of a variety of cancers(7–9). The uptake of this radiolabeled hexose analogue into malignant cells is facilitated by the increased expression of several members of the facilitative hexose transporter (GLUT) family. It is evident that malignant transformation results in the altered expression of genes encoding members responsible not only for hexose transport, but also metabolism(10–12). Fourteen genes encoding facilitative glucose transporter proteins have been identified (GLUT1-13, and

HMIT) (13,14). It has been suggested that overexpression of the GLUT1 and GLUT3 proteins is responsible for the increased uptake of glucose and [¹⁸F]FDG in malignancies(15). Like glucose, [¹⁸F]FDG uptake in cells is followed by phosphorylation to [¹⁸F]FDG 6-phosphate through hexokinase, the first enzymatic step in glycolysis. [¹⁸F]FDG 6-phosphate is not further metabolized, which leads to its metabolic trapping and accumulation within malignant cells, as it is unable to be transported back out of the cell (16,17).

[¹⁸F]FDG displays some important limitations for tumor detection which has led to the clinical use of alternative PET tracers(18,19). Macrophages and other immune cells readily transport high levels of glucose and [¹⁸F]FDG, and uptake into these cells has been implicated in the generation of false positive diagnoses(20–22). An additional limitation of [¹⁸F]FDG in tumor diagnosis is increased uptake in inflammatory lesions, restricting the distinction between inflammation and tumor tissue and frequently leading to an overestimation in tumor size and to complications for assessment of cancer treatment efficacy.

A recent review assessing the clinical value of [¹⁸F]FDG-PET in breast cancer diagnosis indicated 76 to 89% sensitivity and 73 to 80% specificity for the diagnosis of primary breast cancer(23). Low and very variable sensitivity (20 to 50%) was observed for the detection of auxiliary lymph node metastases. Several clinical studies have investigated GLUT1 expression in breast cancers, revealing that 28 to 47% of selected patient samples were GLUT1 negative(24–27). The

low or absent tumor expression of GLUT1 in these patients seems to account for the low sensitivity of [¹⁸F]FDG-PET in detecting these breast cancers.

About 15 years ago, Zamora-Leon *et al.* postulated that the relatively high-affinity fructose transporter GLUT5 expressed in human breast cancer cells could provide an interesting alternative targeting strategy for earlier diagnosis and treatment of breast cancer (28). Recently, it has been shown that the fructose transporting Class I facilitative hexose transporter GLUT2 and the Class II facilitative hexose transporter GLUT5 are overexpressed in breast as well as other cancers (29). The authors found that 91% of the breast tumor tissue samples studied expressed GLUT2 and 85% expressed GLUT5. It has been suggested that increased fructose metabolism may play an important role in cancer progression (29–32). It has also been postulated that tumor cells can switch or supplement their nutrient pool through an increase of GLUT2 and GLUT5 expression, thus allowing a larger array of substrates to enter their metabolic pathways. Unfortunately, GLUT5 overexpression in these tumors does not contribute to the utility of [¹⁸F]FDG, as it is not a substrate for GLUT5. This makes GLUT5 a promising molecular target for the PET imaging of breast cancer and other cancers by means of radiolabeled fructose derivatives.

Rational design of [¹⁸F]labelled fructose derivatives is essential because incorporation of fluorine is critical for both proper binding and trafficking across the membrane via GLUT2 and GLUT5, as well as for its intracellular metabolism.

Intracellular phosphorylation of fructose occurs via two distinct enzymes: either by hexokinase at the 6-position, or ketohexokinase (KHK) at the 1-position. Haradahira and co-workers described the labelling of fructose with [^{18}F] at the 1-position to yield 1-deoxy-1- ^{18}F fluoro-D-fructose (1- ^{18}F FDF) which would be susceptible to phosphorylation by hexokinase. 1- ^{18}F FDF was evaluated in fibrosarcoma tumor-bearing mice; however, no trapping of 1- ^{18}F FDF in the tumor was observed (33). More recently, Levi *et al.* labelled fructose with small fluorophores at the 1-position and apparently showed uptake in GLUT5-expressing human breast cancer cells versus no uptake in cells lacking GLUT5 (31).

Alternatively, labelling of fructose with [^{18}F] could be performed at the 6-position. Previous work by Holman's group indicated that a compound labelled at the 6-position would still be handled properly by the transporter (GLUT5) and in some cases may actually increase the compound's affinity for binding (34,35). In addition to the reported labelling of position 1 of fructose with fluorine and fluorophores, we have synthesized the fructose analogue 6-deoxy-6-fluoro-D-fructose (6-FDF; (36)). Initial experiments using 6-FDF have shown its transport into two human breast cancer cell lines and dose-dependent competitive inhibition of D-fructose transport, as well as transport of [^{14}C]6-FDF via GLUT5 in a cell culture transport model (36).

Herein we describe the synthesis and radiopharmacological evaluation of 6-¹⁸F]fluoro-6-deoxy-D-fructose (6-¹⁸F]FDF) as a novel radiotracer for PET imaging of GLUT5 expression. We have analyzed the *in vitro* transport of 6-¹⁸F]FDF and ¹⁸F]FDG in two different breast cancer cell lines known to express GLUT5. Biodistribution and metabolism of 6-¹⁸F]FDF was studied in wild-type BALB/c mice. Furthermore, we have studied solid tumor uptake of 6-¹⁸F]FDF and of ¹⁸F]FDG in a murine (EMT-6) and human (MCF-7) breast tumor-bearing mouse model using dynamic small animal PET.

3.2 Materials and Methods

Please see **Appendix A** for a detailed materials list.

3.2.1 Radiotracer synthesis

6-Deoxy-6-¹⁸F]fluoro-D-fructose (6-¹⁸F]FDF) was synthesized in an automated Eckert & Ziegler Modular-Lab synthesis unit (Berlin, Germany). The synthesis of reference compound 6-FDF was accomplished in eight steps in 15% overall yield starting with readily available D-fructose (36). This route provides the triflate labeling precursor (methyl 1,3,4-tri-O-acetyl-6-O-(trifluoromethanesulfonyl)- α/β -D-fructofuranoside) for radiofluorinations in milligram-scale quantities. Since the triflate is not stable to prolonged storage, it had to be freshly synthesized prior to each radiosynthesis. Radiolabelling and deprotection were carried out in two steps: a) reaction of methyl 1,3,4-tri-O-acetyl-6-O-(trifluoromethanesulfonyl)- α/β -D-fructofuranoside with potassium [¹⁸F]fluoride in the presence of Kryptofix

(K₂₂₂) in acetonitrile at 85°C, and b) deprotection with 2 N HCl for 8 min at 110°C. The crude hydrolysis mixture was purified by HPLC (PhenomenexC18 10 x 10 x 250 µm column) running at 4 mL/min. Purification provided 6-[¹⁸F]FDF using an increasing acetonitrile : water gradient as the eluent (R_T = 4.1 min). 6-[¹⁸F]FDF was obtained in >98% radiochemical purity. The total synthesis time was 120 min from the start of radiofluorination and the overall yield ranged between 25-35% (decay corrected).

3.2.2 *Western Blots of MCF-7, MDA-MB-231 and EMT-6*

Isolated whole cell samples were lysed with Cellytic™ M (Sigma), combined with a protease inhibitor cocktail as per the manufacturers specifications (Sigma, Canada). BCA protein quantification assay was run as per manufacturers specifications (Pierce, USA). 25 µg samples were then run on a 10% separating gel, and then transferred to a nitrocellulose membrane where the protein was labelled using the particular rabbit primary polyclonal antibodies protein being examined with concentrations ranging from 1:250 to 1:1000 (GLUT5 - Biogenesis, KHK - Sigma). After the primary antibody was applied overnight, it was then labelled with ECL™ Antirabbit IgG Horseradish peroxidase linked whole antibody and then was visualized using the ECL™ Western Blot detection reagents (Amersham Biosciences).

3.2.3 *In vitro cell uptake and efflux studies*

Both EMT-6 and MCF-7 cells were grown in a CO₂ incubator at 37°C, in Gibco[®] DMEM-F-12 supplemented with 15 mM HEPES, L-glutamine, 10% fetal bovine serum and 1% penicillin/streptomycin with media renewal every 2-3 days. For radiotracer uptake studies, cells were grown to confluence in 12-well plates using the same media. One hour prior to the experiment, the media was removed and the cells were washed two times with phosphate-buffered saline solution (PBS). Next, glucose-free Krebs-Ringer solution (120 mM NaCl, 4 mM KCl, 1.2 mM KH₂PO₄, 2.5 mM MgSO₄, 25 mM NaHCO₃, 70 μM CaCl₂, pH 7.4) was added to the cells. 300 μl Krebs-Ringer (with or without 5 mM glucose or 30 mM fructose) solution with 0.1-0.5 MBq [¹⁸F]FDG or 6-[¹⁸F]FDF was added to each well and the plates were incubated at 37°C for specific periods of time (5, 10, 15, 30 and 60 min). After incubation, cells were rinsed twice with ice-cold Krebs-Ringer solution to stop transport and then immediately lysed using 500 μL of 5% trichloroacetic acid (TCA) for one hour. The cell lysate was counted in a γ-counter (Wallac 1480 Wizard-3, Perkin-Elmer, Woodbridge, Ontario, Canada). Protein levels were quantified using the BCA protein assay kit (Pierce, Rockford, IL, U.S.A.) according to the manufacturer's recommendations and bovine serum albumin was used as the protein standard. Cell uptake levels were normalized to percent of the total added amount of radioactivity corresponding to injected dose (%ID) per mg protein.

For the efflux experiments, cells were incubated in glucose-free Krebs-Ringer solution containing 6- ^{18}F]FDF or ^{18}F]FDG for 60 min at 37°C as described above. The cells were then washed twice using room temperature Krebs-Ringer solution, and 1 mL of 37°C Krebs-Ringer solution was carefully added to each well. At the time points of interest (10, 20, 40 and 60 min), the cells were washed twice with ice cold Krebs-Ringer solution, lysed using 500 μL of TCA and counted in a γ -counter (see above). Cell efflux levels were normalized to the radioactivity uptake at time point zero.

To estimate the affinity of cold 6-FDF for GLUT5 in comparison to that of fructose, half-maximum inhibition coefficients (IC_{50}) values of both compounds were determined. EMT-6 cells were incubated with glucose-free Krebs-Ringer buffer containing 6- ^{18}F]FDF and different concentrations of either 6-FDF (10^{-8} – 10^{-2} M) or fructose (10^{-5} – 1 M) and no compound at all for the control. After 60 min cells were rinsed with ice-cold Krebs-Ringer solution, lysed and counted in a γ -counter as described above.

3.2.4 Animals

All animal experiments were carried out in accordance with guidelines of the Canadian Council on Animal Care (CCAC) and were approved by the local animal care committee of the Cross Cancer Institute.

Murine EMT-6 cells (5×10^6 cells in 100 μL PBS) were injected into the upper left flank of female BALB/c mice (20-24 g, Charles River, Saint-Constant, Quebec,

Canada). The EMT-6 tumor-bearing mice were imaged and used for *ex vivo* biodistribution experiments after allowing 8 to 11 days for the tumors to reach sizes of 518 ± 87 mg (n = 9).

Human MCF-7 cells, which form xenografts in female athymic mice, were injected subcutaneously ($2-5 \times 10^6$ cells in 100 μ L PBS) into 8-10 weeks old female NIH-III nu/nu mice (Charles River, Wilmington, MA, U.S.A.). Before injection of the cells, all mice received a 0.72 mg/pellet containing 17β -estradiol in a 60-day release preparation (Innovative Research of America, Sarasota, FL, U.S.A.). The pellet was implanted subcutaneously into the upper right flank in order to provide a constant level of 17β -estradiol needed by the estrogen-receptor positive MCF-7 cells. Tumors were imaged 20 to 30 days after injection, with the tumors reaching sizes ranging from 200 to 400 mm³.

3.2.5 *Biodistribution experiments*

Biodistribution studies were performed in EMT-6 tumor-bearing BALB/c mice. After intravenous injection of 1-2 MBq 6-^[18F]FDG in 80 to 120 μ L saline (0.91% w/v of NaCl) into the tail vein of anesthetized mice, the animals were allowed to regain consciousness until sacrifice. Animals were euthanized by decapitation at 5, 30 and 120 min post injection and rapidly dissected. Organs of interest including blood, heart, lung, liver, kidneys, gallbladder, spleen, duodenum, small and large intestine, pancreas, right femur, muscle, ovaries, brain, fat and tumors were collected and weighed. Radioactivity in all tissues was measured in the γ -

counter and results were analyzed as percentage of injected dose per gram of tissue (%ID/g).

3.2.6 *Small animal PET in normal and tumor-bearing mice*

Positron emission tomography (PET) experiments were performed on normal BALB/c mice, on BALB/c mice bearing EMT-6 tumors, and on NIH-III nu/nu mice bearing MCF-7 tumors on the upper left flank. The mice were not fasted prior to imaging experiments. The animals were anesthetized through inhalation of isoflurane in 40% oxygen / 60% nitrogen (gas flow, 1 L/min) and body temperature was kept constant at 37°C for the entire experiment. Mice were positioned and immobilized in the prone position with their medial axis parallel to the axial axis of the scanner and their thorax, abdomen and hind legs (organs of interest: heart, kidneys, bladder, tumors) in the centre of the field of view of the microPET[®] R4 scanner (Siemens Preclinical Solutions, Knoxville, TN, U.S.A.). A transmission scan for attenuation correction was not acquired. The amount of radioactivity present in the injection solution in a 0.5 mL syringe was determined with a dose calibrator (AtomLab[™] 300, Biodex Medical Systems, Shirley, NY, U.S.A.), which was cross calibrated with the scanner. The emission scan of 120-min PET acquisition was started. After a delay of approximately 15 s, 4-5 MBq of the radiotracer of interest (6-[¹⁸F]FDF or [¹⁸F]FDG) in 100 -150 µL saline was injected through a needle catheter into the tail vein. Data acquisition continued for 120 min in 3D list mode. The list mode data were sorted into sinograms with 59 time frames (10 x 2 s, 8 x 5 s, 6 x 10 s, 6 x 20 s, 8 x 60 s, 10 x 120 s, 10 x 300 s).

The frames were reconstructed using the Ordered Subset Expectation Maximization applied to the 2D sinograms (2D OSEM). The pixel size was 0.085 by 0.085 by 0.12 cm and the resolution in the centre field of view was 1.8 mm. No correction for partial volume effects was performed. The image files were further processed using the ROVER v2.0.21 software (ABX GmbH, Radeberg, Germany). Masks for defining 3D regions of interest (ROI) were set and the ROI's were defined by thresholding. ROI time-activity curves (TAC) were generated for subsequent data analysis. Standardized uptake values (SUV = (activity/mL tissue) / (injected activity/body weight), mL/g) were calculated for each ROI.

3.2.7 **Phosphorylation with KHK**

The *in vitro* enzymatic reaction of 6-¹⁸F]FDF and human recombinant KHK or human recombinant hexokinase-II (both 1 mg/mL; ATGen, Seongnam City, South Korea) was carried out in a TRIS buffer solution for up to 60 min at 37°C using a thermomixer. The final buffer solution contained 600 µL TRIS-HCl (100 mM), 200 µL KH₂PO₄ (100 mM), 50 µL MgCl₂ (40 mM), 50 µL Na₂ATP (100 mM), 50 or 150 µg KHK or 120 µg hexokinase-II and 1.7 MBq 6-¹⁸F]FDF in 50 µl deionized water. After 5, 10, 30 and 60 min, aliquots of the reaction mixture were spotted on standard phase TLC plates, developed in 95% acetonitrile and 5% water and analyzed by radio-TLC. The samples were compared to a control solution mixture with no enzyme added.

3.2.8 Determination of radioactive metabolites in mouse blood and urine

15 to 25 MBq 6-¹⁸F]FDF in 100 to 150 μ L saline was injected as a bolus through a catheter into the tail vein of isoflurane anesthetized BALB/c mice. Before radiotracer injection, mice were heparinized by subcutaneous injection of 50 μ L heparin (1000 I.U.) and kept under anesthesia during the course of the experiment. At selected time points of 5, 30, or 60 min, the animal was sacrificed and a whole blood sample (approximately 500 μ L) was collected. Blood cells were separated by immediate centrifugation (5 min at 13,000 rpm). Proteins within the sample were precipitated by adding ~800 μ L methanol to the supernatant following a second centrifugation step (5 min at 13,000 rpm). TLC samples from the plasma fraction were developed and analyzed using radio-TLC as described above. The experiments were carried out at least three times per time point. Each fraction (blood cells, proteins and plasma) was counted for its radioactivity content in the dose calibrator in order to determine radioactivity percentage distribution in the blood compartments.

3.2.9 Data analysis

All data are expressed as means \pm S.E.M. from n investigated animals. All TACs were constructed using GraphPad Prism[®] 4.0 (GraphPad Software, San Diego, CA, U.S.A.). Where applicable, statistical differences were tested by Student's t-test and were considered significant for $p < 0.05$. IC₅₀ values (molar concentrations

producing half-maximum inhibition of the maximum uptake of 6-¹⁸F]FDF in EMT-6 cells) were determined by non-linear regression.

3.3 Results

3.3.1 Radiotracer synthesis

The radiosynthesis of 6-¹⁸F]FDF was performed in a remotely-controlled synthesis unit via a two-step procedure through treatment of a triflate precursor **1** with no-carrier-added potassium [¹⁸F]fluoride and kryptofix K₂₂₂ in acetonitrile at 85°C. Intermediate **2** was subsequently deprotected by treatment with 2 N HCl at 110°C for 8 min (**Figure 3.1**). [¹⁸F]Fluoride incorporation by nucleophilic displacement of the triflate leaving group in the labeling precursor **1** and subsequent acidic hydrolysis of intermediate **2** gave 6-¹⁸F]FDF in radiochemical yields of 25-35% (decay-corrected) within 120 min including HPLC purification. The radiochemical purity exceeded 95%.

The UV detection limit for 6-FDF was determined to be 0.1 mg/mL, which translates to a maximum amount of 15 µg of cold 6-FDF in a mouse after injection of a maximum of 150 µL of product solution. However, the exact amount of unlabelled 6-FDF in the final product solution should be much lower, since the UV trace of the analytical HPLC at 220 nm showed no mass peak corresponding to unlabelled 6-FDF.

3.3.2 *Western Blots of MCF-7, MDA-MB-231 and EMT-6*

Western blots probing for GLUT5 in EMT-6 and KHK in the MCF-7, MDA-MB-231 and EMT-6 cell lines using 25 µg of whole cell lysate were performed and bands corresponding to GLUT5 in EMT-6 at ~55 KDa, although nothing was observed for KHK staining in all three cell lines in agreement with previously published data (**Figure 3.2**) (31). The control lane containing 25 µg of lysate from a human liver lysate sample (gift from Dr. Elaine Leslie) had a band at ~30 KDa, agreeing with previously published data on liver expression of KHK (31).

3.3.3 *Cell uptake studies*

Radiotracer uptake of 6-¹⁸F]FDF in the murine breast cancer cell line EMT-6 and in the human breast cancer cell line MCF-7 were compared to the uptake of ¹⁸F]FDG (**Figure 3. 3 left**). Uptake of 6-¹⁸F]FDF was similar in both cell lines, whereas uptake of ¹⁸F]FDG was about 5- to 8-fold higher in EMT-6 versus MCF-7 cells. In the presence of 5 mM glucose ¹⁸F]FDG uptake was significantly reduced in EMT-6 cells. In MCF-7 cells, the ¹⁸F]FDG uptake was also decreased by the presence of external glucose but to a lesser extent than in EMT-6 cells. In contrast, addition of 5 mM glucose to the extracellular test media did not influence uptake levels of 6-¹⁸F]FDF. The presence of extracellular glucose competitively inhibited ¹⁸F]FDG binding and transport through GLUT1, but did not affect GLUT5-mediated 6-¹⁸F]FDF transport.

Uptake of 6-^[18F]FDF into both cell lines was also measured in the absence and presence of extracellular fructose (**Figure 3.3 middle**). A concentration of 30 mM fructose reduced radiotracer uptake levels from 22 ± 1 to 15 ± 0.6 %ID/g protein in EMT-6 cells and from 17 ± 2 to 8 ± 2 %ID/g protein in MCF-7 cells after 60 min incubation, confirming that 6-^[18F]FDF is indeed being transported through GLUT5 and thus competes with extracellular fructose for entry into the cell.

Radiotracer efflux experiments in both cell lines (**Figure 3.3 right**) showed that ^[18F]FDG was not transported out of the cells, consistent with the accepted hypothesis for trapping by phosphorylation. 6-^[18F]FDF, on the other hand, was rapidly transported back out of the cells, which implies the lack of a trapping mechanism in both cell lines *in vitro*.

Analysis of the intracellular radioactivity after a 60 min incubation revealed that $\geq 75\%$ and $\geq 65\%$ intact 6-^[18F]FDF was found in murine EMT-6 cells and human MCF-7 cells, respectively.

To estimate the affinity of 6-FDF for GLUT5, cell uptake of 6-^[18F]FDF into EMT-6 cells was analyzed in the presence of different concentrations of cold 6-FDF and fructose. **Figure 3.4** shows the resulting concentration-response curve for 6-FDF inhibiting 6-^[18F]FDF uptake in comparison to that for fructose. Non-linear regression analysis resulted in an IC_{50} of 19 ± 6 mM ($n=3$) for 6-FDF and of 322 ± 33 mM ($p < 0.05$; $n=3$) for fructose, indicating that the potency and

therefore also the affinity of 6-FDF for GLUT5 is about 10-fold higher than that of fructose, the natural substrate for GLUT5.

3.3.4 *Biodistribution in normal mice*

Table 3.1 depicts the organ biodistribution of 6- ^{18}F]FDF in EMT-6 tumor bearing BALB/c mice at 5 min, 30 min and 120 min post injection. A similar overall organ biodistribution was also found in non-tumor-bearing BALB/c mice. Aside from initial high blood levels, large amounts of radioactivity uptake were found in liver and kidney at 5 min post injection. The radioactivity was cleared from all tissues and organs over time, except for the bone, indicating either radio-defluorination or uptake into the bone. Interestingly, radioactivity uptake was observed in the brain within the first 30 min post injection followed by a decrease again at 120 min post injection.

Figure 3.5 shows a timecourse of the radioactivity levels using dynamic small-animal PET experiments after injection into a normal BALB/c mouse. Clearance of 6- ^{18}F]FDF mainly occurred through the kidneys. The skeleton was clearly visible at 30 min post injection. After 60 min, radioactivity accumulation in the bone was even more pronounced. At 120 min, radioactivity was cleared from most tissues and organs, which is consistent with the findings of the biodistribution studies.

In **Figure 3.6**, time-activity curves (TACs) over 120 min for 6- ^{18}F]FDF in normal BALB/c mice are presented. Blood clearance occurred quickly over the time

course of the experiment as observed from the analysis of the blood pool over the heart and most of the injected radioactivity was accumulated in the bladder (compare to **Table 3.1** and **Figure 3.5**) radioactivity uptake in the brain reached a maximum SUV of 0.98 ± 0.08 at 50 min post injection, which then decreased slightly to 0.80 ± 0.12 ($n = 3$; $p = 0.055$) at the end of the experiment (**Figure 3.6**). The maximum uptake level in the brain seemed to stay relatively constant after slow uptake over the first half hour. Interestingly, the TAC for bone suggests two phases in the kinetics of radioactivity uptake as indicated by two different slopes in the curve. After a rapid initial uptake reaching an SUV of 0.99 ± 0.09 at 4.5 min post injection, an increase of uptake was observed after 30 min, reaching a final SUV of 2.41 ± 0.45 at 120 min post injection (**Figure 3.6**).

3.3.5 *In vivo studies in tumor-bearing mice*

In this study, two different mouse models were analyzed: the murine EMT-6 tumor-bearing BALB/c mouse model and the xenografted human MCF-7-bearing NIH-III mouse model. **Figure 3.7** shows the maximum intensity projections for 6- ^{18}F FDF in an EMT-6 tumor-bearing mouse at 15 min (**Figure 3.7A**) and 120 min (**Figure 3.7B**) post injection. Tumor uptake of 6- ^{18}F FDF was visible at both time points, and at 120 min bone uptake of fluoride was apparent as well. For comparison, the same mouse was also imaged 48 h later with ^{18}F FDG (**Figure 3.7C and D**) and the EMT-6 tumor was again clearly visible at both time points. **Figure 3.8** shows the imaging experiments with both tracers in the human MCF-7 tumor model. Tumor uptake of 6- ^{18}F FDF was less visible than in the EMT-6

tumor possibly due to a decreased tumor-to-muscle ratio. In the MCF-7 tumors the tumor-to-muscle ratio also seemed to be low for [¹⁸F]FDG when measured in the same tumor within 24 h.

Figure 3.9 summarizes the TACs over 120 min for both tracers in both tumor models (upper panels) and the corresponding tumor-to-muscle ratios (lower panels). After the injection of 6-[¹⁸F]FDF, rapid uptake of the radioactivity into EMT-6 tumors was observed, reaching a maximum level (SUV 1.23 ± 0.09 , $n = 3$) after 10-15 min. At later time points, the radioactivity concentration decreased in the tumor reaching a SUV of 0.54 ± 0.06 ($n = 3$) after 120 min post injection. [¹⁸F]FDG showed a completely different accumulation pattern in EMT-6 tumors compared to 6-[¹⁸F]FDF; its uptake levels increased consistently over two hours, reaching a maximum SUV of 1.80 ± 0.25 ($n = 3$). The tumor uptake profile of both tracers was quite different in the human MCF-7 tumor xenograft. Radioactivity uptake levels of both tracers were lower in the MCF-7 tumors and did not change significantly after the initial uptake phase at 5 to 10 min post injection (SUV of 0.76 ± 0.05 , $n = 3$ for 6-[¹⁸F]FDF and 0.74 ± 0.12 , $n = 3$ for [¹⁸F]FDG). Interestingly, maximum uptake levels of the two radiotracers in MCF-7 tumors seemed to be very similar despite the fact that the tracers use different uptake and trapping mechanisms. Analysis of tumor-to-muscle ratios in MCF-7 tumors revealed higher ratios for [¹⁸F]FDG versus 6-[¹⁸F]FDF, which was mainly due to the lower muscle uptake of [¹⁸F]FDG. In addition, tumor-to-muscle ratios for both radiotracers in MCF-7 tumors remained constant over time, whereas

tumor-to-muscle ratios increased in EMT-6 tumors for [¹⁸F]FDG but not for 6-[¹⁸F]FDF.

3.3.6 *Phosphorylation with KHK*

6-[¹⁸F]FDF metabolism is examined in **Figure 3.10A-G**. 6-[¹⁸F]FDF was phosphorylated by the human recombinant KHK as analyzed in a direct reaction between the radiotracer and the enzyme. **Figure 3.10A** illustrates the time-dependence of the enzyme reaction resulting in the formation of phosphorylated product at two different concentrations of KHK. In the presence of 50 µg enzyme 84% of 6-[¹⁸F]FDF was phosphorylated after 60 min; with 150 µg enzyme, this increase amounted to 97%. In contrast, ≥ 90% of intact 6-[¹⁸F]FDF was detectable after a 60 min incubation with the human recombinant hexokinase-II (**Figure 3.10B**). These findings indicate that 6-[¹⁸F]FDF is a selective substrate for recombinant human KHK *in vitro*.

3.3.7 *Metabolite analysis*

Figures 3.10C-G summarizes the analysis of blood and urine samples. At 5 min post injection, 33 ± 2% of the total amount of the radioactivity in the blood was found in blood cells, 10 ± 2% was bound to plasma proteins and 57 ± 3% was present within the plasma (n = 3), with only the latter amount available for delivery to the target organs (**Figure 3.10C**). The overall distribution in the different blood compartments did not change over time, which suggests the rapid establishment of equilibrium between the different blood compartments.

Analysis of the plasma samples at different time points with radio-TLC revealed at least two detectable radiometabolites: one more polar radiometabolite 1 ($R_f = 0.1$), and a more lipophilic radiometabolite 2 ($R_f = 0.7-0.8$; **Figure 3.10E**). Over time, the amount of intact 6- ^{18}F FDF decreased rapidly. At 5 min post injection, only 24% of intact 6- ^{18}F FDF was detected in the plasma. At 30 min and at 60 min the amount of intact 6- ^{18}F FDF further decreased to 9-11% (**Figure 3.10F**). This is consistent with the profile observed in urine samples (**Figure 3.10G**). At 5 min post-injection, about 16% of the total radioactivity was found to be intact 6- ^{18}F FDF in the urine, whereas at 60 min only 4% of 6- ^{18}F FDF remained unmetabolized. The overall metabolite analysis thus revealed rapid metabolism of 6- ^{18}F FDF in mice.

3.4 Discussion

3.4.1 Summary

The goal of the present study was to investigate the radiopharmacological profile of the fructose derivative 6- ^{18}F FDF *in vitro* and *in vivo*. We found that (i) EMT-6 expresses GLUT5 and uptake of 6- ^{18}F FDF in mouse EMT-6 as well as human MCF-7 breast tumor cells is mediated via GLUT5, (ii) 6-FDF possesses a 10-fold higher potency than fructose to inhibit 6- ^{18}F FDF uptake in EMT-6 cells via GLUT5, (iii) 6- ^{18}F FDF is rapidly cleared from the body and radioactivity is accumulated in the bladder, (iv) 6- ^{18}F FDF undergoes radiodefluorination, (v) 6-

[¹⁸F]FDF exhibits uptake in murine and human xenograft breast tumors *in vivo*, and (vi) 6-[¹⁸F]FDF is rapidly metabolized in mice.

3.4.2 *In vitro studies*

Western blots used to identify the expression of GLUT5 and KHK in the MCF-7, MDA-MB-231 and EMT-6 cell lines identified that as previous studies suggested, neither MCF-7 or MDA-MB-231 expressed KHK (31). EMT-6 however, did have expression of GLUT5. The typically observed doublet indicating the mature glycosylated and the immature unglycosylated forms, EMT-6 showed a singlet perhaps due to the varied affinity of the human antibody for the murine isoform of GLUT5.

[¹⁸F]FDG was used in the experiments as the “gold standard” for hexose transport and metabolism to compare the putative properties of the fructose derivative 6-[¹⁸F]FDF as a novel radiotracer for breast cancer imaging. [¹⁸F]FDG uptake into EMT-6 and MCF-7 cells was clearly dependent on the presence of extracellular glucose levels that competitively inhibited [¹⁸F]FDG transport through GLUT1, which is the major uptake mechanism for this standard radiotracer. In the absence of glucose in the extracellular media, uptake of [¹⁸F]FDG was about 4-fold higher in the murine than in the human cell line. This difference suggests that the expression profile of GLUT1 may differ in these two tumor cell lines. It also suggests that the murine transport kinetics and affinity for [¹⁸F]FDG and/or the expression and enzyme activity of the intracellular

hexokinase II, which phosphorylates [^{18}F]FDG, may also be different. MCF-7 cells show lower [^{18}F]FDG uptake compared to other human tumor cell lines such as HT-29, FaDu, HDMEC, HUVEC, HAEC. In addition, estrogen receptor (ER)-positive breast cancer cells such as MCF-7 are known to show lower [^{18}F]FDG uptake compared to that of ER-negative cells such as MDA-MB-231 (26,37) since the ER status may alter the expression of other proteins such as GLUT1. It has been shown that mRNA expression levels of GLUT1 in ER-negative cell lines such as MDA-MB-231 were higher than those of ER-positive cells such as MCF-7(38). Immunocytochemical analysis within a group of GLUT1-positive breast cancer patients revealed that more tumors were ER negative than ER positive (26). However, under saturation conditions in the presence of high extracellular glucose concentrations (5 mM) we found no significant differences in the uptake of [^{18}F]FDG between EMT-6 and MCF-7 cells.

Uptake of the fructose derivative 6-[^{18}F]FDF was independent of glucose (5 mM), indicating a GLUT1/GLUT2-independent transport of 6-[^{18}F]FDF. In contrast, excess of extracellular fructose (30 mM) competitively inhibited 6-[^{18}F]FDF uptake, confirming that the transport of the radiotracer is indeed mediated through the fructose transporting GLUT5. Uptake of 6-[^{18}F]FDF in EMT-6 cells was 2-fold higher than in MCF-7 cells. This may suggest a difference in the expression profile of GLUT5 in the two cell lines, which is the main transporter for fructose and 6-[^{18}F]FDF in these cells(28,36). In EMT-6 cells, unlabelled 6-FDF has a 10-fold higher potency for inhibiting 6-[^{18}F]FDF uptake via GLUT5

compared to the natural substrate fructose, indicating that transport of 6-¹⁸F]FDF through GLUT5 would be favoured when both compounds are present. Fructose itself possesses an order of magnitude lower affinity for GLUT2 (apparent $K_m > 50$ mM (28) or 66.7 ± 18.3 mM (39)) versus GLUT5 ($K_m=8$ mM (28) or 5 mM (40)). On the other hand, glucose has a higher affinity for both GLUT1 ($K_m=5$ mM) and GLUT2 ($K_m=11$ mM (14)). In the presence of normal circulating glucose concentrations (~5mM), only GLUT5 will be available for the transport of 6-¹⁸F]FDF due to glucose inhibiting fructose transport via GLUT2. The observed differences in transport between the two cell lines are likely attributed to a difference in GLUT5 expression levels as well as perhaps substrate affinity variability between the human and murine transporter homologues. When comparing *in vitro* uptake of [¹⁸F]FDG and 6-¹⁸F]FDF in the presence of 5 mM glucose, radiotracer uptake levels of 6-¹⁸F]FDF were substantially lower than those for [¹⁸F]FDG.

Radiotracer efflux experiments showed no (EMT-6) or only low (10%, MCF-7) amounts of [¹⁸F]FDG efflux out of the cells and into the extracellular medium, which is consistent with the accepted hypothesis of intracellular phosphorylation by hexokinase as the metabolic trapping mechanism(41,42). On the other hand, 6-¹⁸F]FDF displayed substantial efflux for both cell types, which is indicative of a lack of trapping mechanism via KHK-mediated phosphorylation. These findings are consistent with previous work that shows that the breast cancer cell lines MCF-7, MDA-MB-231 and MDA-MB-435 do not express the enzyme KHK *in*

vitro(31). When comparing the efflux curves of 6-[¹⁸F]FDF from both lines, efflux from MCF-7 cells occurs more slowly than from EMT-6 cells.

Incubation of 6-[¹⁸F]FDF with various concentrations of recombinant human KHK resulted in the formation of phosphorylated 6-[¹⁸F]FDF, which identifies 6-[¹⁸F]FDF as an *in vitro* substrate for KHK. KHK is the principal fructose-metabolizing enzyme, and it is found in large amounts in kidneys, liver and the pancreas [41]. It is obvious that fructose derivatives labelled in position 6 cannot be phosphorylated by hexokinase and therefore, position 1 of 6-[¹⁸F]FDF is available for phosphorylation by KHK only(31,33,43). Indeed, no phosphorylated product was detectable after incubation of 6-[¹⁸F]FDF with human recombinant hexokinase-II.

3.4.3 *In vivo studies*

Fructose transport *in vivo* and uptake into target organs is dependent on expression levels of the fructose transporting GLUT isoforms GLUT2 and GLUT5. High levels of GLUT5 are found in small intestine, kidneys, testes and sperm, skeletal muscle, adipocytes and in different cell types of the brain (32). Biodistribution of 6-[¹⁸F]FDF indicated initial high uptake in kidneys, small intestine and brain of normal mice, which remains high after 120 min post injection when compared to the biodistribution pattern of [¹⁸F]FDG in these organs(44). [¹⁸F]FDG uptake in the kidneys is about 7-times lower than 6-[¹⁸F]FDF and only half of the uptake is found in the whole intestine at 60 min post

injection when compared with 6-[¹⁸F]FDF. Biodistribution of 6-[¹⁸F]FDF in mice showed a similar pattern in small intestine, kidney and brain compared to the previously reported ¹⁸F-labeled fructose derivative 1-[¹⁸F]FDF (33). This finding suggests that both of the radiolabeled fructose derivatives are accumulated in tissues expressing high levels of GLUT5 in contact with the bloodstream. When 1-[¹⁸F]FDF was first evaluated in 1995, GLUT5 expression had not yet been associated with cancer (28). It has been reported that labelling of fructose in position 1 would favour GLUT5-mediated transport (35,45).

6-[¹⁸F]FDF and 1-[¹⁸F]FDF show a comparable biodistribution pattern in all tissues and organs studied except for a higher brain uptake in the case of 6-[¹⁸F]FDF. However, no information on the GLUT5 affinity and transport capacity of 1-[¹⁸F]FDF is available, which would allow a more meaningful comparison between the two ¹⁸F-labeled fructose derivatives. Further work in this area is warranted in lieu of the information ascertained since the original synthesis and characterization of 1-[¹⁸F]FDF (33–35).

One major difference between 6-[¹⁸F]FDF and 1-[¹⁸F]FDF is what appears to be high radio-defluorination of 6-[¹⁸F]FDF, which results in increased bone uptake of 6.39 %ID/g at 120 min post injection. A comparable high bone uptake was not reported for 1-[¹⁸F]FDF (0.78 %ID/g at 120 min post injection (33)). Based on later investigation discussed in the next chapter, large quantities of radio-defluorination may not be taking place, as radioactivity was observed to be

washed out of bone tissue after an extended observation window in rats. GLUT5 expression has been identified within chondrocytes in rats(46), and the observable high concentration of radioactivity within the joints after two hours may be a consequence of GLUT5 mediated chondrocyte uptake of the tracer. Unfortunately, expression of GLUT5 within other cell types associated with bone is unknown at this time.

Oncogenesis is known to alter the expression levels of many components of the pathways of hexose metabolism, which includes an increased expression of GLUT1 and hexokinase II that, in concert, act as the main mechanism for transport and trapping of [^{18}F]FDG (47,48). GLUT5 mRNA and protein expression has also been identified as influential in the development of tumors in certain organ systems (32). About two decades ago, studies failed to detect GLUT5 in several types of cancer (15), but in 1996, Zamora-Leon and co-workers found evidence for GLUT5 expression in two breast cancer cell lines (28). GLUT5 expression was not detectable in normal breast tissue and, based on the later finding that 6-[^{18}F]FDF is a GLUT5 substrate, 6-[^{18}F]FDF was further studied here in two different mouse breast tumor models *in vivo*. The radioactivity uptake could be shown in both the murine EMT-6 and the human xenograft MCF-7 tumors, although initial uptake as well as accumulation and retention of radioactivity were significantly different in the two tumors. This suggests that uptake mechanisms and possibly also trapping are different in the two tumor models investigated. According to Levi et al., MCF-7 cells do not express KHK and

therefore are not able to further metabolize 6- ^{18}F FDG via phosphorylation after GLUT5-mediated uptake (31,43). In contrast to the *in vitro* experiments, no clearance of radioactivity was observed in MCF-7 tumors, whereas results consistent with the *in vitro* findings were found in the EMT-6 tumors. Interestingly, ^{18}F FDG uptake in EMT-6 and MCF-7 tumors also showed a markedly different radioactivity accumulation pattern. EMT-6 tumors showed increasing radioactivity accumulation over time whereas ^{18}F FDG uptake into MCF-7 tumors was significantly lower and uptake plateaued at relatively low levels after the first initial radiotracer uptake phase. This finding has also been previously observed in ^{18}F FDG MCF-7 cell uptake studies (49). Moreover, analysis of ^{18}F FDG in biodistribution studies also reported low (< 1% ID/g) uptake levels of radioactivity in MCF-7 tumor xenografts (44). Radioactivity uptake levels did not increase between 60 to 180 min post injection (44). Although MCF-7 cells express GLUT1 (28,38) and hexokinase I and II *in vitro* (31), ^{18}F FDG uptake proceeds at a low rate *in vivo*. Thus, the determinants of ^{18}F FDG uptake in MCF-7 cells seem to be more complex than in EMT-6 cells. Uptake of 6- ^{18}F FDG and ^{18}F FDG in the MCF-7 xenograft tumor model results in comparable SUV values and accumulation patterns. This occurs despite obviously different uptake mechanisms involving GLUT1 and hexokinase in the case of ^{18}F FDG, and GLUT5 and the absence of KHK (31) in the case of ^{18}F FDG.

Various clinical studies in breast cancer patients have revealed low or no GLUT1 expression in tumor tissue biopsies (24–27). This finding suggests that further

research on alternative hexose transporters and hexose transporter substrates such as GLUT5 and fructose derivatives is warranted. It is becoming clearer that fructose metabolism might play an important role during growth and progression of breast tumors and possibly in other types of cancers (28–30,36). As a first step it could be determined whether there is any correlation between a reduced GLUT1 expression in tumor cells and an increased expression of the fructose transporting GLUT2 and GLUT5. Robey and co-workers showed that glucose uptake in breast cancer cells is not necessarily dependent on high GLUT1 expression (50). The authors found that low GLUT1 mRNA expressing MDA-MB-231 cells still showed high glucose uptake, conversely, high GLUT1 mRNA expressing MDA-MB-435 cells showed only low glucose uptake. However, since the protein expression was not determined, it still remains to be further elucidated what the reasons for low uptake of [¹⁸F]FDG in breast cancer patients are and if alternative targets such as GLUT5 could be used effectively for PET imaging in a clinical setting.

However, it appears that intracellular trapping mechanisms may be a key determinant of hexose uptake in breast cancer cells. Further research should be directed to radiolabeled fructose derivatives combining facilitated transport via GLUT5 and possible phosphorylation through hexokinase and/or KHK. Additionally, a correlation between low GLUT1 expressing breast cancer cells and increased GLUT2/GLUT5 expression should be investigated.

3.5 Conclusion

6-^[18F]FDF represents a novel PET radiotracer for imaging of GLUT5 expression *in vivo*. It is a substrate for human KHK and it is rapidly metabolized in mice. Radiopharmacological evaluation *in vitro* and *in vivo* has demonstrated radioactivity uptake in murine and human breast tumor models, indicating its potential application for molecular imaging of cells expressing GLUT5. However, after 2 hours, 6-^[18F]FDF showed no advantages over ^[18F]FDG for imaging in the two mouse models and even in the MCF-7 tumor which has low ^[18F]FDG accumulation. Despite the significant loss of F-18 from the 6-^[18F]FDF molecule *in vivo*, F-18-labeled fructose analogues might represent a useful tool for studying alternate hexose pathways in GLUT1 low- or no-expressing tumors which are GLUT5 positive, provided that a correlation with GLUT5 and KHK expression can be established.

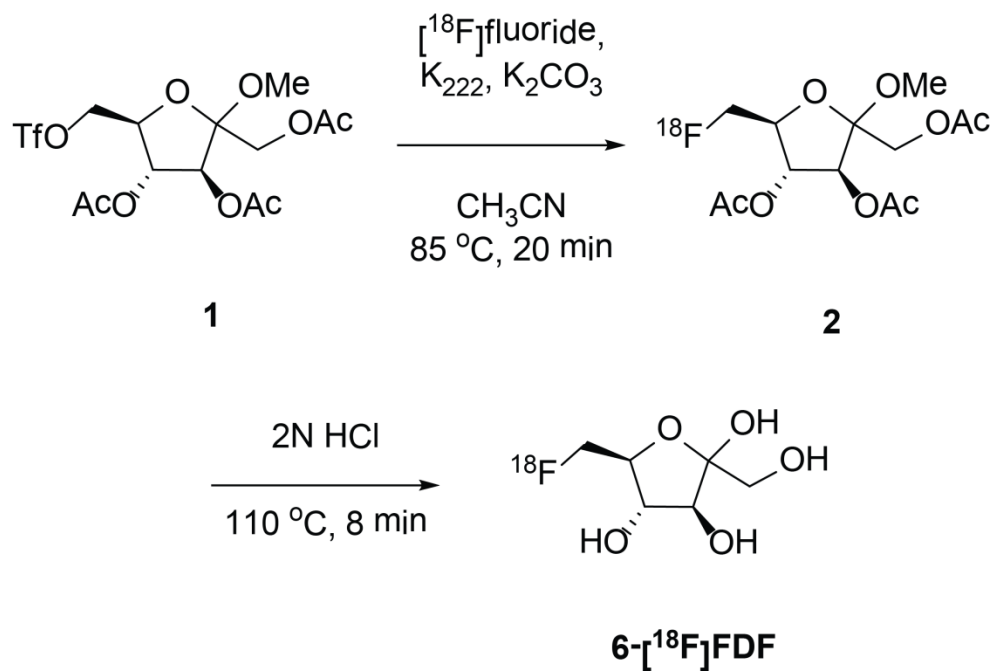


Figure 3.1: Radiosynthesis of 6-[¹⁸F]FDF

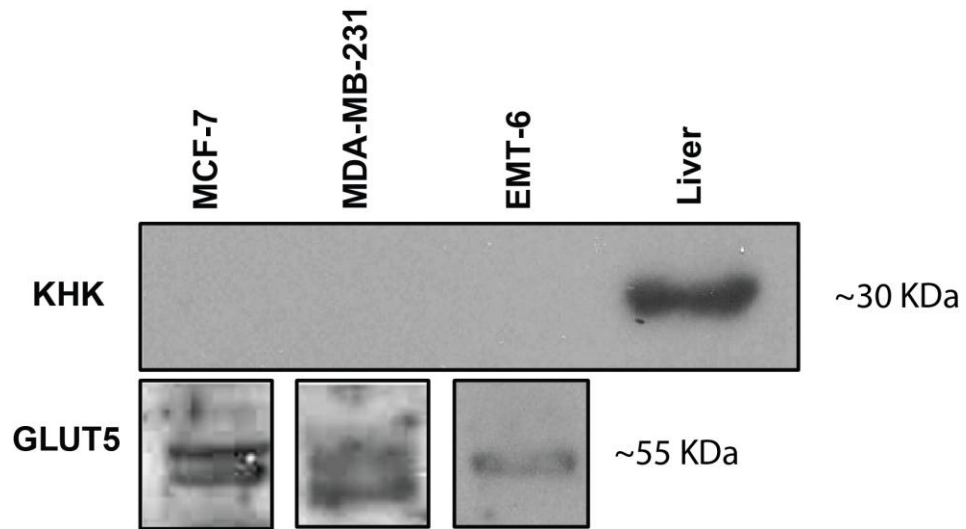
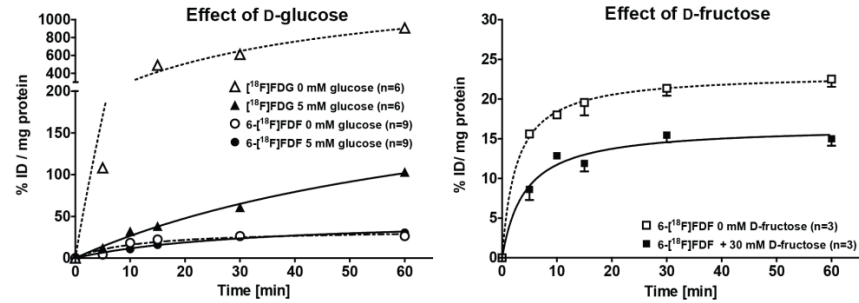
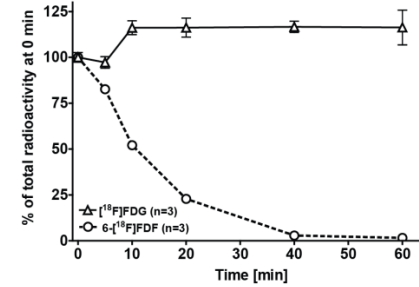


Figure 3.2: Western blots of MCF-7, MDA-MB-231, EMT-6 and human liver homogenate using 25 g of whole cell lysate. All three breast cancer models are negative for ketohexokinase (KHK) expression, while positive for GLUT5. The doublet in MCF-7 and MDA-MB-231 represents both glycosylated and unglycosylated copies of the isoform. Human liver homogenate acted as a positive control for KHK.

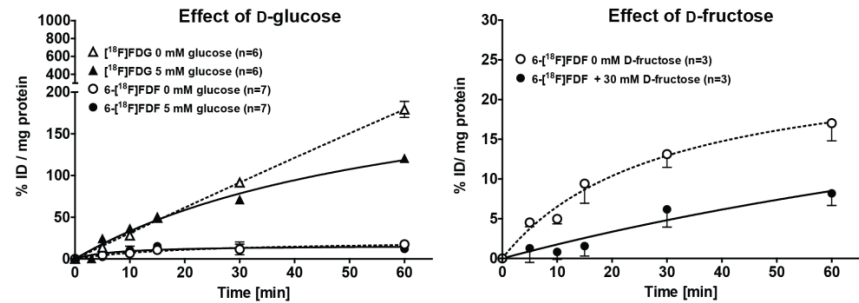
Cell uptake in EMT-6 cells



Cell efflux in EMT-6 cells



Cell uptake in MCF-7 cells



Cell efflux in MCF-7 cells

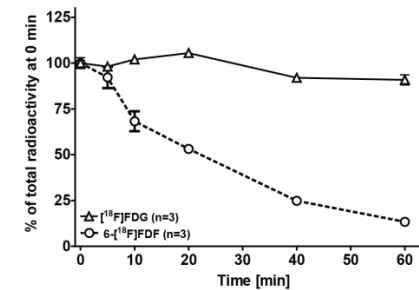


Figure 3.3: In vitro uptake studies Cellular uptake (left and middle) and efflux (right) of $6\text{-}[^{18}\text{F}]\text{FDF}$ and $[^{18}\text{F}]\text{FDG}$ in murine EMT-6 and human MCF-7 breast cancer cells. Experiments were done in the presence (full symbols) or absence (open symbols) of 5 mM glucose (left) or 30 mM fructose (middle) in the extracellular buffer. Data are shown as %ID/mg protein uptake (uptake) or as % of the total radioactivity at time point 0 (efflux) over 60 min. Data are shown as means \pm S.E.M. from n experiments.

Inhibition of 6-[¹⁸F]FDF cell uptake in EMT-6 cells

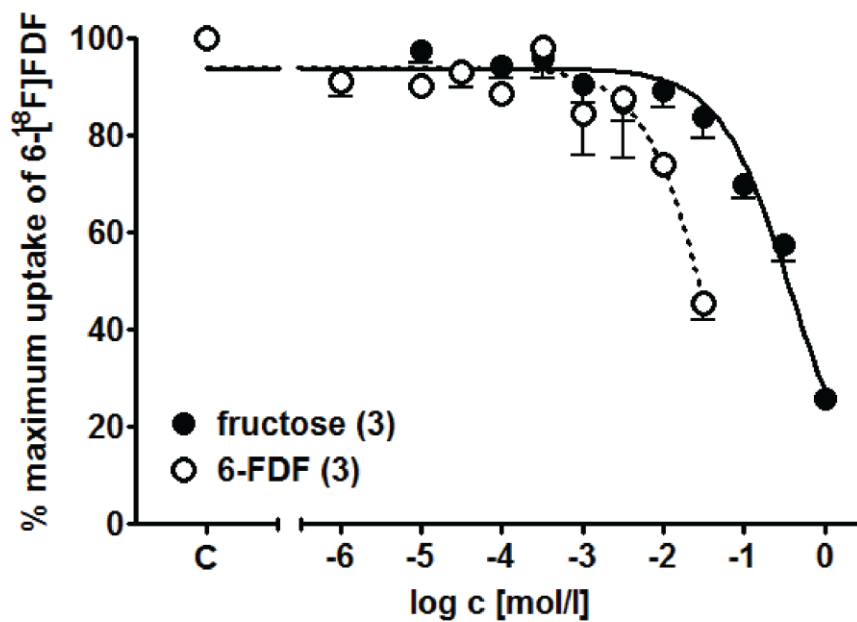


Figure 3.4: Concentration-response curves: 6-FDF and fructose having inhibiting effects of both substrates on the cell uptake of 6-[¹⁸F]FDF into EMT-6 cells. Data are shown as % maximum radiotracer uptake (control = 100%) and as means \pm S.E.M. from 3 different experiments.

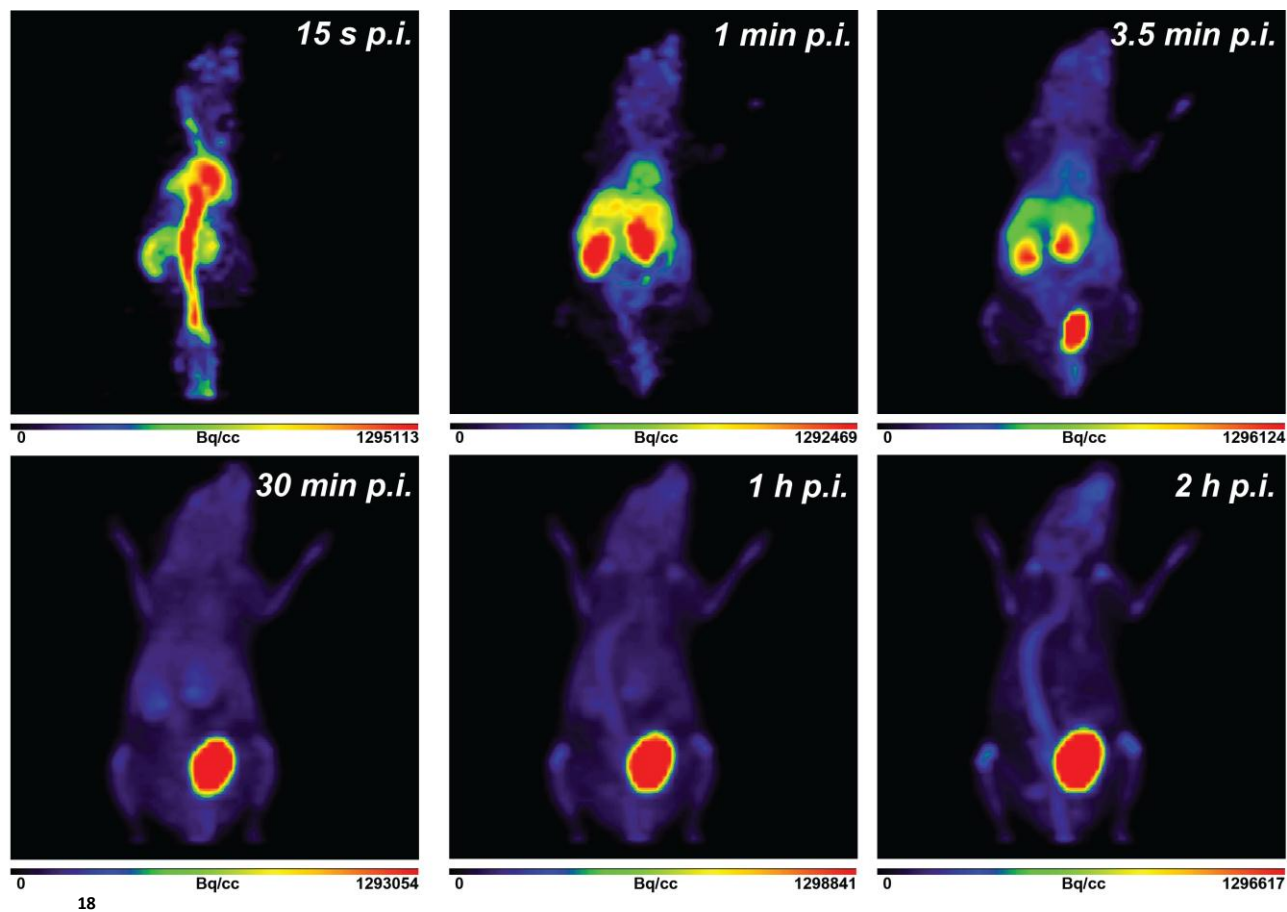


Figure 3.5: 6-[¹⁸F]FDF in a normal BALB/c mouse - Representative dynamic small animal PET images (up to 120 min) of 6-[¹⁸F]FDF in a normal BALB/c mouse after injection of 4.5 MBq. Isoflurane was utilized for anesthetizing the mouse

Organ	5 min	30 min	120 min
Blood	7.67 ± 0.70	4.07 ± 0.44	1.53 ± 0.13
Heart	6.00 ± 0.29	3.06 ± 0.23	1.40 ± 0.20
Lung	4.81 ± 0.55	2.88 ± 0.47	1.08 ± 0.03
Liver	7.26 ± 0.64	3.80 ± 0.44	1.38 ± 0.14
Kidney (right)	12.65 ± 0.55	5.07 ± 0.62	1.67 ± 0.17
Kidney (left)	12.00 ± 0.84	5.23 ± 0.89	1.64 ± 0.16
Intestine (small)	5.87 ± 0.44	2.97 ± 0.38	1.19 ± 0.07
Intestine (large)	3.76 ± 0.29	2.25 ± 0.18	2.09 ± 0.05
Duodenum	5.18 ± 0.77	3.23 ± 1.00	1.20 ± 0.09
Spleen	4.97 ± 0.21	2.54 ± 0.22	1.02 ± 0.07
Bone	1.32 ± 0.36	2.46 ± 0.36	6.39 ± 1.06
Muscle	1.56 ± 0.27	1.41 ± 0.16	0.90 ± 0.18
Gallbladder	4.86 ± 0.12	2.73 ± 0.17	1.31 ± 0.53
Ovaries	1.89 ± 0.32	0.95 ± 0.07	0.41 ± 0.04
Brain	1.67 ± 0.20	1.97 ± 0.15	1.22 ± 0.07
Pancreas	2.85 ± 0.35	1.73 ± 0.28	0.72 ± 0.08
Fat	1.19 ± 0.33	0.50 ± 0.07	0.20 ± 0.07
Tumor	3.65 ± 0.30	3.52 ± 0.34	1.75 ± 0.03
Tumor / Blood	0.48 ± 0.05	0.87 ± 0.06	1.16 ± 0.08
Tumor / Muscle	2.42 ± 0.26	2.51 ± 0.13	2.09 ± 0.37
Tumor / Kidney	0.31 ± 0.03	0.70 ± 0.10	1.09 ± 0.09

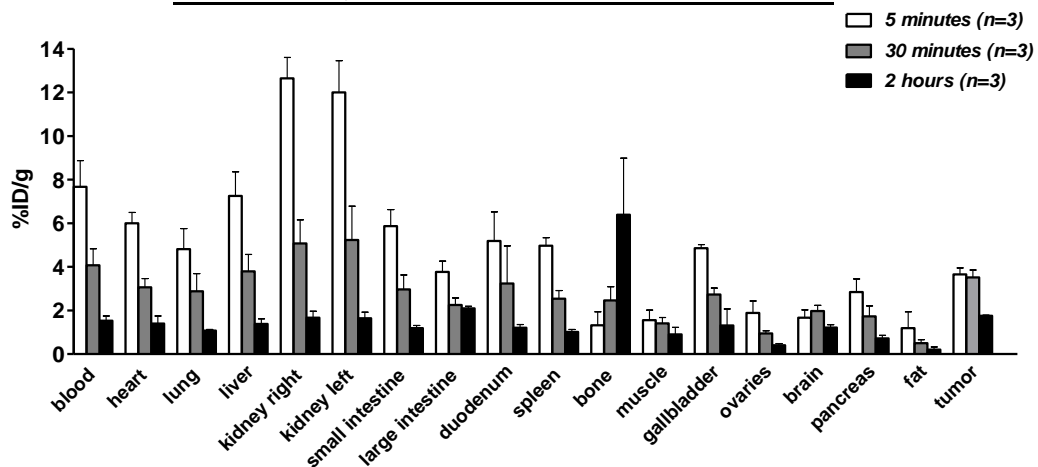


Table 3.1: Biodistribution table and graphical representation of 6-[¹⁸F]FDF in EMT-6 tumor bearing BALB/c mice - Data are the means ± SEM %ID/ g from n = 3 animals per time point.

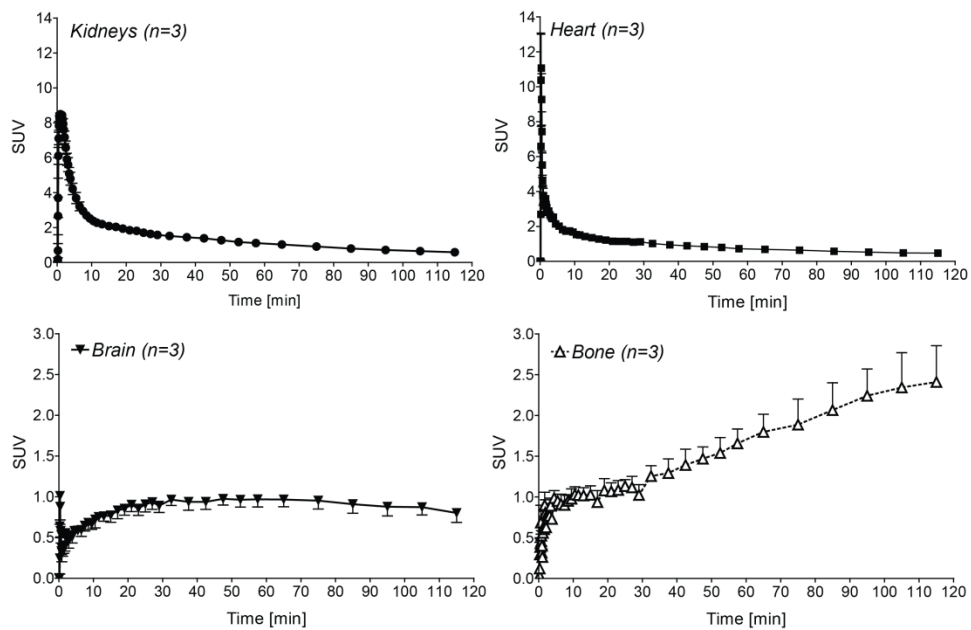


Figure 3.6: 6-¹⁸F]FDF in normal BALB/c mice - Time-activity curves (TAC) of the radioactivity profile in kidney, heart (blood pool), brain and bone after a single intravenous injection of 6-¹⁸F]FDF. Data are shown as SUV and means \pm S.E.M. from 3 normal BALB/c mice.

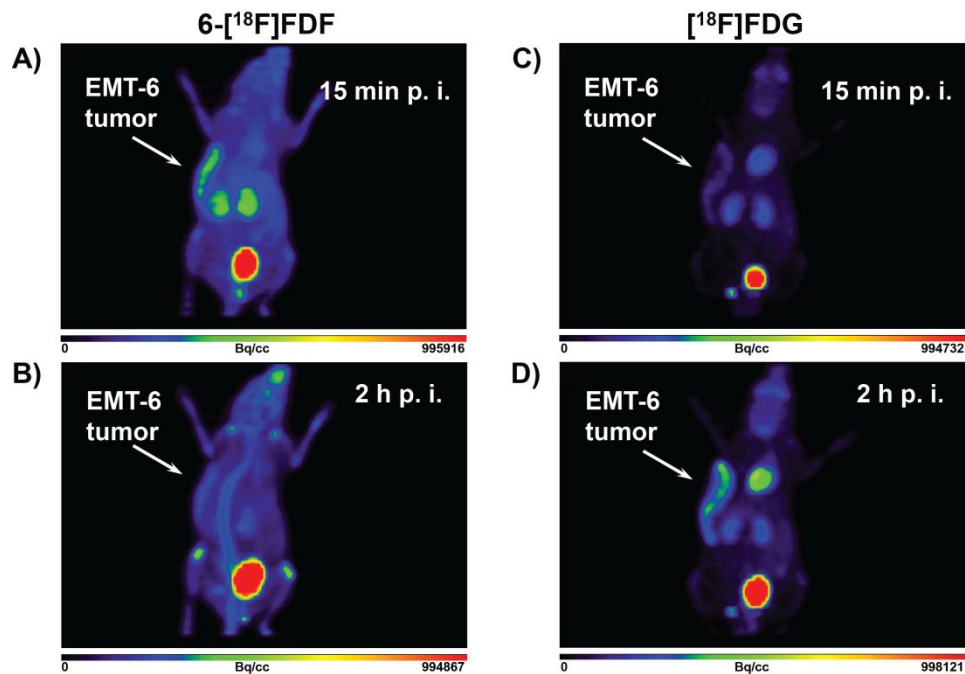


Figure 3.7: EMT-6 tumor-bearing BALB/c mouse - Representative dynamic small animal PET images of 6-[¹⁸F]FDF (A and B; 4.6 MBq injected) and [¹⁸F]FDG (C and D; 5.7 MBq injected) in the same EMT-6 tumor bearing BALB/c mouse after 15 and 120 min post injection. The [¹⁸F]FDG experiment was performed 48 h after 6-[¹⁸F]FDF. Isoflurane was used for anesthesia.

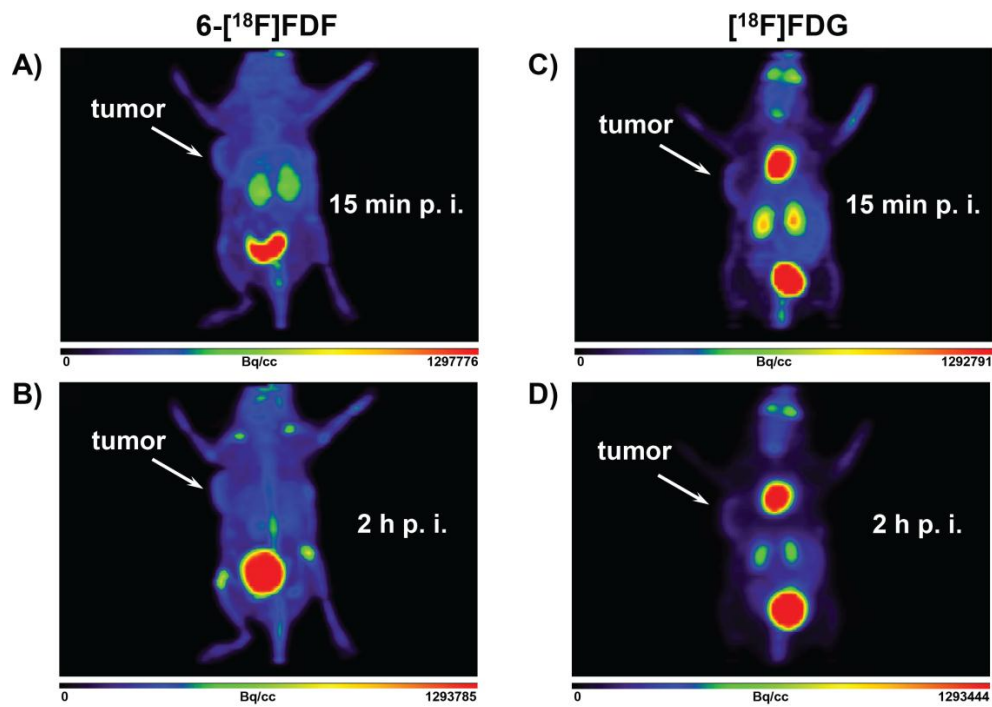


Figure 3.8: PET images of an MCF-7 tumor-bearing NIH-III mouse - Representative dynamic small animal PET images of 6- ^{18}F FDF (left; 5.5 MBq injected) and ^{18}F FDG (right; 4.1 MBq injected) in the same MCF-7 tumor-bearing NIH-III nu/nu mouse after 15 and 120 min post injection. The ^{18}F FDG experiment was performed 24 h after 6- ^{18}F FDF. Isoflurane was used for anesthesia.

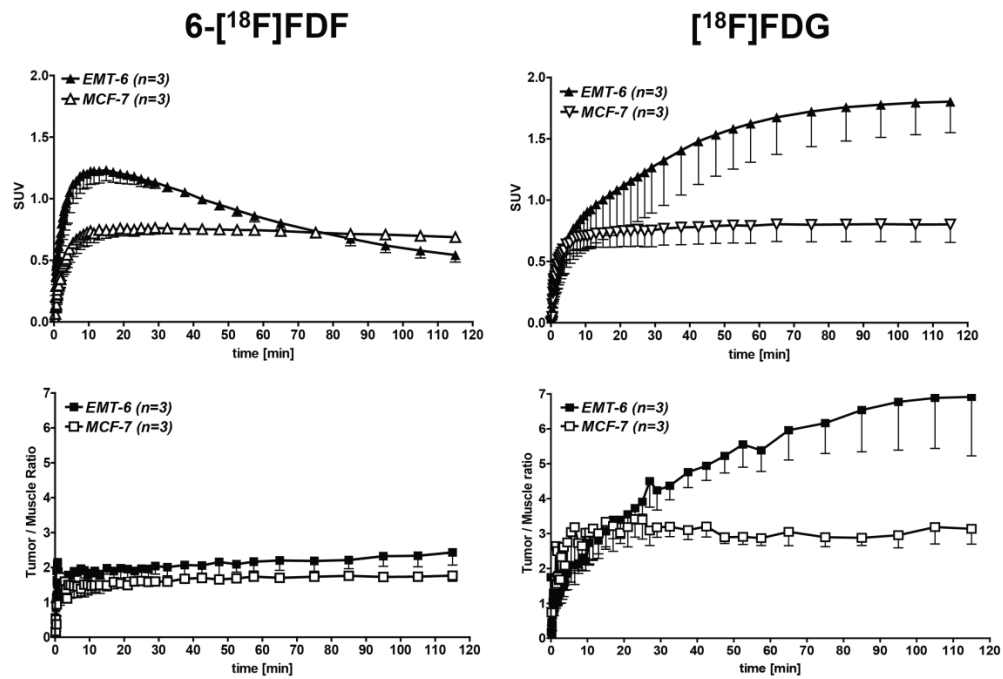


Figure 3.9: Time-activity curves (TAC) - of the radioactivity profile in EMT-6 and MCF-7 tumors (upper panels) as well as tumor/muscle ratios (lower panels) after a single intravenous injection of 6-[¹⁸F]FDF. Data are shown as SUV (top) or as SUV-ratios (bottom) and as means \pm S.E.M. from 3 tumor-bearing mice of each model.

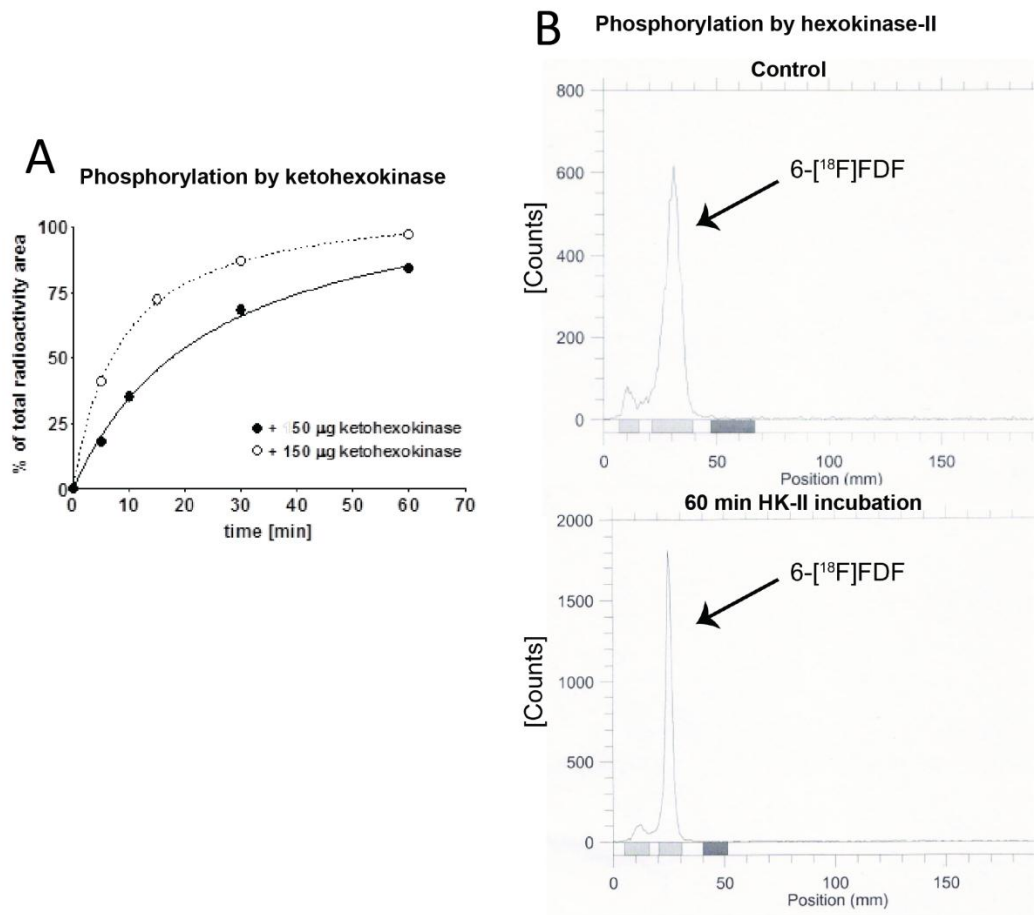


Figure 3.10A-B: Phosphorylation by ketohexokinase in vitro and distribution of radioactivity in blood compartments – (A) Phosphorylation of 6-[¹⁸F]FDF by human recombinant ketohexokinase (50 and 150 µg). Data are shown as % of total radioactivity area over time from a single experiment. **(B)** ≥ 90% of intact 6-[¹⁸F]FDF was detectable after a 60 min incubation with the human recombinant hexokinase-II. A similar trace was observed with 6-[¹⁸F]FDF being incubated in the buffer without enzyme.

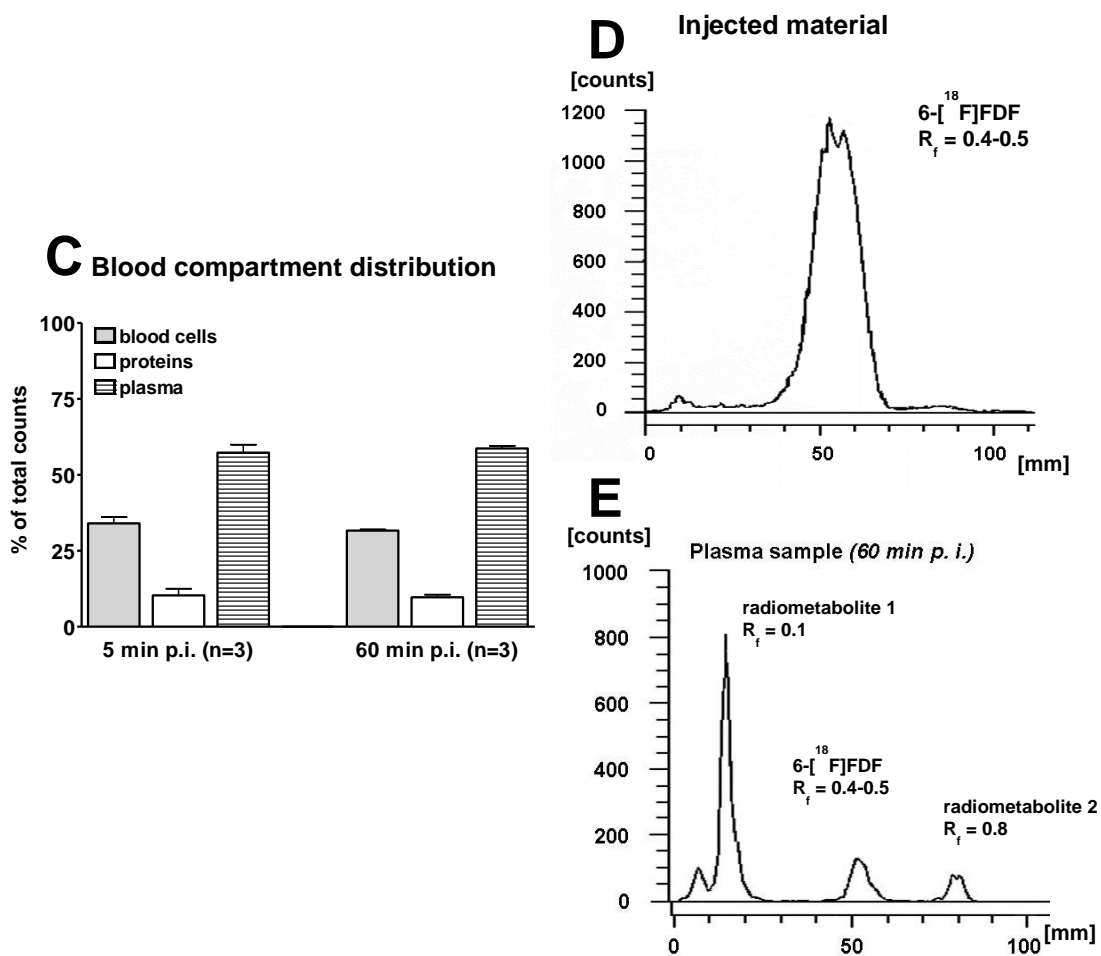


Figure 3.10C-E: Radio TLC of 6-¹⁸F]FDF in saline and mouse plasma and blood compartments- (C) Distribution of radioactivity in blood cells, protein and plasma after 5 and 60 min post-injection (p.i.) Data are presented as % of total counts and means \pm S.E.M. from n BALB/c mice (D) Original traces of radio-TLC samples of 6-¹⁸F]FDF in saline as used for injection and (E) of a mouse plasma sample after 60 min p.i.

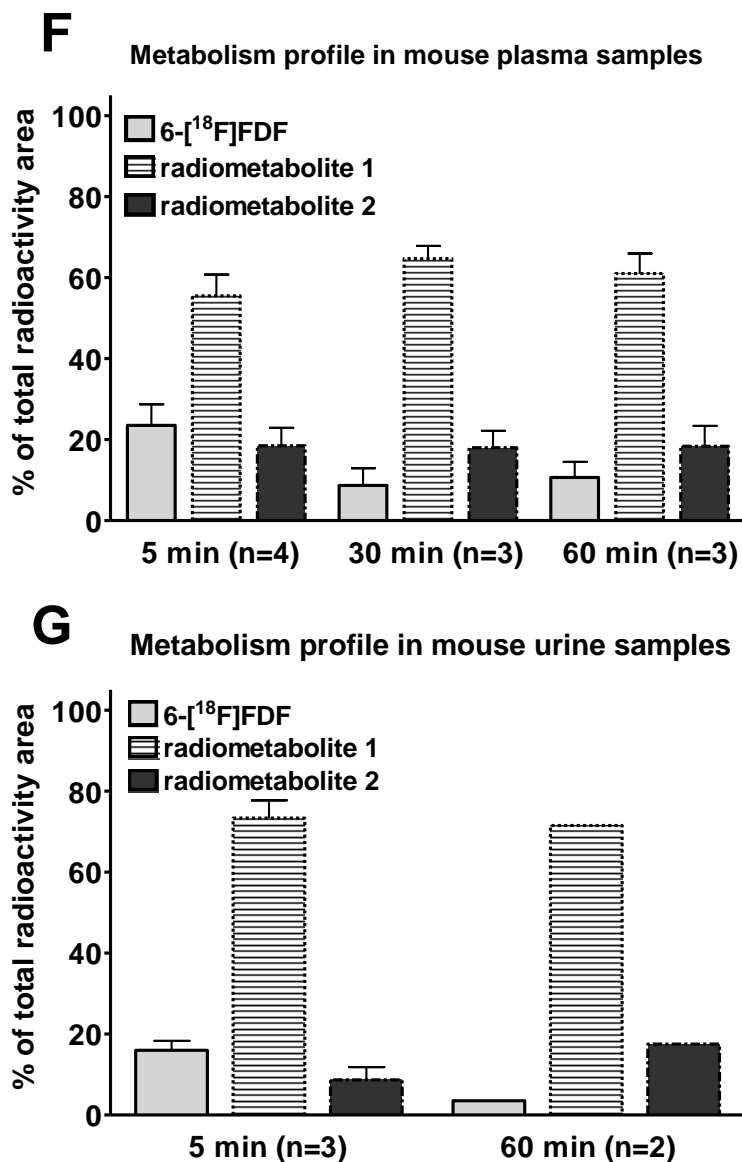


Figure 3.109F-G: Metabolism profile in mouse plasma and urine samples –(F) Metabolism profile of 6-[¹⁸F]FDF in mouse plasma samples after 5, 30 and 60 min p.i. Areas for potential radiometabolite 1 and 2 were defined from their different R_f values as analyzed from radio-TLC (see above). Data are shown as % of total radioactivity area and means ± S.E.M. from n BALB/c mice. **(G)** Metabolism profile of 6-[¹⁸F]FDF in mouse urine after 5 and 60 min p.i.

3.6 Bibliography

1. Mankoff DA. Molecular imaging as a tool for translating breast cancer science. *Breast cancer research : BCR*. 2008 Jan;10 Suppl 1:S3.
2. Iagaru A, Masamed R, Keesara S, Conti PS. Breast MRI and 18F FDG PET/CT in the management of breast cancer. *Annals of nuclear medicine*. 2007 Jan;21(1):33–8.
3. Kluetz PG, Meltzer CC, Villemagne VL, Kinahan PE, Chander S, Martinelli MA, et al. Combined PET/CT Imaging in Oncology. Impact on Patient Management. *Clinical positron imaging : official journal of the Institute for Clinical P.E.T*. 2000 Nov;3(6):223–30.
4. Lim HS, Yoon W, Chung TW, Kim JK, Park JG, Kang HK, et al. FDG PET/CT for the detection and evaluation of breast diseases: usefulness and limitations. *Radiographics : a review publication of the Radiological Society of North America, Inc*. 2007 Oct;27 Suppl 1:S197–213.
5. Lavayssière R, Cabée A-E, Filmont J-E. Positron Emission Tomography (PET) and breast cancer in clinical practice. *European journal of radiology*. 2009 Jan;69(1):50–8.
6. Quon A, Gambhir SS. FDG-PET and beyond: molecular breast cancer imaging. *Journal of clinical oncology : official journal of the American Society of Clinical Oncology*. 2005 Mar 10;23(8):1664–73.
7. Eubank WB, Mankoff DA. Evolving Role of Positron Emission Tomography in Breast Cancer Imaging. *Semin Nucl Med*. 2005 Apr;35(2):84-99.
8. Buerkle A, Weber W a. Imaging of tumor glucose utilization with positron emission tomography. *Cancer metastasis reviews*. 2008 Dec;27(4):545–54.
9. Bastiaannet E, Groen H, Jager PL, Cobben DCP, van der Graaf WTA, Vaalburg W, et al. The value of FDG-PET in the detection, grading and response to therapy of soft tissue and bone sarcomas; a systematic review and meta-analysis. *Cancer treatment reviews*. 2004 Feb;30(1):83–101.
10. Hennipman A, Smits J, van Oirschot B, van Houwelingen JC, Rijksen G, Neyt JP, et al. Glycolytic enzymes in breast cancer, benign breast disease and normal breast tissue. *Tumor biology : the journal of the International Society for Oncodevelopmental Biology and Medicine*. 1987 Jan;8(5):251–63.

11. Brown RS, Goodman TM, Zasadny KR, Greenson JK, Wahl RL. Expression of hexokinase II and Glut-1 in untreated human breast cancer. *Nuclear medicine and biology*. 2002 May;29(4):443–53.
12. Hennipman A, van Oirschot BA, Smits J, Rijksen G, Staal GE. Glycolytic enzyme activities in breast cancer metastases. *Tumor biology : the journal of the International Society for Oncodevelopmental Biology and Medicine*. 1988 Jan;9(5):241–8.
13. Macheda ML, Rogers S, Best JD. Molecular and cellular regulation of glucose transporter (GLUT) proteins in cancer. *Journal of cellular physiology*. 2005 Mar;202(3):654–62.
14. Manolescu AR, Witkowska K, Kinnaird A, Cessford T, Cheeseman C. Facilitated hexose transporters: new perspectives on form and function. *Physiology*. 2007 Aug;22:234–40.
15. Yamamoto T, Seino Y, Fukumoto H, Koh G, Yano H, Inagaki N, et al. Over-expression of facilitative glucose transporter genes in human cancer. *Biochemical and biophysical research communications*. 1990 Jul 16;170(1):223–30.
16. Thongwatchara P, Promwikorn W, Srisomsap C, Chokchaichamnankit D, Boonyaphiphat P, Thongsuksai P. Differential protein expression in primary breast cancer and matched axillary node metastasis. *Oncology reports*. 2011 Jul;26(1):185–91.
17. Santiago JFY, Gonen M, Yeung H, Macapinlac H, Larson S. A retrospective analysis of the impact of 18F-FDG PET scans on clinical management of 133 breast cancer patients. *The quarterly journal of nuclear medicine and molecular imaging : official publication of the Italian Association of Nuclear Medicine (AIMN) [and] the International Association of Radiopharmacology (IAR), [and] Section of the Society of Radiopharmaceutica*. 2006 Mar;50(1):61–7.
18. Sundararajan L, Linden HM, Link JM, Krohn KA, Mankoff DA. 18F-Fluoroestradiol. *Seminars in nuclear medicine*. 2007 Nov;37(6):470–6.
19. Buck AK, Schirrmester H, Mattfeldt T, Reske SN. Biological characterisation of breast cancer by means of PET. *Eur J Nucl Med Mol Imaging*. 2004 Jun;31 Suppl 1:S80-7.
20. Alavi A, Zhuang H. Finding infection--help from PET. *Lancet*. 2001 Oct 27;358(9291):1386.
21. Schirmer M, Calamia KT, Wenger M, Klauser A, Salvarani C, Moncayo R. 18F-fluorodeoxyglucose-positron emission tomography: a new

- explorative perspective. *Experimental gerontology*. 2003 Apr;38(4):463–70.
22. Kubota R, Kubota K, Yamada S, Tada M, Ido T, Tamahashi N. Microautoradiographic study for the differentiation of intratumoral macrophages, granulation tissues and cancer cells by the dynamics of fluorine-18-fluorodeoxyglucose uptake. *Journal of nuclear medicine : official publication, Society of Nuclear Medicine*. 1994 Jan;35(1):104–12.
 23. Facey K, Bradbury I, Laking G, Payne E. Overview of the clinical effectiveness of positron emission tomography imaging in selected cancers. *Health technology assessment (Winchester, England)*. 2007 Oct;11(44):iii-iv, xi–267.
 24. Younes M, Brown RW, Mody DR, Fernandez L, Laucirica R. GLUT1 expression in human breast carcinoma: correlation with known prognostic markers. *Anticancer research*. 15(6B):2895–8.
 25. Ravazoula P, Batistatou A, Aletra C, Ladopoulos J, Kourounis G, Tzigounis B. Immunohistochemical expression of glucose transporter Glut1 and cyclin D1 in breast carcinomas with negative lymph nodes. *European journal of gynaecological oncology*. 2003 Jan;24(6):544–6.
 26. Laudański P, Koda M, Kozłowski L, Swiatecka J, Wojtukiewicz M, Sulkowski S, et al. Expression of glucose transporter GLUT-1 and estrogen receptors ER-alpha and ER-beta in human breast cancer. *Neoplasma*. 2004 Jan;51(3):164–8.
 27. Kuo S-J, Wu Y-C, Chen C-P, Tseng H-S, Chen D-R. Expression of glucose transporter-1 in Taiwanese patients with breast carcinoma--a preliminary report. *The Kaohsiung journal of medical sciences*. 2006 Jul;22(7):339–45.
 28. Zamora-León SP, Golde DW, Concha II, Rivas CI, Delgado-López F, Baselga J, et al. Expression of the fructose transporter GLUT5 in human breast cancer. *Proceedings of the National Academy of Sciences of the United States of America*. 1996 Mar 5;93(5):1847–52.
 29. Reinicke K, Godoy A, Ulloa V, Rodri F, Medina RA, Yan AJ, et al. Differential Subcellular Distribution of Glucose Transporters GLUT1 – 6 and GLUT9 in Human Cancer : Ultrastructural Localization of GLUT1 and GLUT5 in Breast Tumor Tissues. 2006;627(April 2005):614–27.
 30. Chan KK, Chan JYW, Chung KKW, Fung K-P. Inhibition of cell proliferation in human breast tumor cells by antisense oligonucleotides against facilitative glucose transporter 5. *Journal of cellular biochemistry*. 2004 Dec 15;93(6):1134–42.

31. Levi J, Cheng Z, Gheysens O, Patel M, Chan CT, Wang Y, et al. Fluorescent fructose derivatives for imaging breast cancer cells. *Bioconjugate chemistry*. 2007;18(3):628–34.
32. Douard V, Ferraris RP. Regulation of the fructose transporter GLUT5 in health and disease. *American journal of physiology. Endocrinology and metabolism*. 2008 Aug;295(2):E227–37.
33. Haradahira T, Tanaka A, Maeda M, Kanazawa Y, Ichiya YI, Masuda K. Radiosynthesis, rodent biodistribution, and metabolism of 1-deoxy-1-[18F]fluoro-D-fructose. *Nuclear medicine and biology*. 1995 Aug;22(6):719–25.
34. Yang J, Dowden J, Tatibouët A, Hatanaka Y, Holman GD. Development of high-affinity ligands and photoaffinity labels for the D-fructose transporter GLUT5. *The Biochemical journal*. 2002 Oct 15;367(Pt 2):533–9.
35. Tatibouët A, Yang J, Morin C, Holman GD. Synthesis and evaluation of fructose analogues as inhibitors of the D-fructose transporter GLUT5. *Bioorganic & medicinal chemistry*. 2000 Jul;8(7):1825–33.
36. Trayner BJ, Grant TN, West FG, Cheeseman CI. Synthesis and characterization of 6-deoxy-6-fluoro-D-fructose as a potential compound for imaging breast cancer with PET. *Bioorganic & medicinal chemistry*. 2009 Aug 1;17(15):5488–95.
37. Aliaga A, Rousseau JA, Ouellette R, Cadorette J, van Lier JE, Lecomte R, et al. Breast cancer models to study the expression of estrogen receptors with small animal PET imaging. *Nuclear medicine and biology*. 2004 Aug;31(6):761–70.
38. Laudański P, Swiatecka J, Kovalchuk O, Wołczyński S. Expression of GLUT1 gene in breast cancer cell lines MCF-7 and MDA-MB-231. *Ginekologia polska*. 2003 Sep;74(9):782–5.
39. Colville CA, Seatter MJ, Jess TJ, Gould GW, Thomas HM. Kinetic analysis of the liver-type (GLUT2) and brain-type (GLUT3) glucose transporters in *Xenopus* oocytes: substrate specificities and effects of transport inhibitors. *The Biochemical journal*. 1993 Mar 15;290 (Pt 3):701–6.
40. Burant CF, Takeda J, Brot-Laroche E, Bell GI, Davidson NO. Fructose transporter in human spermatozoa and small intestine is GLUT5. *The Journal of biological chemistry*. 1992 Jul 25;267(21):14523–6.
41. Ong L-C, Jin Y, Song I-C, Yu S, Zhang K, Chow PKH. 2-[18F]-2-deoxy-D-glucose (FDG) uptake in human tumor cells is related to the expression of

- GLUT-1 and hexokinase II. *Acta radiologica* (Stockholm, Sweden : 1987). 2008 Dec;49(10):1145–53.
42. Ong LC, Jin Y, Song IC, Yu S, Zhang K, Chow PK. 2-[18F]-2-deoxy-D-glucose (FDG) uptake in human tumor cells is related to the expression of GLUT-1 and hexokinase II. *Acta Radiol.* 2008 Dec;49(10):1145-53.
 43. Heman RH, Zakim D. Fructose metabolism. I. The fructose metabolic pathway. *The American journal of clinical nutrition.* 1968 Mar;21(3):245–9.
 44. Amano S, Inoue T, Tomiyoshi K, Ando T, Endo K. In vivo comparison of PET and SPECT radiopharmaceuticals in detecting breast cancer. *Journal of nuclear medicine : official publication, Society of Nuclear Medicine.* 1998 Aug;39(8):1424–7.
 45. Yang J, Dowden J, Tatiboue A, Hatanaka Y, Holman GD. Development of high-affinity ligands and photoaffinity labels for the D-fructose transporter GLUT5. *Biochem J.* 2002 Oct 15;367(Pt 2):533-9.
 46. Ohara H, Tamayama T, Maemura K, Kanbara K, Hayasaki H, Abe M, et al. Immunocytochemical demonstration of glucose transporters in epiphyseal growth plate chondrocytes of young rats in correlation with autoradiographic distribution of 2-deoxyglucose in chondrocytes of mice. *Acta histochemica.* 2001 Oct;103(4):365–78.
 47. Marín-Hernández A, Rodríguez-Enríquez S, Vital-González PA, Flores-Rodríguez FL, Macías-Silva M, Sosa-Garrocho M, et al. Determining and understanding the control of glycolysis in fast-growth tumor cells. Flux control by an over-expressed but strongly product-inhibited hexokinase. *The FEBS journal.* 2006 May;273(9):1975–88.
 48. Mathupala SP, Ko YH, Pedersen PL. Hexokinase-2 bound to mitochondria: cancer's stygian link to the "Warburg Effect" and a pivotal target for effective therapy. *Seminars in cancer biology.* 2009 Feb;19(1):17–24.
 49. Haberkorn U, Ziegler SI, Oberdorfer F, Trojan H, Haag D, Peschke P, et al. FDG uptake, tumor proliferation and expression of glycolysis associated genes in animal tumor models. *Nuclear medicine and biology.* 1994 Aug;21(6):827–34.
 50. Robey IF, Stephen RM, Brown KS, Baggett BK, Gatenby RA, Gillies RJ. Regulation of the Warburg effect in early-passage breast cancer cells. *Neoplasia* (New York, N.Y.). 2008 Aug;10(8):745–56.

Chapter 4 - Dosimetry of 6-deoxy-6-¹⁸Ffluoro- D-fructose (6-¹⁸F)FDF) for PET imaging of GLUT5 derived from a study in rats

A version of this chapter has been submitted for publication:

Jans H-S, Wuest M, Bouvet V, **Trayner BJ**, Grant TN, West FG, McEwan AGB, Cheeseman CI.

This work presented in this chapter represents a collaboration. HSJ performed dosimetry analysis from biodistribution and PET data acquired by MW and BJT. Chemical syntheses were performed by VB and TNJ.

4.1 Introduction

6-[¹⁸F]FDF was developed as a PET radiotracer for imaging GLUT5 in vivo(1). It is a substrate for the human ketohexokinase and it is rapidly metabolized in mice. Radiopharmacological evaluation in vitro and in vivo has demonstrated radioactivity uptake in murine and human breast tumor models, indicating its potential application for molecular imaging of cells expressing GLUT5 (2). Human normal-organ estimates for 6-[¹⁸F]FDF are a prerequisite for a first study in man according to Health Canada regulations. These apply to the clinical use of diagnostic PET radiotracers and are comparable to data required for an exploratory investigational new drug application (eIND) as described in the U.S. Food and Drug Administration (FDA) regulations (3). This study presents the first calculated human dose estimates for 6-[¹⁸F]FDF based on a biodistribution in normal, healthy rats.

4.2 Methods

Please see **Appendix A** for a detailed materials list.

4.2.1 *Synthesis of 6-[¹⁸F]FDF*

6-Deoxy-6-[¹⁸F]fluoro-D-fructose (6-[¹⁸F]FDF) was synthesized according to the following procedure. [¹⁸F]Fluoride was dried in the NanoTek Microfluidic System (AdvionBioSciences, Inc., Ithaca, NY, U.S.A.) concentrator module:(i) cyclotron-produced [¹⁸F]fluoride (2.5 mL ¹⁸O-enriched H₂O) passed through a Sep-Pak plus QMA cartridge, (ii) cartridge dried with air, (iii) [¹⁸F]fluoride was eluted (800 µL of

K222/K₂CO₃ solution [kryptofix K222 (40 mg) in acetonitrile (1.7 mL); K₂CO₃ (10 mg) in 0.5 mL H₂O], (iv) solvent was evaporated to dryness, and cartridge eluted a second time with 800 µL of K222/K₂CO₃ and (v) resulting solution was distilled three times azeotropically at 100°C (500 µL acetonitrile per step). The overall process required 19 min. [¹⁸F]Fluoride was re-dissolved in 350 µL acetonitrile containing 15 mg (33 µM) triflate precursor methyl 1,3,4-tri-O-acetyl-6-O-(trifluoromethane-sulfonyl)- α/β -D-fructofuranoside (1,2), which was freshly prepared for each radiosynthesis. Radiofluorination was proceeded at 60°C (15 min), cooled and filtered with 2 mL acetonitrile through a silica cartridge (Waters Sep-Pak Silica). At this step the radio-corrected recovery yield was ~60% with a radiochemical purity of >95% (radio-TLC; 7/3 : ethyl acetate/hexane). That solution was concentrated to dryness (N₂) and 0.7 mL of 2 N HCl added following stirring for 7 min at 100°C. Then 10 mL cold acetonitrile, 0.5 mL NaHCO₃sat and 0.2 mL 2 N NaOH was added and the resulting solution was filtered through alumina (Waters Sep-Pak Alumina N) and silica (Waters Sep-Pak Si+) cartridges. An extra 5 mL of acetonitrile/water (95/5) was passed through to fully extract the compound from the cartridges. The final solution was concentrated under reduced pressure and purified using HPLC (Luna C18 column 100 Å, 10 µm, 250×10 mm; increasing acetonitrile : water gradient as eluent; 4 mL/min; R_T = 3 - 4 min). 6-[¹⁸F]FDF was obtained in >98% radiochemical purity and the overall yield ~30% (decay corrected).

4.2.2 Animals

All animal experiments were carried out in accordance with guidelines of the Canadian Council on Animal Care (CCAC) and were approved by the local animal care committee of the Cross Cancer Institute. Imaging and biodistribution studies were carried out with adult female Sprague-Dawley rats (Charles-River, Canada).

4.2.3 Positron Emission Tomography

Rats were injected with 15-17 MBq of 6-[¹⁸F]FDF in 150 to 200 µL saline. The actual administered activity was calculated as difference between the syringe activity before and after injection; activities were determined in a dose calibrator (Atomlab 300, Biodex Medical Systems, Shirley, NY, USA). Rats were then anesthetized through inhalation of isoflurane in 40% oxygen / 60% nitrogen (gas flow, 1 L/min), and body temperature was kept constant at 37°C for the entire experiment. Rats were positioned and immobilized in the prone position with their medial axis parallel to the central axis of the microPET R4 scanner (Siemens Preclinical Solutions, Knoxville, TN, USA). Static whole body emission scan was started 60 min post injection with moving bed positions for the next 60 min to obtain a whole body PET image after 120 min post injection. List mode data was sorted into sinograms and reconstructed using Ordered Subset Expectation Maximization (OSEM). Prior to injection, transmission data for the purpose of attenuation correction was acquired using a Co-57 point source.

4.2.4 *Biodistribution experiments*

After intravenous injection of 1.5 - 4 MBq 6-^[18F]FDF in 150 to 350 µL saline into the tail vein of isofluorane-anesthetized rat, the animals were allowed to regain consciousness until sacrifice. While under isofluorane anesthesia, animals were euthanized by decapitation at 5 and 30 min as well as 1, 2, 3, 4 and 6 h post injection and rapidly dissected. Organs of interest including blood, heart, lung, liver, kidneys, thymus, spleen, duodenum, small and large intestine, pancreas, right femur, muscle, stomach, ovaries, brain, fat and bladder were collected and weighed. Radioactivity in all tissues was measured in a γ-counter and results were analyzed as percentage of injected dose per gram of tissue (%ID/g).

4.2.5 *Radiation Dosimetry Analysis*

Radiation dosimetry analysis for the determination of the normal organ-absorbed doses and the effective dose was performed using Organ Level Internal Dose Assessment/EXponential Modeling (OLINDA/EXM - version 1.1, Vanderbilt University, Nashville, TN, U.S.A.).

The scaling of the animal-obtained values to human values was carried out by weighting the organ uptake with the relative organ mass in the animal and human:

$$\left(\frac{\%ID}{organ}\right)_{human} = \left(\frac{\%ID}{organ}\right)_{rat} \cdot \left[\left(\frac{m_{organ}}{m_{body}}\right)_{human} / \left(\frac{m_{organ}}{m_{body}}\right)_{rat} \right]$$

(1)

In practice, the concentrations $\left(\frac{\%ID}{organ}\right)_{rat} / (m_{organ})_{rat} \equiv \left(\frac{\%ID}{m_{organ}}\right)_{rat}$ are

determined experimentally. This also accounts for organs that cannot be excised in their entirety, such as muscle, blood and bone. Equation 1 then becomes

$$\left(\frac{\%ID}{m_{organ}}\right)_{human} = \left(\frac{\%ID}{m_{organ}}\right)_{rat} \cdot \frac{(m_{body})_{rat}}{(m_{body})_{human}} \quad (2)$$

The values for $\left(\frac{\%ID}{m_{organ}}\right)_{human}$ are obtained by first averaging the values $\left(\frac{\%ID}{m_{organ}}\right)_{rat} \cdot (m_{body})_{rat}$ for the three individual animals sacrificed at each time point and then dividing by the weight of the adult human of 73.7 kg(4,5). To obtain the cumulated activity in each organ, these curves were multiplied by the human organ mass, using the values implemented in the OLINDA/EXM code(5), and integrated: for the first 6 hours numerically by evaluating the area under the measured curve and beyond 6 hours by fitting a mono-exponential function to the last four data points of each curve and integrating it from 6 hrs to infinity.

Not in all cases did the organs for which cumulated activity was determined by means of the biodistribution (see above) correspond to the source organs as defined in OLINDA/EXM. The following assumptions were made to derive the cumulated activity for the OLINDA-defined source organs: (i) It was assumed that all activity detected in the stomach, intestines and the urinary bladder originated from their contents. (ii) Since lower large intestine (LLI) and upper large intestine

(ULI) were not measured separately, the measured total activity was distributed to LLI and ULI activity according to their mass ratio, using the masses for LLI and ULI walls as defined in the OLINDA/EXM code. (iii) Since exact quantities of the small amounts of bone and muscle contained in the remainder of the body were unknown, they were not subtracted from the whole body activity. (iv) The activity of the heart's content was determined from the blood concentration (decays/mL) and multiplied with the volume of the heart (510 mL, (6)). (v) It was assumed that activity is uniformly distributed to cortical and trabecular bone and red marrow. The number of decays in each is assigned according to their weight ratio, based on the weight of the human skeleton of 10.45 kg (6), the ratio of cortical to trabecular bone of 4/1 and the fact that red marrow constitutes 4% of the total body mass (4,6).

The values determined for cumulated activity in each source organ were then used as input for the OLINDA/EXM code.

4.2.6 Statistics

Biodistribution experiments were repeated with three animals at each time point and the values for cumulated activity averaged at each time point. Standard errors of the means (SEM) were calculated for each mean value.

4.3 Results

Figure 4.1 shows the whole body distribution of 6-^[18F]FDF at 2 h post injection in a rat. Clearly visible is the bone uptake and the radioactivity in the urinary

bladder after clearance from the rest of the body. Table 1 summarizes the biodistribution data for 6- ^{18}F]FDF at 5 min, 1, 2 and 6 hours post injection. **Figure 4.2** presents the resulting time-activity curves $(\%ID/kg)_{\text{human}}$ for some of the Medical Internal Radiation Dose (MIRD) source organs (blood, liver, lung, brain, bone and kidneys), scaled to human-equivalent values using Equation 2. Clearance of the radioactivity through organs such as the blood and liver, lung and kidneys is evident. The initial brain uptake peaks at 30 min post injection and then decreases similar to the clearance patterns in blood, liver and lung tissue. Remarkable was the observed bone uptake, which increased to a maximum value at 1 hr post injection and remained constant within error up to 3 h post injection. Activity in the bones decreased significantly after 4 and 6 hrs, indicating a washout of radioactivity. **Table 4.2** presents the calculated human absorbed doses and effective dose for 6- ^{18}F]FDF as determined using OLINDA/EXM, compared to results found in a recent study using state of the art combined PET/CT in human patients with ^{18}F]FDG (7). The highest absorbed doses resulted for the red marrow and osteogenic cells, corresponding to the high amounts of radioactivity detected in the bone and bone marrow (**Figure 4.2**).

4.4 Discussion

This study presents human radiation dose estimates for 6- ^{18}F]FDF, a ^{18}F] labelled fructose derivative developed for imaging GLUT5 in vivo.

The highest absorbed doses are observed for the bone forming cells, the red marrow and the osteogenic cells. This is consistent with the findings from mouse and rat PET image analysis, where bone was found to possess the highest radioactivity levels at 1 h post injection (2) and continued to increase for up to 2 hours. Higher radiation dose levels are also expected for the clearance organs kidneys and urinary bladder since 6-¹⁸F]FDF has shown mainly a renal clearance pattern.

The Food and Drug Administration's Radioactive Drug Research Committee (FDA-RDRC), in its Code of Federal Regulations 21CFR361.1 (8), limits the single dose of radiation to the whole body, active blood-forming organs, lens of the eye and gonads to 30 mSv and for other organs to 50 mSv. The data presented here indicates that an injected dose of 370 MBq (10 mCi), based on a typical prescribed dose of 5.2 MBq/kg for FDG (9), would not exceed these limits. The critical organs, i.e. the osteogenic cells and the red bone marrow, would absorb 11.7 and 4.4 mSv in this case, where in comparison, a typical full body CT scan would expose an individual to 10 – 30 mSv (10).

The effective dose to the patient determined from this investigation is 0.0089 mSv/MBq. This value compares favourably with the one reported for FDG in the SNM procedure guidelines of 0.027 mSv/MBq (11), the International Commission on Radiological Protection of 0.019 mSv/MBq (8) and a recent study with a value of 0.015 mSv/MBq (7).

To date [^{18}F]FDG is still the most widely used PET radiotracer, being used in >90% of all PET exams, and has proven its usefulness for diagnosis, staging and detection of residual / recurrent cancer(12). However, [^{18}F]FDG displays some important limitations for tumor detection because of possible immune reactions; furthermore, its uptake into inflammatory lesions might confound the adequate differentiation between post-therapy inflammation and tumor site (13,14). In breast cancer patients [^{18}F]FDG-PET has been shown to possess a 76-89% sensitivity and 73-80% specificity for the primary diagnosis. It shows, however, only low and very variable sensitivity of 20-50% to detect auxiliary lymph node metastasis (12). This has led to the development of alternative PET and SPECT radiotracers using different targeting approaches (15). Fructose transport through GLUT5, which is highly expressed in breast cancer, is one such alternative targeting strategy that could lead to earlier diagnosis and treatment of breast cancer (16–18). This transport mechanism has been targeted by the recently developed and pre-clinically evaluated ^{18}F -labeled fructose-derivative 6-[^{18}F]FDF, which may thus represent an alternative new PET radiotracer for imaging breast cancer (1,2).

In conclusion, the favourable dosimetry estimates, as well as non-observable toxicological effects for 6-[^{18}F]FDF and the advantageous clearance properties of this radiolabeled fructose-derivative support a further testing of this new PET tracer in a first in human trial.

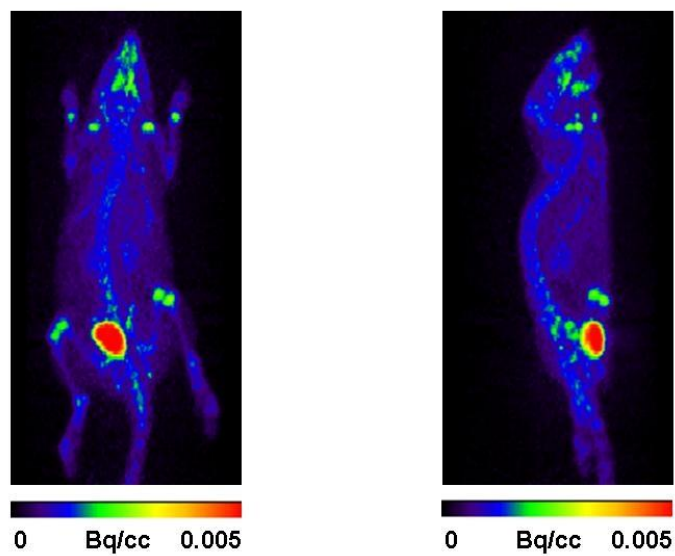


Figure 4.1: Whole body distribution of 6-[¹⁸F]FDF at 2 h post injection in a rat - Clearly visible is uptake into the bone and radioactivity in the urinary bladder after clearance from the rest of the body.

Organs	5 min	1 hour	2 hours	6 hours
Blood	0.739 ± 0.011	0.398 ± 0.026	0.183 ± 0.026	0.034 ± 0.005
Heart	0.636 ± 0.011	0.303 ± 0.023	0.179 ± 0.046	0.029 ± 0.003
Lung	0.607 ± 0.040	0.322 ± 0.028	0.152 ± 0.023	0.037 ± 0.004
Liver	0.577 ± 0.009	0.347 ± 0.028	0.218 ± 0.051	0.064 ± 0.012
Kidneys	3.052 ± 0.300	0.875 ± 0.105	0.420 ± 0.078	0.064 ± 0.016
Thymus	0.489 ± 0.020	0.280 ± 0.032	0.156 ± 0.385	0.023 ± 0.002
Spleen	0.449 ± 0.013	0.284 ± 0.016	0.147 ± 0.005	0.053 ± 0.003
Duodenum	0.704 ± 0.011	0.327 ± 0.006	0.189 ± 0.021	0.051 ± 0.015
Small Intestine	0.627 ± 0.004	0.340 ± 0.009	0.236 ± 0.055	0.046 ± 0.010
Large Intestine	0.230 ± 0.005	0.279 ± 0.007	0.534 ± 0.218	0.495 ± 0.046
Pancreas	0.283 ± 0.015	0.179 ± 0.015	0.095 ± 0.016	0.024 ± 0.002
Bone	0.234 ± 0.025	0.795 ± 0.046	0.786 ± 0.344	0.094 ± 0.026
Muscle	0.240 ± 0.010	0.310 ± 0.024	0.156 ± 0.020	0.023 ± 0.003
Stomach	0.274 ± 0.090	0.245 ± 0.020	0.147 ± 0.027	0.020 ± 0.001
Ovaries	0.470 ± 0.064	0.323 ± 0.029	0.145 ± 0.042	0.025 ± 0.005
Brain	0.129 ± 0.016	0.240 ± 0.015	0.186 ± 0.005	0.043 ± 0.005
Bladder	0.831 ± 0.119	1.305 ± 0.171	1.095 ± 0.621	0.153 ± 0.044
Fat	0.077 ± 0.016	0.053 ± 0.009	0.016 ± 0.003	0.005 ± 0.001

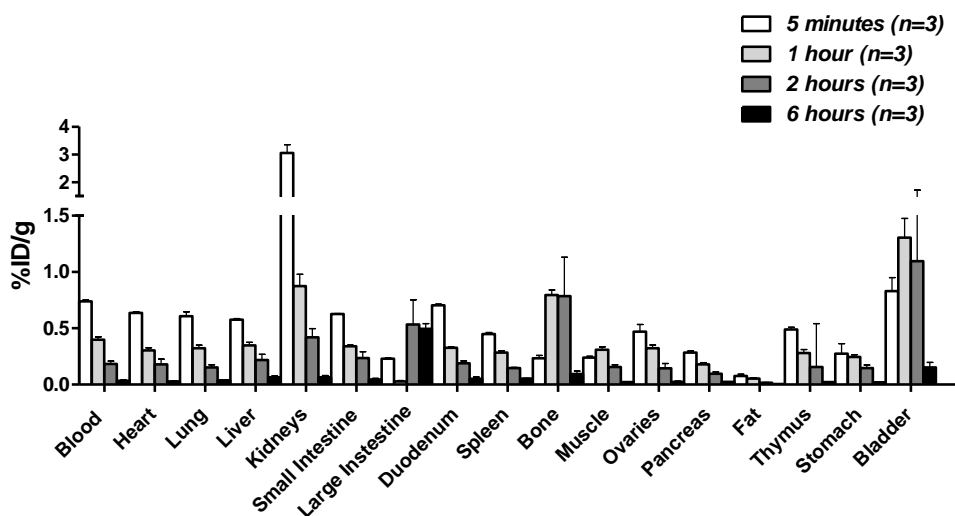


Table 4.1: Biodistribution table and graphical representation of 6-[¹⁸F]FDF in rats - Data presented are the means means ± SEM %ID/ g from n = 3 animals per time point.

Organs	Absorbed dose for 6- ¹⁸ F]FDF [mGy/MBq]	Absorbed dose for ¹⁸ F]FDG [mGy/MBq]
Adrenals	0.0069	
Brain	0.0051	0.050±0.019
Breasts	0.0037	
Gallbladder wall	0.0074	
Lower low intestine wall	0.0118	0.013±0.001
Small intestine	0.0151	
Stomach wall	0.0060	
Upper low intestine wall	0.0117	0.013±0.001
Heart wall	0.0075	0.025±0.010
Kidneys	0.0202	0.024±0.012
Liver	0.0132	0.016±0.004
Lungs	0.0059	0.013±0.03
Muscle	0.0055	0.010±0.002
Ovaries	0.0092	0.018±0.001
Pancreas	0.0065	
Red marrow	0.0119	0.010±0.001
Osteogenic cells	0.0315	
Skin	0.0036	
Spleen	0.0063	0.015 ± 0.0021
Testes	0.0045	0.021±0.001
Thymus	0.0049	
Thyroid	0.0048	
Urinary bladder wall	0.0179	0.052±0.014
Uterus	0.0073	
Total body	0.0071	0.012 ± 0.00077
Effective dose	0.0089 mSv/MBq	0.015±0.001 mSv/MBq
Effective dose equivalent	0.0108 mSv/MBq	

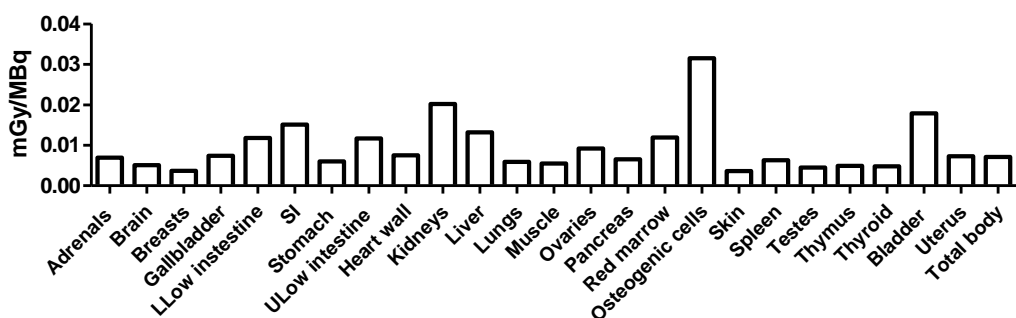


Table 4.2: Table and graphical representation of the calculated human absorbed doses and effective dose for 6-¹⁸F]FDF as determined using OLINDA/EXM and compared to estimated doses for ¹⁸F]FDG use in patients from a recent study (7). Higher absorbed dose values with ¹⁸F]FDG are in bold.

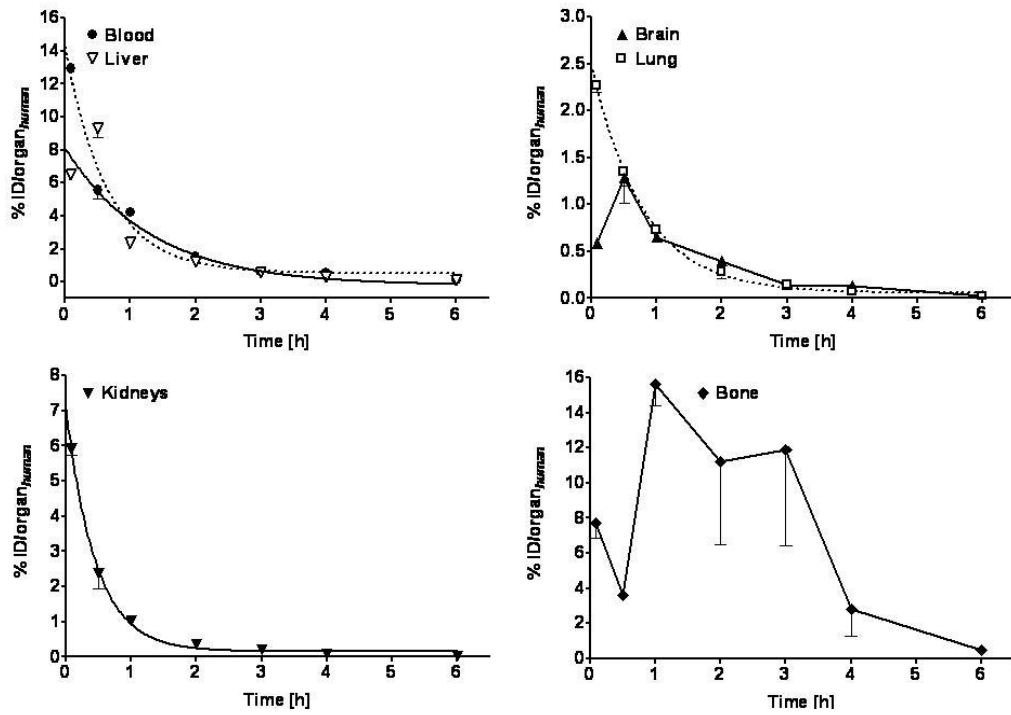


Figure 4.2: Time-activity curves ($\%ID/kg$)_{human} for some of the Medical Internal Radiation Dose (MIRD) source organs (blood, liver, lung, brain, bone and kidneys), scaled to human-equivalent values.

4.5 Bibliography

1. Trayner BJ, Grant TN, West FG, Cheeseman CI. Synthesis and characterization of 6-deoxy-6-fluoro-D-fructose as a potential compound for imaging breast cancer with PET. *Bioorganic & medicinal chemistry*. 2009 Aug 1;17(15):5488–95.
2. Wuest M, Trayner BJ, Grant TN, Jans H-S, Mercer JR, Murray D, et al. Radiopharmacological evaluation of 6-deoxy-6-[18F]fluoro-D-fructose as a radiotracer for PET imaging of GLUT5 in breast cancer. *Nuclear medicine and biology*. 2011 May;38(4):461–75.
3. U.S. Food and Drug Administration. Guidance for Industry, investigators and reviewers: exploratory IND studies. 2006:
<http://www.fda.gov/downloads/Drugs/GuidanceComplianceRegulatoryInformation/Guidances/ucm078933.pdf>
4. ICRP Publication. Basic anatomical and physiological data for use in radiological protection: reference values. A report of age- and gender-related differences in the anatomical and physiological characteristics of reference individuals. *Ann ICRP*. 2002;32:5–265.
5. Stabin MG, Sparks RB, Crowe E. OLINDA/EXM: the second-generation personal computer software for internal dose assessment in nuclear medicine. *Journal of nuclear medicine : official publication, Society of Nuclear Medicine*. 2005 Jun;46(6):1023–7.
6. Stabin M, Emmons M, Segars W, Fernald M, Brill A. ICRP-89 based adult and pediatric phantom series. *Journal of nuclear medicine : official publication, Society of Nuclear Medicine*. 2008;49(Suppl 1):14P.
7. Staaf J, Jacobsson H, Sanchez-Crespo A. A revision of the organ radiation doses from 2-fluoro-2-deoxy-D-glucose with reference to tumor presence. *Radiation protection dosimetry. Radiat Prot Dosimetry*. 2012;151(1):43-50.
8. U.S. Food and Drug Administration. Prescription drugs for human use generally recognized as safe and effective and not misbranded: drugs used in research.
<http://www.accessdata.fda.gov/scripts/cdrh/cfdocs/cfCFR/CFRSearch.cfm?CFRPart=361&showFR=1>

9. Abele JT, Fung CI. Effect of hepatic steatosis on liver FDG uptake measured in mean standard uptake values. *Radiology*. 2010 Mar;254(3):917–24.
10. Brenner DJ, Hall EJ. Computed tomography--an increasing source of radiation exposure. *The New England journal of medicine*. 2007 Nov 29;357(22):2277–84.
11. ICRP Publication. Radiation dose to patients from radiopharmaceuticals. *Ann ICRP*. 2007;106(38):1–2.
12. Fleming IN, Gilbert FJ, Miles KA, Cameron D. Opportunities for PET to deliver clinical benefit in cancer: breast cancer as a paradigm. *Cancer imaging : the official publication of the International Cancer Imaging Society*. 2010 Jan;10:144–52.
13. Yang WT, Le-Petross HT, Macapinlac H, Carkaci S, Gonzalez-Angulo AM, Dawood S, et al. Inflammatory breast cancer: PET/CT, MRI, mammography, and sonography findings. *Breast cancer research and treatment*. 2008 Jun;109(3):417–26.
14. Alavi A, Zhuang H. Finding infection--help from PET. *Lancet*. 2001 Oct 27;358(9291):1386.
15. Oude Munnink TH, Nagengast WB, Brouwers AH, Schröder CP, Hospers GA, Lub-de Hooge MN, et al. Molecular imaging of breast cancer. *Breast (Edinburgh, Scotland)*. 2009 Oct;18 Suppl 3:S66–73.
16. Zamora-León SP, Golde DW, Concha II, Rivas CI, Delgado-López F, Baselga J, et al. Expression of the fructose transporter GLUT5 in human breast cancer. *Proceedings of the National Academy of Sciences of the United States of America*. 1996 Mar 5;93(5):1847–52.
17. Haradahira T, Tanaka A, Maeda M, Kanazawa Y, Ichiya YI, Masuda K. Radiosynthesis, rodent biodistribution, and metabolism of 1-deoxy-1-[18F]fluoro-D-fructose. *Nuclear medicine and biology*. 1995 Aug;22(6):719–25.
18. Levi J, Cheng Z, Gheysens O, Patel M, Chan CT, Wang Y, et al. Fluorescent fructose derivatives for imaging breast cancer cells. *Bioconjugate chemistry*. 2007;18(3):628–34.

Chapter 5 - In vitro and in vivo evaluation of 1-deoxy-1-fluoro-2,5-anhydro-D-mannitol as a potential radiotracer for PET imaging of GLUT5 in breast cancer

Trayner BJ, Wuest M, Soueidan M, Bouvet V, Henderson J, Grant TN, Jans H-S, Mercer JR, Murray D, West FG, Wuest F, McEwan AJB, Cheeseman CI.

The work presented in this chapter represents a collaboration. BJT performed all *in vitro* experiments and analysis. *In vivo* experiments and analysis were performed by MW. All chemical syntheses were performed by MS, VB, JH and TNG.

5.1 Introduction

Breast cancer represents the second leading cause of cancer related deaths in women, presenting clinicians and health care providers a challenge to improve on detection methods. While advances in detection and treatment regimens have decreased cancer related mortality, further investigation is warranted into the improvement of various diagnostic modalities. Positron emission tomography (PET), magnetic resonance imaging (MRI), computed tomography (CT) and ultrasound used to complement often poorly sensitive detection methods such as mammography and physical exams, have seen more widespread use in the diagnosis and staging of breast cancer (1–5).

Diagnosis and therapy monitoring of tumors in breast cancer patients has seen increasing use of PET with the glucose analogue 2-deoxy-2-[¹⁸F]fluoro-D-glucose ([¹⁸F]FDG) being the most broadly utilized radiotracer (6–10). The efficacy of this technique has been attributed to cancer's hypermetabolic phenotype with a much higher demand for glucose than that of normal tissue (11–13). This observed increase in glucose uptake has been attributed to the overexpression of several of the SLC2A family of facilitative hexose transporters (GLUTs) (13,14). So far fourteen facilitative hexose transporter genes have been identified to be expressed within human tissues. Studies have implicated the overexpression of the high affinity glucose transporters GLUT1 and GLUT3 for the bulk of glucose and also [¹⁸F]FDG transport into cancer cells (15–20). After being translocated across the cell membrane, [¹⁸F]FDG is phosphorylated by hexokinase at position

6 by the initial enzymatic step of glycolysis. The members of the hexokinase family, and in particular hexokinase II, are upregulated in many tumors (21–23). After this initial step, no subsequent metabolism or efflux occurs allowing [¹⁸F]FDG to be accumulated and trapped within malignant cells and to generate a signal detectable by PET.

Despite its widespread clinical acceptance, [¹⁸F]FDG-PET possesses some significant limitations in detecting tumors which has stimulated the development of alternative PET radiotracers. Macrophages and neutrophils present within inflammatory tissue display high levels of glucose and [¹⁸F]FDG uptake, and [¹⁸F]FDG scans of these regions have been implicated in false positive diagnoses (4,24). Inflammatory tissue surrounding tumors may also lead to overestimation of tumor size based on the higher uptake of [¹⁸F]FDG in inflamed cells, and can be confounding when evaluating treatment efficacy. [¹⁸F]FDG has also been shown to be ineffective at identifying small (<1 cm in size) breast tumors and in a recent review, [¹⁸F]FDG-PET was assessed to have 76-89% sensitivity and 73-80% specificity for the diagnosis of primary breast cancers (25). Additionally, auxiliary lymph node metastases have had low and quite variable sensitivity in diagnoses (25–27).

One possible explanation for variable [¹⁸F]FDG-PET sensitivity in breast tumors may be due to the well documented altered expression of the facilitative hexose transporter family after malignant transformation; a phenomenon observed in

breast tumor cell lines as well as clinical patient samples (14,28,29). Whilst GLUT1 has been implicated as the main transporter for the cellular uptake of [^{18}F]FDG, studies have shown that 28 to 47% of selected breast cancer patient samples were GLUT1 negative (30–32). It has been suggested that other GLUT isoforms would be upregulated in order to provide the cell with its required metabolic fuel (14,28). Other reports have shown that the fructose transporters GLUT2 and GLUT5 display selective expression in human breast cancer tissue but not in healthy breast tissue suggesting that perhaps fructose may be an additional or alternative metabolic substrate in addition to glucose (14). While GLUT2 is able to transport both fructose and glucose at a low affinity, GLUT5 is exclusively a fructose transporter possessing a relatively high affinity for its substrate. GLUT5 may represent the more ideal target of the two as circulating plasma concentrations of glucose would compete for the binding site of GLUT2, limiting the ability of the radiotracer to enter the cell (16,33,34). GLUT5 expression in cancerous breast tissue compared to that of healthy breast tissue may represent a unique opportunity to design new fructose-based radiotracers for improved imaging of breast cancer (28,33,34).

Rational design of a ^{18}F -labelled fructose-based compound is essential as the structural requirements of GLUT5 and binding of the substrate to the transporter must be taken into account, as well as for phosphorylation of the compound by the primary glycolytic enzymes within the cell. Phosphorylation of fructose can

occur at either the 1 position by ketohexokinase (KHK) or at the 6 position by the hexokinase family, and thus placement of ^{18}F must take this into account (29,35).

Initial work on the development of fluorinated fructose derivatives started with Hadahira et al.'s work wherein fructose was labelled at position 1 yielding 1-deoxy-1- ^{18}F fluoro-D-fructose (36). Tumor cell uptake was examined in a fibrosarcoma-bearing mouse model, and despite the availability of the 6 position for phosphorylation via hexokinase, washout from tumor tissue was observed over time. Additionally, at that time they were not analyzing the uptake of the radiotracer for the imaging of breast tumors in a preclinical setting utilizing small animal PET, as GLUT5 was identified in breast cancer in 1996 (28). More recent labelling attempts at the position 1 with fluorophores have also been undertaken, although the investigators have suggested that due to the size and electronic changes modified by the addition of such bulky fluorescent groups, uptake of their derivatives cannot be used as an analogue of fructose for transport through GLUT5 (29).

Pioneering studies done by Holman and colleagues have suggested that labelling fructose at position 6 would provide analogues that would be properly handled by GLUT5 (37,38), and that there may also be an increase the affinity of the compound for binding and subsequent transport. Using this as a starting point, the initial work mentioned in the previous 3 chapters has focused on the synthesis and characterization of the fructose analogue 6-FDF. The ability of the

compound to be handled readily by GLUT5 in two breast cancer models, utilized for PET imaging of two murine xenograft models of breast cancer and a favourable clearance and dosimetry profile in a rat model was described (33,34). Being fluorinated at the 6 position allowed the fructose derivative to enter the cells rapidly, but due to the lack of expression of the enzyme KHK in either model it was effluxed due to the lack of phosphorylation and subsequent metabolic trapping (39).

Later work in 2002 done by Yang et al. has led to the identification of second generation fluorinated 2,5-anhydro-D-mannitol (2,5-AM) derivatives as potential innovative PET imaging agents (38). 2,5-AM is a C_2 -symmetric, stable fructose mimic that is known to be transported by GLUT5 (40). A 2,5-AM derivative shows several key advantages over a fructose analogue for imaging of GLUT5 expressing tumors. It possesses an affinity for GLUT5 comparable to that of fructose, as GLUT5 prefers the 2,5-AM furanose configuration for transport since it is more symmetrical than the pyranose form (41); [6-FDF is in the furanose ring form (34)] and lastly, being C_2 symmetric, the positions 1 and 6 are equivalent allowing for labelling at either position with proper handling by GLUT5 and ensuing phosphorylation by either KHK or hexokinase (38,42). As it was found previously that position 6 is amicable for proper transport via GLUT5 (33,34), and as both position 1 and 6 are equivalent, it is hypothesized that labelling at this position would provide compound amenable for transport via GLUT5 and metabolic trapping after phosphorylation by either KHK or hexokinase (29).

Cold 2,5-AM was synthesized, as well as the 2,5-AM derivative 1-deoxy-1-fluoro-2,5-anhydro-D-mannitol (1-FDAM) and herein the *in vitro* analysis of their transport characteristics in two breast cancer cell lines is described. Additionally, a suitable method for the synthesis of ^{18}F -labelled 1-FDAM was developed and initial analysis of 1- ^{18}F FDAM in *in vitro* transport assays and *in vivo* experiments utilizing the previously characterized EMT-6 xenograft mouse model are described. The obtained data for 1- ^{18}F FDAM are compared to the previously described 1- ^{18}F FDF in the same animal model and to previous data collected for the GLUT5 substrate 6- ^{18}F FDF and the glucose analogue ^{18}F FDG (33,36).

5.2 Materials and methods

Please see **Appendix A** for a detailed materials list.

5.2.1 *Synthesis of 1-deoxy-1-fluoro-2,5-anhydro-D-mannitol*

Reactions were carried out in flame-dried glassware under a positive argon atmosphere unless otherwise stated (**Figure 5.1**). Transfer of anhydrous solvents and reagents was accomplished with oven-dried syringes or cannulae. Solvents were distilled before use: methylene chloride (CH_2Cl_2) and *t*-amyl alcohol from calcium hydride, and pyridine from KOH. Thin layer chromatography was performed on glass plates precoated with 0.25 mm Kieselgel 60 F₂₅₄ (Merck). Flash chromatography columns were packed with 230–400 mesh silica gel (Silicycle). Optical rotations were measured at 22 ± 2 °C. Proton nuclear magnetic resonance spectra (^1H NMR) were recorded at 300 MHz, 400 MHz or 500 MHz and coupling constants (*J*) are reported in Hertz (Hz). Standard notation was used

to describe the multiplicity of signals observed in ^1H NMR spectra: broad (br), multiple (m), singlet (s), doublet (d), triplet (t), etc. Carbon nuclear magnetic resonance spectra (^{13}C NMR) were recorded at 100 MHz or 125 MHz and are reported (ppm) relative to the centre line of the triplet from chloroform-d (77.00 ppm). Fluorine nuclear magnetic resonance spectra (^{19}F NMR) were recorded at 377 MHz and are reported (ppm) relative to trifluoroacetic acid (-76.55 ppm). Infrared (IR) spectra were measured with a Mattson Galaxy Series FT-IR 3000 spectrophotometer. Mass spectra were determined on a PerSeptiveBiosystems Mariner high-resolution electrospray positive ion mode spectrometer.

2,5-Anhydro-D-mannitol (1): D-Glucosamine (1.03 g, 4.78 mmol) was dissolved in distilled water (14 mL) and mixed at room temperature for 3 hours to achieve mutarotational equilibrium. Solid sodium nitrite (1.0 g, 14.5 mmol) was added and the solution was cooled to 0 °C. Glacial acetic acid (0.54 mL) was added dropwise which caused the evolution of nitrogen gas. After mixing at 0 °C for two hours, the solution was warmed to room temperature and argon gas was bubbled through the solution for 30 minutes. The resulting yellow solution was re-cooled to 0 °C and solid NaBH_4 (0.900 g, 23.9 mmol) was added in small portions. After completion of gas evolution, the solution was warmed to room temperature and mixed for 18 hours. The mixture was filtered off and then quenched with Amberlite IR120 (H^+). The resin was filtered off and the resulting filtrate was concentrated in *vacuo* to give a white solid.

As previously reported (45), it was convenient to peracetylate crude 2,5-anhydro-D-mannitol for purification. Therefore, crude 2,5-anhydro-D-mannitol was dissolved in pyridine (5 mL). Acetic anhydride (5 mL) was added and the solution was cooled to 0°C. Then, 4-Dimethylaminopyridine was carefully added in a small portion at 0 °C and the solution was warmed up to room temperature. After 18 hours, the solution was cooled to 0 °C and H₂O was added (10 mL). The solution was extracted with CH₂Cl₂ (3 x 15 mL) and the combined organic layers were washed with 10% H₂SO_{4(aq)} (20 mL) and H₂O (20 mL). The solution was dried over anhydrous MgSO₄, filtered and concentrated to a viscous off yellow oil. The crude mixture was then purified *via* column chromatography (9:1 to 1:1 Hex:EtOAc) to afford the desired compound as a clear colourless oil that matched previously reported data² (1.19 g, 3.59 mmol, 75% yield from D-glucosamine).: ¹H NMR (300 MHz, CDCl₃): δ 5.17 (m, 2H), 4.25 (m, 6H), 2.09 (s, 9H).

Peracetylated 2,5-anhydro-D-mannitol (1.19 g, 3.59 mmol) was dissolved in methanol (10 mL) and 1.5 M NaOMe in methanol (0.68 mL) was added. The solution was mixed at room temperature for 1 h and subsequently neutralized with Amberlite IR-120 (H⁺). The resin was filtered off and the filtrate concentrated to afford 2,5-anhydromannitol as a viscous, slightly yellow oil (0.560 g, 3.41 mmol, 95 % yield). The crude mixture was then purified *via* column chromatography (acetone with 1% of methanol) or crystallized with

(MeCN/MeOH) to afford the 2,5-anhydro-D-mannitol (**1**) as clear crystals that matched previously reported characterization data (46).

^1H NMR (300 MHz, D_2O): δ 4.07 (m, 2H), 3.90 (m, 2H), 3.79 (dd, 2H, $J=12.2$, 3.1 Hz), 3.70 (dd, 2H, $J=12.6$, 5.57 Hz).

Trityl 3,4,6-tri-O-acetyl-2,5-anhydro-D-mannitol (2): 2,5-Anhydromannitol (0.568 g, 3.46 mmol) was dissolved in pyridine (6 mL) and trityl chloride (0.975 g, 3.50 mmol) was added. Subsequently, the solution was equipped with a reflux condenser and heated at 90 °C for 3 hours. The resulting yellow solution was cooled to 0 °C and acetic anhydride (5 mL) was added dropwise. The reaction was slowly warmed to room temperature overnight and was quenched by the addition of water (15 mL) and extracted with CH_2Cl_2 (3 x 20 mL). The combined organic layers were washed with 5% $\text{H}_2\text{SO}_{4(\text{aq})}$ (20 mL) and water (20 mL) and dried over anhydrous MgSO_4 . Filtration and concentration in vacuo afforded an oil residue that was purified via column chromatography (9:1 to 1:1 Hex:EtOAc) to afford (**2**) as a clear colourless oil that matched previously reported characterization data (46) (0.747 g, 1.40 mmol, 40% yield).: ^1H NMR (500 MHz, CDCl_3): δ 7.48 (d, 6H, $J=7.52$ Hz), 7.32 (t, 6H, $J=7.79$ Hz), 7.25 (t, 3H, $J=7.27$ Hz), 5.14 (t, 1H, $J=3.22$ Hz), 5.14 (dd, 1H, $J=4.34$, 2.67 Hz), 4.27 (m, 4H), 3.34 (dd, 1H, $J=9.74$, 4.40 Hz), 3.30 (dd, 1H, $J=9.74$, 5.56 Hz), 2.12 (s, 3H), 2.09 (s, 3H), 2.02 (s, 3H); ^{13}C NMR (125 MHz, CDCl_3): δ 170.72, 169.95, 169.90, 143.75, 128.74, 127.85, 127.11, 86.95, 82.59, 80.95, 78.79, 78.51, 63.59, 63.48, 20.88, 20.85, 20.79.

3,4,6-tri-O-acetyl-2,5-anhydro-D-mannitol (3): Trifluoroacetic acid (2 mL, 5% solution in CH₂Cl₂) was added to a mixture of compound **(2)** (136 mg, 0.20 mmol) and triethylsilane (38 g/L, 0.24 mmol). The solution was stirred for 30 min and quenched with aqueous saturated NaHCO₃. The resulting mixture was extracted with CH₂Cl₂ (3x25 mL) and the combined organic layers were dried over anhydrous MgSO₄. Filtration and concentration in *vacuo*, followed by flash column chromatography (9:1 to 1:1 Hex:EtOAc) afforded alcohol **(3)** as a clear colourless oil that matched previously reported data³ (0.607 g, 2.09 mmol, 85% yield).: ¹H NMR (500 MHz, CDCl₃): δ 5.23 (m, 1H), 5.19 (s, 1H), 4.25 (s, 3H), 4.10 (q, 1H, *J*=4.92 Hz), 3.78 (m, 2H), 2.28 (t, 1H, *J*=6.09 Hz), 2.11 (s, 6H), 2.10 (s, 3H); ¹³C NMR (125 MHz, CDCl₃): δ 170.67, 170.32, 170.07, 83.44, 80.71, 78.42, 77.80, 63.13, 62.00, 20.82, 20.78.

Triflyl 3,4,6-tri-O-acetyl-2,5-anhydro-D-mannitol (4): Alcohol **(3)** (0.607 g, 2.09 mmol) was dissolved in freshly distilled CH₂Cl₂ (21 mL) and cooled to -10 °C. Pyridine (0.24 mL) and triflic anhydride (0.39 mL) were added dropwise and the resulting solution was mixed at -10 °C. After one hour, water (10 mL) was added and the solution was extracted with CH₂Cl₂ (3 x 20 mL). The combined organic layers were washed with 10% H₂SO_{4(aq)} (20 mL), dried over anhydrous MgSO₄, filtered and concentrated to afford **(4)** as a viscous yellow oil that was used without further purification in the next reaction.: [α]_D²⁰=+15.81 (c 0.956, CHCl₃); IR (film) ν_{max} 1746, 1415, 1373, 1227, 1147, 1049, 956 cm⁻¹; ¹H NMR (500 MHz, CDCl₃): δ 5.20 (t, 1H, *J*=2.45 Hz), 5.12 (dd, 1H, *J*=4.08, 2.45 Hz), 4.68 (d, 2H,

$J=4.22$ Hz), 4.36-4.16 (m, 4H), 2.13 (s, 3H), 2.11 (s, 6H); ^{13}C NMR (125 MHz, CDCl_3): δ 170.57, 170.15, 169.96, 119.86, 117.32, 81.68, 80.97, 78.03, 77.73, 74.29, 62.63, 20.76, 20.64, 20.63; HRMS (ESI, $[\text{M}+\text{Na}^+]$) calcd for $\text{C}_{13}\text{H}_{17}\text{O}_{10}\text{SF}_3\text{Na}$ 445.0387, found 445.0380.

3,4,6-tri-O-acetyl-1-deoxy-1-fluoro-2,5-anhydro-D-mannitol (5): Crude triflate **(4)** (≤ 2.09 mmol) was dissolved in distilled *t*-amyl alcohol (6.3 mL) and cesium fluoride (0.93 g) was added as a single portion. The reaction was heated to $95\text{ }^\circ\text{C}$ for 25 minutes and then cooled to room temperature again. Water (10 mL) was added and the mixture was extracted with CH_2Cl_2 (3 x 10 mL). The combined organic layers were then washed with water (10 mL), dried over anhydrous MgSO_4 , filtered and concentrated. Flash column chromatography (9:1 to 1:1 EtOAc:Hex) afforded fluorinated **(5)** as a clear, colourless oil (0.488 g, 1.67 mmol, 80% yield over two steps): $[\alpha]_{\text{D}}^{20} = +18.39$ (c 0.8200, CHCl_3); IR (film) ν_{max} 1744, 1436, 1232, 1041 cm^{-1} ; ^1H NMR (400 MHz, CDCl_3): δ 5.20 (t, 1H, $J=3.77$ Hz), 5.15 (t, 1H, $J=3.41$ Hz), 4.55 (dd, 2H, $J=46.84, 3.77$ Hz), 4.27-4.12 (m, 4H), 2.07 (s, 3H), 2.06 (s, 3H), 2.05 (s, 3H); ^{13}C NMR (100 MHz, CDCl_3): δ 170.52, 170.00, 169.93, 82.38 (d, $J_{\text{C-F}}=174.81$ Hz), 81.81 (d, $J_{\text{C-F}}=15.25$ Hz), 81.01, 77.91, 77.49 (d, $J_{\text{C-F}}=6.49$ Hz), 63.00, 20.70, 20.66; ^{19}F NMR (400 MHz, CDCl_3): δ -230.05 (ddd, $J=46.84, 25.07$ Hz); HRMS (ESI, $[\text{M}+\text{Na}^+]$) calcd for $\text{C}_{12}\text{H}_{17}\text{O}_7\text{FNa}$ 315.0851, found 315.0851.

1-Deoxy-1-fluoro-2,5-anhydro-D-mannitol (6): Peracetylated **(5)** (0.488 g, 1.67 mmol) was dissolved in anhydrous MeOH (15 mL) and NaOMe in MeOH (1.5 M,

0.35 mL) was added dropwise. The solution was mixed at room temperature for 30 minutes and neutralized with the addition of Amberlite IR-120 (H⁺). The resin was filtered off and the filtrate was concentrated in *vacuo* to afford **(6)** as a clear colourless oil that crystallized over time (166.15 g, 1.59 mmol, 95% yield): mp 84-86 °C; [α]_D²⁰=+39.99 (c 0.7800, MeOH); IR (film) ν_{\max} 3365, 2924, 1456, 1119, 1058 cm⁻¹; ¹H NMR (400 MHz, D₂O): δ 4.61 (ddd, 2H, *J*=47.56, 10.50, 5.47 Hz), 4.14-3.99 (m, 3H), 3.92 (m, 1H), 3.78 (dd, 1H, *J*=12.57, 2.73 Hz), 3.69 (dd, 1H, *J*=12.75, 5.47 Hz); ¹³C NMR (100 MHz, CDCl₃): δ 83.58 (d, *J*_{C-F}= 168.87 Hz), 83.32, 81.49 (d, *J*_{C-F}=14.60 Hz), 76.84, 76.26 (d, *J*_{C-F}=8.22 Hz), 61.76; ¹⁹F NMR (400 MHz, CDCl₃): δ -229.79 (ddd, *J*=47.56, 24.54 Hz); HRMS (ESI, [M+Na⁺]) calcd for C₆H₁₁O₄FNa 189.0534, found 189.0532; anal. calcd for C₆H₁₁O₄F C: 43.37; H, 6.67 found: C, 43.35; H, 6.68.

5.2.2 Cell culture and transport experiments

EMT-6 and MCF-7 cells were grown in a CO₂ incubator at 37° in Gibco DMEM/F12 media supplemented with 15mM HEPES, L-glutamine, 10% fetal bovine serum and 1% penicillin/streptomycin with media renewal every 2 days. Uptake studies were performed once allowing the cells to reach confluence in 12 well plates. One hour before the initiation of an experiment, the media was removed, the plate rinsed twice with PBS and then replaced with glucose-free Krebs-Ringer solution (120 mMNaCl, 4 mMKCl, 1.2 mM KH₂PO₄, 2.5 mM, MgSO₄, 25 mM NaHCO₃, 70 μ M CaCl₂, pH 7.4). After the hour long incubation period, the glucose-free Krebs-Ringer solution was removed, and 300 μ L of a radiotracer

containing Krebs-Ringer solution was added to each well with a specific activity of 0.3 $\mu\text{Ci}/\text{mL}$ of ^{14}C -labeled D-fructose (Moravek Biochemicals), or 1-FDAM (proprietary), or approximately 0.3 MBq/mL of 1- ^{18}F FDAM. This was left to incubate within the wells for specific periods of time in a 37°C incubator until the media was aspirated and rinsed with ice-cold Krebs-Ringer to stop further transport. 500 μL of 5% trichloroacetic acid was then added to each well lysing the cells on a rotating rocker for an hour. The cell lysate was then transferred into scintillation vials containing 4 mL of ScintiSafe™ liquid scintillation fluid for counting in a liquid scintillation counter (Beckman LS 6500 multi-purpose liquid scintillation counter). Protein quantification was performed by lysing the cells using Cellytic™ M (Sigma) and then performing a BCA protein assay (Pierce, Rockford, IL, U.S.A.) according to the manufacturer's specifications. For the in vitro 1- ^{18}F FDAM experiments, the cell lysate was counted in a γ -counter (Wallac 1480 Wizard-3, Perkin-Elmer, Woodbridge, Ontario, Canada). Inhibition studies were performed as described in previous chapters.

5.2.1 *Animals*

All animal experiments were carried out in accordance with guidelines of the Canadian Council on Animal Care (CCAC) and were approved by the local animal care committee of the Cross Cancer Institute.

Murine EMT-6 cells (5×10^6 cells in 100 μL PBS) were injected into the upper left flank of female BALB/c mice (20-23 g, Charles River, Saint-Constant, Quebec,

Canada). Tumors were approximately 7-8 days old and ranged in size from 200-400 mm³.

5.2.2 *Small animal PET in EMT-6 tumor-bearing mice*

Positron emission tomography (PET) experiments were performed on BALB/c mice bearing EMT-6 tumors on the upper left flank. The mice were not fasted prior to the imaging experiments as the circulating glucose concentrations within the plasma would not effect GLUT5 mediated transport of 1-[¹⁸F]FDAM. The animals were anesthetized through inhalation of isoflurane in 40% oxygen / 60% nitrogen (gas flow, 1 L/min) and body temperature was kept constant at 37°C for the entire experiment. Mice were positioned and immobilized in the prone position with their medial axis parallel to the axial axis of the scanner and their thorax, abdomen and hind legs (organs of interest: heart, kidneys, bladder, tumors) in the centre of the field of view of a Concorde microPET[®] R4 scanner (Siemens Preclinical Solutions, Knoxville, TN, U.S.A.). A transmission scan for attenuation correction was not acquired. The amount of radioactivity present in the injection solution in a 0.5 mL syringe was determined with a dose calibrator (Atomlab[™] 300, Biodex Medical Systems, Shirley, NY, U.S.A.), which was cross calibrated with the scanner. The emission scan of 120-min PET acquisition was started. After a delay of approximately 15 s, 4-5 MBq of the radiotracer of interest (6-[¹⁸F]FDF, or 1-[¹⁸F]FDAM) in 100 -150 µL saline was injected through a needle catheter into the tail vein. Data acquisition continued for 120 min in 3D list mode. The list mode data were sorted into sinograms with 59 time frames

(10 x 2 s, 8 x 5 s, 6 x 10 s, 6 x 20 s, 8 x 60 s, 10 x 120 s, 10 x 300 s). The frames were reconstructed using the Ordered Subset Expectation Maximization applied to the 2D sinograms (2D OSEM) and MAP. The pixel size was 0.085 by 0.085 by 0.12 cm and the resolution in the centre field of view was 1.8 mm. No additional correction for partial volume effects was performed. The image files were further processed using the ROVER v2.0.21 software (ABX GmbH, Radeberg, Germany). Masks for defining 3D regions of interest (ROI) were set and the ROI's were defined by thresholding. ROI time-activity curves (TAC) were generated for subsequent data analysis. Standardized uptake values (SUV = (activity/mL tissue) / (injected activity/body weight), mL/g) were calculated for each ROI.

5.2.1 Phosphorylation with KHK and HK

The *in vitro* enzymatic reaction of 1-[¹⁸F]FDAM and 1-[¹⁸F]FDF with human recombinant KHK or human recombinant hexokinase-II (both 1 mg/mL; ATGen, Seongnam City, South Korea) was carried out in a TRIS buffer solution for up to 60 min at 37°C using a thermomixer. The final buffer solution contained 600 µL TRIS-HCl (100 mM), 200 µL KH₂PO₄ (100 mM), 50 µL MgCl₂ (40 mM), 50 µL Na₂ATP (100 mM), 50 or 150 µg KHK or 120 µg hexokinase-II and 1.7 MBq 6-[¹⁸F]FDF in 50 µL deionized water. After 5, 10, 30 and 60 min, aliquots of the reaction mixture were spotted on standard phase TLC plates, developed in 95% acetonitrile and 5% water and analyzed by radio-TLC. The samples were compared to a control solution mixture with no enzyme added.

5.2.2 *Data analysis*

In the inhibition experiments performed, counts per minute (CPM) were normalized to standards, background levels of substrate subtracted and then plotted against the maximum uptake of the radiolabeled tracer (ie. [¹⁴C]1-FDAM or [¹⁴C]D-fructose). For time courses, values were corrected with standards and to the protein levels present per well. IC₅₀ values (concentration at which half maximum inhibition of cellular uptake of a radiotracer was observed) were determined using non-linear regression analysis in GraphPad Prism 5 (GraphPad Software, San Diego, CA, USA), and significance was determined at p < 0.05 using a student's t-test.

5.3 Results

5.3.1 *Inhibition of [¹⁴C]D-fructose transport with 2,5-AM*

In order to fully understand 2,5-AM and its derivatives ability to bind to and be transported by GLUT5, 2,5-AM was used as a competitive inhibitor against [¹⁴C]D-fructose transport and its IC₅₀ determined. **Figure 5.2** shows inhibition of [¹⁴C]D-fructose transport in both the EMT-6 and MCF-7 cell lines known to endogenously express GLUT5 (28,29,33,34). Concentrations of 2,5-AM reached 10 mM in these studies and the IC₅₀ calculated from a 60 min incubation was 1.06 ± 0.58 μM in EMT-6 (n=3) and 0.16 ± 0.094 μM in MCF-7 cells (n=3). At 10 mM, transport of [¹⁴C]D-fructose was inhibited by 62% in both EMT-6 and MCF-7 cells.

5.3.2 Inhibition of [¹⁴C]D-fructose transport by 1-FDAM

Figure 5.3 shows initial experiments ascertaining the viability of 1-FDAM as a substrate for GLUT5. The previously characterized GLUT5 expressing breast cancer cell lines EMT6 and MCF-7 (28,29,33,34) were utilized for dose-dependent competitive inhibition of [¹⁴C]D-fructose uptake by 1-FDAM and to elucidate the relative affinity for the transporter. After 60 min incubation with increasing concentrations of non-radiolabeled 1-FDAM in the extracellular media, inhibition of [¹⁴C]D-fructose uptake was observed. Non-linear regression ascertained an IC₅₀ of 6.823 ± 3.0 μM (n=3) in EMT-6 and 3.96 ± 2.6 μM (n=3) in MCF-7 cells. At the highest examined concentration of 10 mM 1-FDAM, there was 68% inhibition of total [¹⁴C]D-fructose transport in EMT-6, and 76% in MCF-7 cells.

5.3.3 Uptake of [¹⁴C]1-FDAM

While it was observed that 1-FDAM was able to competitively inhibit [¹⁴C]D-fructose's entry into the cell in a dose dependent manner, it still was not clear whether it was binding and being translocated across the membrane, or just binding to the extracellular binding site of GLUT5 and thus preventing [¹⁴C]D-fructose from binding and crossing the cell membrane. To ascertain 1-FDAM's ability to be properly transported, uptake of newly synthesized [¹⁴C]1-FDAM (0.3 μCi/mL) was studied over time at tracer concentrations (**Figure 5.4**). Cells were incubated for 0, 1, 5, 10, 20, 30 and 60 minutes, and then lysed to determine how much compound was internalized in each breast cancer cell line. After 60

min it was observed that EMT-6 had approximately 1.7 times more uptake per mg of protein than MCF-7 (0.48 corrected CPM/mg protein, n=3 vs. 0.29 corrected CPM/mg protein, n=3). Uptake into EMT-6 elicited an almost linear uptake while MCF-7 on the other hand began to plateau after 30 minutes.

5.3.4 Inhibition of [¹⁴C]1-FDAM uptake by cytochalasin B

Cells were incubated in the presence of 0.3 μCi/ml of [¹⁴C]1-FDAM and 50 μM of the Class I GLUT inhibitor cytochalasin B (CB) for 60 minutes to fully elucidate GLUT2's influence on total [¹⁴C]1-FDAM flux (**Figure 5.5**). After 60 min incubation, EMT-6 in the presence of CB had 12% inhibition compared to the control (n=3), and MCF-7 had 11% (n=3) inhibition suggesting that GLUT5 mediates the remaining portion of the flux (88 - 89%). A student's t-test found no significant difference between the control and CB treated cells in either cell line indicating that uptake of [¹⁴C]1-FDAM mainly if not exclusively is mediated through GLUT5 only.

5.3.5 Inhibition of [¹⁴C]1-FDAM transport with D-fructose

In order to further examine the characteristics of [¹⁴C]1-FDAM's ability to bind to GLUT5, transport was inhibited through increasing concentrations of the natural substrate D-fructose to fully elucidate the relative affinity of both substrates (**Figure 5.6**). Dose dependent inhibition was observed in both cell lines, and non-linear analysis resulted in the similar IC₅₀ values of 34±27 mM for EMT-6 (n=3) and 75±36 mM for MCF-7 cells (n=3). These IC₅₀ values were significantly higher

than those for the inhibition of [¹⁴C]D-fructose transport with 1-FDAM, suggesting that like previously described for the fluorinated tracers, they may have a higher affinity for the transporter than the natural substrate D-fructose (33,34).

5.3.6 Inhibition of 6-[¹⁸F]FDF uptake with 1-FDAM

To estimate the affinity of 1-FDAM for GLUT5 in comparison to the natural substrate D-fructose and 6-FDF, cell uptake of 6-[¹⁸F]FDF (known to be almost exclusively transported through GLUT5 as outlined in earlier chapters) into EMT-6 cells was analyzed in the presence of increasing concentrations of cold 1-FDAM and 1-FDF. **Figure 5.7** shows the resulting concentration-response curve for 1-FDAM inhibiting 6-[¹⁸F]FDF uptake in comparison to fructose, 1-FDF and 6-FDF. Non-linear regression analysis resulted in an IC₅₀ value of 19 ± 6 mM (n=3) for 6-FDF and of 322 ± 33 mM (n=3) for fructose (33). 1-FDAM however possesses an apparently higher affinity in inhibiting 6-[¹⁸F]FDF transport than that of 6-FDF, suggesting an improved ability to bind to the transporter, although a full analysis of the concentration-response curve resulting in a solid IC₅₀ value was not possible with the limited data available so far. Similarly, 1-FDF appears to have a very similar trend for inhibition of 6-[¹⁸F]FDF as well.

5.3.7 Uptake of 1-[¹⁸F]FDAM into EMT-6 cells

The ¹⁸F-labelled version of 1-FDAM was synthesized and subsequently examined for its ability to be transported into the murine breast cancer cell line EMT-6 and

compared with previous data determined for 6-FDF (**Figure 5.8**) (33). Uptake was analyzed over a time course of 60 min at 37°C with timepoints at 2, 5, 10, 15, 30 and 60 min. Two conditions were used – normal Krebs buffer with approximately 0.3 MBq/mL of 1-[¹⁸F]FDAM, and Krebs solution with the radiotracer and supplemented with 100 mM D-fructose. After 60 min, an uptake of 2.89 ± 0.13 %ID/mg protein was observed in the control condition, and a reduced uptake of 1.91 ± 1.3 %ID/mg protein was observed in the presence of D-fructose. A statistically significant 44% reduction in uptake levels was observed after 60 minutes.

5.3.8 Uptake of 1-[¹⁸F]FDAM, 1-[¹⁸F]FDF, 6-[¹⁸F]FDF and [¹⁸F]FDG into BALB/c mice with xenografted EMT-6 tumors

Murine EMT-6 tumor-bearing BALB/c mice were used for the evaluation of the in vivo uptake of 1-[¹⁸F]FDAM. **Figure 5.9** shows maximum density projections for 1-[¹⁸F]FDAM at 10 and 30 min post injection. Tumor uptake was visible at both time points with clearance through the kidneys into the urinary bladder. **Figure 5.10** shows a comparison of the time-activity curves for tumor and muscle uptake of 1-[¹⁸F]FDAM over 110 min in comparison to the previously characterized GLUT5 substrate 6-[¹⁸F]FDF. After injection of 1-[¹⁸F]FDAM, lower uptake compared to 6-[¹⁸F]FDF was observed in the EMT-6 tumor. Uptake increased to a maximum SUV of 0.59 ± 0.09 (n=3) after approximately 20 min, and then slowly decreased over time. This contrasts with the previously profile observed for 6-[¹⁸F]FDF that peaked at a SUV of 1.23 ± 0.09 (n=3) after 10-15

min. Muscle uptake was also somewhat lower compared to 6- ^{18}F FDF, but this does not provide enough of a difference to increase the tumor/muscle ratio to that of 6- ^{18}F FDF. In **Figure 5.11** comparison of tumor uptake for 6- ^{18}F FDF, 1- ^{18}F FDF, 1- ^{18}F FDAM and ^{18}F FDG is summarized. Uptake of 1- ^{18}F FDAM was similar to 1- ^{18}F FDF with a maximum SUV of 0.48 ± 0.07 (n=3) after 20 min compared to that of 0.59 ± 0.09 (n=3) determined for 1- ^{18}F FDAM. Initial uptake levels during the first 30 min as well as later at almost 2 h post injection were significantly lower for both radiotracers compared to 6- ^{18}F FDF. However all three radiotracers have shown a washout from tumor tissue over time indicating no intracellular trapping in EMT-6 tumors while ^{18}F FDG is being accumulated over time and therefore trapped in the tumor cells.

5.3.1 Phosphorylation with KHK and HK

1- ^{18}F FDAM and 1- ^{18}F FDF was not phosphorylated by either human recombinant KHK or HK as analyzed in a direct reaction between the radiotracer and the enzyme (data not shown). There was no time-dependent reaction of either enzyme with both substrates. These findings indicate that 1- ^{18}F FDAM and 1- ^{18}F FDF are not substrates for either recombinant human KHK or HK *in vitro*.

5.4 Discussion

The objective of this study was to examine the fluorinated 2,5-AM derivative 1-FDAM and its ability to be transported into two models of breast cancer, and

characterize and compare 1-[¹⁸F]FDAM's profile to that of 6-[¹⁸F]FDF both *in vitro* and *in vivo*. This work has identified that i) 1-FDAM, like 2,5-AM, is a high affinity substrate for the facilitative hexose transporter GLUT5, ii) it is transported into human MCF-7 and murine EMT-6 cells, iii) it is rapidly cleared from the blood stream and cleared fast into the bladder in mice, iv) 1-[¹⁸F]FDAM shows uptake into the EMT-6 murine breast cancer model both *in vitro* and *in vivo* but v) it has a poorer ability to be transported into the EMT-6 tumor in BALB/c mice than that of 6-[¹⁸F]FDF and therefore leads to overall less uptake.

2,5-AM was synthesized to provide a benchmark to 1-FDAM and context on how the C-1 addition of fluorine impacts transport and handling via GLUT5. Inhibition studies show a marked decrease in the affinity of 1-FDAM versus that of 2,5-AM. 2,5-AM showed inhibition as low as the sub-micromolar range (EMT-6: $1.06 \pm 0.58 \mu\text{M}$ and MCF-7: $0.16 \pm 0.09 \mu\text{M}$) compared to an almost one order of magnitude larger IC_{50} for 1-FDAM (EMT-6: $7.11 \pm 3.2 \mu\text{M}$ and MCF-7: $3.96 \pm 2.6 \mu\text{M}$). The variability of the IC_{50} between cell lines may be indicative of variability in the structure and binding of 1-FDAM to murine GLUT5 compared to that of the human homologue, as well as the possible expression of other fructose transporting GLUTs that may also show some variable affinity for the substrate. Due to the lack of specific inhibitors for the Class II and III GLUTs, it is not possible to fully analyse their contribution to overall transport. 2,5-AMs superior ability to inhibit fructose transport compared to 1-FDAM seems to suggest that

the hydroxyl group present at positions 1 or 6 increases its relative affinity for binding.

[¹⁴C] labelled transport studies indicate that 1-FDAM is taken up into murine EMT-6 cells (0.48 ± 0.06 corrected CPM/mg protein), as well as the human MCF-7 cells (0.25 ± 0.03 corrected CPM/mg protein). The higher level of uptake in EMT-6 compared to MCF-7 cells is consistent to what was observed in previous studies done with 6-FDF and D-fructose (33,34).

To verify the hypothesis that 1-FDAM uptake is mediated by GLUT5, co-incubation of the Class I GLUT inhibitor cytochalasin B (CB) and [¹⁴C]1-FDAM indicates that the majority of cellular influx is for the most part CB insensitive, pointing towards GLUT5 as the major mediator of 1-FDAM's transport. This coincides with previous data for 6-FDF as described in chapter 2. Interestingly, and in agreement with previous data looking at 6-[¹⁸F]FDF transport inhibition with D-fructose (33), the IC₅₀ for inhibiting [¹⁴C]1-FDAM transport with D-fructose is also substantially higher than 1-FDAM inhibition of [¹⁴C]D-fructose transport suggesting that 1-FDAM's affinity for the transporter is much higher than the one of the natural substrate (EMT-6: 34 ± 27 mM; MCF-7: 75 ± 36 mM). Uptake of tracer concentrations of 1-[¹⁸F]FDAM was significantly inhibited by 44% in the presence of 100 mM D-fructose adding credence to the thought that perhaps 1-FDAM does indeed have higher affinity for the transporter than the natural substrate.

However, and despite the appearance of 1-FDAM being a high affinity substrate and well-handled by the transporter, *in vitro* uptake of 6-[¹⁸F]FDF (33) (22 ± 1 %ID/mg protein) was much higher compared to 1-[¹⁸F]FDAM (2.88 ± 0.1 %ID/mg protein) in murine EMT-6 cells after 60 min. This result was less expected as inhibition studies of 6-[¹⁸F]FDF transport using increasing concentrations of 1-FDAM suggested that perhaps it is a more effective inhibitor than either D-fructose or 6-FDF. It appears as if the initial step of binding to GLUT5 may not be a proper indication of the levels of substrate that will be translocated via action of GLUT5. 1-FDAM is very effective in binding to the extracellular vestibule in the initial steps of transport, but it appears that 1-[¹⁸F]FDAM despite this favourable characteristic is not being transported at the levels observed with 6-[¹⁸F]FDF. 6-FDF on the other hand may have less affinity for the first steps of translocation, but it seems to be more amenable to transport in the latter stages during conformational change and facilitative transport via GLUT5 (33). These *in vitro* results may indicate that 1-[¹⁸F]FDAM would maybe possessing somewhat lower uptake in GLUT5 expressing tumors *in vivo* compared to 6-[¹⁸F]FDF.

To verify this hypothesis, animal studies with injected 1-[¹⁸F]FDAM in the murine EMT-6 xenograft model have shown that the compound can be taken up into tumor tissue. After injection, 1-[¹⁸F]FDAM was visible clearing through the heart, kidneys and into the urinary bladder. TACs looking at tumor uptake of 1-[¹⁸F]FDAM show a maximum radioactivity level after approximately 20 minutes not unlike that of 6-[¹⁸F]FDF, albeit maximum levels are significantly lower (33).

The tumor/muscle ratios steadily rise in both 1-[¹⁸F]FDAM and 6-[¹⁸F]FDF injected animals, however after approximately 2 hours 6-[¹⁸F]FDF has a markedly higher ratio of 2.43 compared to 2.03 in the case of 1-[¹⁸F]FDAM. This in context with the *in vitro* data, indicates that 6-[¹⁸F]FDF has a stronger ability to image GLUT5 *in vivo* in the murine EMT-6 tumor model compared to 1-[¹⁸F]FDAM.

The observed similar level of uptake of the C-1 labelled fructose analogue 1-[¹⁸F]FDF (36) into the EMT-6 BALB/c xenografted tumor compared to 1-[¹⁸F]FDAM may be attributed to the symmetrical nature of the 2,5-AM molecule. This characteristic that was originally thought to perhaps provide this compound with an advantage over 6-[¹⁸F]FDF for binding, as it would be able to bind to the transporter with either C-1 or C-6, but the transport data suggests that this is not the case.

Incubation of 1-[¹⁸F]FDAM and 1-[¹⁸F]FDF with various concentrations of recombinant human KHK and HK led to no phosphorylated product suggesting that both compounds are not substrates for either enzyme. This is contrary to earlier work as this data indicates that perhaps the C-1 hydroxyl is crucial for the enzymatic reaction of fructose with HK and KHK (36). The lack of phosphorylation by either enzyme may also contribute to the low levels of uptake that were observed in both the *in vitro* and *in vivo* models examined.

Further work however needs to be done to ascertain 1-FDAM's biodistribution profile, metabolic stability within mice, and its transport behaviour into a human

model of breast cancer such as that described in chapter 3. This information will allow a more detailed comparison between 6-[¹⁸F]FDF and 1-[¹⁸F]FDAM as radiolabeled PET imaging agents targeting GLUT5 expression *in vivo*.

5.5 Conclusion

1-[¹⁸F]FDAM is a novel compound developed for imaging of GLUT5 expressing breast cancer tissue using PET. Uptake into both human and murine tissues has been observed, suggesting its ability to be a potential radiotracer for imaging of these tissues. Unfortunately, 1-[¹⁸F]FDAM has shown no favourable properties over the previously described radiotracer 6-[¹⁸F]FDF which is also a substrate for GLUT5. Further work needs to be done to analyse its transport characteristics in a human model of breast cancer and its metabolic status *in vivo*.

Fructose transport via GLUT5 and metabolism appears to be an important player in breast cancer growth and proliferation (14,28,29,33,34,43). Fortunately, the characterization of 1-[¹⁸F]FDAM has shed further light into the development of radiolabeled GLUT5 substrates, and this information may lead to the identification of other, more promising radiotracers useful for non-invasive molecular imaging approaches.

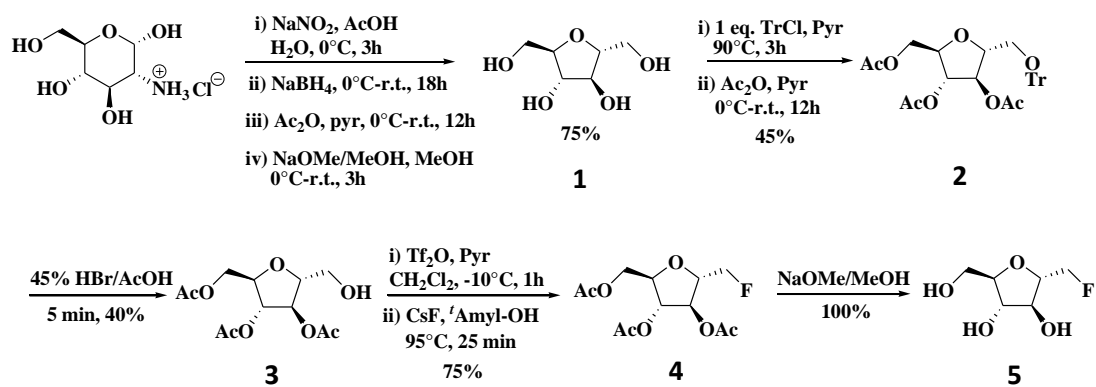


Figure 5.1: Synthesis of 1-FDAM

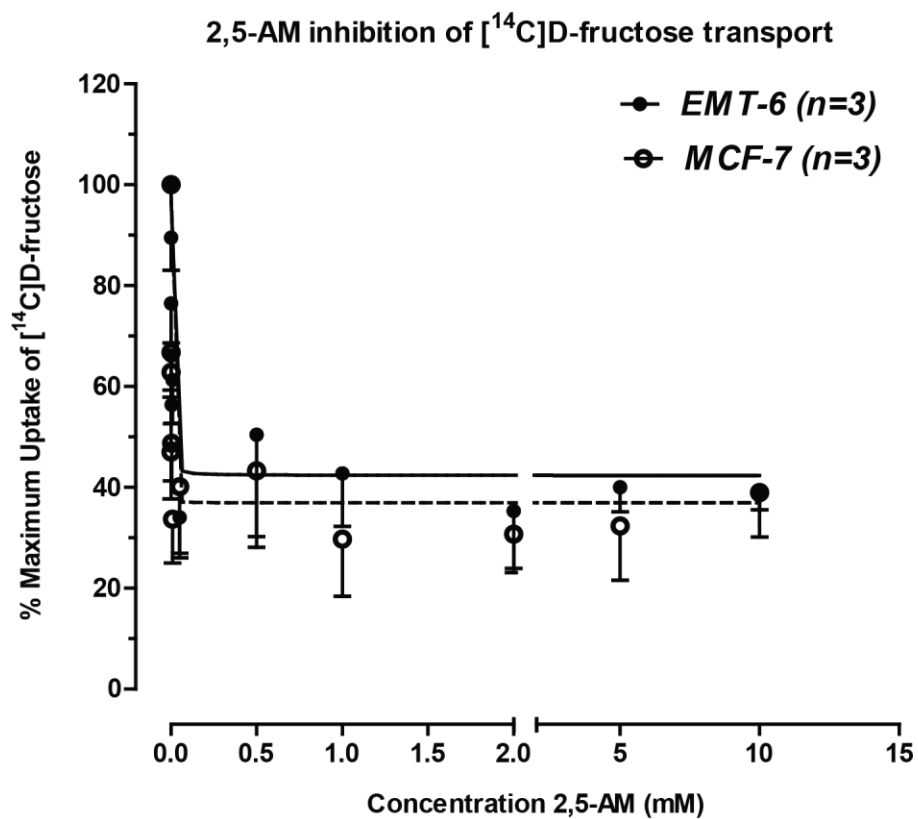


Figure 5.2: 2,5-AM inhibition of [¹⁴C]D-fructose transport - after a 60 min incubation at 37°C with both EMT-6 and MCF-7 using increasing concentrations of 2,5-AM. Fructose transport was inhibited by increasing concentrations of 2,5-AM, and the IC₅₀ obtained for EMT-6(●) was 1.06 ± 0.58 μM and 0.16 ± 0.09 μM in MCF-7(○). Error bars represent the SEM.

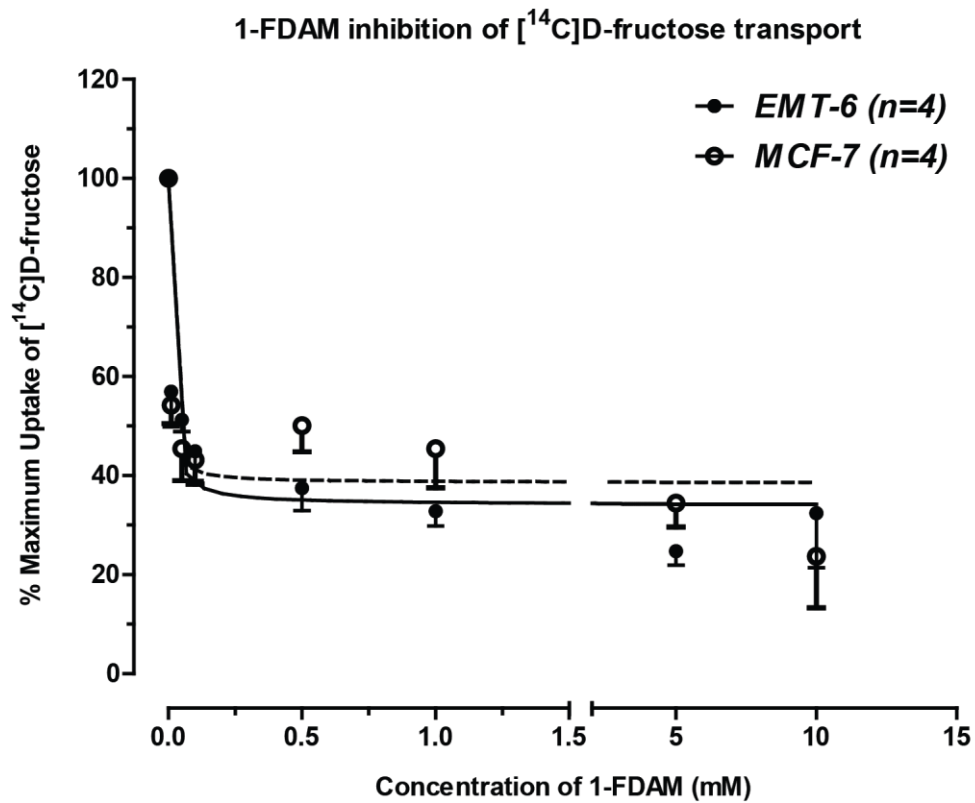


Figure 5.3: 1-FDAM inhibition of [¹⁴C]D-fructose transport - after a 60 min incubation at 37°C with both EMT-6 and MCF-7 using increasing concentrations of 1-FDAM. Fructose transport was inhibited by increasing concentrations of 1-FDAM, and the IC₅₀ obtained for EMT-6 was EMT-6 (●) 6.823 ± 3.0 μM, and MCF-7(○) 3.96 ± 2.6 μM. Error bars represent the SEM.

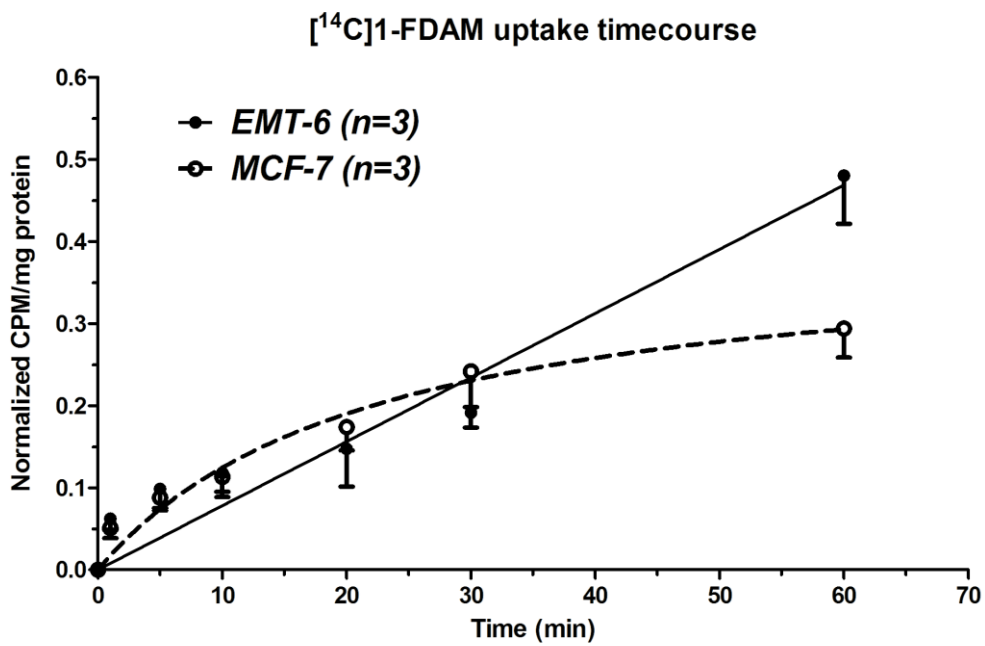


Figure 5.4: [¹⁴C]1-FDAM 60 minute time course in both MCF-7 (○) and EMT-6 (●) - corrected for non-mediated hexose uptake at 37°C. Uptake is observed in both cell types after a 60 min incubation. Error bars represent the SEM.

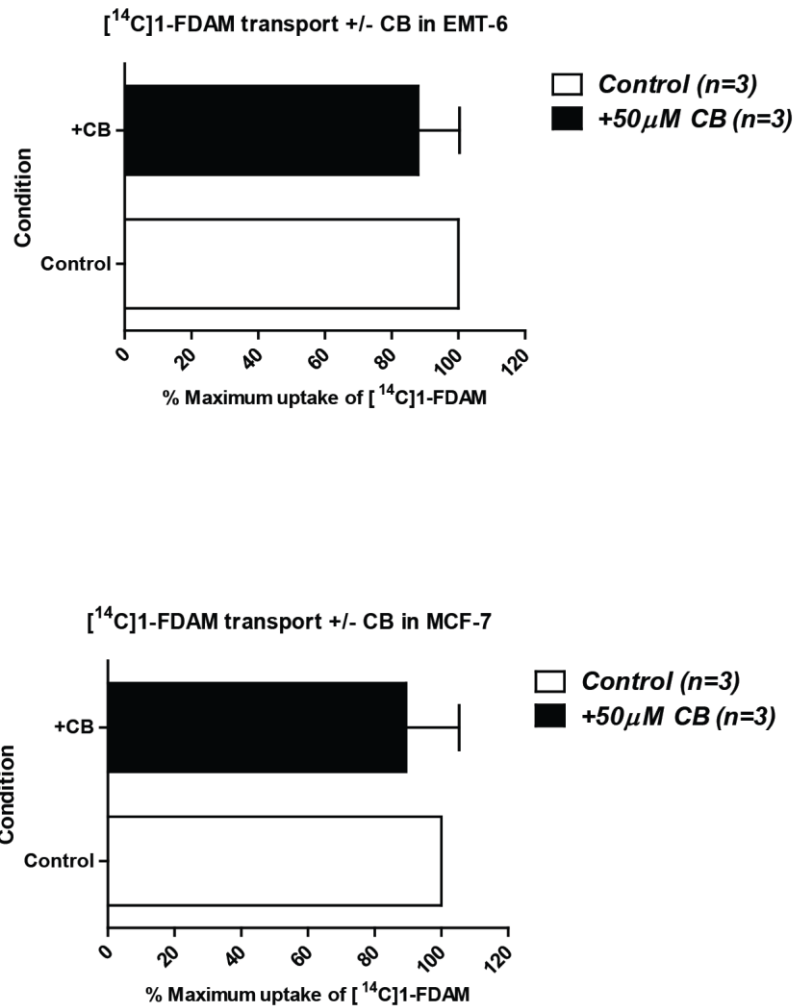


Figure 5.5: Inhibition of [¹⁴C]1-FDAM by 50 μM cytochalasin B(+CB) - is represented by the shaded bars of [¹⁴C]1-FDAM uptake into EMT-6 and MCF-7 cells. 37°C incubations lasted 60 min and uptakes were corrected for non-mediated fluxes. Error bars represent the SEM. No significant difference was observed between the control and treated groups.

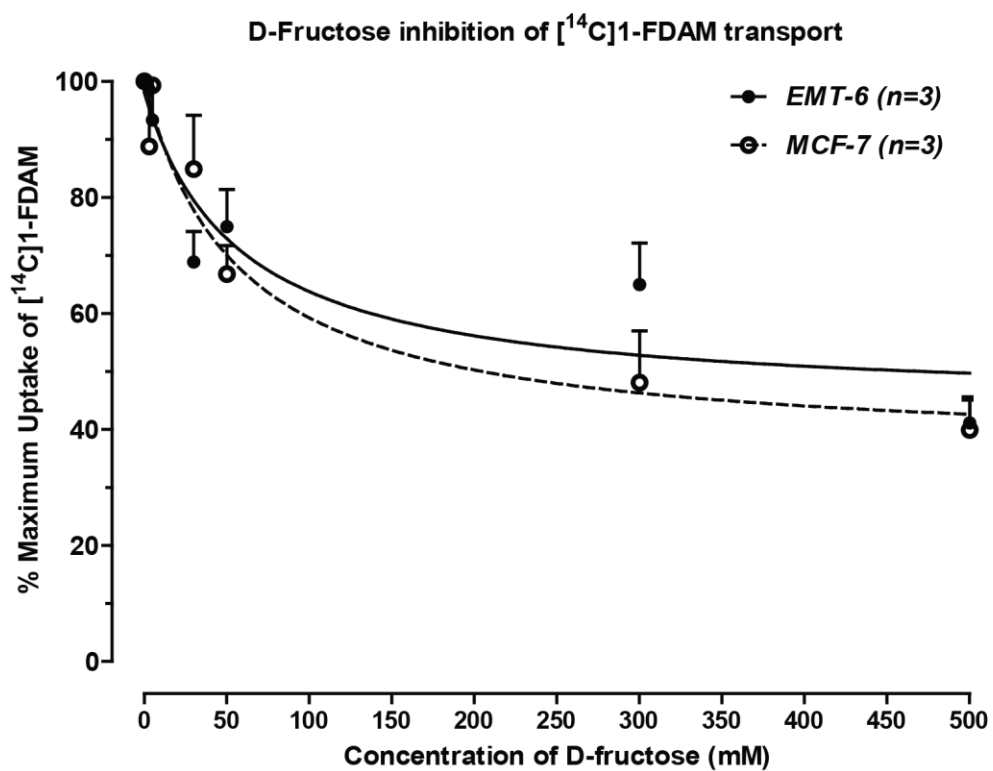


Figure 5.6: Fructose inhibition studies of [¹⁴C]1-FDAM transport - after a 60 min incubation at 37°C in both EMT-6 and MCF-7 using increasing concentrations of D-fructose. Transport was inhibited by D-fructose with a IC_{50} of approximately 34 ± 27 mM for EMT-6(●) and 75 ± 36 mM for MCF-7(○). Error bars represent the SEM.

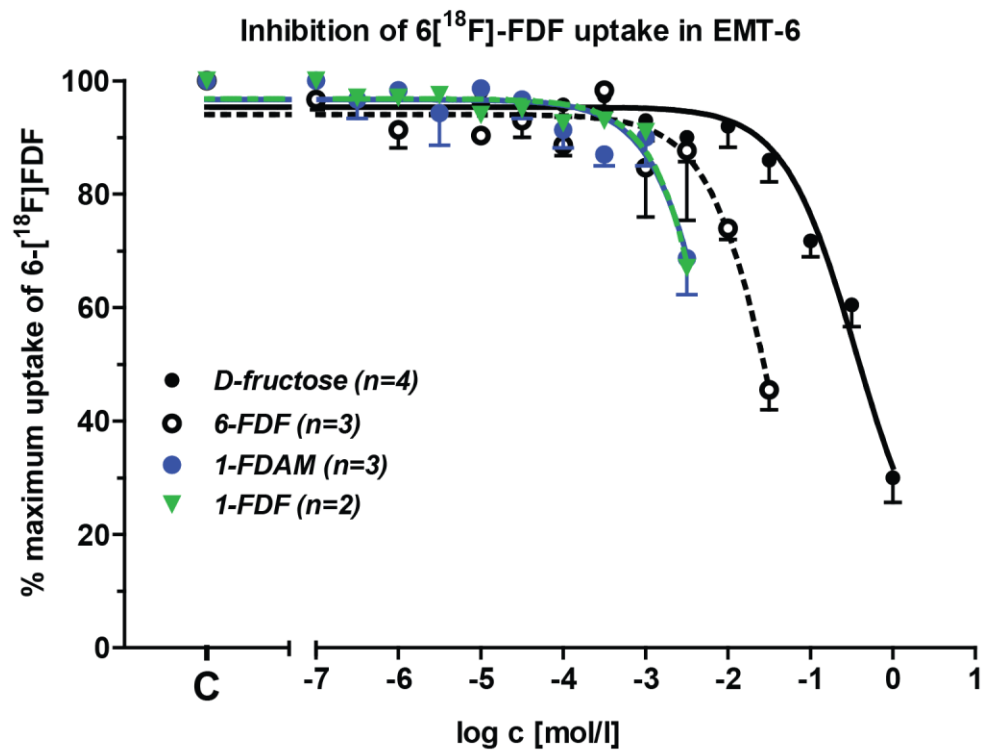


Figure 5.7: Concentration-response curves for 6-FDF, fructose, 1-FDAM and 1-FDF- the inhibiting effects of each substrate on the cell uptake of 6-[¹⁸F]FDF into EMT-6 cells. Data are shown as % maximum radiotracer uptake (control = 100%) and error bars represent the SEM.

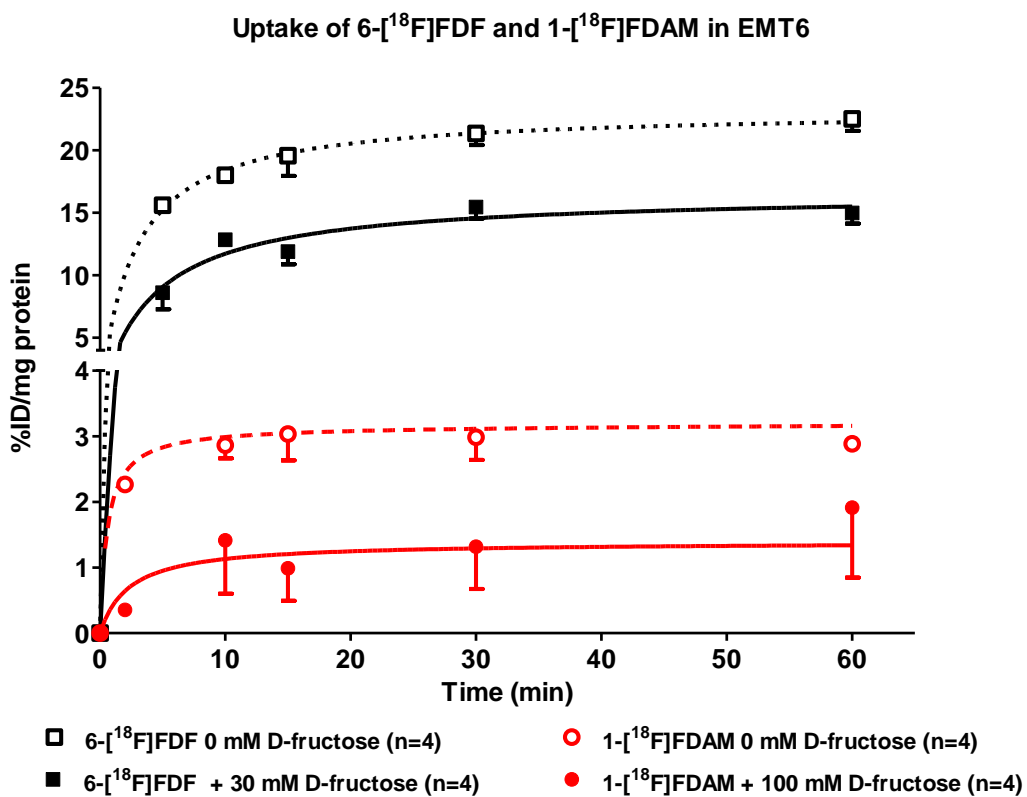


Figure 5.8: *In vitro* 1-^{[18]F}FDAM uptake studies- Cellular uptake of 1-^{[18]F}FDAM and 6-^{[18]F}FDF in murine EMT-6 breast cancer cells. Experiments were done in the presence (●) or absence (○) of 100 or 30 mM fructose in the extracellular buffer. Data are shown as %ID/mg protein uptake. Error bars represent the SEM.

1-¹⁸F]FDAM uptake in tumor bearing BALB/c

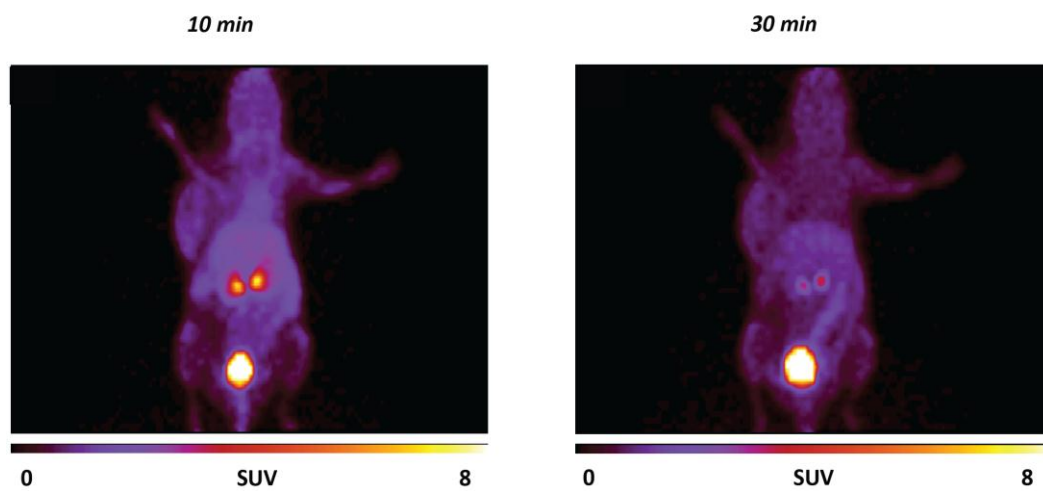


Figure 5.9: 1-¹⁸F]FDAM uptake into an EMT-6 tumor-bearing BALB/c mouse - Representative dynamic small animal PET images of 1-¹⁸F]FDAM after 10 and 30 min post injection. Isoflurane was used for anesthesia.

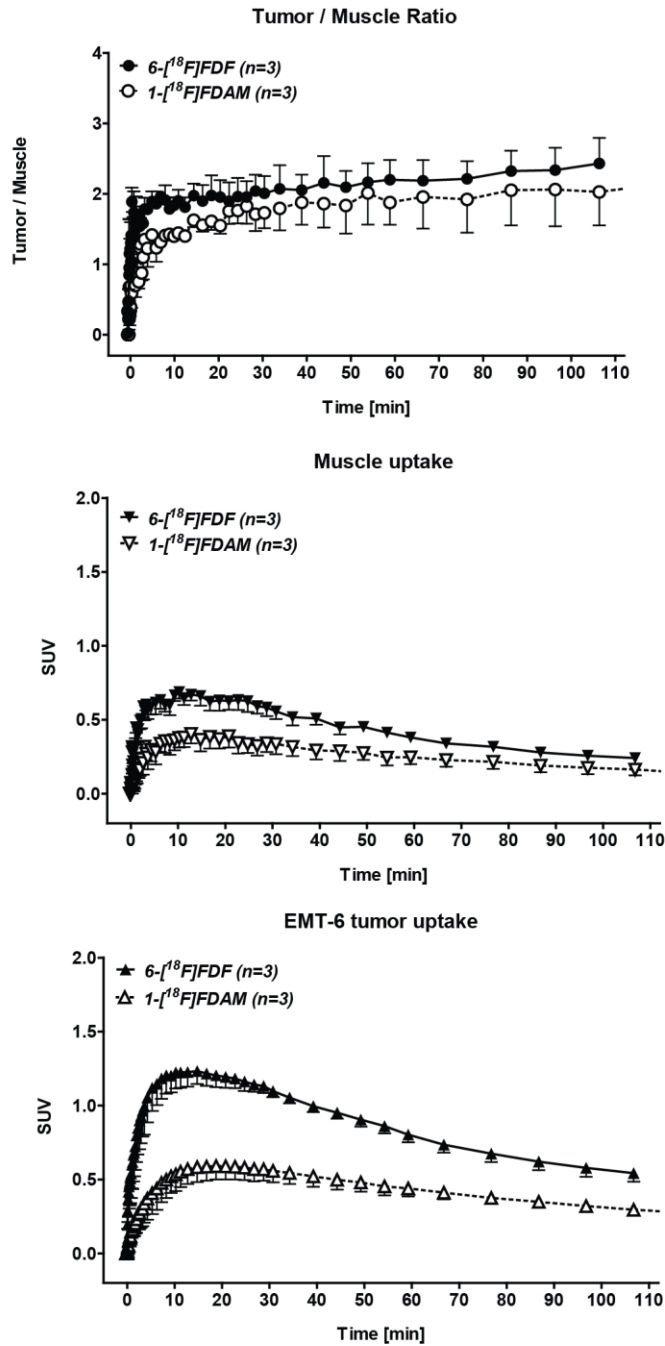


Figure 5.10: 1-[¹⁸F]FDAM and 6-[¹⁸F]FDF in EMT-6 bearing BALB/c mice -Time-activity curves (TAC) of the radioactivity profile in muscle and the xenografted tumor (bottom two panels). Tumor and muscle ratios for both tracers are shown in the top panel. Data is shown as SUV and error bars represent the SEM.

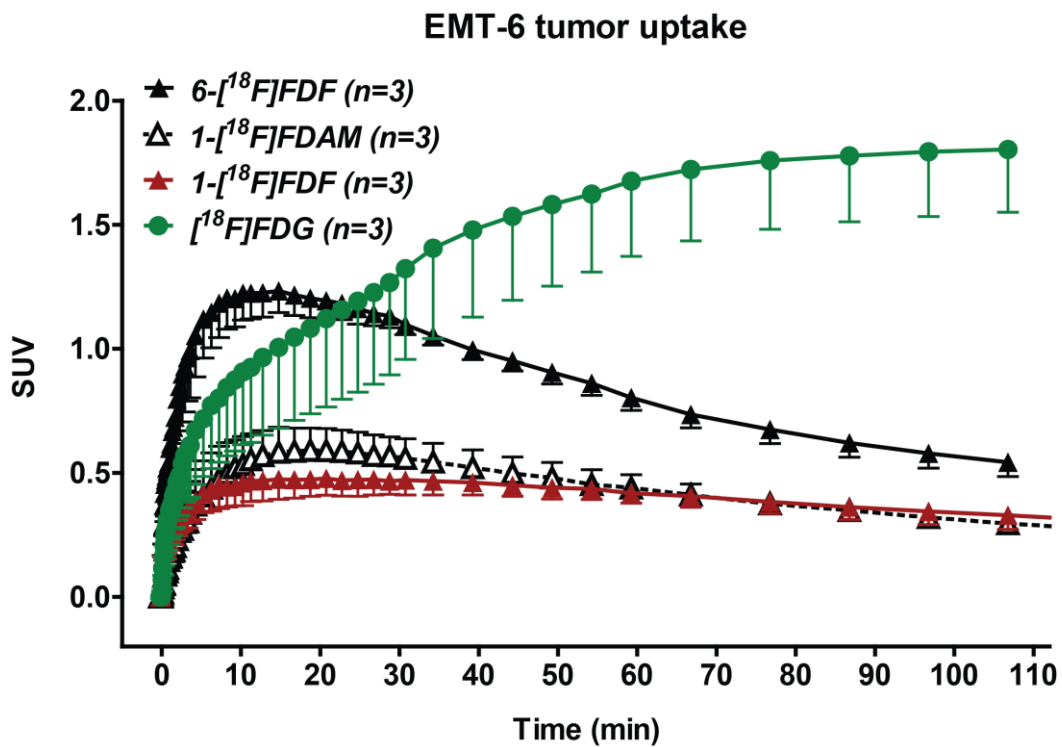


Figure 5.11: Time-activity curves (TAC) - of the uptake of 1- ^{18}F FDAM, 6- ^{18}F FDF, 1- ^{18}F FDF and ^{18}F FDG in EMT-6 tumors after a single intravenous injection of each respective radiotracer. Data is shown as SUV and the error bars represent the SEM.

5.6 Bibliography

1. Ginat DT, Puri S. FDG PET/CT manifestations of hematopoietic malignancies of the breast. *Academic radiology*. 2010 Aug;17(8):1026–30.
2. Iagaru A, Masamed R, Keesara S, Conti PS. Breast MRI and 18F FDG PET/CT in the management of breast cancer. *Annals of nuclear medicine*. 2007 Jan;21(1):33–8.
3. Lim HS, Yoon W, Chung TW, Kim JK, Park JG, Kang HK, et al. FDG PET/CT for the detection and evaluation of breast diseases: usefulness and limitations. *Radiographics : a review publication of the Radiological Society of North America, Inc*. 2007 Oct;27Suppl 1:S197–213.
4. Yang WT, Le-Petross HT, Macapinlac H, Carkaci S, Gonzalez-Angulo AM, Dawood S, et al. Inflammatory breast cancer: PET/CT, MRI, mammography, and sonography findings. *Breast cancer research and treatment*. 2008 Jun;109(3):417–26.
5. Berg WA, Weinberg IN, Narayanan D, Lobrano ME, Ross E, Amodei L, et al. High-resolution fluorodeoxyglucose positron emission tomography with compression (“positron emission mammography”) is highly accurate in depicting primary breast cancer. *The breast journal*. 2006;12(4):309–23.
6. Santiago JFY, Gonen M, Yeung H, Macapinlac H, Larson S. A retrospective analysis of the impact of 18F-FDG PET scans on clinical management of 133 breast cancer patients. *The quarterly journal of nuclear medicine and molecular imaging : official publication of the Italian Association of Nuclear Medicine (AIMN) [and] the International Association of Radiopharmacology (IAR), [and] Section of the Society of Radiopharmaceutica*. 2006 Mar;50(1):61–7.
7. Quon A, Gambhir SS. FDG-PET and beyond: molecular breast cancer imaging. *Journal of clinical oncology : official journal of the American Society of Clinical Oncology*. 2005 Mar 10;23(8):1664–73.
8. Oude Munnink TH, Nagengast WB, Brouwers AH, Schröder CP, Hospers GA, Lub-de Hooge MN, et al. Molecular imaging of breast cancer. *Breast (Edinburgh, Scotland)*. 2009 Oct;18Suppl 3:S66–73.
9. Buck AK, Schirrmester H, Mattfeldt T, Reske SN. Biological characterisation of breast cancer by means of PET. *Eur J Nucl Med Mol Imaging*. 2004 Jun;31 Suppl 1:S80-7.

10. Mavi A, Urhan M, Yu JQ, Zhuang H, Houseni M, Cermik TF, et al. Dual time point 18F-FDG PET imaging detects breast cancer with high sensitivity and correlates well with histologic subtypes. *Journal of nuclear medicine : official publication, Society of Nuclear Medicine*. 2006 Sep;47(9):1440–6.
11. Hanahan D, Weinberg RA. Hallmarks of cancer: the next generation. *Cell*. 2011 Mar 4;144(5):646–74.
12. Warburg O. On the origin of cancer cells. *Science (New York, N.Y.)*. 1956 Feb 24;123(3191):309–14.
13. Shaw RJ. Glucose metabolism and cancer. *Current opinion in cell biology*. 2006 Dec;18(6):598–608.
14. Reinicke K, Godoy A, Ulloa V, Rodri F, Medina RA, Yan AJ, et al. Differential Subcellular Distribution of Glucose Transporters GLUT1 – 6 and GLUT9 in Human Cancer : Ultrastructural Localization of GLUT1 and GLUT5 in Breast Tumor Tissues. *J Cell Physiol*. 2006 Jun;207(3):614–27.
15. Krzeslak A, Wojcik-Krowiranda K, Forma E, Jozwiak P, Romanowicz H, Bienkiewicz A, et al. Expression of GLUT1 and GLUT3 Glucose Transporters in Endometrial and Breast Cancers. *Pathology oncology research : POR*. 2012 Jul;18(3):721–8.
16. Manolescu AR, Witkowska K, Kinnaird A, Cessford T, Cheeseman C. Facilitated hexose transporters: new perspectives on form and function. *Physiology (Bethesda, Md.)*. 2007 Aug;22:234–40.
17. Khandani AH, Dunphy CH, Meteesatien P, Dufault DL, Ivanovic M, Shea TC. Glut1 and Glut3 expression in lymphoma and their association with tumor intensity on 18F-fluorodeoxyglucose positron emission tomography. *Nuclear medicine communications*. 2009 Aug;30(8):594–601.
18. Meneses AM, Medina RA, Kato S, Pinto M, Jaque MP, Lizama I, et al. Regulation of GLUT3 and glucose uptake by the cAMP signalling pathway in the breast cancer cell line ZR-75. *Journal of cellular physiology*. 2008 Jan;214(1):110–6.
19. Laudański P, Swiatecka J, Kovalchuk O, Wołczyński S. Expression of GLUT1 gene in breast cancer cell lines MCF-7 and MDA-MB-231. *Ginekologiapolska*. 2003 Sep;74(9):782–5.

20. Rodríguez-Enríquez S, Marín-Hernández A, Gallardo-Pérez JC, Moreno-Sánchez R. Kinetics of transport and phosphorylation of glucose in cancer cells. *Journal of cellular physiology*. 2009 Dec;221(3):552–9.
21. Mathupala SP, Ko YH, Pedersen PL. Hexokinase-2 bound to mitochondria: cancer's stygian link to the "Warburg Effect" and a pivotal target for effective therapy. *Seminars in cancer biology*. 2009 Feb;19(1):17–24.
22. Brown RS, Goodman TM, Zasadny KR, Greenson JK, Wahl RL. Expression of hexokinase II and Glut-1 in untreated human breast cancer. *Nuclear medicine and biology*. 2002 May;29(4):443–53.
23. Pedersen PL, Mathupala S, Rempel A, Geschwind JF, Ko YH. Mitochondrial bound type II hexokinase: a key player in the growth and survival of many cancers and an ideal prospect for therapeutic intervention. *Biochimica et biophysica acta*. 2002 Sep 10;1555(1-3):14–20.
24. Bleeker-Rovers CP, de Kleijn EMH a, Corstens FHM, van der Meer JWM, Oyen WJG. Clinical value of FDG PET in patients with fever of unknown origin and patients suspected of focal infection or inflammation. *European journal of nuclear medicine and molecular imaging*. 2004 Jan;31(1):29–37.
25. Facey K, Bradbury I, Laking G, Payne E. Overview of the clinical effectiveness of positron emission tomography imaging in selected cancers. *Health technology assessment (Winchester, England)*. 2007 Oct;11(44):iii-iv, xi–267.
26. Fletcher JW, Djulbegovic B, Soares HP, Siegel BA, Lowe VJ, Lyman GH, et al. Recommendations on the use of 18F-FDG PET in oncology. *Journal of nuclear medicine : official publication, Society of Nuclear Medicine*. 2008 Mar;49(3):480–508.
27. Hodgson NC, Gulenchyn KY. Is there a role for positron emission tomography in breast cancer staging? *Journal of clinical oncology : official journal of the American Society of Clinical Oncology*. 2008 Feb 10;26(5):712–20.
28. Zamora-León SP, Golde DW, Concha II, Rivas CI, Delgado-López F, Baselga J, et al. Expression of the fructose transporter GLUT5 in human breast cancer. *Proceedings of the National Academy of Sciences of the United States of America*. 1996 Mar 5;93(5):1847–52.

29. Levi J, Cheng Z, Gheysens O, Patel M, Chan CT, Wang Y, et al. Fluorescent fructose derivatives for imaging breast cancer cells. *Bioconjugate chemistry*. 2007;18(3):628–34.
30. Younes M, Brown RW, Mody DR, Fernandez L, Laucirica R. GLUT1 expression in human breast carcinoma: correlation with known prognostic markers. *Anticancer research*. 15(6B):2895–8.
31. Ravazoula P, Batistatou A, Aletra C, Ladopoulos J, Kourounis G, Tzigounis B. Immunohistochemical expression of glucose transporter Glut1 and cyclin D1 in breast carcinomas with negative lymph nodes. *European journal of gynaecological oncology*. 2003 Jan;24(6):544–6.
32. Laudański P, Koda M, Kozłowski L, Swiatecka J, Wojtukiewicz M, Sulkowski S, et al. Expression of glucose transporter GLUT-1 and estrogen receptors ER-alpha and ER-beta in human breast cancer. *Neoplasma*. 2004 Jan;51(3):164–8.
33. Wuest M, Trayner BJ, Grant TN, Jans H-S, Mercer JR, Murray D, et al. Radiopharmacological evaluation of 6-deoxy-6-[18F]fluoro-D-fructose as a radiotracer for PET imaging of GLUT5 in breast cancer. *Nuclear medicine and biology*. 2011 May;38(4):461–75.
34. Trayner BJ, Grant TN, West FG, Cheeseman CI. Synthesis and characterization of 6-deoxy-6-fluoro-D-fructose as a potential compound for imaging breast cancer with PET. *Bioorganic & medicinal chemistry*. 2009 Aug 1;17(15):5488–95.
35. Heman RH, Zakim D. Fructose metabolism. I. The fructose metabolic pathway. *The American journal of clinical nutrition*. 1968 Mar;21(3):245–9.
36. Haradahira T, Tanaka A, Maeda M, Kanazawa Y, Ichiya YI, Masuda K. Radiosynthesis, rodent biodistribution, and metabolism of 1-deoxy-1-[18F]fluoro-D-fructose. *Nuclear medicine and biology*. 1995 Aug;22(6):719–25.
37. Tatibouët a, Yang J, Morin C, Holman GD. Synthesis and evaluation of fructose analogues as inhibitors of the D-fructose transporter GLUT5. *Bioorganic & medicinal chemistry*. 2000 Jul;8(7):1825–33.

38. Yang J, Dowden J, Tatibouët A, Hatanaka Y, Holman GD. Development of high-affinity ligands and photoaffinity labels for the D-fructose transporter GLUT5. *The Biochemical journal*. 2002 Oct 15;367(Pt 2):533–9.
39. Thomas P, Bessel EM. The effect of substitution at C-2 of D-glucose 6-phosphate on the rate of dehydrogenation by yeast glucose 6-phosphate dehydrogenase. *The Biochemical journal*. 1972 Nov;130(1):21P.
40. Yang J, Dowden J, Tatiboué A, Hatanaka Y, Holman GD. Development of high-affinity ligands and photoaffinity labels for the D-fructose transporter GLUT5. *Biochem J*. 2002 Oct 15;367(Pt 2):533-9.
41. Girniene J, Tatibouët A, Sackus A, Yang J, Holman GD, Rollin P. Inhibition of the d-fructose transporter protein GLUT5 by fused-ring glyco-1,3-oxazolidin-2-thiones and -oxazolidin-2-ones. *Carbohydrate Research*. 2003 Apr;338(8):711–9.
42. Dills WL, Geller JI, Gianola KM, McDonough GM. Enzymatic analysis of 2,5-anhydro-D-mannitol and related compounds. *Analytical biochemistry*. 1983 Sep;133(2):344–9.
43. Wlaschin KF, Hu W-S. Engineering cell metabolism for high-density cell culture via manipulation of sugar transport. *Journal of biotechnology*. 2007 Aug 31;131(2):168–76.
44. Cassel S, Debaig C, Benvegno T, Chaimbault P, Lafosse M, Plusquellec D, Rollin P, *European Journal of Organic Chemistry*. 2001, 875-896.
45. Guthrie RD, Jenkins ID, Watters JJ, Wright MW, Yamasaki R, *Australian Journal of Chemistry*. 1982. 35, 2169-2173.

**Chapter 6 - General Discussion, conclusions and
future directions.**

6.1 Hypothesis revisited

The goal of this thesis was to ascertain the viability of radiolabeled, novel fructose based substrates for the facilitative hexose transporter GLUT5 to image GLUT5 expressing breast cancers *in vivo*, and to have a favourable metabolic profile for the initiation of clinical trials in man. In this chapter the proceeding body of work will be summarized, the main findings highlighted and future directions described.

6.2 Fructose derivatives for molecular imaging

6.2.1 *Molecular imaging of GLUT5*

Molecular imaging has been defined as the “visualization, characterization and measurement of biological processes at the molecular and cellular level in humans and other living systems” by the Society of Nuclear Medicine (1). To visualize a biological process with PET, a compound must:

- i) Have a target that is able to be distinguished from other tissues.
- ii) Be specific for that target.
- iii) Be transported/diffused readily into the cell/have a target that is on the exterior of the cell.
- iv) Have good binding affinity.
- v) Be non-toxic.
- vi) Be excreted easily.

vii) Be accumulated in the target in order to generate a good signal/noise ratio.

Lastly, and uniquely the case with PET tracers is that the synthesis of the compound must be rapid enough for the effective labelling with short-lived radionuclides.

The discovery of GLUT5 expression in breast cancer opened the door for the exploration of a new target for the *in vivo* imaging of tumors using PET – an idea which was originally suggested in Zamora-Léon's initial paper (2). The compounds described within this thesis are specific, readily transported, high affinity, non-toxic, easily excreted and are able to generate a good signal/noise ratio in our model systems. In this case we have been successful in visualizing and characterize breast cancer fructose transport and metabolism and have assessed the viability of several of these probes for clinical utility (2,3).

6.2.2 History and critique of previous work in the field

Investigation into the creation of novel substrates for the labelling of GLUT5 expressing breast cancers has only been explored twice – the first being by the Haradahira (4) group in 1995 where they synthesized 1-FDF in an effort to visualize fructose metabolism with PET and secondly by Gambhir's group who added fluorophore groups on the C-1 of fructose (13). Haradahira's group was unfortunately at a distinct disadvantage for several reasons: i) they were unaware and/or did not mention whether the fructose transporting GLUT2 or

GLUT5 was expressed in the fibrosarcoma model that they used ii) the 1996 paper by Zamora-Leon et al. (2) describing the expression of GLUT5 in the two breast cancer models MCF-7 and MDA-468 had yet to be published which may have given them a better xenograft model to use to examine tumor uptake and iii) the seminal papers by Holman's group (5,6) had yet to be released describing the binding site and its inability to handle fructose labelled at the one position with GLUT5. They did observe rapid uptake into liver, kidneys and small intestine – all areas with high levels of fructose transport that is primarily mediated by expression of the glucose/fructose transporter GLUT2 (7). Curiously, the studies by Holman indicated that the one position would not be amenable for labelling as it was required for transport with GLUT5, but the work done by Gould's group indicates that GLUT2 is able to handle fructose but not glucose compounds labelled at the 1 position (8). This might suggest that the bulk of the uptake of 1-FDF is GLUT2 mediated, and due to the high levels of glucose perfusing through the liver via the hepatic portal vein and in the normal circulation, 1-FDF was outcompeted for binding by glucose to the hexokinase family. Hexokinase affinity for glucose is several orders of magnitude higher than fructose, and thus 1-FDF was not metabolized or metabolically trapped (9–12). To determine whether or not this is the case, uptake studies using the *Xenopus laevis* heterologous expression system expressing GLUT2 should be undertaken to clarify if C-1 labelled fructose analogue uptake is indeed mediated by GLUT2.

Additionally, phosphorylation studies examining 1-FDF's ability to be phosphorylated by the hexokinase family should be done as well.

The first attempt to use GLUT5 expression as a target for molecular imaging of breast cancer was that of the Gambhir's group in 2007. In this study they synthesized a class of fluorescent compounds for the imaging of three GLUT5 expressing breast cancer cell lines: MCF-7, MDA-MB-231, MDA-MB-435 (13). Like Haradahira's (4) group, they also chose to label at the one position with both the NBD or Cy5.5 groups – bulky fluorophores that are respectively 294 and 1128 g/mol in size and coupled to fructose by an amine group. Their focus was the initial phosphorylation step after entrance into the cell, so the 6 position for labelling was disregarded as it would be unable to be phosphorylated by the hexokinase family, and the cell lines examined did not express KHK. Holman's work in 2002 used an allylamine group at the one position of fructose to take the place of the missing hydroxyl for hydrogen bonding and found it to be moderately well handled by the transporter, and thus they believed that an amine linker would increase the affinity of the compound for the binding site of GLUT5 even with a bulky group present.

Transport assays were performed using confocal microscopy to ascertain the ability of the two compounds to enter the three model breast cancer cell lines. Strangely, no competition studies examining the two compounds' effect on normal fructose uptake were undertaken. Flow cytometry was used to examine

uptake of the molecules and found that uptake was proportional to their concentration in the extracellular fluid. This data however was not included in the paper, nor was the technique used further to give a clearer, more quantitative picture of the behaviour of the compounds and their entrance into the model cell lines. The only competition studies that were done was using high levels of extracellular fructose concentrations (50mM) to show competitive inhibition of the two substrates. This paper lacks significant quantitative descriptions of the transport of their compound, and the quality of the work suffers substantially because of it.

As there is no quantitative dissection of the transport characteristics of these compounds, one must conclude that further work needs to be done in order to properly clarify their behaviour within their model system. While they do admit that the size and charge of the bulky groups would prevent the two analogues from being representative of fructose transport, they have not provided quantitative data to back up that conclusion either way. These publications do not provide a great deal of insight into the binding and transport of novel GLUT5 substrates other than perhaps that labelling at the C-1 may not be amenable for proper transport as was originally suggested by Holman and associates (5).

6.2.3 Initial in vitro characterization of 6-FDF, and model systems

The C-6 fluorinated fructose analogue was the initial attempt to ascertain the viability of using GLUT5 as a target for imaging of breast cancer with PET and its

initial characterization is presented in chapter 2. Following Holman's work which suggested that labelling at the six carbon position was readily handled by GLUT5, cold 6-FDF was synthesized in 7-steps from fructose. It was then used to first examine the inhibition of [¹⁴C]D-fructose uptake in the human, MDA-MB-231 and MCF-7 cell lines – models that were chosen from their previous use in exploring GLUT5 mediated uptake of fructose analogues (13). After further examination of the GLUT expression profile it became quite clear that while the characteristic expression of GLUT1 and 5 was apparent there were also a multitude of Class I, Class II and Class III transporters expressed in both lines such as GLUT2, 4, 7, 9, and 11. Contrary to previous work done by the Rogers group, we did not identify GLUT12 expression in either of the cell lines (14). The expression profile of other GLUTs is a limitation of using cell lines as a model system for analysing the transport characteristics of novel substrates. The *Xenopus laevis* heterologous expression system however allows for the specific expression of single transporters and allows for a detailed kinetic dissection of uptake. The down side of using the *X. laevis* system is that not only is very labour intensive, it is an amphibian cell expressing mammalian transporters and thus it is difficult to conclude that the same behaviour would be observed in a mammalian transport system. Unfortunately, attempts at getting reliable GLUT5 or GLUT2 expression in *X. laevis* has been shown to be difficult, and thus a cell culture model became the preferred method of determining the transport characteristics of the novel compounds described herein.

When using cell models for transport, some tools are available to determine the relative contribution of different GLUTs from the overall flux (such as the Class I inhibitor cytochalasin B), although there are no specific inhibitors currently available for GLUTs that belong to Class II or III. The cell culture transport system may give more insight into the *in vivo* behaviour of the compound as it is a mammalian cell line that can be used as xenografts in animal PET imaging studies using ^{18}F -labelled compounds. Ideally, a model that is GLUT1 negative, GLUT5 positive should be identified in order to validate that a fructose analogue would be able to successfully image cells unable to take up [^{18}F]FDG. Unfortunately, current techniques for cell culture use high glucose media and thus would select for those cells expressing high quantities of GLUT1 and not GLUT5. Work on GLUT5 expressing cell culture models has shown that fructose supplemented media is sufficient to allow for the proliferation of cells *in vitro*, suggesting that a primary tumor line found to express high levels of GLUT5 and low levels of GLUT1 would be able to maintain that phenotype in fructose supplemented media as well as sustain normal growth and a proliferative phenotype (15).

Effort was dedicated to determining the relative uptake of the natural substrates D-glucose and D-fructose to ascertain their proportional level of uptake in both MCF-7 and MDA-MB-231. Due to the conditions under which they were cultured, high levels of glucose uptake were observed compared to that of fructose – while not ideal, was not surprising. Initial experiments using cold 6-FDF described in chapter 2 saw high affinity inhibition of fructose transport in both cell lines.

Cytochalasin B (CB) inhibition of fructose transport indicates that the majority of fructose transport in both lines was mediated by a Class II or Class III GLUT, but was assumed to be mainly mediated by GLUT5 due to its physiological role as the primary fructose transporter of the GLUT family (16,17). Both MDA-MB-231 and MCF-7 cell uptake studies with [¹⁴C]6-FDF indicated uptake over 90 minutes, with relative uptake not unlike what was observed with glucose transport in other studies (18). The more poorly differentiated MDA-MB-231 cell line took up higher levels of the compound compared to MCF-7 suggesting that perhaps GLUT5 expression and fructose metabolism is more upregulated in those cells as well (18). [¹⁴C]6-FDF uptake was further confirmed to be GLUT5 mediated via inhibition studies using CB in MCF-7. Our focus then shifted to modifying the synthetic pathway to be amenable for ¹⁸F-labelling.

Using the Eckert & Ziegler modular synthesis unit and the triflate precursor, the ¹⁸F-labelled substrate was synthesized. Unfortunately the triflate had to be made fresh before each synthesis as it was shown to decompose over time. Later unpublished work has identified that a tosylate labelled precursor allows for increased stability over time and thus will be utilized for further syntheses and eventual clinical trials. The synthesis of the compound used in chapter 3 from the triflate precursor took 120 minutes and was used for both the *in vitro* cell uptake and *in vivo* animal studies .

We undertook further *in vitro* trials to more fully understand the nature of the transport of the compound and to confirm the findings of the previous chapter as well as compare the uptake of 6-[¹⁸F]FDF to that of the gold standard PET imaging agent, [¹⁸F]FDG (19–21). The murine EMT-6 breast cancer model was adopted instead of the MDA-MB-231 cell line since EMT-6 has been shown to be a very robust breast cancer xenograft model, to grow rapidly and reliably *in vitro* and which has been used in previous studies by our collaborators (22–24). After the confirmed GLUT5 expression and uptake of 6-[¹⁸F]FDF as described in chapter 3, it was deemed a viable model for GLUT5 expressing breast cancer.

The data on D-glucose and D-fructose uptake in chapter 2 was consistent with with the proportional difference in uptake between the higher levels of [¹⁸F]FDG transport and that of 6-[¹⁸F]FDF. Extracellular 5mM glucose was used to mimic the circulating plasma concentrations present in mammals and it readily inhibited [¹⁸F]FDG uptake confirming a GLUT1 mediated transport process. 6-[¹⁸F]FDF transport was unaffected confirming a GLUT5 mediated process. Inhibition of 6-[¹⁸F]FDF was observed with increasing concentrations of D-fructose, albeit at an order of magnitude lower affinity than 6-FDF suggesting that the addition of the fluorine at the 6 position perhaps grants it an increased ability to bind to the transporter over the natural substrate. Holman's group only examined the replacement of the C-6 hydroxyl with an allyl group and that was readily accepted by the transporter, so the fact that fluorine has a higher affinity for the transporter may suggest hydrogen bonds being formed between that

fluorine and the amino acid side chains present in the binding pocket of GLUT5. Since little other work has been done to ascertain the structure of the binding pocket for GLUT5, it is unclear what the exact mechanism is that allows for this increase in affinity.

6-[¹⁸F]FDF was identified to be a substrate for human recombinant fructokinase and as such, efflux studies clearly indicate washout of the compound from both cell lines that were confirmed to have no KHK expression. Questions need to be asked when considering whether or not KHK expression is somehow correlated to GLUT5 expression in cancerous breast tissue. Regrettably, the only work examining levels of KHK in breast cancer have been that of Gambhir's paper group looking at three cell lines (13) – cells that have been cultured in high glucose conditions for several decades and thus likely have their metabolic machinery more geared to the metabolism of glucose. This would likely manifest in the higher expression of GLUT1, and the primary steps of glucose metabolism covered in more detail in chapter 1.

6.2.4 6-FDF *in vivo* studies and preclinical work

In conjunction with the *in vitro* studies present in chapter 3, *in vivo* imaging, biodistribution and metabolic studies were undertaken to fully grasp the utility of 6-[¹⁸F]FDF in a living system. Two xenograft models were used: the BALB/c EMT-6, a rapidly growing murine cell line in a non immunocompromised mouse as well as the slow growing NIH-III MCF-7 model whose growth is dependent on

estradiol supplementation. The downside to using subcutaneously implanted tumors is that they can show marked differences in the behaviour of the cell line than when implanted orthotopically (25). The downside of orthotopic implantation is that often there is difficulty in creating a robust model where the tumors “take” reliably and are consistent in their growth patterns (26,27). Additionally, in the case of the MCF-7 tumors, implanted estradiol tablets were required in order for the human tumor line to grow in an immunocompromised mouse which may add uncertainty when translating the *in vitro* model into an *in vivo* experimental system.

Healthy BALB/c mice injected with 6-¹⁸F]FDF were examined first to observe clearance of the compound as well as normal tissue accumulation. Rapid transit through the heart and kidneys was observed, leading to good clearance within the urinary bladder. After two hours, bone uptake was also observed, although it was not clear whether this was due to radio-defluorination of the compound or uptake from cells present within the bone and cartilage. Chapter 4 expanded on this by using longer timeframes and surprisingly, saw washout of 6-¹⁸F]FDF after 6 hours post injection. This leads us to believe that perhaps it is not just radio defluorination, but instead is uptake of the compound itself. The biphasic shape of the TAC curve for bone uptake supports this, indicating that perhaps several transport and metabolic processes are occurring simultaneously. Recent literature has identified chondrocytes in rats to express GLUT5, and uptake is readily apparent in joints such as the knee suggesting uptake of 6-¹⁸F]FDF.

Additionally, unpublished data in human chondrocytes indicates that GLUT5 is also expressed and as such may show a similar pattern of uptake in patients (personal communication – David Cinats). Currently the fate of 6-^[18F]6FDF in bone is unknown. Further examination is warranted to determine the true mechanism of uptake and the identity of the chemical species involved. Interestingly, brain uptake was also observed with a peak after 30 minutes which could be attributed to glial expression of GLUT5, cerebellar uptake or another currently unknown mechanism (28–31).

6-^[18F]FDF and ^[18F]FDG uptake in the two xenograft models allowed a comparison between the compounds' clearance as well as normal tissue and tumor accumulation. With regards to the rapidly growing murine cell line EMT-6 in BALB/c mice, the rapid uptake of 6-^[18F]FDF versus that of ^[18F]FDG indicates that perhaps the compound has a very high affinity for the GLUT5 transporter and due to the lack of circulating fructose in the bloodstream, competitive inhibition for GLUT5 did not occur. The washout of 6-^[18F]FDF after 15 minutes in the EMT-6 tumors verifies what was observed in the *in vitro* model – no metabolic trapping was occurring due to the lack of KHK expression. ^[18F]FDG showed slow uptake, most likely due to competition for the binding site of GLUT1 by normal circulating concentrations of glucose. Metabolic trapping via action of the hexokinase family is readily apparent, and again correlates to the *in vitro* efflux studies. While this may indicate that perhaps 6-^[18F]FDF may not have clinical utility when compared to the “gold standard” ^[18F]FDG in the EMT-6

model, several factors must be recognized: Firstly, large studies examining GLUT5 and concurrent KHK expression that would allow for phosphorylation and metabolic trapping have not been performed on patient samples. Secondly, the rapid uptake may provide some advantages to that of [^{18}F]FDG, as patients would be able to be injected and visualized rapidly as opposed to waiting the prescribed 90 minute timeframe before scanning (21). This is assuming that this data does translate well into what would be observed in trials in man.

The estrogen sensitive human adenocarcinoma cell line MCF-7 implanted in the immunocompromised NIH-III mice shows markedly different uptake patterns of [^{18}F]FDG and 6-[^{18}F]FDF than that of the EMT-6 BALB/c model. Rapid uptake was observed over the first 5 minutes using both tracers, but strangely, and unlike what was observed with the EMT-6 line, uptake plateaued after that initial phase. Most surprisingly was MCF-7's inability to continually accumulate [^{18}F]FDG like that observed in EMT-6 despite of the fact that MCF-7 has been shown to express GLUT1, HKI and HKII in vitro (2,13,32). With that, both radiotracers displayed comparable SUV values and accumulation in the MCF-7 model, something that may be indicative of perhaps slower and less active glucose and fructose metabolism. EMT-6 tumors were able to be implanted and ready for imaging in approximately a week whilst MCF-7 took almost a month. The proliferative ability of EMT-6 may be tied into its ability to metabolize large quantities of glucose rapidly, an aspect that can be visualized using [^{18}F]FDG. In conjunction with large levels of [^{18}F]FDG uptake in EMT-6, higher levels of 6-

[¹⁸F]FDF uptake were observed perhaps also indicating that in order to achieve the rapidly proliferating phenotype observed in vivo, have also broadened their substrate specificity to incorporate higher levels of fructose uptake – something that has been suggested previously in the literature (2,3,13,15).

The nature of the MCF-7 xenograft model adds uncertainty to the translatability of its behaviour to a human system. What is not clear is the impact on the behaviour of the cells by implanting human tissue in an immunocompromised mouse, as well as the impact of estradiol supplementation that is required for growth. Ideally we would like to implant a GLUT5 positive, GLUT1 negative xenograft tumor that would clearly show the utility of 6-[¹⁸F]FDF over [¹⁸F]FDG, but as mentioned earlier, one has yet to be identified.

Rapid metabolism and equilibrium of the compound between blood compartments is apparent after 5 minutes in BALB/c mice. Two radiolabeled metabolites have also been identified: one polar and one more lipophilic than the parent compound with only approximately 10% of the parent compound remaining in the plasma after 60 minutes. While the identification of these two compounds will require further investigation, their identity can be hypothesized due to their relative polarity and the metabolic pathway of fructose (33). After 6-[¹⁸F]FDF was injected into the tail vein, it was rapidly carried through all the major organs including the liver where fructokinase can phosphorylate the compound and produce the initial high levels of the more polar radiometabolite

1 described in chapter 3. Subsequent catalysis of 6-¹⁸F]FDF-1-phosphate by the next enzymatic step aldolase B, cleaving 6-¹⁸F]FDF-1-phosphate into dihydroxyacetone phosphate and 3-¹⁸F]fluoro-3-deoxy-D-glyceraldehyde may represent the more lipophilic radiometabolite 2 observed on the radio TLCs of murine blood and urine (**Figure 6.1**). The relative levels in both urine and blood suggest that 6-¹⁸F]FDF is being rapidly metabolized into the phosphorylated 6-¹⁸F]FDF-1-phosphate which makes up the bulk of the radioactivity and then is slowly converted into DHAP and 3-¹⁸F]fluoro-3-deoxy-D-glyceraldehyde, increasing over 60 minutes. The lack of total metabolism over the observed timeframe to 3-¹⁸F]fluoro-3-deoxy-D-glyceraldehyde may indicate aldolase B's inability to handle fluorine at the 6 position of fructose and thus catalysis might be slowed. The apparent lack of appearance of any other metabolites suggests that perhaps 3-¹⁸F]fluoro-3-deoxy-D-glyceraldehyde is not further metabolized by glyceraldehyde phosphate dehydrogenase.

Chapter 4 was the next step undertaken to determine whether or not 6-¹⁸F]FDF biodistribution and dosimetry would be acceptable for clinical trials, thus radiation dosage estimates using rats was undertaken. Biodistribution data determining organ levels of radioactivity at 5 and 30 minutes as well as 1, 2, 3, 4 and 6 hours post injection was analyzed using Organ Level INTERNAL Dose Assessment/EXponential Modeling (OLINDA/EXM) to scale up to human values as well as determine absorbed doses in organs. The findings suggest that the dosimetry estimates determined through modelling are within the guidelines

recommended by the Food and Drug Administration's Radioactive Drug Research Committee (34) and in conjunction with 6-[¹⁸F]FDF's favourable clearance profile and unobservable toxicological effects, it would be safe to initiate a clinical trial in humans.

6-[¹⁸F]FDF promising characteristics prompted us to start exploring other options for substrates to be transported by GLUT5 – although our focus shifted to compounds that would have the ability to be phosphorylated by the known upregulation of HK in many tumors (35,36).

6.2.5 1-FDAM *in vitro* characterization

Not unlike 6-FDF, 1-FDAM was born out of the work done by Holman's group in the early 2000s examining 2,5-AM analogues and their ability to inhibit D-fructose entry into a cell culture model expressing GLUT5 (37). They found that labelling 2,5-AM at the C-1 with allylamine and dinitrophenyl groups as well as large photolabel moieties readily inhibited normal D-fructose transport. They attributed this to the C₂ symmetry present in the structure of 2,5-AM that prevents GLUT5 from recognizing the difference between the 1 and 6 positions allowing the bulky groups to protrude into the extracellular space from the binding pocket (6). Additionally, the allyl group was suggested to strengthen hydrophobic interactions with the transporter and the amine group would be able to take the place of the missing hydroxyl group and form hydrogen bonds with the protein. Not unlike the amine group, fluorine has also been indicated in

forming hydrogen bonds and additionally, due to the symmetrical nature of the molecule it would be able to be phosphorylated by either the HK family or KHK allowing for metabolic trapping. For these reasons we hypothesized that substitution at the C-1 position of 2,5-AM with ^{18}F would be a suitable candidate for transport and labelling of GLUT5 expressing breast cancer.

Chapter 5 details the synthesis of cold 1-FDAM that was accomplished in 5 steps from 2,5-AM to be used in initial inhibition trials with [^{14}C]D-fructose. Not unlike 6-FDF, 1-FDAM showed a high potency to inhibit the transport of D-fructose, albeit to a lesser extent than what was observed with the parent compound 2,5-AM suggesting despite the compounds symmetry, the removal of the hydroxyl group had somehow interrupted its ability to bind to the transporter. Despite this, synthesized ^{14}C labelled 1-FDAM was examined for its transport behaviour. Proportionally larger uptake into the EMT-6 cells than MCF-7 was again observed, and was not significantly inhibited by CB treatment insinuating that, not unlike 6-FDF, transport is mediated by GLUT5. D-fructose was found to have a high IC_{50} for inhibition of [^{14}C]1-FDAM suggesting that it possesses a higher affinity for the transporter than the natural substrate.

6.2.6 *Insight into binding to GLUT5 from 6- ^{18}F FDF and 1- ^{18}F FDAM*

1- ^{18}F FDAM uptake studies provided fascinating insight into substrate binding when compared the uptake data to that of 6- ^{18}F FDF. 1- ^{18}F FDAM had an order of magnitude lower uptake into the EMT-6 cell line than that of 6- ^{18}F FDF,

indicating a poorer ability to be translocated by GLUT5. This was also the case in the *in vivo* imaging studies as the TACs for 1-[¹⁸F]FDAM in the tumor did not reach the levels that were identified with that seen with 6-FDF. Despite the apparent ability of 1-FDAM to inhibit both fructose and 6-[¹⁸F]FDF at a high level as was discussed in chapter 5, it may just represent the compound just binding to and “clogging” up the transporter instead of being transported (37). While the initial interaction of the substrate binding to the binding pocket is necessary for transport and relatively easily observed via inhibition studies, it is still unknown how these substrates are eventually shuttled through the interior of the pore into the cytosol. On top of the uncertainty, 2,5-AM derivatives and their ability to be phosphorylated by the HK family or KHK needs to be ascertained.

Structurally, 6-FDF and 1-FDAM are quite similar, although 6-FDF possesses a hydroxyl group present on the anomeric carbon that through the action of binding to the protein can be linearized (**Figure 6.2**). This additional hydroxyl present at the front the fructose molecule enters via the C-1 as suggested by Holman’s work (38) and may provide additional, and required hydrogen bonds for the eventual translocation of the substrate. This anomeric hydroxyl may not be necessary for binding however, as Holman’s multitude of high affinity 2,5-AM analogues were able to inhibit D-fructose transport at very high affinities. This ability to inhibit at very low concentrations may be indicative of the rate of 1-FDAM binding as perhaps the additional hydroxyl group on the anomeric carbon may slow this process, but may be necessary for proper facilitative transport. D-

fructose and 6-FDF unlike 2,5-AM and its derivatives are able to linearize – a process that may facilitate the “threading” of the substrate through the transport pore and into the cytosol. A similar process has been observed with polypeptide chains unfolding in order to reach an energetically favourable state for transport, so it is natural to think that similar behaviour would be witnessed in other transport systems (39). While 1-FDF is also able to be linearized, it would enter with the fluorinated C-1, and thus proper hydrogen bonds leading to transport would not form as they would with the hydroxyl group (5). 1-FDAM, while symmetrical, can enter the pore with the non-labelled C-1/6 position, but lacks the hydroxyl group present on the anomeric position to form the hydrogen bonds that may be important for translocation. If true, and based on what was found with the studies done by Holman, a C-6 labelled fructose compound labelled with a long amine linker to a bulky group may be able to bind, linearize, be transported and then “plug” the transporter with a fluorescent or radiolabeled bulky group at the end. This strategy would permit the efficient labelling of GLUT5 expression in breast cancer and accumulation without worrying about the action of the primary phosphorylating enzymes.

With these novel GLUT5 substrates there may be a disconnect between their ability to bind to the transporter and the process of translocation across the membrane. They are distinct processes suggested by the simple carrier model discussed in chapter 1, and must be treated as such. While it may be possible to ascertain the first step of this process using simple inhibition assays and non-

radiolabeled substrates, the next step of substrates actually entering the cells is of more interest to us due to the clinical nature of this project. This is where Holman's studies fall short, as while they have done an excellent job synthesizing and analysing these potential substrates for competitive binding to GLUT5, the transport data is one unfortunate missing component to what happens to be an extremely excellent group of publications (5,37,38).

6.3 Special comment on Gowrishankar et al. 2011 – GLUT 5 Is Not Over-Expressed in Breast Cancer Cells and Patient Breast Cancer Tissues.

The same group which published the fluorescent fructose derivative paper in 2007 (13) released the publication: GLUT 5 Is Not Over-Expressed in Breast Cancer Cells and Patient Breast Cancer Tissues in the journal PLoS ONE. The primary tenet of the paper is that GLUT5 is not essential for fructose uptake in breast cancer cells, something which, based on the data presented, cannot be supported (40).

Firstly, there are some crucial experiments missing that have not been performed in order to fully validate their hypothesis. No western blots were done to examine membrane expression of GLUT5 +/- siRNA treatment. Instead, they relied on RNA levels as a determinant of expression despite the fact they saw no correlation with RNA levels

and fructose uptake in the earlier experiments. The authors also state: "In further support of our IHC results, an examination of GLUT5 mRNA levels by microarray analysis did not show a significant difference between breast cancer tissue and normal breast tissues (data not shown)." The use of RNA levels as an indicator of protein expression and functional activity as an indicator of expression is unfounded and unrealistic.

Although the authors suggest that tumor lines are not expressing higher level of GLUT5, they do see uptake of fructose in all three cell lines. The "healthy" model for breast tissue showed the lowest uptake (MCF-10A) suggesting that the tumor lines do indeed take up more, and that perhaps the metabolic machinery behind fructose transport is upregulated as well.

The authors additionally state: "This uptake of fructose in the breast cancer cell lines MCF-7 and MDA-MB-468 was sensitive to CB (Fig 4) a potent inhibitor of glucose uptake by GLUT1." (40) This statement is accurate if instead of GLUT1, they considered the Class I glucose/fructose transporter GLUT2, an isoform that has been shown to be expressed in MCF-7 in chapter 2. Additionally, and a common theme with both this and their previous publication on the fluorophore labelled fructose analogues, crucial data was not shown in the paper regarding MCF-7 fructose uptake inhibition via action of CB. Without this data being shown, it is difficult to fully grasp how they came upon their conclusions.

The paper confirms the discussion: "A limitation of the current study is the lack of Western blotting data showing protein expression or lack of in the MCF-7 and MDA-MB-468 cells. We did attempt Western blotting with different GLUT5 antibodies but were unable to see a clear band of the right size in MDA-MB-468 cells (data not shown). We did however see some bands in the MCF-7 cells. Since our focus was to evaluate GLUT5 expression in tissue sections by IHC we did not further pursue the Western blotting."⁽⁴⁰⁾ This is a large oversight by Gowrishankar and associates. In order to say with certainty that the siRNA knockdowns were effective, reduced membrane expression would need to be correlated to functional data in order to back up the crux of their argument.

And finally the authors state: "More studies are needed to determine if radiolabeled fructose/fructose analogues could be used as metabolic PET tracers in the imaging of breast."⁽⁴⁰⁾ It appears that they have not examined the literature before the submission of this paper (32,41).

Overall this publication muddies the water more than it clears it, and unfortunately due to its publication in a relatively high impact journal, it may steer research groups from exploring GLUT5 expression and fructose metabolism in breast tumors – a field which at this current moment is wide open and needs further exploration.

6.4 Future directions

6.4.1 6-[¹⁸F]FDF, GLUT expression in breast cancer and beyond

Preclinical work examining the *in vitro* and *in vivo* characteristics of 6-FDF have indicated that it may hold some clinical utility in the imaging of GLUT5 expressing breast cancers. More research needs to be undertaken in order to fully grasp its usefulness in patients however, such as determining if there is any correlation between low GLUT1 and increased GLUT5 expression. KHK expression patterns and its linkage with GLUT expression will also need to be fully ascertained from patient samples as only cell line expression has been examined. To aid in this search and to further the understanding and perhaps allow for more personalized care, the metabolic status of these tumors as well as the identification of biomarkers in patient blood and urine can be determined. This may indicate whether or not GLUT1 or GLUT5 are expressed at high levels and if this has additional promise to aid clinicians when diagnosing and treating patients.

The field of cancer metabolomics has recently exploded, and novel work on the categorization of differences in metabolites between cancer patients and their healthy counterparts based on their metabolic profile is extremely promising (42). Metabolomics is defined as an analytical tool that combines analytical chemistry, pattern recognition and bioinformatic approaches to describe and follow the chemical composition changes in biofluids or tissue (42). The

examination of metabolites allows us to gain insight into the functional environment of the cell and it has become an extremely powerful tool in the diagnosis of cancer, and many biomarkers related to progression in transformed tissues have been identified (43–46).

While metabolomic techniques are extremely powerful in understanding the “endpoint” of altered metabolic processes, a combined approach with genomic analysis and proteomics is needed to obtain a more detailed picture of what and how is effected in the altered genome / metabolome of cancer tissues. Sensitive analytical chemistry methods, genomic investigation and proper statistical analyses undertaken simultaneously creates potential for the determination of unique biomarkers that might allow us to determine the hexose transporter status of tumors. Not only can we then describe what is occurring within GLUT1 negative cells, but also describe the genomic and proteomic adaptation of certain breast tumors to a GLUT5 mediated, fructose supplemented phenotype. It is feasible that the classification of the differences in the metabolic phenotype would be able to distinguish between GLUT1 positive and negative breast cancers and the recognition of distinguishable biomarkers present within patients’ plasma and urine, would allow us to design a much more rigorous PET imaging strategy using 6-^[18F]FDF and/or ^[18F]FDG to image tumors based on their GLUT expression profile. In addition, through proper genomic, proteomic and metabolic descriptions of normal tissue as well as GLUT1 positive and negative breast tumors, we would be able to clarify GLUT5’s role in breast cancer

tumorigenesis with relation to GLUT1 expression. The exact genomic and metabolic alterations in breast tumors that result in increased levels of GLUT5 expression and fructose metabolism are unknown, but we expect that a quantifiable change between GLUT5 expressing breast tissues and GLUT5 non-expressing tissues will be able to be observed.

Immunohistochemical studies examining HK, KHK, GLUT1, GLUT2 and GLUT5 expression in tissue microarrays containing patient breast tumor samples should also be done to combat the recent publication suggesting that breast cancer does not express increased levels of GLUT5 compared to normal breast tissue (13). A robust analysis would be able to be performed using these arrays, reinforcing the theory that that GLUT5 is indeed more highly expressed in cancerous breast tissue. This would also give insight into the interplay between glucose and fructose metabolism in these cancers.

Outside of breast cancer, there may be opportunities for GLUT5 mediate imaging of other tumor types. Godoy and associates have suggested that perhaps colon, lung and even uterine cancers may have an increase in GLUT5 expression and thus might be able to be imaged by 6-^[18F]FDF (3).

As for 6-^[18F]FDF, further work needs to be done to determine the identity of the two radiometabolites observed and their origin. Bone uptake needs to be revisited as well, as it may shed light into fructose uptake and metabolism that has not been previously investigated. Brain uptake has sparked some interest

from the perspective of examining fructose uptake and KHK expression, so perhaps autoradiograph and immunohistological studies of rat brain sections looking at areas of accumulation would be an interesting and novel perspective in the world of neuroscience.

Fructose metabolism and its related disease states are becoming more and more at the forefront of nutritional research (17,33). Gavage studies with 6-[¹⁸F]FDF and real time imaging of luminal transport in the small intestine and patterns of accumulation through the action of KHK expression would be another novel vein of research that could be explored as well.

6.4.2 **1-FDAM**

Initial trials in the EMT-6 BALB/c model system indicate that perhaps 1-[¹⁸F]FDAM does not hold as much promise as 6-[¹⁸F]FDF, but further investigation is still warranted. Determining its uptake profile in the MCF-7 cell line *in vitro* and in the NIH-III model would be fascinating when compared with the data from the *in vivo* trials with 6-[¹⁸F]FDF. Based on what has been seen before, 1-[¹⁸F]FDAM would probably show a similar if not lower uptake profile than that of 6-[¹⁸F]FDF highlighting its inability to be quickly translocated through the membrane.

Metabolic studies should also be done to determine the stability of the compound *in vivo*. Phosphorylation studies using both the cell culture efflux

model and recombinant HK and KHK will give insight to 2,5-AM analogues ability to be phosphorylated by both enzymes.

6.4.3 **Other 2,5-AM analogues**

AC-AM as well as other 2,5-AM analogues were thought to be amenable for binding and transport via GLUT5, but the current data for 1-FDAM – arguably the simplest compound of this class is not encouraging. Perhaps the missing hydroxyl at the anomeric carbon and linearization of the substrate is necessary for large quantities of transport via GLUT5. The data presented on initial trials with 2-fluoro-*N*-(1-deoxy-2,5-anhydro-*D*-mannitol)acetamide (AC-AM) in Appendix B is not very supportive of pursuing this compound since the IC₅₀ for the inhibition of fructose transport shows values that are an order of magnitude higher than that observed with 1-FDAM, 2,5-AM and 3-FDF. Whether or not these substrates will have success in labelling GLUT5 expressing tissues will not be known fully until they are labelled with ¹⁸F and are fully characterized in the model systems previously characterised within the previous chapters.

6.4.4 **3-FDF**

Appendix B includes the data from the initial *in vitro* analysis of 3-FDF. Not unlike 1-FDAM and 6-FDF before it, it shows promise to be a potential candidate for the *in vivo* imaging of GLUT5 expressing breast tumors. Inhibiting [¹⁴C]D-fructose transport at low concentrations and also having a trend to inhibit 6-[¹⁸F]FDF uptake with the highest affinity of the analysed compounds, it displays all the

characteristics for a successful tracer. Holman's work labelling the 3 position with a bulky allyl group suggested that the position was not well tolerated – fluorine is much smaller than the allyl group and may also act to form hydrogen bonds with the transporter and thus the same decrease in affinity may not be occurring. 3-FDF also possesses the anomeric hydroxyl group that is not present on 1-FDAM, and could be linearized through binding to the transporter. We observed high affinity inhibition with both 1-FDF and 1-FDAM which led us to believe in its potential efficacy, so judgement must be reserved until 3-FDF can be labelled with [¹⁸F] and uptake examined in both model systems.

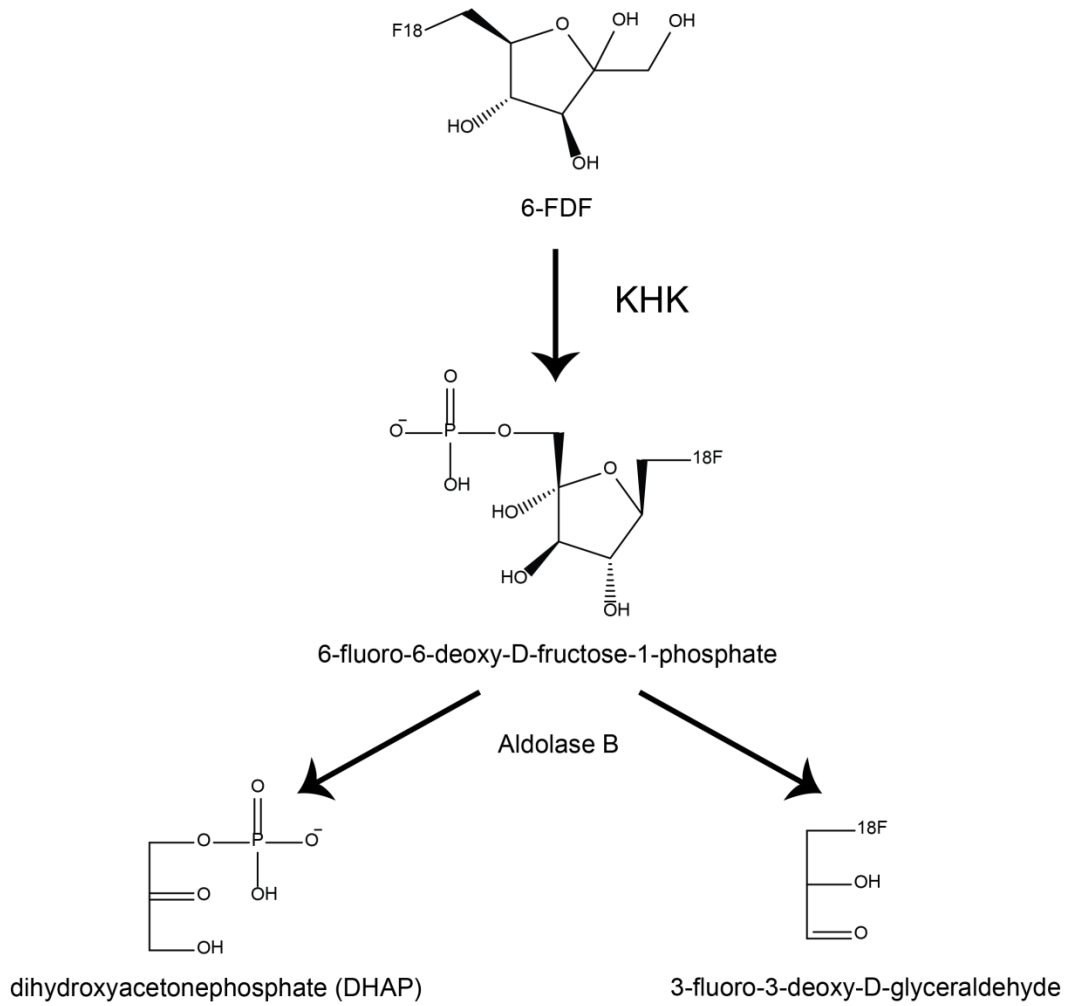


Figure 6.1 – Proposed metabolic pathway of 6-[¹⁸F]FDF

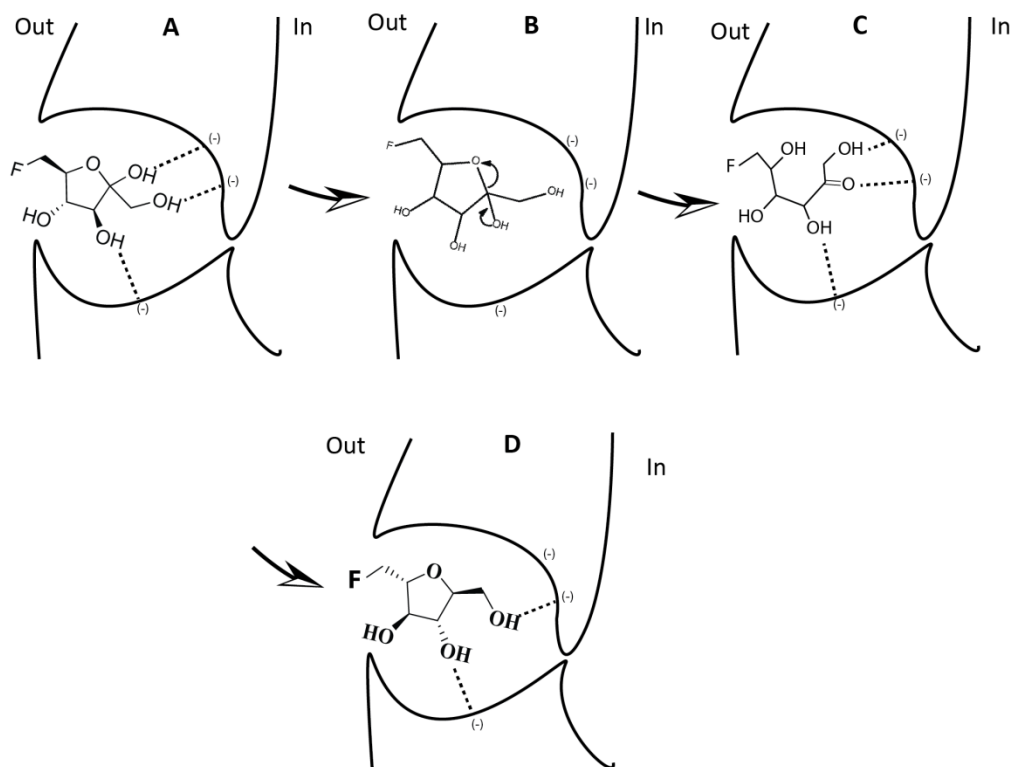


Figure 6.2 Binding of 6-FDF and 1-FDAM to GLUT5 – After 6-FDF makes its initial (A) hydrogen bonds between the C-1 hydroxyl and anomeric carbon to negative amino acid sidechains in the binding vestibule, the proton on the anomeric hydroxyl is removed which allows the electrons to cascade and “unfurl” and linearize the substrate (B-C). This then is able to be threaded through the transporter. 1-FDAM (D), while able to readily bind to the transporter, lacks the anomeric hydroxyl and ability to linearize, decreasing the ability of the substrate to be translocated by GLUT5.

6.5 Bibliography

1. Mankoff DA. A definition of molecular imaging. *Journal of nuclear medicine : official publication, Society of Nuclear Medicine*. 2007 Jun;48(6):18N, 21N.
2. Zamora-León SP, Golde DW, Concha II, Rivas CI, Delgado-López F, Baselga J, et al. Expression of the fructose transporter GLUT5 in human breast cancer. *Proceedings of the National Academy of Sciences of the United States of America*. 1996 Mar 5;93(5):1847–52.
3. Reinicke K, Godoy A, Ulloa V, Rodri F, Medina RA, Yan AJ, et al. Differential Subcellular Distribution of Glucose Transporters GLUT1 – 6 and GLUT9 in Human Cancer : Ultrastructural Localization of GLUT1 and GLUT5 in Breast Tumor Tissues. *J Cell Physiol*. 2006 Jun;207(3):614–27.
4. Haradahira T, Tanaka A, Maeda M, Kanazawa Y, Ichiya YI, Masuda K. Radiosynthesis, rodent biodistribution, and metabolism of 1-deoxy-1-[18F]fluoro-D-fructose. *Nuclear medicine and biology*. 1995 Aug;22(6):719–25.
5. Tatibouët a, Yang J, Morin C, Holman GD. Synthesis and evaluation of fructose analogues as inhibitors of the D-fructose transporter GLUT5. *Bioorganic & medicinal chemistry*. 2000 Jul;8(7):1825–33.
6. Yang J, Dowden J, Tatibouët A, Hatanaka Y, Holman GD. Development of high-affinity ligands and photoaffinity labels for the D-fructose transporter GLUT5. *The Biochemical journal*. 2002 Oct 15;367(Pt 2):533–9.
7. Leturque A, Brot-Laroche E, Le Gall M, Stolarczyk E, Tobin V. The role of GLUT2 in dietary sugar handling. *Journal of physiology and biochemistry*. 2005 Dec;61(4):529–37.
8. Colville CA, Seatter MJ, Jess TJ, Gould GW, Thomas HM. Kinetic analysis of the liver-type (GLUT2) and brain-type (GLUT3) glucose transporters in *Xenopus* oocytes: substrate specificities and effects of transport inhibitors. *The Biochemical journal*. 1993 Mar 15;290 (Pt 3):701–6.
9. Froesch E, Ginsberg J. Fructose Metabolism of Adipose Tissue. *Acta Med Scand Suppl*. 1972;542:37-46.
10. Diggle CP, Shires M, Leitch D, Brooke D, Carr IM, Markham AF, et al. Ketohexokinase: expression and localization of the principal fructose-

metabolizing enzyme. *The journal of histochemistry and cytochemistry : official journal of the Histochemistry Society*. 2009 Aug;57(8):763–74.

11. Cárdenas ML, Rabajille E, Niemeyer H. Fructose is a good substrate for rat liver “glucokinase” (hexokinase D). *The Biochemical journal*. 1984 Sep 1;222(2):363–70.
12. Cárdenas ML, Cornish-Bowden A, Ureta T. Evolution and regulatory role of the hexokinases. *Biochimica et biophysica acta*. 1998 Mar 5;1401(3):242–64.
13. Levi J, Cheng Z, Gheysens O, Patel M, Chan CT, Wang Y, et al. Fluorescent fructose derivatives for imaging breast cancer cells. *Bioconjugate chemistry*. 2007;18(3):628–34.
14. Macheda ML, Rogers S, Best JD. Molecular and cellular regulation of glucose transporter (GLUT) proteins in cancer. *Journal of cellular physiology*. 2005 Mar;202(3):654–62.
15. Wlaschin KF, Hu W-S. Engineering cell metabolism for high-density cell culture via manipulation of sugar transport. *Journal of biotechnology*. 2007 Aug 31;131(2):168–76.
16. Manolescu AR, Witkowska K, Kinnaird A, Cessford T, Cheeseman C. Facilitated hexose transporters: new perspectives on form and function. *Physiology (Bethesda, Md.)*. 2007 Aug;22:234–40.
17. Douard V, Ferraris RP. Regulation of the fructose transporter GLUT5 in health and disease. *American journal of physiology. Endocrinology and metabolism*. 2008 Aug;295(2):E227–37.
18. Laudański P, Swiatecka J, Kovalchuk O, Wołczyński S. Expression of GLUT1 gene in breast cancer cell lines MCF-7 and MDA-MB-231. *Ginekologia polska*. 2003 Sep;74(9):782–5.
19. Lavayssière R, Cabée A-E, Filmont J-E. Positron Emission Tomography (PET) and breast cancer in clinical practice. *European journal of radiology*. 2009 Jan;69(1):50–8.
20. Quon A, Gambhir SS. FDG-PET and beyond: molecular breast cancer imaging. *Journal of clinical oncology : official journal of the American Society of Clinical Oncology*. 2005 Mar 10;23(8):1664–73.

21. Oude Munnink TH, Nagengast WB, Brouwers AH, Schröder CP, Hospers GA, Lub-de Hooge MN, et al. Molecular imaging of breast cancer. *Breast (Edinburgh, Scotland)*. 2009 Oct;18 Suppl 3:S66–73.
22. Taper HS, Roberfroid M. Influence of inulin and oligofructose on breast cancer and tumor growth. *The Journal of nutrition*. 1999 Jul;129(7 Suppl):1488S–91S.
23. Kelly CJ, Hussien K, Muschel RJ. 3D tumor spheroids as a model to assess the suitability of [¹⁸F]FDG-PET as an early indicator of response to PI3K inhibition. *Nuclear medicine and biology*. 2012 Jun 8;
24. Demicheli R, Pratesi G, Foroni R. The exponential-Gompertzian tumor growth model: data from six tumor cell lines in vitro and in vivo. Estimate of the transition point from exponential to Gompertzian growth and potential clinical implications. *Tumori*. 1991 Jun 30;77(3):189–95.
25. Loi M, Di Paolo D, Becherini P, Zorzoli A, Perri P, Carosio R, et al. The use of the orthotopic model to validate antivasular therapies for cancer. *The International journal of developmental biology*. 2011 Jan;55(4-5):547–55.
26. Chan E, Patel A, Heston W, Larchian W. Mouse orthotopic models for bladder cancer research. *BJU international*. 2009 Nov;104(9):1286–91.
27. Sano D, Myers JN. Xenograft models of head and neck cancers. *Head & neck oncology*. 2009 Jan;1:32.
28. Shepherd PR, Gibbs EM, Wesslau C, Gould GW, Kahn BB. Human small intestine facilitative fructose/glucose transporter (GLUT5) is also present in insulin-responsive tissues and brain. Investigation of biochemical characteristics and translocation. *Diabetes*. 1992 Oct;41(10):1360–5.
29. Payne J, Maher F, Simpson I, Mattice L, Davies P. Glucose transporter Glut 5 expression in microglial cells. *Glia*. 1997 Nov;21(3):327–31.
30. Funari VA, Crandall JE, Tolan DR. Fructose metabolism in the cerebellum. *Cerebellum (London, England)*. 2007 Jan;6(2):130–40.
31. Funari V a, Herrera VLM, Freeman D, Tolan DR. Genes required for fructose metabolism are expressed in Purkinje cells in the cerebellum. *Brain research. Molecular brain research*. 2005 Dec 14;142(2):115–22.
32. Trayner BJ, Grant TN, West FG, Cheeseman CI. Synthesis and characterization of 6-deoxy-6-fluoro-D-fructose as a potential compound

for imaging breast cancer with PET. *Bioorganic & medicinal chemistry*. 2009 Aug 1;17(15):5488–95.

33. Heman RH, Zakim D. Fructose metabolism. I. The fructose metabolic pathway. *The American journal of clinical nutrition*. 1968 Mar;21(3):245–9.
34. U.S. Food and Drug Administration. Guidance for Industry, investigators and reviewers: exploratory IND studies. 2006; <http://www.fda.gov/downloads/Drugs/GuidanceComplianceRegulatoryInformation/Guidances/ucm078933.pdf>
35. Brown RS, Goodman TM, Zasadny KR, Greenson JK, Wahl RL. Expression of hexokinase II and Glut-1 in untreated human breast cancer. *Nuclear medicine and biology*. 2002 May;29(4):443–53.
36. Mathupala SP, Ko YH, Pedersen PL. Hexokinase-2 bound to mitochondria: cancer's stygian link to the "Warburg Effect" and a pivotal target for effective therapy. *Seminars in cancer biology*. 2009 Feb;19(1):17–24.
37. Yang J, Dowden J, Tatiboue A, Hatanaka Y, Holman GD. Development of high-affinity ligands and photoaffinity labels for the D-fructose transporter GLUT5. *Biochem J*. 2002 Oct 15;367(Pt 2):533–9.
38. Girniene J, Tatibouët A, Sackus A, Yang J, Holman GD, Rollin P. Inhibition of the d-fructose transporter protein GLUT5 by fused-ring glyco-1,3-oxazolidin-2-thiones and -oxazolidin-2-ones. *Carbohydrate Research*. 2003 Apr;338(8):711–9.
39. Neupert W, Hartl FU, Craig EA, Pfanner N. How do polypeptides cross the mitochondrial membranes? *Cell*. 1990 Nov 2;63(3):447–50.
40. Gowrishankar G, Zitzmann-Kolbe S, Junutula A, Reeves R, Levi J, Srinivasan A, et al. GLUT 5 is not over-expressed in breast cancer cells and patient breast cancer tissues. *PloS one*. 2011 Jan;6(11):e26902.
41. Wuest M, Trayner BJ, Grant TN, Jans H-S, Mercer JR, Murray D, et al. Radiopharmacological evaluation of 6-deoxy-6-[18F]fluoro-D-fructose as a radiotracer for PET imaging of GLUT5 in breast cancer. *Nuclear medicine and biology*. 2011 May;38(4):461–75.
42. Spratlin JL, Serkova NJ, Eckhardt SG. Clinical applications of metabolomics in oncology: a review. *Clinical cancer research : an official journal of the American Association for Cancer Research*. 2009 Jan 15;15(2):431–40.

43. Nam H, Chung BC, Kim Y, Lee K, Lee D. Combining tissue transcriptomics and urine metabolomics for breast cancer biomarker identification. *Bioinformatics (Oxford, England)*. 2009 Dec 1;25(23):3151–7.
44. Urayama S, Zou W, Brooks K, Tolstikov V. Comprehensive mass spectrometry based metabolic profiling of blood plasma reveals potent discriminatory classifiers of pancreatic cancer. *Rapid communications in mass spectrometry : RCM*. 2010 Mar 15;24(5):613–20.
45. Sitter B, Bathen TF, Singstad TE, Fjøsne HE, Lundgren S, Halgunset J, et al. Quantification of metabolites in breast cancer patients with different clinical prognosis using HR MAS MR spectroscopy. *NMR in biomedicine*. 2010 May;23(4):424–31.
46. Ong ES, Zou L, Li S, Cheah PY, Eu KW, Ong CN. Metabolic profiling in colorectal cancer reveals signature metabolic shifts during tumorigenesis. *Molecular & cellular proteomics : MCP*. 2010 Feb 10;

Appendix A – Materials

A.1 Materials

Standard reagents and materials for this work were ordered from either Fisher Scientific (Ontario, Canada) or Sigma Aldrich (Oakville, Canada). Other reagents used in cell culture and transport assays are listed in **Table A.1**, antibodies and recombinant enzymes in **Table A.2**, and equipment and software in **Table A.3**. Lastly, **Table A.4-6** will detail the composition of buffers used within the previous chapters.

Table A.1: Cell culture, transport assay and western blot materials

Reagent/Material	Manufacturer/Provider
Cell culture	
DMEM-F12 cell culture media supplemented with 15mM HEPES, L-Glutamine	Gibco - Invitrogen, USA
Fetal Bovine Serum	Invitrogen, USA
Penicillin/Streptomycin	Invitrogen, USA
Radiolabeled transport assay materials	
[¹⁴ C]D-glucose	Amersham. USA
[¹⁴ C]D-fructose	Moravek Biochemicals, USA
[¹⁴ C]6-FDF	Proprietary
[¹⁴ C]3-FDF	Proprietary
[¹⁴ C]1-FDAM	Proprietary
6-[¹⁸ F]FDF	Proprietary
1-[¹⁸ F]FDAM	Proprietary
1-[¹⁸ F]FDF	Proprietary
Cold transport assay materials	
6-FDF	Proprietary
3-FDF	Proprietary
1-FDF	Proprietary
2,5-AM	Proprietary
AC-AM	Proprietary
1-FDAM	Proprietary
Other cell culture materials	
BCA protein assay kit	Pierce, USA

Cellytic™ M lysis buffer	Sigma Aldrich, Canada
Protease inhibitor cocktail	Sigma Aldrich, Canada
ProLong® Gold anti-fade reagent with DAPI	Invitrogen, USA
Western Blot materials	
ECL™ AntirabbitIgG Horseradish peroxidase	Amersham Biosciences, USA
ECL™ Western Blot detection reagents	Amersham Biosciences, USA
Anti-rabbit Alexafluor 488	Invitrogen, USA
30% acrylamide/Bis	Bio-Rad Laboratories, USA
Triton X-100	Sigma Aldrich, Canada
TEMED	Sigma Aldrich, Canada
Ammonium Persulfate	Sigma Aldrich, Canada
1.5M Tris-HCl, pH 8.8	Bio-Rad Laboratories, USA
0.5M Tris-HCL, pH 8.8	Bio-Rad Laboratories, USA
Bio-Rad Precision Plus™ dual colour protein standards ladder	Bio-Rad Laboratories, USA

Table A.2: Antibodies and Recombinant Enzymes

Reagent/Material	Manufacturer/Provider
Antibodies	
Fructokinase antibody	Sigma Aldrich Prestige antibodies, USA
hGLUT1 antibody	Chemicon, USA
hGLUT2 antibody	Chemicon, USA
hGLUT4 antibody	Chemicon, USA
hGLUT5 antibody	Biogenesis, USA
hGLUT7 antibody	Chemicon, USA
hGLUT9 antibody	Gift from Dr. Kelle Molle
hGLUT11 antibody	Gift from Dr. Sue Rogers
hGLUT12 antibody	Gift from Dr. Sue Rogers
Recombinant Enzymes	
Recombinant Human Hexokinase II	ATGen, South Korea
Recombinant Human Fructokinase	ATGen, South Korea

Table A.3: Software and Equipment

Software	
Data entry and calculations	Microsoft Excel – Microsoft Corp.
Statistical analysis and plotting	GraphPad Prism 5 – GraphPad Software Inc. USA
Confocal image software	LSM confocal software – Carl Zeiss Microscopy Inc.
microPET image processing	ROVER v2.0.21 ABX GmbH, Germany
Dosimetry analysis and modelling	OLINDA/EXM version 1.1 Vanderbilt University, USA
Equipment	
LS 6500 β Liquid Scintillation counter	Beckman, USA
Wallac 1480 Wizard-3 γ -Counter	Perkin-Elmer, Canada
ZEISS LSM 510 Confocal Microscope	Carl Zeiss Microscopy Inc.
PowerPac™ Basic power supply	Bio-Rad Laboratories Inc.
Atomlab™ 300 Dose calibrator	Biodex Medical Systems, USA
microPET® R4 scanner	Siemens Preclinical Solutions, USA
Eckert & Ziegler Modular-Lab synthesis unit	Ecker & Ziegler, Germany

Table A.4 Composition of Phosphate buffered saline (PBS)

Component	Concentration
NaCl	135 mM
KCl	1.3 mM
KH ₂ PO ₄	3.2 mM
Na ₂ HPO ₄	0.5 mM
pH – 7.4	

Table A.5 Composition of Krebs-Ringer solution

Component	Concentration
NaCl	120 mM
KCl	4 mM
KH ₂ PO ₄	1.2 mM
MgSO ₄	2.5 mM
NaHCO ₃	25 mM
CaCl ₂	70 μM
pH – 7.4	

Table A.6 Western Blot Buffers

Component	Concentration
Running buffer (1X)	
Tris Base	24.8 mM
Glycine	192 mM
SDS	3.5 mM
pH – 8.3	
Transfer Buffer (1X)	
Glycine	384 mM
Tris Base	50 mM
Methanol	20% (v/w)
pH ~ 8.1 - 8.4	

**Appendix B - Characterization of
1-deoxy-1-fluoro-D-fructose (1-FDF),
3-deoxy-3-fluoro-D-fructose (3-FDF),
and 2-fluoro-N-(1-deoxy-2,5-anhydro-D-
mannitol)acetamide (AC-AM)
for breast cancer imaging via PET**

Trayner BJ, Wuest M, Soueidan M, Bouvet V, Henderson J, Grant TN

This work presented represents a collaboration. BJT performed all *in vitro* experiments and analysis. *In vivo* experiments and analysis were performed by MW with assistance by BJT. All chemical syntheses were performed by MS, VB, JH and TNG.

B.1 2-fluoro-*N*-(1-deoxy-2,5-anhydro-*D*-mannitol)acetamide (AC-AM)

8.1.1 B.1.1 Experimental Design

These experiments were done in order to ascertain the ability of the 1 labelled 2,5-AM derivative 2-fluoro-*N*-(1-deoxy-2,5-anhydro-*D*-mannitol)acetamide (AC-AM) to be a substrate for GLUT5 expressing breast cancer models, not unlike the previous chapters work on other compounds (**Figure B.1**). Work by Holman and associates have suggested that replacement of the hydroxyl at the 1 position on 2,5-AM with an amide groups may actually increase the affinity of the substrate for the transporter¹. Compound was synthesized in house. Uptake and inhibition experiments with AC-AM were done as described earlier in chapter 5, with inhibition experiments performed at 60 minutes. All [¹⁴C] labelled samples were counted in the scintillation counter and analyzed using Graphpad Prism 5.

8.1.2 B.1.2 Results and Discussion

Figure B.2 illustrates dose dependent inhibition of [¹⁴C]D-fructose transport by AC-AM in both EMT-6 and MCF-7 cell lines. Like the other compounds, AC-AM readily inhibits [¹⁴C]D-fructose transport, albeit at a lower level than previously described compounds (EMT-6: 18.3 ± 8.8 μM, n=3 and MCF-7: 32.5 ± 24μM,

¹ From :Yang J, Dowden J, Tatibouët A, Hatanaka Y, Holman GD. Development of high-affinity ligands and photoaffinity labels for the D-fructose transporter GLUT5. *The Biochemical journal*. 2002 Oct 15;367(Pt 2):533–9.

n=3). This data suggests that perhaps AC-AM would not be as readily able to be taken up into GLUT5 expressing tissues as well as previously described compounds. Further experiments are required examining the ability of AC-AM to enter GLUT5 expressing.

B.2 1-Deoxy-1-fluoro-D-fructose (1-FDF)

8.1.3 B.2.1 Experimental Design

As it is a previously characterized compound, 1-FDF was synthesized in order to ascertain its viability as a tracer for GLUT5 expressing tissues in the EMT-6 model system (**Figure B.1**). Previous work had used a fibrosarcoma model in rats whose GLUT5 status is unknown². Inhibition of 6-[¹⁸F]FDF uptake and *in vivo* imaging using dynamic PET was performed as described in chapters 3, 4 and 5. Chemical syntheses of 1-[¹⁸F]FDF was performed by colleagues using previously published synthesis methods³.

8.1.4 B.2.2 Results and Discussion

Figure B.3 illustrates both the dynamic PET images obtained with 1-[¹⁸F]FDF. When compared to 1-[¹⁸F]FDAM, 1-[¹⁸F]FDF appears to have strikingly similar uptake into the tumor over the initial phase of 20 minutes, and then slowly washes out to equivalent levels after 110 minutes. This suggests that perhaps 1-

²From: Haradahira T, Tanaka A, Maeda M, Kanazawa Y, Ichiya YI, Masuda K. Radiosynthesis, rodent biodistribution, and metabolism of 1-deoxy-1-[¹⁸F]fluoro-D-fructose. *Nuclear medicine and biology*. 1995 Aug;22(6):719–25.

FDF and 1-FDAM have very similar binding characteristics, and that the symmetry present in the structure of 1-FDAM affords only marginal levels of increased uptake.

B.3 3-Deoxy-3-fluoro-D-fructose (3-FDF)

8.1.5 B.3.1 Experimental Design

These experiments were done in order to ascertain the ability of the 3 position labelled fructose derivative 3-deoxy-3-fluoro-D-fructose (3-FDF) to be a substrate for GLUT5 expressing breast cancer models (**Figure B.1**). Work by Holman and associates have suggested that replacement of the hydroxyl at the 3 position with a bulky group would not be well tolerated by the transporter – and while this may be the case for allyl derivatives that were explored, a fluorine at position 3 may satisfy the size and hydrogen bonding requirements for proper recognition and translocation by GLUT5³. Uptake and inhibition experiments were done as was earlier described in chapter 5, with inhibition experiments performed at 60 minutes. All [¹⁴C] labelled samples were counted in the scintillation counter, [¹⁸F] counted with a γ counter and analyzed using Graphpad Prism 5. Radiolabeled [¹⁴C]3-FDF was synthesized in house.

³From: Tatibouët a, Yang J, Morin C, Holman GD. Synthesis and evaluation of fructose analogues as inhibitors of the D-fructose transporter GLUT5. *Bioorganic & medicinal chemistry*. 2000 Jul;8(7):1825–33

8.1.6 B.3.2 Results and Discussion

Figure B.4 illustrates that 3-FDF is able to inhibit [¹⁴C]D-fructose transport in a dose dependent manner and with a IC₅₀ of 1.16 ± 0.7μM in EMT-6 and 2.37 ± 1.5μM in MCF-7. These values compare quite well to that of 1-FDAM and its parent compound 2,5-AM suggesting that it may be a high affinity substrate for GLUT5. Next, cell uptake experiments, and inhibition studies using the [¹⁴C] labelled 3-FDF indicates that (**Figure B.5**) i) it is transported into both cell lines, ii) EMT-6 has higher uptake than that of MCF-7 which agrees with previous findings, iii) uptake is not significantly inhibited by cytochalasin B (**Figure B.6**), and iv) 3-FDF appears to have higher relative affinity for binding to GLUT5 than D-fructose due to the poor ability of 500mM D-fructose to inhibit [¹⁴C]3-FDF transport (**Figure B.6**). This in concert with data acquired from 3-FDF inhibition of 6-[¹⁸F]FDF transport in EMT-6 (**Figure B.7**) shows that out of all the analyzed compounds, 3-FDF possesses a trend suggesting it may have the highest affinity for inhibition of 6-[¹⁸F]FDF transport (n=2). Based on this preliminary information, 3-FDF may be a promising compound for *in vivo* imaging of GLUT5 expressing tumors.

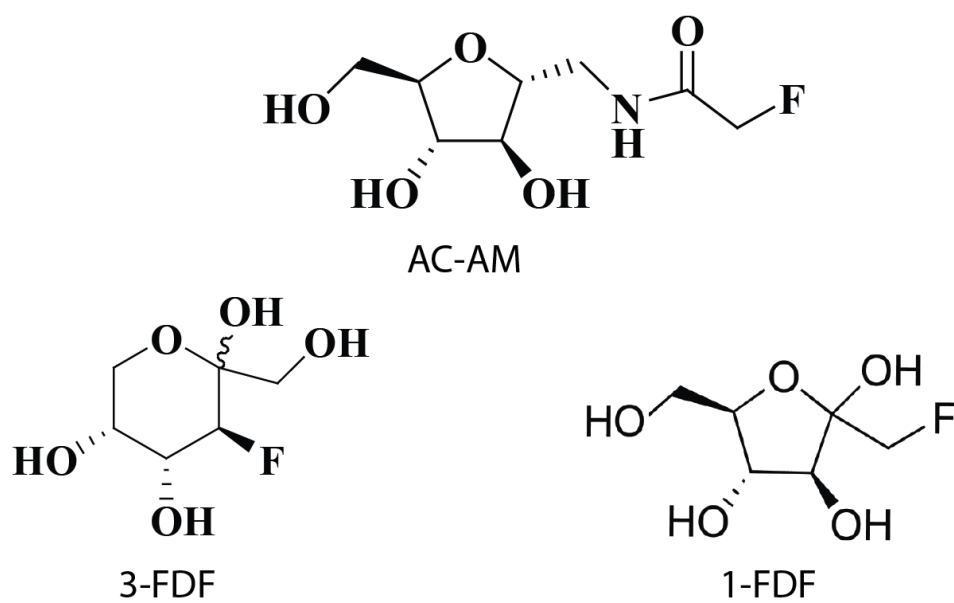


Figure B.1: Structures of AC-AM, 3-FDF and 1-FDF

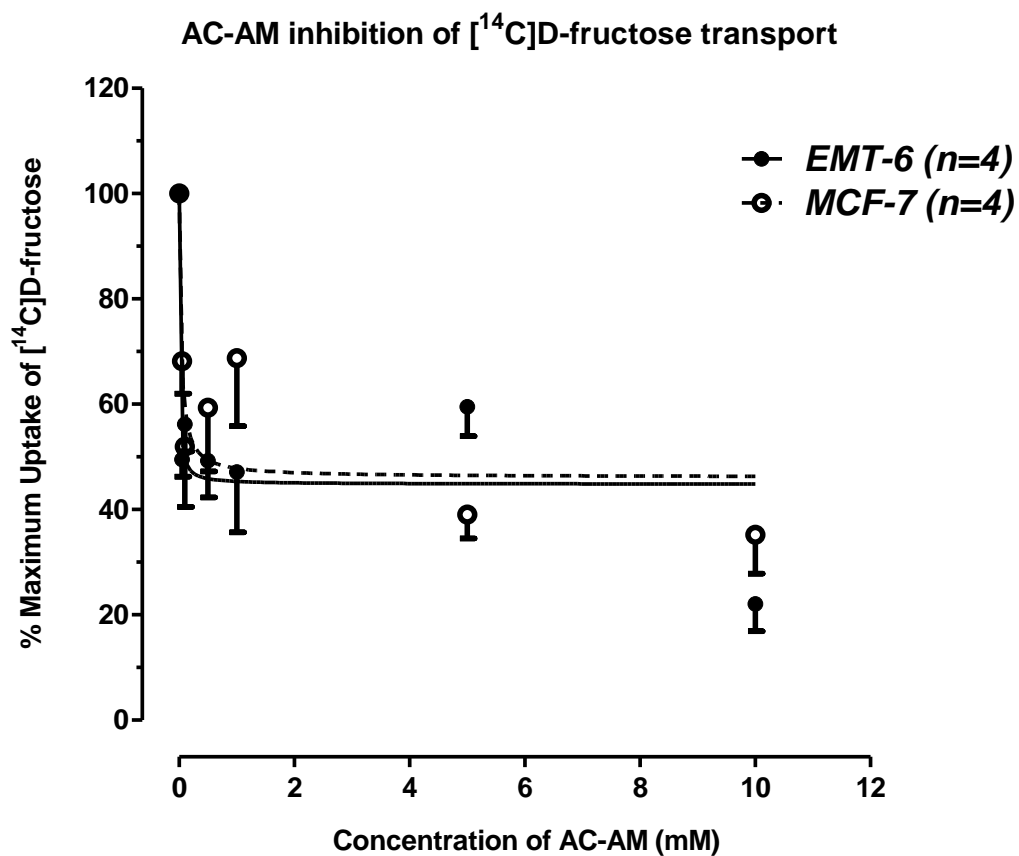


Figure B.2: AC-AM inhibition of [¹⁴C]D-fructose transport - after a 60 min incubation at 37°C with both EMT-6 and MCF-7 using increasing concentrations of AC-AM. Fructose transport was inhibited by increasing concentrations of AC-AM, and the IC₅₀ obtained for EMT-6 (●) was 18.3 ± 8.8 μM and 32.54 ± 24 μM in MCF-7(o). Error bars represent the SEM.

1-[¹⁸F]FDF in EMT-6 tumor-bearing BALB/c

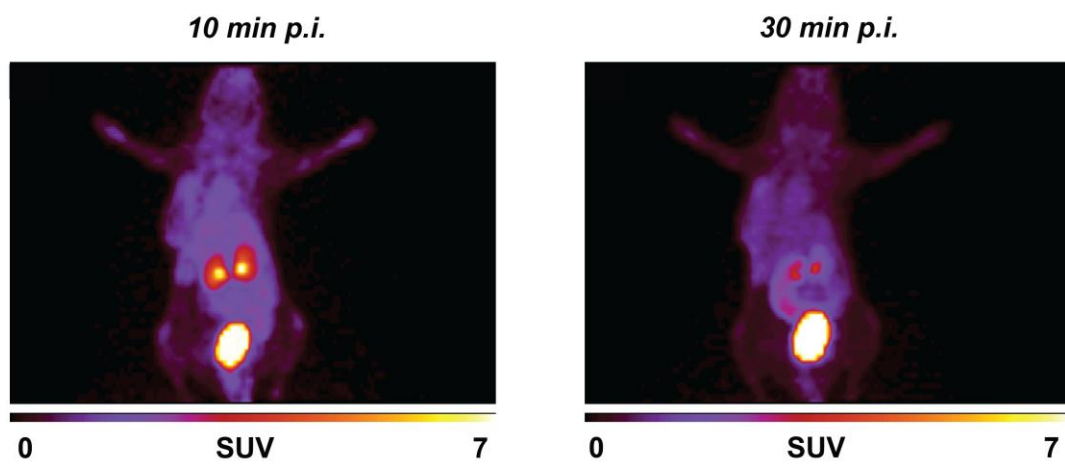


Figure B.3: 1-[¹⁸F]FDF injected EMT-6 tumor-bearing BALB/c mouse PET image - Representative dynamic small animal PET images of 1-[¹⁸F]FDF after 10 and 30 min post injection. Isoflurane was used for anesthesia.

3-FDF inhibition of [¹⁴C] D-fructose transport

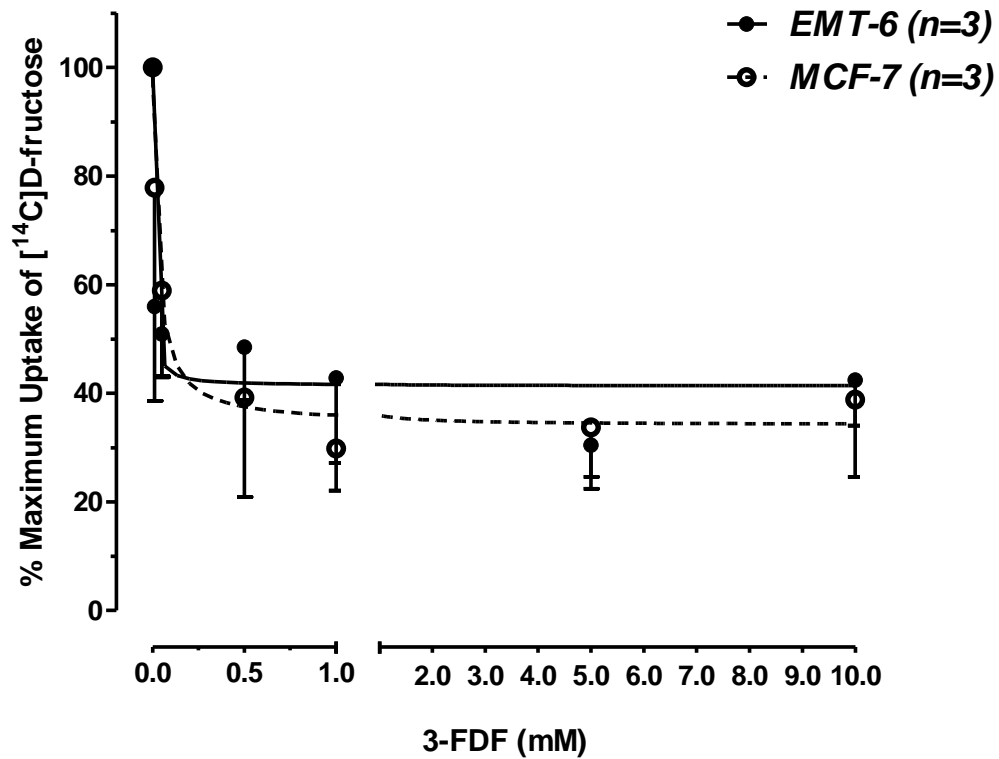


Figure B.4: 3-FDF inhibition of [¹⁴C]D-fructose transport - after a 60 min incubation at 37°C with both EMT-6 and MCF-7 using increasing concentrations of 3-FDF. Fructose transport was inhibited by increasing concentrations of 3-FDF, and the IC₅₀ obtained for EMT-6 (●) was 1.16 ± 0.67 μM and 2.37 ± 1.5 μM in MCF-7(o). Error bars represent the SEM.

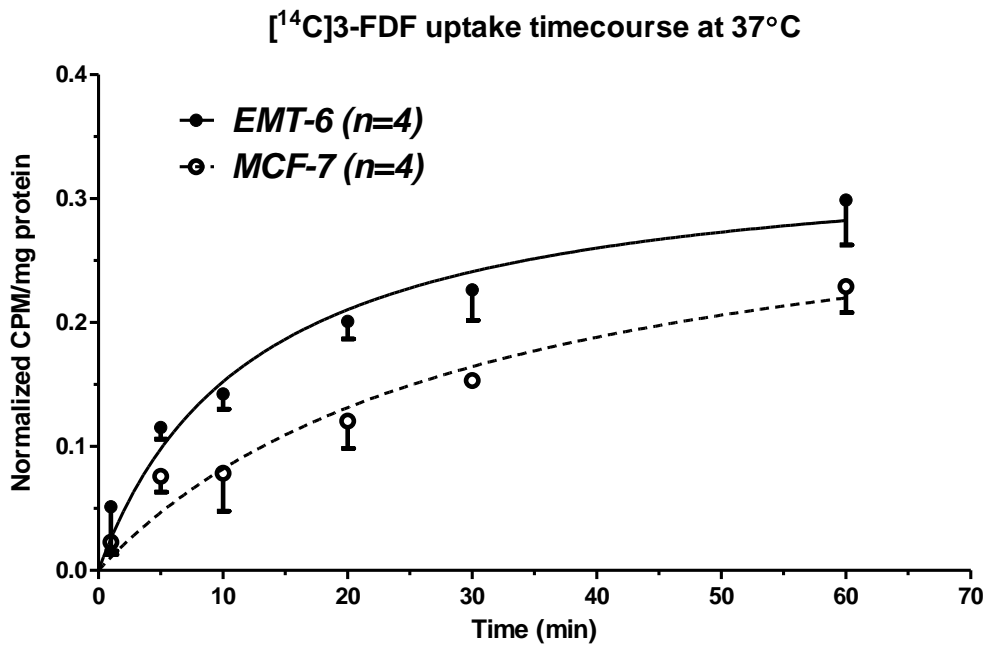
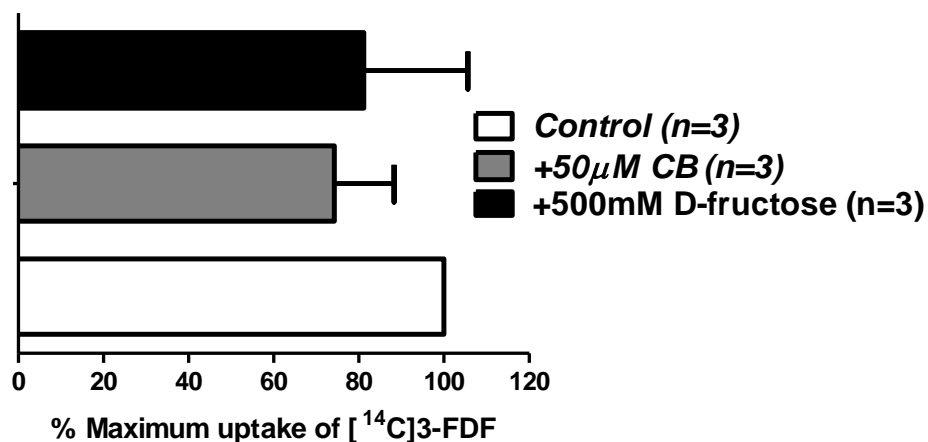


Figure B.5: [¹⁴C]3-FDF 60 minute time course in both MCF-7 (○) and EMT-6 (●) - corrected for non-mediated hexose uptake at 37°C. Uptake is observed in both cell types after a 60 min incubation. Error bars represent the SEM.

[¹⁴C]3-FDF transport +/- CB in EMT-6



[¹⁴C]3-FDF transport +/- CB in MCF-7

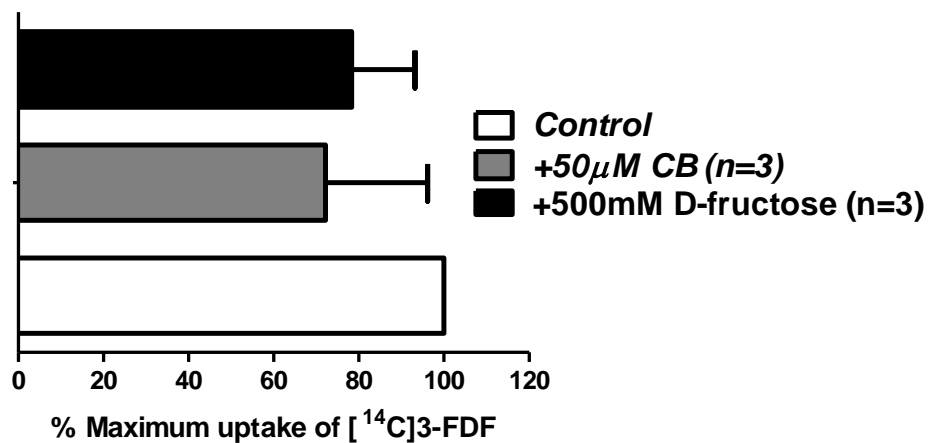


Figure B.6: Inhibition of [¹⁴C]3-FDF uptake by 50 μM cytochalasin B (+CB) and 500mM D-fructose. 37°C incubations lasted 60 min and uptakes were corrected for non-mediated fluxes. Error bars represent the SEM. No significant difference was observed between the control and treated groups.

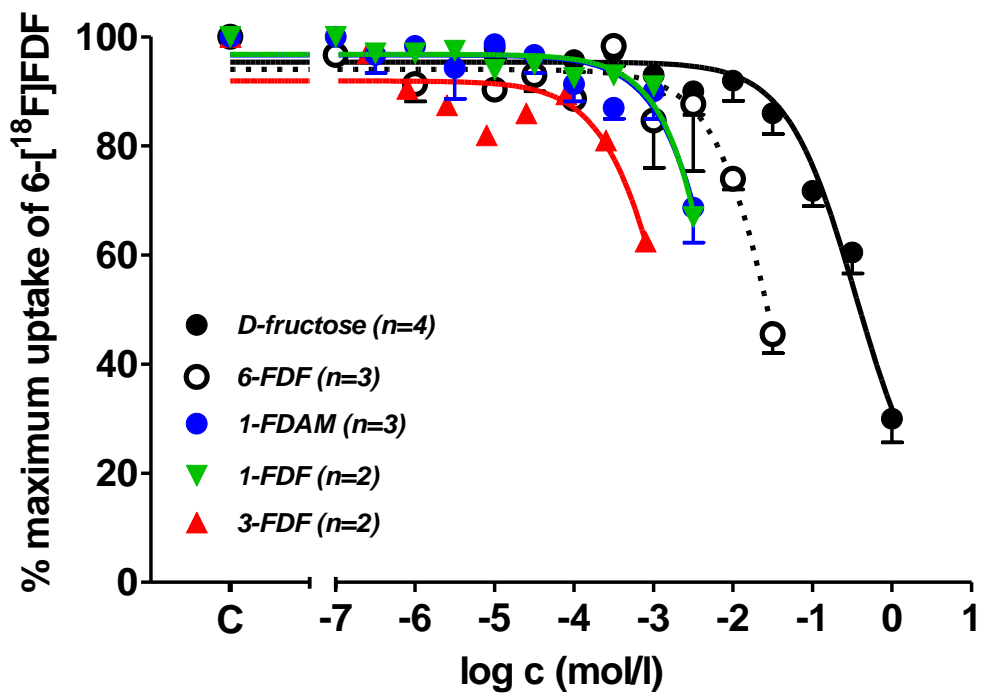


Figure B.7: Concentration-response curves for 6-FDF, fructose, 1-FDAM 3-FDF and 1-FDF - the inhibiting effects of each substrate on the cell uptake of 6-[¹⁸F]FDF into EMT-6 cells. Data are shown as % maximum radiotracer uptake (control = 100%) and error bars represent the SEM.